

Gamma-Ray Bursts

Contents

1	Topics	73
2	Participants	75
2.1	ICRANet participants	75
2.2	Past collaborators	75
2.3	Ongoing collaborations	76
2.4	Students	78
3	Brief summary of recent progresses	79
4	Selected publications before 2005	81
4.1	Refereed journals	81
4.2	Conference proceedings	88
5	Publications (2005–2015)	93
5.1	Refereed journals	93
5.2	Conference proceedings	120

1 Topics

- GRB classification
- GRB empirical correlations
- “Genuine short” GRBs: Possible identifications and selection effects
- A modified spectral energy distribution for highly energetic GRBs
- The observed spectra of the P-GRBs
- GRB prompt emission spectra below 5 keV: challenges for future missions
- Interpretation of the ultra high energy emission from GRBs observed by Fermi and AGILE
- Analysis of different families of progenitors for GRBs with different energetics
- GRBs at redshift $z > 6$
- GRBs originating from a multiple collapse
- Prompt emission and X-ray flares: the clumpiness of CBM
- Microphysical description of the interaction between the fireshell and the CBM
- Theoretical interpretation of the “plateau” phase in the X-ray afterglow
- Emission from newly born neutron stars, or “neo neutron stars”.
- Induced Gravitational Collapse process for GRBs associated with supernovae.
- Redshift estimators for GRBs with no measured redshift.

- Binary Driven Hypernovae (BdHNe) as progenitor of GRBs via Induced Gravitational Collapse.
- GRB light curves as composed of four different episodes.
- Different kinds of binary systems as GRB progenitors.
- “Cosmic Matrix” for GRBs.

2 Participants

2.1 ICRANet participants

- David Arnett
- Carlo Luciano Bianco
- Massimo Della Valle
- Luca Izzo
- Jorge Armando Rueda Hernandez
- Remo Ruffini
- Gregory Vereshchagin
- She-Sheng Xue

2.2 Past collaborators

- Andrey Baranov
- Maria Grazia Bernardini (OAB, Italy)
- Joao Braga (INPE, Brazil)
- Sabrina Casanova (MPIK, Germany)
- Letizia Caito
- Pascal Chardonnet (Université de Savoie, France)
- Guido Chincarini (Universit di Milano "Bicocca", Italy)

- Demetrios Christodoulou (ETH Zurich, Switzerland)
- Alessandra Corsi (INAF-IASF Roma, Italy)
- Valeri Chechetkin
- Maria Giovanna Dainotti
- Thibault Damour (IHES, France)
- Walter Ferrara
- Federico Fraschetti (CEA Saclay, France)
- Roberto Guida
- Vahe Gurzadyan (Yerevan Physics Institute, Armenia)
- Wen-Biao Han
- Massimiliano Lattanzi (Oxford Astrophysics, UK)
- Vincenzo Liccardo
- Nino Panagia
- Elena Pian
- Giuliano Preparata (Università di Milano, Italy)
- Jay D. Salmonson (Livermore Lab, USA)
- Vineeth Valsan
- Jim Wilson (Livermore Lab, USA)

2.3 Ongoing collaborations

- Alexey Aksenov (ITEP, Russia)
- Lorenzo Amati (INAF-IASF Bologna, Italy)
- Riccardo Belvedere (ICRANet-Rio, Brazil)

- Sandip Kumar Chakrabarti (S.N. Bose National Centre and Indian Centre for Space Physics, India)
- Alessandro Chieffi (INAF-IASF Roma, Italy)
- Stefano Covino (OAB, Italy)
- Gustavo de Barros (UFRJ, Brazil)
- Filippo Frontera (Universit di Ferrara, Italy)
- Chris Fryer (Los Alamos National Laboratories, USA).
- Dafne Guetta (OAR, Italy)
- Cristiano Guidorzi (OAB, Italy)
- Stanislav Kelner (MEPhI, Russia, and MPIK, Germany)
- Marco Limongi (OAR, Italy)
- Vanessa Mangano (INAF-IASF Palermo, Italy)
- Barbara Patricelli (Astronomy Institute - UNAM, México))
- Ana Virginia Penacchioni (INPE, Brazil)
- Luis Juracy Rangel Lemos (Fundao Universidade Federal do Tocantins, Brazil)
- Ivan Siutsou (ICRANet-Rio, Brazil)
- Susanna Vergani (Dunsink Observatory, Ireland)
- Francesco Vissani (INFN, Italy)
- Elena Zaninoni (ICRANet-Rio, Brazil)

2.4 **Students**

- Cristina Barbarino (IRAP PhD, Italy)
- Maxime Enderli (IRAP PhD, France)
- Milos Kovacevic (IRAP PhD, Serbia)
- Hendrik Ludwig (IRAP PhD, Germany)
- Marco Muccino (IRAP PhD, Italy)
- Giovanni Battista Pisani (IRAP PhD, Italy)
- Yu Wang (IRAP PhD, China)

3 Brief summary of recent progresses

Major progresses have been accomplished this year in the following aspects:

- In discovering a “nesting” in the late x-ray light curves of BdHN systems.
- In reviewing old BATSE data finding the same characteristic features of BdHN systems.
- In dividing GRBs in two different families, based on their energetics, thanks to the results of the analysis of GRB 130427A, associated with SN 2013cq, within the BdHN scenario.
- In applying this new classification in two different families, based on the energetics, also to short GRBs.
- In studying the different configurations of the binary progenitor system within the IGC paradigm.

4 Selected publications before 2005

4.1 Refereed journals

1. D. Christodoulou, R. Ruffini; “Reversible Transformations of a Charged Black Hole”; *Physical Review D*, 4, 3552 (1971).

A formula is derived for the mass of a black hole as a function of its “irreducible mass”, its angular momentum, and its charge. It is shown that 50% of the mass of an extreme charged black hole can be converted into energy as contrasted with 29% for an extreme rotating black hole.

2. T. Damour, R. Ruffini; “Quantum electrodynamical effects in Kerr-Newman geometries”; *Physical Review Letters*, 35, 463 (1975).

Following the classical approach of Sauter, of Heisenberg and Euler and of Schwinger the process of vacuum polarization in the field of a “bare” Kerr-Newman geometry is studied. The value of the critical strength of the electromagnetic fields is given together with an analysis of the feedback of the discharge on the geometry. The relevance of this analysis for current astrophysical observations is mentioned.

3. G. Preparata, R. Ruffini, S.-S. Xue; “The dyadosphere of black holes and gamma-ray bursts”; *Astronomy & Astrophysics*, 338, L87 (1999).

The “dyadosphere” has been defined as the region outside the horizon of a black hole endowed with an electromagnetic field (abbreviated to EMBH for “electromagnetic black hole”) where the electromagnetic field exceeds the critical value, predicted by Heisenberg & Euler for e^\pm pair production. In a very short time ($\sim O(\hbar/mc^2)$) a very large number of pairs is created there. We here give limits on the EMBH parameters leading to a Dyadosphere for $10M_\odot$ and 10^5M_\odot EMBH’s, and give as well the pair densities as functions of the radial coordinate. We here assume that the pairs reach thermodynamic equilibrium

with a photon gas and estimate the average energy per pair as a function of the EMBH mass. These data give the initial conditions for the analysis of an enormous pair-electromagnetic-pulse or "P.E.M. pulse" which naturally leads to relativistic expansion. Basic energy requirements for gamma ray bursts (GRB), including GRB971214 recently observed at $z=3.4$, can be accounted for by processes occurring in the dyadosphere. In this letter we do not address the problem of forming either the EMBH or the dyadosphere: we establish some inequalities which must be satisfied during their formation process.

4. R. Ruffini, J.D. Salmonson, J.R. Wilson, S.-S. Xue; "On the pair electromagnetic pulse of a black hole with electromagnetic structure"; *Astronomy & Astrophysics*, 350, 334 (1999).

We study the relativistically expanding electron-positron pair plasma formed by the process of vacuum polarization around an electromagnetic black hole (EMBH). Such processes can occur for EMBH's with mass all the way up to $6 \times 10^5 M_{\odot}$. Beginning with a idealized model of a Reissner-Nordstrom EMBH with charge to mass ratio $\zeta = 0.1$, numerical hydrodynamic calculations are made to model the expansion of the pair-electromagnetic pulse (PEM pulse) to the point that the system is transparent to photons. Three idealized special relativistic models have been compared and contrasted with the results of the numerically integrated general relativistic hydrodynamic equations. One of the three models has been validated: a PEM pulse of constant thickness in the laboratory frame is shown to be in excellent agreement with results of the general relativistic hydrodynamic code. It is remarkable that this precise model, starting from the fundamental parameters of the EMBH, leads uniquely to the explicit evaluation of the parameters of the PEM pulse, including the energy spectrum and the astrophysically unprecedented large Lorentz factors (up to 6×10^3 for a $10^3 M_{\odot}$ EMBH). The observed photon energy at the peak of the photon spectrum at the moment of photon decoupling is shown to range from 0.1 MeV to 4 MeV as a function of the EMBH mass. Correspondingly the total energy in photons is in the range of 10^{52} to 10^{54} ergs, consistent with observed gamma-ray bursts. In these computations we neglect the presence of baryonic matter which will be the subject of forthcoming publications.

5. R. Ruffini, J.D. Salmonson, J.R. Wilson, S.-S. Xue; "On the pair-electromagnetic pulse from an electromagnetic black hole surrounded by a baryonic remnant"; *Astronomy & Astrophysics*, 359, 855 (2000).

The interaction of an expanding Pair-Electromagnetic pulse (PEM pulse) with

a shell of baryonic matter surrounding a Black Hole with electromagnetic structure (EMBH) is analyzed for selected values of the baryonic mass at selected distances well outside the dyadosphere of an EMBH. The dyadosphere, the region in which a super critical field exists for the creation of e^+e^- pairs, is here considered in the special case of a Reissner-Nordstrom geometry. The interaction of the PEM pulse with the baryonic matter is described using a simplified model of a slab of constant thickness in the laboratory frame (constant-thickness approximation) as well as performing the integration of the general relativistic hydrodynamical equations. The validation of the constant-thickness approximation, already presented in a previous paper Ruffini et al. (1999) for a PEM pulse in vacuum, is here generalized to the presence of baryonic matter. It is found that for a baryonic shell of mass-energy less than 1% of the total energy of the dyadosphere, the constant-thickness approximation is in excellent agreement with full general relativistic computations. The approximation breaks down for larger values of the baryonic shell mass, however such cases are of less interest for observed Gamma Ray Bursts (GRBs). On the basis of numerical computations of the slab model for PEM pulses, we describe (i) the properties of relativistic evolution of a PEM pulse colliding with a baryonic shell; (ii) the details of the expected emission energy and observed temperature of the associated GRBs for a given value of the EMBH mass; $10^3 M_\odot$, and for baryonic mass-energies in the range 10^{-8} to 10^{-2} the total energy of the dyadosphere.

6. C.L. Bianco, R. Ruffini, S.-S. Xue; "The elementary spike produced by a pure e^+e^- pair-electromagnetic pulse from a Black Hole: The PEM Pulse"; *Astronomy & Astrophysics*, 368, 377 (2001).

In the framework of the model that uses black holes endowed with electromagnetic structure (EMBH) as the energy source, we study how an elementary spike appears to the detectors. We consider the simplest possible case of a pulse produced by a pure e^+e^- pair-electro-magnetic plasma, the PEM pulse, in the absence of any baryonic matter. The resulting time profiles show a *Fast-Rise-Exponential-Decay* shape, followed by a power-law tail. This is obtained without any special fitting procedure, but only by fixing the energetics of the process taking place in a given EMBH of selected mass, varying in the range from 10 to $10^3 M_\odot$ and considering the relativistic effects to be expected in an electron-positron plasma gradually reaching transparency. Special attention is given to the contributions from all regimes with Lorentz γ factor varying from $\gamma = 1$ to $\gamma = 10^4$ in a few hundreds of the PEM pulse travel time. Although the

main goal of this paper is to obtain the elementary spike intensity as a function of the arrival time, and its observed duration, some qualitative considerations are also presented regarding the expected spectrum and on its departure from the thermal one. The results of this paper will be comparable, when data will become available, with a subfamily of particularly short GRBs not followed by any afterglow. They can also be propedeutical to the study of longer bursts in presence of baryonic matter currently observed in GRBs.

7. R. Ruffini, C.L. Bianco, P. Chardonnet, F. Fraschetti, S.-S. Xue; "Relative spacetime transformations in Gamma-Ray Bursts"; *The Astrophysical Journal*, 555, L107 (2001).

The GRB 991216 and its relevant data acquired from the BATSE experiment and RXTE and Chandra satellites are used as a prototypical case to test the theory linking the origin of gamma ray bursts (GRBs) to the process of vacuum polarization occurring during the formation phase of a black hole endowed with electromagnetic structure (EMBH). The relative space-time transformation paradigm (RSTT paradigm) is presented. It relates the observed signals of GRBs to their past light cones, defining the events on the worldline of the source essential for the interpretation of the data. Since GRBs present regimes with unprecedentedly large Lorentz γ factor, also sharply varying with time, particular attention is given to the constitutive equations relating the four time variables: the comoving time, the laboratory time, the arrival time at the detector, duly corrected by the cosmological effects. This paradigm is at the very foundation of any possible interpretation of the data of GRBs.

8. R. Ruffini, C.L. Bianco, P. Chardonnet, F. Fraschetti, S.-S. Xue; "On the interpretation of the burst structure of Gamma-Ray Bursts"; *The Astrophysical Journal*, 555, L113 (2001).

Given the very accurate data from the BATSE experiment and RXTE and Chandra satellites, we use the GRB 991216 as a prototypical case to test the EMBH theory linking the origin of the energy of GRBs to the electromagnetic energy of black holes. The fit of the afterglow fixes the only two free parameters of the model and leads to a new paradigm for the interpretation of the burst structure, the IBS paradigm. It leads as well to a reconsideration of the relative roles of the afterglow and burst in GRBs by defining two new phases in this complex phenomenon: a) the injector phase, giving rise to the proper-GRB (P-GRB), and b) the beam-target phase, giving rise to the extended afterglow peak emission (E-APE) and to the afterglow. Such differentiation leads to a

natural possible explanation of the bimodal distribution of GRBs observed by BATSE. The agreement with the observational data in regions extending from the horizon of the EMBH all the way out to the distant observer confirms the uniqueness of the model.

9. R. Ruffini, C.L. Bianco, P. Chardonnet, F. Frascchetti, S.-S. Xue; "On a possible Gamma-Ray Burst-Supernova time sequence"; *The Astrophysical Journal*, 555, L117 (2001).

The data from the Chandra satellite on the iron emission lines in the afterglow of GRB 991216 are used to give further support for the EMBH theory, which links the origin of the energy of GRBs to the extractable energy of electromagnetic black holes (EMBHs), leading to an interpretation of the GRB-supernova correlation. Following the relative space-time transformation (RSTT) paradigm and the interpretation of the burst structure (IBS) paradigm, we introduce a paradigm for the correlation between GRBs and supernovae. The following sequence of events is shown as kinematically possible and consistent with the available data: a) the GRB-progenitor star P_1 first collapses to an EMBH, b) the proper GRB (P-GRB) and the peak of the afterglow (E-APE) propagate in interstellar space until the impact on a supernova-progenitor star P_2 at a distance $\leq 2.69 \times 10^{17}$ cm, and they induce the supernova explosion, c) the accelerated baryonic matter (ABM) pulse, originating the afterglow, reaches the supernova remnants 18.5 hours after the supernova explosion and gives rise to the iron emission lines. Some considerations on the dynamical implementation of the paradigm are presented. The concept of induced supernova explosion introduced here specifically for the GRB-supernova correlation may have more general application in relativistic astrophysics.

10. R. Ruffini, C.L. Bianco, P. Chardonnet, F. Frascchetti, S.-S. Xue; "On the physical processes which lie at the bases of time variability of GRBs"; *Il Nuovo Cimento B*, 116, 99 (2001).

The relative-space-time-transformation (RSTT) paradigm and the interpretation of the burst-structure (IBS) paradigm are applied to probe the origin of the time variability of GRBs. Again GRB 991216 is used as a prototypical case, thanks to the precise data from the CGRO, RXTE and Chandra satellites. It is found that with the exception of the relatively inconspicuous but scientifically very important signal originating from the initial "proper gamma ray burst" (P-GRB), all the other spikes and time variabilities can be explained by the interaction of the accelerated-baryonic-matter pulse with inhomogeneities in the

interstellar matter. This can be demonstrated by using the RSTT paradigm as well as the IBS paradigm, to trace a typical spike observed in arrival time back to the corresponding one in the laboratory time. Using these paradigms, the identification of the physical nature of the time variability of the GRBs can be made most convincingly. It is made explicit the dependence of a) the intensities of the afterglow, b) the spikes amplitude and c) the actual time structure on the Lorentz gamma factor of the accelerated-baryonic-matter pulse. In principle it is possible to read off from the spike structure the detailed density contrast of the interstellar medium in the host galaxy, even at very high redshift.

11. R. Ruffini, C.L. Bianco, P. Chardonnet, F. Fraschetti, S.-S. Xue; "On the structures in the afterglow peak emission of gamma ray bursts"; *The Astrophysical Journal*, 581, L19 (2002).

Using GRB 991216 as a prototype, it is shown that the intensity substructures observed in what is generally called the "prompt emission" in gamma ray bursts (GRBs) do originate in the collision between the accelerated baryonic matter (ABM) pulse with inhomogeneities in the interstellar medium (ISM). The initial phase of such process occurs at a Lorentz factor $\gamma \sim 310$. The crossing of ISM inhomogeneities of sizes $\Delta R \sim 10^{15}$ cm occurs in a detector arrival time interval of ~ 0.4 s implying an apparent superluminal behavior of $\sim 10^5 c$. The long lasting debate between the validity of the external shock model vs. the internal shock model for GRBs is solved in favor of the first.

12. R. Ruffini, C.L. Bianco, P. Chardonnet, F. Fraschetti, S.-S. Xue; "On the structure of the burst and afterglow of Gamma-Ray Bursts I: the radial approximation"; *International Journal of Modern Physics D*, 12, 173 (2003).

We have recently proposed three paradigms for the theoretical interpretation of gamma-ray bursts (GRBs). (1) The relative space-time transformation (RSTT) paradigm emphasizes how the knowledge of the entire world-line of the source from the moment of gravitational collapse is a necessary condition in order to interpret GRB data. (2) The interpretation of the burst structure (IBS) paradigm differentiates in all GRBs between an injector phase and a beam-target phase. (3) The GRB-supernova time sequence (GSTS) paradigm introduces the concept of *induced supernova explosion* in the supernovae-GRB association. In the introduction the RSTT and IBS paradigms are enunciated and illustrated using our theory based on the vacuum polarization process occurring around an electromagnetic black hole (EMBH theory). The results are summarized

using figures, diagrams and a complete table with the space-time grid, the fundamental parameters and the corresponding values of the Lorentz gamma factor for GRB 991216 used as a prototype. In the following sections the detailed treatment of the EMBH theory needed to understand the results of the three above letters is presented. We start from the considerations on the dyadosphere formation. We then review the basic hydrodynamic and rate equations, the equations leading to the relative space-time transformations as well as the adopted numerical integration techniques. We then illustrate the five fundamental eras of the EMBH theory: the self acceleration of the e^+e^- pair-electromagnetic plasma (PEM pulse), its interaction with the baryonic remnant of the progenitor star, the further self acceleration of the e^+e^- pair-electromagnetic radiation and baryon plasma (PEMB pulse). We then study the approach of the PEMB pulse to transparency, the emission of the proper GRB (P-GRB) and its relation to the “short GRBs”. Particular attention is given to the free parameters of the theory and to the values of the thermodynamical quantities at transparency. Finally the three different regimes of the afterglow are described within the fully radiative and radial approximations: the ultrarelativistic, the relativistic and the nonrelativistic regimes. The best fit of the theory leads to an unequivocal identification of the “long GRBs” as extended emission occurring at the afterglow peak (E-APE). The relative intensities, the time separation and the hardness ratio of the P-GRB and the E-APE are used as distinctive observational test of the EMBH theory and the excellent agreement between our theoretical predictions and the observations are documented. The afterglow power-law indexes in the EMBH theory are compared and contrasted with the ones in the literature, and no beaming process is found for GRB 991216. Finally, some preliminary results relating the observed time variability of the E-APE to the inhomogeneities in the interstellar medium are presented, as well as some general considerations on the EMBH formation. The issue of the GSTS paradigm will be the object of a forthcoming publication and the relevance of the iron-lines observed in GRB 991216 is shortly reviewed. The general conclusions are then presented based on the three fundamental parameters of the EMBH theory: the dyadosphere energy, the baryonic mass of the remnant, the interstellar medium density. An in depth discussion and comparison of the EMBH theory with alternative theories is presented as well as indications of further developments beyond the radial approximation, which will be the subject of paper II in this series. Future needs for specific GRB observations are outlined.

13. R. Ruffini, C.L. Bianco, P. Chardonnet, F. Fraschetti, V. Gurzadyan, S.-S. Xue; "On the instantaneous spectrum of gamma ray bursts"; *International Journal of Modern Physics D*, 13, 843 (2004).

A theoretical attempt to identify the physical process responsible for the afterglow emission of Gamma-Ray Bursts (GRBs) is presented, leading to the occurrence of thermal emission in the comoving frame of the shock wave giving rise to the bursts. The determination of the luminosities and spectra involves integration over an infinite number of Planckian spectra, weighted by appropriate relativistic transformations, each one corresponding to a different viewing angle in the past light cone of the observer. The relativistic transformations have been computed using the equations of motion of GRBs within our theory, giving special attention to the determination of the equitemporal surfaces. The only free parameter of the present theory is the "effective emitting area" in the shock wave front. A self consistent model for the observed hard-to-soft transition in GRBs is also presented. When applied to GRB 991216 a precise fit ($\chi^2 \simeq 1.078$) of the observed luminosity in the 2–10 keV band is obtained. Similarly, detailed estimates of the observed luminosity in the 50–300 keV and in the 10–50 keV bands are obtained.

4.2 Conference proceedings

1. R. Ruffini; "Beyond the critical mass: The dyadosphere of black holes"; in "Black Holes and High Energy Astrophysics", H. sato, N. Sugiyama, Editors; p. 167; Universal Academy Press (Tokyo, Japan, 1998).

The "dyadosphere" (from the Greek word "duas-duados" for pairs) is here defined as the region outside the horizon of a black hole endowed with an electromagnetic field (abbreviated to EMBH for "electromagnetic black hole") where the electromagnetic field exceeds the critical value, predicted by Heisenberg and Euler for e^+e^- pair production. In a very short time ($\sim O(\hbar/mc^2)$), a very large number of pairs is created there. I give limits on the EMBH parameters leading to a Dyadosphere for $10M_\odot$ and 10^5M_\odot EMBH's, and give as well the pair densities as functions of the radial coordinate. These data give the initial conditions for the analysis of an enormous pair-electromagnetic-pulse or "PEM-pulse" which naturally leads to relativistic expansion. Basic energy requirements for gamma ray bursts (GRB), including GRB971214 recently observed at $z = 3.4$, can be accounted for by processes occurring in the dyado-

sphere.

2. R. Ruffini, C.L. Bianco, P. Chardonnet, F. Fraschetti, L. Vitagliano, S.-S. Xue; "New perspectives in physics and astrophysics from the theoretical understanding of Gamma-Ray Bursts"; in "COSMOLOGY AND GRAVITATION: Xth Brazilian School of Cosmology and Gravitation; 25th Anniversary (1977-2002)", Proceedings of the Xth Brazilian School on Cosmology and Gravitation, Mangaratiba, Rio de Janeiro (Brazil), July - August 2002, M. Novello, S.E. Perez Bergliaffa, Editors; AIP Conference Proceedings, 668, 16 (2003).

If due attention is given in formulating the basic equations for the Gamma-Ray Burst (GRB) phenomenon and in performing the corresponding quantitative analysis, GRBs open a main avenue of inquiring on totally new physical and astrophysical regimes. This program is very likely one of the greatest computational efforts in physics and astrophysics and cannot be actuated using shortcuts. A systematic approach is needed which has been highlighted in three basic new paradigms: the relative space-time transformation (RSTT) paradigm, the interpretation of the burst structure (IBS) paradigm, the GRB-supernova time sequence (GSTS) paradigm. From the point of view of fundamental physics new regimes are explored: (1) the process of energy extraction from black holes; (2) the quantum and general relativistic effects of matter-antimatter creation near the black hole horizon; (3) the physics of ultrarelativistic shock waves with Lorentz gamma factor $\gamma > 100$. From the point of view of astronomy and astrophysics also new regimes are explored: (i) the occurrence of gravitational collapse to a black hole from a critical mass core of mass $M \gtrsim 10M_{\odot}$, which clearly differs from the values of the critical mass encountered in the study of stars "catalyzed at the endpoint of thermonuclear evolution" (white dwarfs and neutron stars); (ii) the extremely high efficiency of the spherical collapse to a black hole, where almost 99.99% of the core mass collapses leaving negligible remnant; (iii) the necessity of developing a fine tuning in the final phases of thermonuclear evolution of the stars, both for the star collapsing to the black hole and the surrounding ones, in order to explain the possible occurrence of the "induced gravitational collapse". New regimes are as well encountered from the point of view of nature of GRBs: (I) the basic structure of GRBs is uniquely composed by a proper-GRB (P-GRB) and the afterglow; (II) the long bursts are then simply explained as the peak of the afterglow (the E-APE) and their observed time variability is explained in terms of inhomogeneities in the interstellar medium (ISM); (III) the short bursts are

identified with the P-GRBs and the crucial information on general relativistic and vacuum polarization effects are encoded in their spectra and intensity time variability. A new class of space missions to acquire information on such extreme new regimes are urgently needed.

3. R. Ruffini, C.L. Bianco, P. Chardonnet, F. Fraschetti, S.-S. Xue; "The EMBH Model in GRB 991216 and GRB 980425"; in Proceedings of "Third Rome Workshop on Gamma-Ray Burst in the Afterglow Era", 17-20 September 2002; M. Feroci, F. Frontera, N. Masetti, L. Piro, Editors; ASP Conference Series, 312, 349 (2004).

This is a summary of the two talks presented at the Rome GRB meeting by C.L. Bianco and R. Ruffini. It is shown that by respecting the Relative Space-Time Transformation (RSTT) paradigm and the Interpretation of the Burst Structure (IBS) paradigm, important inferences are possible: a) in the new physics occurring in the energy sources of GRBs, b) on the structure of the bursts and c) on the composition of the interstellar matter surrounding the source.

4. M.G. Bernardini, C.L. Bianco, P. Chardonnet, F. Fraschetti, R. Ruffini, S.-S. Xue; "A New Astrophysical 'Triptych': GRB030329/SN2003dh/URCA-2"; in "GAMMA-RAY BURSTS: 30 YEARS OF DISCOVERY", Proceedings of the Los Alamos "Gamma Ray Burst Symposium", Santa Fe, New Mexico, 8-12 September 2003, E.E. Fenimore, M. Galassi, Editors; AIP Conference Proceedings, 727, 312 (2004).

We analyze the data of the Gamma-Ray Burst/Supernova GRB030329/SN2003dh system obtained by HETE-2, R-XTE, XMM and VLT within our theory for GRB030329. By fitting the only three free parameters of the EMBH theory, we obtain the luminosity in fixed energy bands for the prompt emission and the afterglow. Since the Gamma-Ray Burst (GRB) analysis is consistent with a spherically symmetric expansion, the energy of GRB030329 is $E = 2.1 \times 10^{52}$ erg, namely $\sim 2 \times 10^3$ times larger than the Supernova energy. We conclude that either the GRB is triggering an induced-supernova event or both the GRB and the Supernova are triggered by the same relativistic process. In no way the GRB can be originated from the supernova. We also evidence that the XMM observations, much like in the system GRB980425/SN1998bw, are not part of the GRB afterglow, as interpreted in the literature, but are associated to the Supernova phenomenon. A dedicated campaign of observations is needed to confirm the nature of this XMM source as a newly born neutron star cooling by generalized URCA processes.

5. F. Frascchetti, M.G. Bernardini, C.L. Bianco, P. Chardonnet, R. Ruffini, S.-S. Xue; "The GRB980425-SN1998bw Association in the EMBH Model"; in "GAMMA-RAY BURSTS: 30 YEARS OF DISCOVERY", Proceedings of the Los Alamos "Gamma Ray Burst Symposium", Santa Fe, New Mexico, 8-12 September 2003, E.E. Fenimore, M. Galassi, Editors; AIP Conference Proceedings, 727, 424 (2004).

Our GRB theory, previously developed using GRB 991216 as a prototype, is here applied to GRB 980425. We fit the luminosity observed in the 40–700 keV, 2–26 keV and 2–10 keV bands by the BeppoSAX satellite. In addition the supernova SN1998bw is the outcome of an "induced gravitational collapse" triggered by GRB 980425, in agreement with the GRB-Supernova Time Sequence (GSTS) paradigm. A further outcome of this astrophysically exceptional sequence of events is the formation of a young neutron star generated by the SN1998bw event. A coordinated observational activity is recommended to further enlighten the underlying scenario of this most unique astrophysical system.

6. A. Corsi, M.G. Bernardini, C.L. Bianco, P. Chardonnet, F. Frascchetti, R. Ruffini, S.-S. Xue; "GRB 970228 Within the EMBH Model"; in "GAMMA-RAY BURSTS: 30 YEARS OF DISCOVERY", Proceedings of the Los Alamos "Gamma Ray Burst Symposium", Santa Fe, New Mexico, 8-12 September 2003, E.E. Fenimore, M. Galassi, Editors; AIP Conference Proceedings, 727, 428 (2004).

We consider the gamma-ray burst of 1997 February 28 (GRB 970228) within the ElectroMagnetic Black Hole (EMBH) model. We first determine the value of the two free parameters that characterize energetically the GRB phenomenon in the EMBH model, that is to say the dyadosphere energy, $E_{dya} = 5.1 \times 10^{52}$ ergs, and the baryonic remnant mass M_B in units of E_{dya} , $B = M_B c^2 / E_{dya} = 3.0 \times 10^{-3}$. Having in this way estimated the energy emitted during the beam-target phase, we evaluate the role of the InterStellar Medium (ISM) number density (n_{ISM}) and of the ratio \mathcal{R} between the effective emitting area and the total surface area of the GRB source, in reproducing the observed profiles of the GRB 970228 prompt emission and X-ray (2-10 keV energy band) afterglow. The importance of the ISM distribution three-dimensional treatment around the central black hole is also stressed in this analysis.

5 Publications (2005–2015)

5.1 Refereed journals

1. R. Ruffini, C.L. Bianco, P. Chardonnet, F. Fraschetti, V. Gurzadyan, S.-S. Xue; “Emergence of a filamentary structure in the fireball from GRB spectra”; *International Journal of Modern Physics D*, 14, 97 (2005).

It is shown that the concept of a fireball with a definite filamentary structure naturally emerges from the analysis of the spectra of Gamma-Ray Bursts (GRBs). These results, made possible by the recently obtained analytic expressions of the equitemporal surfaces in the GRB afterglow, depend crucially on the single parameter R describing the effective area of the fireball emitting the X-ray and gamma-ray radiation. The X-ray and gamma-ray components of the afterglow radiation are shown to have a thermal spectrum in the co-moving frame of the fireball and originate from a stable shock front described self-consistently by the Rankine-Hugoniot equations. Precise predictions are presented on a correlation between spectral changes and intensity variations in the prompt radiation verifiable, e.g., by the Swift and future missions. The highly variable optical and radio emission depends instead on the parameters of the surrounding medium. The GRB 991216 is used as a prototype for this model.

2. R. Ruffini, M.G. Bernardini, C.L. Bianco, P. Chardonnet, F. Fraschetti, V. Gurzadyan, M. Lattanzi, L. Vitagliano, S.-S. Xue; “Extracting energy from black holes: ‘long’ and ‘short’ GRBs and their astrophysical settings”; *Il Nuovo Cimento C*, 28, 589 (2005).

The introduction of the three interpretational paradigms for Gamma-Ray Bursts (GRBs) and recent progress in understanding the X- and gamma-ray luminosity in the afterglow allow us to make assessments about the astrophysical settings of GRBs. In particular, we evidence the distinct possibility that some GRBs occur in a binary system. This subclass of GRBs manifests itself in a “tryptich”: one component formed by the collapse of a massive star to a black

hole, which originates the GRB; a second component by a supernova and a third one by a young neutron star born in the supernova event. Similarly, the understanding of the physics of quantum relativistic processes during the gravitational collapse makes possible precise predictions about the structure of short GRBs.

3. M.G. Bernardini, C.L. Bianco, P. Chardonnet, F. Fraschetti, R. Ruffini, S.-S. Xue; "Theoretical interpretation of luminosity and spectral properties of GRB 031203"; *The Astrophysical Journal*, 634, L29 (2005).

The X-ray and gamma-ray observations of the source GRB 031203 by INTEGRAL are interpreted within our theoretical model. In addition to a complete spacetime parameterization of the GRB, we specifically assume that the afterglow emission originates from a thermal spectrum in the comoving frame of the expanding baryonic matter shell. By determining the two free parameters of the model and estimating the density and filamentary structure of the ISM, we reproduce the observed luminosity in the 20-200 keV energy band. As in previous sources, the prompt radiation is shown to coincide with the peak of the afterglow, and the luminosity substructure is shown to originate in the filamentary structure of the ISM. We predict a clear hard-to-soft behavior in the instantaneous spectra. The time-integrated spectrum over 20 s observed by INTEGRAL is well fitted. Despite the fact that this source has been considered "unusual", it appears to us to be a normal low-energy GRB.

4. R. Ruffini, M.G. Bernardini, C.L. Bianco, P. Chardonnet, F. Fraschetti, S.-S. Xue; Evidence for isotropic emission in GRB991216; *Advances in Space Research*, 38, 1291 (2006).

The issue of the possible presence or absence of jets in GRBs is here re-examined for GRB991216. We compare and contrast our theoretically predicted afterglow luminosity in the 2–10 keV band for spherically symmetric versus jetted emission. At these wavelengths the jetted emission can be excluded and data analysis confirms spherical symmetry. These theoretical fits are expected to be improved by the forthcoming data of the Swift mission.

5. R. Ruffini, M.G. Bernardini, C.L. Bianco, P. Chardonnet, F. Fraschetti, R. Guida, S.-S. Xue; "GRB 050315: A step toward understanding the uniqueness of the overall GRB structure"; *The Astrophysical Journal*, 645, L109 (2006).

Using the Swift data of GRB 050315, we are making progress toward understanding the uniqueness of our theoretically predicted gamma-ray burst (GRB) structure, which is composed of a proper GRB (P-GRB), emitted at the transparency of an electron-positron plasma with suitable baryon loading, and an afterglow comprising the so-called prompt emission due to external shocks. Thanks to the Swift observations, the P-GRB is identified, and for the first time we can theoretically fit detailed light curves for selected energy bands on a continuous timescale ranging over 10⁶ s. The theoretically predicted instantaneous spectral distribution over the entire afterglow is presented, confirming a clear hard-to-soft behavior encompassing, continuously, the “prompt emission” all the way to the latest phases of the afterglow.

6. C.L. Bianco, L. Caito, R. Ruffini; “Theoretical interpretation of GRB 011121”; *Il Nuovo Cimento B*, 121, 1441 (2006).

GRB011121 is analyzed as a prototype to understand the “flares” recently observed by Swift in the afterglow of many GRB sources. Detailed theoretical computation of the GRB011121 light curves in selected energy bands are presented and compared and contrasted with observational BeppoSAX data.

7. R. Ruffini, M.G. Bernardini, C.L. Bianco, P. Chardonnet, F. Frascchetti, R. Guida, S.-S. Xue; “GRB 050315: A step toward the uniqueness of the overall GRB structure”; *Il Nuovo Cimento B*, 121, 1367 (2006).

Using the *Swift* data of GRB 050315, we progress on the uniqueness of our theoretically predicted Gamma-Ray Burst (GRB) structure as composed by a proper-GRB (P-GRB), emitted at the transparency of an electron-positron plasma with suitable baryon loading, and an afterglow comprising the so called “prompt emission” as due to external shocks. Thanks to the *Swift* observations, we can theoretically fit detailed light curves for selected energy bands on a continuous time scale ranging over 10⁶ seconds. The theoretically predicted instantaneous spectral distribution over the entire afterglow confirms a clear hard-to-soft behavior encompassing, continuously, the “prompt emission” all the way to the latest phases of the afterglow. Consequences of the instrumental threshold on the definition of “short” and “long” GRBs are discussed.

8. M.G. Bernardini, C.L. Bianco, L. Caito, P. Chardonnet, A. Corsi, M.G. Dainotti, F. Frascchetti, R. Guida, R. Ruffini, S.-S. Xue; GRB970228 as a prototype for short GRBs with afterglow; *Il Nuovo Cimento B*, 121, 1439 (2006).

GRB970228 is analyzed as a prototype to understand the relative role of short GRBs and their associated afterglows, recently observed by Swift and HETE-II. Detailed theoretical computation of the GRB970228 light curves in selected energy bands are presented and compared with observational BeppoSAX data.

9. M.G. Dainotti, M.G. Bernardini, C.L. Bianco, L. Caito, R. Guida, R. Ruffini; “GRB060218 and GRBs associated with Supernovae Ib/c”; *Astronomy & Astrophysics*, 471, L29 (2007).

Context: The *Swift* satellite has given continuous data in the range 0.3–150 keV from 0 s to 10^6 s for GRB060218 associated with SN2006aj. This Gamma-Ray Burst (GRB) which has an unusually long duration ($T_{90} \sim 2100$ s) fulfills the Amati relation. These data offer the opportunity to probe theoretical models for GRBs connected with Supernovae (SNe).

Aims: We plan to fit the complete γ - and X-ray light curves of this long duration GRB, including the prompt emission, in order to clarify the nature of the progenitors and the astrophysical scenario of the class of GRBs associated with SNe Ib/c.

Methods: We apply our “fireshell” model based on the formation of a black hole, giving the relevant references. It is characterized by the precise equations of motion and equitemporal surfaces and by the role of thermal emission.

Results: The initial total energy of the electron-positron plasma $E_{e^\pm}^{tot} = 2.32 \times 10^{50}$ erg has a particularly low value, similar to the other GRBs associated with SNe. For the first time, we observe a baryon loading $B = 10^{-2}$ which coincides with the upper limit for the dynamical stability of the fireshell. The effective CircumBurst Medium (CBM) density shows a radial dependence $n_{cbm} \propto r^{-\alpha}$ with $1.0 \lesssim \alpha \lesssim 1.7$ and monotonically decreases from 1 to 10^{-6} particles/cm³. This behavior is interpreted as being due to a fragmentation in the fireshell. Analogies with the fragmented density and filling factor characterizing Novae are outlined. The fit presented is particularly significant in view of the complete data set available for GRB060218 and of the fact that it fulfills the Amati relation.

Conclusions: We fit GRB060218, usually considered as an X-Ray Flash (XRF), as a “canonical GRB” within our theoretical model. The smallest possible black hole, formed by the gravitational collapse of a neutron star in a binary system, is consistent with the especially low energetics of the class of GRBs associated with SNe Ib/c. We provide the first evidence for a fragmentation in the fireshell. This fragmentation is crucial in explaining both the unusually large T_{90} and the consequently inferred abnormally low value of the CBM effective

density.

10. M.G. Bernardini, C.L. Bianco, L. Caito, M.G. Dainotti, R. Guida, R. Ruffini; “GRB970228 and a class of GRBs with an initial spikelike emission”; *Astronomy & Astrophysics*, 474, L13 (2007).

Context: The discovery by *Swift* and HETE-2 of an afterglow emission associated possibly with short GRBs opened the new problematic of their nature and classification. This issue has been further enhanced by the observation of GRB060614 and by a new analysis of the BATSE catalog which led to the identification of a new class of GRBs with “an occasional softer extended emission lasting tenths of seconds after an initial spikelike emission”.

Aims: We plan a twofold task: a) to fit this new class of “hybrid” sources within our “canonical GRB” scenario, where all GRBs are generated by a “common engine” (i.e. the gravitational collapse to a black hole); b) to propose GRB970228 as the prototype of the above mentioned class, since it shares the same morphology and observational features.

Methods: We analyze *BeppoSAX* data on GRB970228 within the “fireshell” model and we determine the parameters describing the source and the CircumBurst Medium (CBM) needed to reproduce its light curves in the 40–700 keV and 2–26 keV energy bands.

Results: We find that GRB970228 is a “canonical GRB”, like e.g. GRB050315, with the main peculiarity of a particularly low average density of the CBM $\langle n_{cbm} \rangle \sim 10^{-3}$ particles/cm³. We also simulate the light curve corresponding to a rescaled CBM density profile with $\langle n_{cbm} \rangle = 1$ particle/cm³. From such a comparison it follows that the total time-integrated luminosity is a faithful indicator of the nature of GRBs, contrary to the peak luminosity which is merely a function of the CBM density.

Conclusions: We call attention on discriminating the short GRBs between the “genuine” and the “fake” ones. The “genuine” ones are intrinsically short, with baryon loading $B \lesssim 10^{-5}$, as stated in our original classification. The “fake” ones, characterized by an initial spikelike emission followed by an extended emission lasting tenths of seconds, have a baryon loading $10^{-4} \lesssim B \leq 10^{-2}$. They are observed as such only due to an underdense CBM consistent with a galactic halo environment which deflates the afterglow intensity.

11. R. Guida, M.G. Bernardini, C.L. Bianco, L. Caito, M.G. Dainotti, R. Ruffini; “The Amati relation in the “fireshell” model”; *Astronomy & Astrophysics*, 487, L37 (2008).

Context: The cosmological origin of gamma-ray bursts (GRBs) has been firmly established, with redshifts up to $z = 6.29$. They are possible candidates for use as “distance indicators” for testing cosmological models in a redshift range hardly achievable by other cosmological probes. Asserting the validity of the empirical relations among GRB observables is now crucial for their calibration.

Aims: Motivated by the relation proposed by Amati and collaborators, we look within the “fireshell” model for a relation between the peak energy E_p of the νF_ν total time-integrated spectrum of the afterglow and the total energy of the afterglow E_{aft} , which in our model encompasses and extends the prompt emission.

Methods: The fit within the fireshell model, as for the “canonical” GRB050315, uses the complete arrival time coverage given by the Swift satellite. It is performed simultaneously, self-consistently, and recursively in the four BAT energy bands (15–25 keV, 25–50 keV, 50–100 keV, and 100–150 keV), as well as in the XRT one (0.2–10 keV). It uniquely determines the two free parameters characterizing the GRB source, the total energy $E_{tot}^{e^\pm}$ of the e^\pm plasma and its baryon loading B , as well as the effective CircumBurst Medium (CBM) distribution. We can then build two sets of “gedanken” GRBs varying the total energy of the electron-positron plasma $E_{tot}^{e^\pm}$ and keeping the same baryon loading B of GRB050315. The first set assumes the one obtained in the fit of GRB050315 for the effective CBM density. The second set assumes instead a constant CBM density equal to the average value of the GRB050315 prompt phase.

Results: For the first set of “gedanken” GRBs we find a relation $E_p \propto (E_{aft})^a$, with $a = 0.45 \pm 0.01$, whose slope strictly agrees with the Amati one. Such a relation, in the limit $B \rightarrow 10^{-2}$, coincides with the Amati one. Instead, no correlation is found in the second set of “gedanken” GRBs.

Conclusions: Our analysis excludes the proper GRB (P-GRB) from the prompt emission, extends all the way to the latest afterglow phases, and is independent of the assumed cosmological model, since all “gedanken” GRBs are at the same redshift. The Amati relation, on the other hand, includes the P-GRB, focuses only on the prompt emission, being therefore influenced by the instrumental threshold that fixes the end of the prompt emission, and depends on the assumed cosmology. This might explain the intrinsic scatter observed in the Amati relation.

12. L. Caito, M.G. Bernardini, C.L. Bianco, M.G. Dainotti, R. Guida, R. Ruffini; “GRB060614: a “fake” short GRB from a merging binary system”; *Astronomy & Astrophysics*, 489, 501 (2009).

Context: GRB060614 observations by VLT and by Swift have infringed the traditionally accepted gamma-ray burst (GRB) collapsar scenario that purports the origin of all long duration GRBs from supernovae (SN). GRB060614 is the first nearby long duration GRB clearly not associated with a bright Ib/c SN. Moreover, its duration ($T_{90} \sim 100$ s) makes it hardly classifiable as a short GRB. It presents strong similarities with GRB970228, the prototype of a new class of “fake” short GRBs that appear to originate from the coalescence of binary neutron stars or white dwarfs spiraled out into the galactic halo. *Aims:* Within the “canonical” GRB scenario based on the “fireshell” model, we test if GRB060614 can be a “fake” or “disguised” short GRB. We model the traditionally termed “prompt emission” and discriminate the signal originating from the gravitational collapse leading to the GRB from the process occurring in the circumburst medium (CBM). *Methods:* We fit GRB060614 light curves in Swift’s BAT (15 – 150 keV) and XRT (0.2 – 10 keV) energy bands. Within the fireshell model, light curves are formed by two well defined and different components: the proper-GRB (P-GRB), emitted when the fireshell becomes transparent, and the extended afterglow, due to the interaction between the leftover accelerated baryonic and leptonic shell and the CBM. *Results:* We determine the two free parameters describing the GRB source within the fireshell model: the total e^\pm plasma energy ($E_{tot}^{e^\pm} = 2.94 \times 10^{51}$ erg) and baryon loading ($B = 2.8 \times 10^{-3}$). A small average CBM density $\sim 10^{-3}$ particles/cm³ is inferred, typical of galactic halos. The first spikelike emission is identified with the P-GRB and the following prolonged emission with the extended afterglow peak. We obtain very good agreement in the BAT (15 – 150 keV) energy band, in what is traditionally called “prompt emission”, and in the XRT (0.2 – 10 keV) one. *Conclusions:* The *anomalous* GRB060614 finds a natural interpretation within our canonical GRB scenario: it is a “disguised” short GRB. The total time-integrated extended afterglow luminosity is greater than the P-GRB one, but its peak luminosity is smaller since it is deflated by the peculiarly low average CBM density of galactic halos. This result points to an old binary system, likely formed by a white dwarf and a neutron star, as the progenitor of GRB060614 and well justifies the absence of an associated SN Ib/c. Particularly important for further studies of the final merging process are the temporal structures in the P-GRB down to 0.1 s.

13. M.G. Bernardini, C.L. Bianco, L. Caito, M.G. Dainotti, R. Guida, R. Ruffini; “GRB970228 in the “canonical GRB” scenario”; *Journal of the Korean Physical Society*, 56, 1575 (2010).

Within the “fireshell” model, we define a “canonical GRB” light curve with two sharply different components: the proper-GRB (P-GRB), emitted when the optically thick fireshell of an electron-positron plasma originating from the phenomenon reaches transparency, and the afterglow, emitted due to the collision between the remaining optically thin fireshell and the circumburst medium (CBM). On the basis of the recent understanding of GRB970228 as the prototype for a new class of GRBs with “an occasional softer extended emission lasting tenths of seconds after an initial spikelike emission”, we outline our “canonical GRB” scenario, originating from the gravitational collapse to a black hole, with special emphasis on the discrimination between “genuine” and “fake” short GRBs. Furthermore, we investigate how the GRB970228 analysis provides a theoretical explanation for the apparent absence of such a correlation for the GRBs belonging to this new class.

14. L. Caito, M.G. Bernardini, C.L. Bianco, M.G. Dainotti, R. Guida, R. Ruffini; “GRB060614: a preliminary result”; *Journal of the Korean Physical Society*, 56, 1579 (2010).

The explosion of GRB 060614 produced a deep break in the GRB scenario and opened new horizons of investigation because it can’t be traced back to any traditional scheme of classification. In fact, it manifests peculiarities both of long bursts and of short bursts, and above all, it is the first case of a long-duration near GRB without any bright Ib/c associated Supernova. We will show that, in our canonical GRB scenario, this “anomalous” situation finds a natural interpretation and allows us to discuss a possible variation in the traditional classification scheme, introducing a distinction between “genuine” and “fake” short bursts.

15. M.G. Dainotti, M.G. Bernardini, C.L. Bianco, L. Caito, R. Guida, R. Ruffini; “The astrophysical tryptic: GRB, SN and URCA can be extended to GRB060218?”; *Journal of the Korean Physical Society*, 56, 1588 (2010).

The *Swift* satellite has given continuous data in the range 0.3–150 keV from 0 s to 10^6 s for GRB060218 associated with SN2006aj. This GRB is the fourth GRB spectroscopically associated with SNe after the cases of GRB980425-SN1998bw, GRB031203-SN2003lw, GRB 030329-SN2003dh. It has an unusually long duration ($T_{90} \sim 2100$ s). These data offer the opportunity to probe theoretical models for Gamma-Ray Bursts (GRBs) connected with Supernovae (SNe). We plan to fit the complete γ - and X-ray light curves of this long duration GRB,

including the prompt emission, in order to clarify the nature of the progenitors and the astrophysical scenario of the class of GRBs associated to SNe Ib/c. We apply our “fireshell” model based on the formation of a black hole, giving the relevant references. The initial total energy of the electron-positron plasma $E_{e^\pm}^{tot} = 2.32 \times 10^{50}$ erg has a particularly low value similarly to the other GRBs associated with SNe. For the first time we observe a baryon loading $B = 10^{-2}$ which coincides with the upper limit for the dynamical stability of the fireshell. The effective CircumBurst Medium (CBM) density shows a radial dependence $n_{cbm} \propto r^{-\alpha}$ with $1.0 \lesssim \alpha \lesssim 1.7$ and monotonically decreases from 1 to 10^{-6} particles/cm³. Such a behavior is interpreted as due to a fragmentation in the fireshell. Such a fragmentation is crucial in explaining both the unusually large T_{90} and the consequently inferred abnormal low value of the CBM effective density. We fit GRB060218, usually considered as an X-Ray Flash (XRF), as a “canonical GRB” within our theoretical model. The smallest possible black hole, formed by the gravitational collapse of a neutron star in a binary system, is consistent with the especially low energetics of the class of GRBs associated with SNe Ib/c. We present the URCA process and the connection between the GRBs associated with SNe extended also to the case of GRB060218.

16. L. Izzo, M.G. Bernardini, C.L. Bianco, L. Caito, B. Patricelli, R. Ruffini; “GRB 090423 at Redshift 8.1: a Theoretical Interpretation”; *Journal of the Korean Physical Society*, 57, 551 (2010).

GRB 090423 is the farthest gamma ray burst ever observed, with a redshift of about 8.1. We present within the fireshell scenario a complete analysis of this GRB. We model the prompt emission and the first rapid flux decay of the afterglow emission as being to the canonical emission of the interaction in the interval $0 \leq t \leq 440$ s by using accelerated baryonic matter with the circumburst medium. After the data reduction of the Swift data in the BAT (15 - 150 keV) and XRT (0.2 - 10 keV) energy bands, we interpret the light curves and the spectral distribution in the context of the fireshell scenario. We also confirm in this source the existence of a second component, a plateau phase, as being responsible for the late emission in the X-ray light curve. This extra component originates from the fact that the ejecta have a range of the bulk Lorentz Γ factor, which starts to interact each other ejecta at the start of the plateau phase.

17. L. Caito, L. Amati, M.G. Bernardini, C.L. Bianco, G. De Barros, L. Izzo, B. Patricelli, R. Ruffini; “GRB 071227: an additional case of a disguised

short burst”; *Astronomy & Astrophysics*, 521, A80 (2010).

Context: Observations of gamma-ray bursts (GRBs) have shown an hybridization between the two classes of long and short bursts. In the context of the fireshell model, the GRB light curves are formed by two different components: the *proper* GRB (P-GRB) and the extended afterglow. Their relative intensity is linked to the fireshell baryon loading B . The GRBs with P-GRB predominance are the short ones, the remainders are long. A new family of *disguised* short bursts has been identified: long bursts with a protracted low instantaneous luminosity due to a low density CircumBurst Medium (CBM). In the 15–150 keV energy band GRB 071227 exhibits a short duration (about 1.8s) spike-like emission followed by a very soft extended tail up to one hundred seconds after the trigger. It is a faint ($E_{iso} = 5.8 \times 10^{50}$) nearby GRB ($z = 0.383$) that does not have an associated type Ib/c bright supernova (SN). For these reasons, GRB 071227 has been classified as a short burst not fulfilling the Amati relation holding for long burst. *Aims:* We check the classification of GRB 071227 provided by the fireshell model. In particular, we test whether this burst is another example of a *disguised* short burst, after GRB 970228 and GRB 060614, and, for this reason, whether it fulfills the Amati relation. *Methods:* We simulate GRB 071227 light curves in the *Swift* BAT 15–50 keV bandpass and in the XRT (0.3–10 keV) energy band within the fireshell model. *Results:* We perform simulations of the tail in the 15–50 keV bandpass, as well as of the first part of the X-ray afterglow. This infers that: $E_{tot}^{e^{\pm}} = 5.04 \times 10^{51}$ erg, $B = 2.0 \times 10^{-4}$, $E_{P-GRB}/E_{aft} \sim 0.25$, and $\langle n_{cbm} \rangle = 3.33$ particles/cm³. These values are consistent with those of “long duration” GRBs. We interpret the observed energy of the first hard emission by identifying it with the P-GRB emission. The remaining long soft tail indeed fulfills the Amati relation. *Conclusions:* Previously classified as a short burst, GRB 071227 on the basis of our analysis performed in the context of the fireshell scenario represents another example of a *disguised* short burst, after GRB 970228 and GRB 060614. Further confirmation of this result is that the soft tail of GRB 071227 fulfills the Amati relation.

18. M.G. Bernardini, C.L. Bianco, L. Caito, L. Izzo, B. Patricelli, R. Ruffini; “Analysis of GRB060607A within the fireshell model: prompt emission, X-ray flares and late afterglow phase”; *Astronomy & Astrophysics*, submitted to.

Context: GRB060607A is a very distant ($z = 3.082$) and energetic event ($E_{iso} \sim 10^{53}$ erg). Its main peculiarity is that the peak of the near-infrared (NIR) af-

terglow has been observed with the REM robotic telescope. This NIR peak has been interpreted as the afterglow onset within the fireball forward shock model, and the initial Lorentz gamma factor of the emitting system has been inferred. *Aims:* We analyze GRB060607A within the fireshell model. We emphasize the central role of the prompt emission in determining the initial Lorentz gamma factor of the extended afterglow and we interpret the X-ray flares as produced by the interaction of the optically thin fireshell with overdense CircumBurst Medium (CBM) clumps. *Methods:* We deal only with the Swift BAT and XRT observations, that are the basic contribution to the GRB emission and that are neglected in the treatment adopted in the current literature. The numerical modeling of the fireshell dynamics allows to calculate all its characteristic quantities, in particular the exact value of the Lorentz gamma factor at the transparency. *Results:* We show that the theoretically computed prompt emission light curves are in good agreement with the observations in all the *Swift* BAT energy bands as well as the spectra integrated over different time intervals. The flares observed in the decaying phase of the X-ray afterglow are also reproduced by the same mechanism, but in a region in which the typical dimensions of the clumps are smaller than the visible area of the fireshell and most energy lies in the X-ray band due to the hard-to-soft evolution. *Conclusions:* We show that it is possible to obtain flares with $\Delta t/t$ compatible with the observations when the three-dimensional structure of the CBM clumps is duly taken into account. We stop our analysis at the beginning of the X-ray plateau phase, since we suppose this originates from the instabilities developed in the collision between different subshells within a structured fireshell.

19. G. de Barros, M. G. Bernardini, C.L. Bianco, L. Caito, L. Izzo, B. Patricelli, R. Ruffini; "On the nature of GRB 050509b: a disguised short GRB"; *Astronomy & Astrophysics*, 529, A130 (2011)

Context: GRB 050509b, detected by the *Swift* satellite, is the first case where an X-ray afterglow has been observed associated with a short gamma-ray burst (GRB). Within the fireshell model, the canonical GRB light curve presents two different components: the proper-GRB (P-GRB) and the extended afterglow. Their relative intensity is a function of the fireshell baryon loading parameter B and of the CircumBurst Medium (CBM) density (n_{CBM}). In particular, the traditionally called short GRBs can be either "genuine" short GRBs (with $B \lesssim 10^{-5}$, where the P-GRB is energetically predominant) or "disguised" short GRBs (with $B \gtrsim 3.0 \times 10^{-4}$ and $n_{CBM} \ll 1$, where the extended afterglow is energetically predominant). *Aims:* We verify whether GRB 050509b can be clas-

sified as a “genuine” short or a “disguised” short GRB, in the fireshell model. *Methods:* We investigate two alternative scenarios. In the first, we start from the assumption that this GRB is a “genuine” short burst. In the second attempt, we assume that this GRB is a “disguised” burst. *Results:* If GRB 050509b were a genuine short GRB, there should initially be very hard emission which is ruled out by the observations. The analysis that assumes that this is a disguised short GRB is compatible with the observations. The theoretical model predicts a value of the extended afterglow energy peak that is consistent with the Amati relation. *Conclusions:* GRB 050509b cannot be classified as a “genuine” short GRB. The observational data are consistent with a “disguised” short GRB classification, i.e., a long burst with a weak extended afterglow “deflated” by the low density of the CBM. We expect that all short GRBs with measured redshifts are disguised short GRBs because of a selection effect: if there is enough energy in the afterglow to measure the redshift, then the proper GRB must be less energetic than the afterglow. The Amati relation is found to be fulfilled only by the extended afterglow excluding the P-GRB.

20. L. Caito, M.G. Bernardini, C.L. Bianco, L. Izzo, B. Patricelli, R. Ruffini; “GRB 071227: another disguised short burst”; *International Journal of Modern Physics D*, 20, 1931 (2011).

Observations of Gamma-ray Bursts (GRBs) put forward in the recent years have revealed, with increasing evidence, that the historical classification between long and short bursts has to be revised. Within the Fireshell scenario, both short and long bursts are canonical bursts, consisting of two different phases. First, a Proper-GRB (P-GRB), that is the emission of photons at the transparency of the fireshell. Then, the Extended Afterglow, multiwavelength emission due to the interaction of the baryonic remnants of the fireshell with the CircumBurst Medium (CBM). We discriminate between long and short bursts by the amount of energy stored in the first phase with respect to the second one. Within the Fireshell scenario, we have introduced a third intermediate class: the disguised GRBs. They appear like short bursts, because their morphology is characterized by a first, short, hard episode and a following deflated tail, but this last part — coincident with the peak of the afterglow — is energetically predominant. The origin of this peculiar kind of sources is inferred to a very low average density of the environment (of the order of 10^{-3}). After GRB 970228 and GRB 060614, we find in GRB 071227 a third example of disguised burst.

21. L. Izzo, M.G. Bernardini, C.L. Bianco, L. Caito, B. Patricelli, L.J. Rangel Lemos, R. Ruffini; “GRB 080916C and the high-energy emission in the fireshell scenario”; *International Journal of Modern Physics D*, 20, 1949 (2011).

In this paper we discuss a possible explanation for the high energy emission (up to \sim GeV) seen in GRB 080916C. We propose that the GeV emission is originated by the collision between relativistic baryons in the fireshell after the transparency and the nucleons located in molecular clouds near the burst site. This collision should give rise pion production, whose immediate decay provides high energy photons, neutrinos and leptons. Using a public code (SYBILL) we simulate these relativistic collisions in their simple form, so that we can draw our preliminar results in this paper. We will present moreover our hypothesis that the delayed onset of this emission identifies in a complete way the P-GRB emission.

22. B. Patricelli, M.G. Bernardini, C.L. Bianco, L. Caito, L. Izzo, R. Ruffini, G. Vereshchagin; “A new spectral energy distribution of photons in the fireshell model of GRBs”; *International Journal of Modern Physics D*, 20, 1983 (2011).

The analysis of various Gamma-Ray Bursts (GRBs) having a low energetics (an isotropic energy $E_{iso} \lesssim 10^{53}$ ergs) within the fireshell model has shown how the $N(E)$ spectrum of their prompt emission can be reproduced in a satisfactory way by a convolution of thermal spectra. Nevertheless, from the study of very energetic bursts ($E_{iso} \lesssim 10^{54}$ ergs) such as, for example, GRB 080319B, some discrepancies between the numerical simulations and the observational data have been observed. We investigate a different spectrum of photons in the comoving frame of the fireshell in order to better reproduce the spectral properties of GRB prompt emission within the fireshell model. We introduce a phenomenologically modified thermal spectrum: a thermal spectrum characterized by a different asymptotic power-law index in the low energy region. Such an index depends on a free parameter α , so that the pure thermal spectrum corresponds to the case $\alpha = 0$. We test this spectrum by comparing the numerical simulations with the observed prompt emission spectra of various GRBs. From this analysis it has emerged that the observational data can be correctly reproduced by assuming a modified thermal spectrum with $\alpha = -1.8$.

23. A.V. Penacchioni, R. Ruffini, L. Izzo, M. Muccino, C.L. Bianco, L. Caito, B. Patricelli, L. Amati; “Evidence for a proto-black hole and a double

astrophysical component in GRB 101023"; *Astronomy & Astrophysics*, 538, A58 (2012).

Context: It has been recently shown that GRB 090618, observed by AGILE, Coronas Photon, Fermi, Konus, Suzaku and Swift, is composed of two very different components: episode 1, lasting 50 s, shows a thermal plus power-law spectrum with a characteristic temperature evolving in time as a power law; episode 2 (the remaining 100 s) is a canonical long GRB. We have associated episode 1 to the progenitor of a collapsing bare core leading to the formation of a black hole: what was defined as a "proto black hole". *Aims:* In precise analogy with GRB 090618 we aim to analyze the 89s of the emission of GRB 101023, observed by Fermi, Gemini, Konus and Swift, to see if there are two different episodes: the first one presenting a characteristic black-body temperature evolving in time as a broken power law, and the second one consistent with a canonical GRB. *Methods:* To obtain information on the spectra, we analyzed the data provided by the GBM detector onboard the Fermi satellite, and we used the heasoft package XSPEC and RMFIT to obtain their spectral distribution. We also used the numerical code GRBsim to simulate the emission in the context of the fireshell scenario for episode 2. *Results:* We confirm that the first episode can be well fit by a black body plus power-law spectral model. The temperature changes with time following a broken power law, and the photon index of the power-law component presents a soft-to-hard evolution. We estimate that the radius of this source increases with time with a velocity of $1.5 \times 10^4 km/s$. The second episode appears to be a canonical GRB. By using the Amati and the Atteia relations, we determined the cosmological redshift, $z \sim 0.9 \pm 0.084(stat.) \pm 0.2(sys.)$. The results of GRB 090618 are compared and contrasted with the results of GRB 101023. Particularly striking is the scaling law of the soft X-ray component of the afterglow. *Conclusions:* We identify GRB 090618 and GRB 101023 with a new family of GRBs related to a single core collapse and presenting two astrophysical components: a first one related to the proto-black hole prior to the process of gravitational collapse (episode 1), and a second one, which is the canonical GRB (episode 2) emitted during the formation of the black hole. For the first time we are witnessing the process of a black hole formation from the instants preceding the gravitational collapse up to the GRB emission. This analysis indicates progress towards developing a GRB distance indicator based on understanding the P-GRB and the prompt emission, as well as the soft X-ray behavior of the late afterglow.

24. R. Negreiros, R. Ruffini, C. L. Bianco, J. A. Rueda; "Cooling of young

neutron stars in GRB associated to supernovae"; *Astronomy & Astrophysics*, 540, A12 (2012).

Context: The traditional study of neutron star cooling has been generally applied to quite old objects such as the Crab Pulsar (957 years) or the central compact object in Cassiopeia A (330 years) with an observed surface temperature $\sim 10^6$ K. However, recent observations of the late ($t = 10^8$ – 10^9 s) emission of the supernovae (SNe) associated to GRBs (GRB-SN) show a distinctive emission in the X-ray regime consistent with temperatures $\sim 10^7$ – 10^8 K. Similar features have been also observed in two Type Ic SNe SN 2002ap and SN 1994I that are not associated to GRBs. *Aims:* We advance the possibility that the late X-ray emission observed in GRB-SN and in isolated SN is associated to a hot neutron star just formed in the SN event, here defined as a neo-neutron star. *Methods:* We discuss the thermal evolution of neo-neutron stars in the age regime that spans from ~ 1 minute (just after the proto-neutron star phase) all the way up to ages < 10 – 100 yr. We examine critically the key factor governing the neo-neutron star cooling with special emphasis on the neutrino emission. We introduce a phenomenological heating source, as well as new boundary conditions, in order to mimic the high temperature of the atmosphere for young neutron stars. In this way we match the neo-neutron star luminosity to the observed late X-ray emission of the GRB-SN events: URCA-1 in GRB980425-SN1998bw, URCA-2 in GRB030329-SN2003dh, and URCA-3 in GRB031203-SN2003lw. *Results:* We identify the major role played by the neutrino emissivity in the thermal evolution of neo-neutron stars. By calibrating our additional heating source at early times to $\sim 10^{12}$ – 10^{15} erg/g/s, we find a striking agreement of the luminosity obtained from the cooling of a neo-neutron stars with the prolonged ($t = 10^8$ – 10^9 s) X-ray emission observed in GRB associated with SN. It is therefore appropriate a revision of the boundary conditions usually used in the thermal cooling theory of neutron stars, to match the proper conditions of the atmosphere at young ages. The traditional thermal processes taking place in the crust might be enhanced by the extreme high-temperature conditions of a neo-neutron star. Additional heating processes that are still not studied within this context, such as e^+e^- pair creation by overcritical fields, nuclear fusion, and fission energy release, might also take place under such conditions and deserve further analysis. *Conclusions:* Observation of GRB-SN has shown the possibility of witnessing the thermal evolution of neo-neutron stars. A new campaign of dedicated observations is recommended both of GRB-SN and of isolated Type Ic SN.

25. L. Izzo, R. Ruffini, A.V. Penacchioni, C.L. Bianco, L. Caito, S.K. Chakrabarti, J.A. Rueda, A. Nandi, B. Patricelli; “A double component in GRB 090618: a proto-black hole and a genuinely long gamma-ray burst”; *Astronomy & Astrophysics*, 543, A10 (2012).

Context: The joint X-ray and gamma-ray observations of GRB 090618 by very many satellites offer an unprecedented possibility of testing crucial aspects of theoretical models. In particular, they allow us to test (a) in the process of gravitational collapse, the formation of an optically thick e^+e^- -baryon plasma self-accelerating to Lorentz factors in the range $200 < \Gamma < 3000$; (b) its transparency condition with the emission of a component of 10^{53-54} baryons in the TeV region and (c) the collision of these baryons with the circumburst medium (CBM) clouds, characterized by dimensions of 10^{15-16} cm. In addition, these observations offer the possibility of testing a new understanding of the thermal and power-law components in the early phase of this GRB. *Aims:* We test the fireshell model of GRBs in one of the closest ($z = 0.54$) and most energetic ($E_{iso} = 2.90 \times 10^{53}$ erg) GRBs, namely GRB 090618. It was observed at ideal conditions by several satellites, namely *Fermi*, *Swift*, *Konus-WIND*, *AGILE*, *RT-2*, and *Suzaku*, as well as from on-ground optical observatories. *Methods:* We analyzed the emission from GRB 090618 using several spectral models, with special attention to the thermal and power-law components. We determined the fundamental parameters of a canonical GRB within the context of the fireshell model, including the identification of the total energy of the e^+e^- plasma, $E_{tot}^{e^+e^-}$, the proper GRB (P-GRB), the baryon load, the density and structure of the CBM. *Results:* We find evidence of the existence of two different episodes in GRB 090618. The first episode lasts 50 s and is characterized by a spectrum consisting of a thermal component, which evolves between $kT = 54$ keV and $kT = 12$ keV, and a power law with an average index $\gamma = 1.75 \pm 0.04$. The second episode, which lasts for ~ 100 s, behaves as a canonical long GRB with a Lorentz gamma factor at transparency of $\Gamma = 495$, a temperature at transparency of 29.22 keV and with a characteristic size of the surrounding clouds of $R_{cl} \sim 10^{15-16}$ cm and masses of $\sim 10^{22-24}$ g. *Conclusions:* We support the recently proposed two-component nature of GRB 090618, namely, episode 1 and episode 2, with a specific theoretical analysis. We furthermore illustrate that episode 1 cannot be considered to be either a GRB or a part of a GRB event, but it appears to be related to the progenitor of the collapsing bare core, leading to the formation of the black hole, which we call a “proto-black hole”. Thus, for the first time, we are witnessing the process of formation of a black

hole from the phases just preceding the gravitational collapse all the way up to the GRB emission.

26. B. Patricelli, M.G. Bernardini, C.L. Bianco, L. Caito, G. De Barros, L. Izzo, R. Ruffini, G.V. Vereshchagin; “Analysis of GRB 080319B and GRB 050904 within the Fireshell Model: Evidence for a Broader Spectral Energy Distribution”; *The Astrophysical Journal*, 756, 16 (2012).

The observation of GRB 080319B, with an isotropic energy $E_{iso} = 1.32 \times 10^{54}$ erg, and GRB 050904, with $E_{iso} = 1.04 \times 10^{54}$ erg, offers the possibility of studying the spectral properties of the prompt radiation of two of the most energetic Gamma Ray Bursts (GRBs). This allows us to probe the validity of the fireshell model for GRBs beyond 10^{54} erg, well outside the energy range where it has been successfully tested up to now (10^{49} – 10^{53} erg). We find that in the low energy region, the prompt emission spectra observed by *Swift* BAT reveals more power than theoretically predicted. The opportunities offered by these observations to improve the fireshell model are outlined in this paper. One of the distinguishing features of the fireshell model is that it relates the observed GRB spectra to the spectrum in the comoving frame of the fireshell. Originally, a fully radiative condition and a comoving thermal spectrum were adopted. An additional power-law in the comoving thermal spectrum is required due to the discrepancy of the theoretical and observed light curves and spectra in the fireshell model for GRBs 080319B and 050904. A new phenomenological parameter α is correspondingly introduced in the model. We perform numerical simulations of the prompt emission in the *Swift* BAT bandpass by assuming different values of α within the fireshell model. We compare them with the GRB 080319B and GRB 050904 observed time-resolved spectra, as well as with their time-integrated spectra and light curves. Although GRB 080319B and GRB 050904 are at very different redshifts ($z=0.937$ and $z=6.29$ respectively), a value of $\alpha = -1.8$ leads for both of them to a good agreement between the numerical simulations and the observed BAT light curves, time-resolved and time-integrated spectra. Such a modified spectrum is also consistent with the observations of previously analyzed less energetic GRBs and reasons for this additional agreement are given. Perspectives for future low energy missions are outlined.

27. M. Muccino, R. Ruffini, C.L. Bianco, L. Izzo, A.V. Penacchioni; “GRB 090227B: The missing link between the genuine short and long GRBs”; *The Astrophysical Journal*, 763, 125 (2013).

The time-resolved spectral analysis of GRB 090227B, made possible by the *Fermi*-GBM data, allows to identify in this source the missing link between the genuine short and long GRBs. Within the Fireshell model of the Gamma-Ray Bursts (GRBs) we predict genuine short GRBs: bursts with the same inner engine of the long bursts but endowed with a severely low value of the Baryon load, $B \lesssim 5 \times 10^{-5}$. A first energetically predominant emission occurs at the transparency of the e^+e^- plasma, the Proper-GRB (P-GRB), followed by a softer emission, the extended afterglow. The typical separation between the two emissions is expected to be of the order of $10^{-3} - 10^{-2}$ s. We identify the P-GRB of GRB 090227B in the first 96 ms of emission, where a thermal component with the temperature $kT = (517 \pm 28)$ keV and a flux comparable with the non thermal part of the spectrum is observed. This non thermal component as well as the subsequent emission, where there is no evidence for a thermal spectrum, is identified with the extended afterglow. We deduce a theoretical cosmological redshift $z = 1.61 \pm 0.14$. We then derive the total energy $E_{e^+e^-}^{tot} = (2.83 \pm 0.15) \times 10^{53}$ ergs, the Baryon load $B = (4.13 \pm 0.05) \times 10^{-5}$, the Lorentz Γ factor at transparency $\Gamma_{tr} = (1.44 \pm 0.01) \times 10^4$, and the intrinsic duration $\Delta t' \sim 0.35$ s. We also determine the average density of the CircumBurst Medium (CBM), $\langle n_{CBM} \rangle = (1.90 \pm 0.20) \times 10^{-5}$ particles/cm³. There is no evidence of beaming in the system. In view of the energetics and of the Baryon load of the source, as well as of the low interstellar medium and of the intrinsic time scale of the signal, we identify the GRB progenitor as a binary neutron star. From the recent progress in the theory of neutron stars, we obtain masses of the stars $m_1 = m_2 = 1.34M_\odot$ and their corresponding radii $R_1 = R_2 = 12.24$ km and thickness of their crusts ~ 0.47 km, consistent with the above values of the Baryon load, of the energetics and of the time duration of the event.

28. A.V. Penacchioni, R. Ruffini, C.L. Bianco, L. Izzo, M. Muccino, G.B. Pisani, J.A. Rueda; “GRB 110709B in the induced gravitational collapse paradigm”; *Astronomy & Astrophysics*, 551, A133 (2013).

Context: GRB 110709B is the first source for which *Swift* BAT triggered twice, with a time separation of ~ 10 minutes. The first emission (called here Episode 1) goes from 40 s before the first trigger up to 60 s after it. The second emission (hereafter Episode 2) goes from 35 s before the second trigger to 100 s after it. These features reproduce the ones of GRB 090618, which has been recently interpreted within the Induced Gravitational Collapse paradigm (IGC). In line with this paradigm we assume the progenitor to be a close binary system composed of a core of an evolved star and a Neutron Star (NS). The evolved star

explodes as a Supernova (SN) and ejects material that is partially accreted by the NS. We identify this process with Episode 1. The accretion process brings the NS over its critical mass, thus gravitationally collapsing to a BH. This process leads to the GRB emission, Episode 2. The double trigger has given for the first time the possibility to have a coverage of the X-ray emission observed by XRT both prior to and during the prompt phase of GRB 110709B. *Aims:* We analyze the spectra and time variability of Episode 1 and 2 and compute the relevant parameters of the binary progenitor, as well as the astrophysical parameters both in the SN and the GRB phase in the IGC paradigm. *Methods:* We perform a time-resolved spectral analysis of Episode 1 by fitting the spectrum with a blackbody (BB) plus a power-law (PL) spectral model. From the BB fluxes and temperatures of Episode 1 and the luminosity distance d_L , we evaluate the evolution with time of the radius of the BB emitter, associated here to the evolution of the SN ejecta. We analyze Episode 2 within the Fireshell model, identifying the Proper-GRB (P-GRB) and simulating the light curve and spectrum. We establish the redshift to be $z = 0.75$, following the phenomenological methods by Amati, by Yonetoku and by Grupe, and our analysis of the late X-ray afterglow. It is most remarkable that the determination of the cosmological redshift on the ground of the scaling of the late X-ray afterglow, already verified in GRB 090618 and GRB 101023, is again verified by this analysis. *Results:* We find for Episode 1 a temperature of the BB component that evolves with time following a broken PL, with the slope of the PL at early times $\alpha = 0$ (constant function) and the slope of the PL at late times $\beta = -4 \pm 2$. The break occurs at $t = 41.21$ s. The total energy of Episode 1 is $E_{iso}^{(1)} = 1.42 \times 10^{53}$ erg. The total energy of Episode 2 is $E_{iso}^{(2)} = 2.43 \times 10^{52}$ erg. We find at transparency a Lorentz factor $\Gamma \sim 1.73 \times 10^2$, laboratory radius of 6.04×10^{13} cm, P-GRB observed temperature $kT_{P-GRB} = 12.36$ keV, baryon load $B = 5.7 \times 10^{-3}$ and P-GRB energy of $E_{P-GRB} = 3.44 \times 10^{50}$ erg. We find a remarkable coincidence of the cosmological redshift by the scaling of the XRT data and with three other phenomenological methods. *Conclusions:* We interpret GRB 110709B as a member of the IGC sources, together with GRB 970828, GRB 090618 and GRB 101023. The existence of the XRT data during the prompt phase of the emission of GRB 110709B (Episode 2) offers an unprecedented tool for improving the diagnostic of GRBs emission.

29. G.B. Pisani, L. Izzo, R. Ruffini, C.L. Bianco, M. Muccino, A.V. Penacchioni, J.A. Rueda, Y. Wang; “Novel distance indicator for gamma-ray bursts associated with supernovae”; *Astronomy & Astrophysics*, 552,

L5 (2013).

Context: In recent years it has been proposed that the temporal coincidence of a Gamma Ray Burst (GRB) and a type Ib/c supernova (SN) can be explained by the concept of Induced Gravitational Collapse (IGC) of a Neutron Star (NS) to a Black Hole (BH) by accretion of matter ejected by a SN Ib/c. This scenario reveals a possible common behavior in the late time X-ray emission of this subclass of GRBs. *Aims:* We want to test if such a common behavior can actually be present in the sources belonging to this GRB sub-class and if this may lead to a redshift estimator for these sources. *Methods:* We build a sample of GRBs belonging to this sub-class, and we rescale the X-ray light curves of all of them both in time and in flux to a common cosmological redshift. *Results:* We found that the X-ray light curves of all the GRBs of the sample with a measured redshift present a common late time behavior when rescaled to a common redshift $z = 1$. We then use this result to estimate the redshift of the GRBs of the sample with no measured redshift. *Conclusions:* The common behavior in the late decay of the X-ray light curves of the GRBs of the sample points to a common physical mechanism in this particular phase of the GRB emission, possibly related to the SN process. This scenario may represent an invaluable tool to estimate the redshift of GRBs belonging to this sub-class of events. More GRBs are therefore needed in order to enlarge the subclass and to make more stringent constraints on the redshift estimates performed with this method for GRBs pertaining to this class.

30. C.L. Bianco, M. G. Bernardini, L. Caito, G. De Barros, L. Izzo, M. Muccino, B. Patricelli, A.V. Penacchioni, G.B. Pisani, R. Ruffini; “The canonical GRB scenario”; *Il Nuovo Cimento C*, 36 s01, 21 (2013).

The canonical GRB scenario implied by the fireshell model is briefly summarized.

31. A.V. Penacchioni, R. Ruffini, L. Izzo, M. Muccino, C.L. Bianco, L. Caito, B. Patricelli; “Evidences for a double component in the emission of GRB 101023”; *Il Nuovo Cimento C*, 36 s01, 117 (2013).

In this work we present the results of the analysis of GRB 101023 in the fireshell scenario. Its redshift is not known, so we attempted to infer it from the Amati Relation, obtaining $z = 0.9$. Its light curve presents a double emission, which makes it very similar to the already studied GRB 090618. We called each part Episode 1 and Episode 2. We performed a time-resolved spectral

analysis with RMFIT using different spectral models, and fitted the light curve with a numerical code integrating the fireshell equations of motion. We used Fermi GBM data to build the light curve, in particular the second NaI detector, in the range (8.5–1000 keV). We considered different hypotheses regarding which part of the light curve could be the GRB and performed the analysis of all of them. We noticed a great variation of the temperature with time in the first episode, as well as almost no variation of the progenitor radius. We found that the first emission does not match the requirements for a GRB, while the second part perfectly agrees with being a canonical GRB, with a P-GRB lasting 4 s.

32. M. Muccino, R. Ruffini, C.L. Bianco, L. Izzo, A.V. Penacchioni, G.B. Pisani; “GRB 090510: A Disguised Short Gamma-Ray Burst with the Highest Lorentz Factor and Circumburst Medium”; *The Astrophysical Journal*, 772, 62 (2013).

GRB 090510, observed both by Fermi and AGILE satellites, is the first bright short-hard Gamma-Ray Burst (GRB) with an emission from the keV up to the GeV energy range. Within the Fireshell model, we interpret the faint precursor in the light curve as the emission at the transparency of the expanding e^+e^- plasma: the Proper-GRB (P-GRB). From the observed isotropic energy we assume a total plasma energy $E_{e^+e^-}^{tot} = (1.10 \pm 0.06) \times 10^{53}$ erg and derive a Baryon load $B = (1.45 \pm 0.28) \times 10^{-3}$ and a Lorentz factor at transparency $\Gamma_{tr} = (6.7 \pm 1.6) \times 10^2$. The main emission ~ 0.4 s after the initial spike is interpreted as the extended afterglow, due to the interaction of the ultrarelativistic baryons with the CircumBurst Medium (CBM). Using the condition of fully radiative regime, we infer a CBM average spherically symmetric density of $\langle n_{CBM} \rangle = (1.85 \pm 0.14) \times 10^3$ particles/cm³, one of the highest found in the Fireshell model. The value of the filling factor, $1.5 \times 10^{-10} \leq \mathcal{R} \leq 3.8 \times 10^{-8}$, leads to the estimate of filaments with densities $n_{fil} = n_{CBM}/\mathcal{R} \approx (10^6 - 10^{14})$ particles/cm³. The sub-MeV and the MeV emissions are well reproduced. When compared to the canonical GRBs with $\langle n_{CBM} \rangle \approx 1$ particles/cm³ and to the disguised short GRBs with $\langle n_{CBM} \rangle \approx 10^{-3}$ particles/cm³, the case of GRB 090510 leads to the existence of a new family of bursts exploding in an over-dense galactic region with $\langle n_{CBM} \rangle \approx 10^3$ particles/cm³. The joint effect of the high Γ_{tr} and the high density compresses in time and “inflates” in intensity the extended afterglow, making it appear as a short burst, which we here define as “disguised short GRB by excess”. The determination of the above parameters values may represent an important step towards the explanation

of the GeV emission.

33. R. Ruffini, M. Muccino, C.L. Bianco, M. Enderli, L. Izzo, M. Kovacevic, A.V. Penacchioni, G.B. Pisani, J.A. Rueda, Y. Wang; “On Binary Driven Hypernovae and their nested late X-ray emission”; *Astronomy & Astrophysics*, 565, L10 (2014).

Context: The induced gravitational collapse (IGC) paradigm addresses the very energetic (10^{52} – 10^{54} erg) long gamma-ray bursts (GRBs) associated to supernovae (SNe). Unlike the traditional “collapsar” model, an evolved FeCO core with a companion neutron star (NS) in a tight binary system is considered as the progenitor. This special class of sources, here named “binary driven hypernovae” (BdHNe), presents a composite sequence composed of four different episodes with precise spectral and luminosity features.

Aims: We first compare and contrast the steep decay, the plateau, and the power-law decay of the X-ray luminosities of three selected BdHNe (GRB 060729, GRB 061121, and GRB 130427A). Second, to explain the different sizes and Lorentz factors of the emitting regions of the four episodes, for definiteness, we use the most complete set of data of GRB 090618. Finally, we show the possible role of r-process, which originates in the binary system of the progenitor.

Methods: We compare and contrast the late X-ray luminosity of the above three BdHNe. We examine correlations between the time at the starting point of the constant late power-law decay t_a^* , the average prompt luminosity $\langle L_{iso} \rangle$, and the luminosity at the end of the plateau L_a . We analyze a thermal emission (~ 0.97 – 0.29 keV), observed during the X-ray steep decay phase of GRB 090618.

Results: The late X-ray luminosities of the three BdHNe, in the rest-frame energy band 0.3–10 keV, show a precisely constrained “nested” structure. In a space-time diagram, we illustrate the different sizes and Lorentz factors of the emitting regions of the three episodes. For GRB 090618, we infer an initial dimension of the thermal emitter of $\sim 7 \times 10^{12}$ cm, expanding at $\Gamma \approx 2$. We find tighter correlations than the Dainotti-Willingale ones.

Conclusions: We confirm a constant slope power-law behavior for the late X-ray luminosity in the source rest frame, which may lead to a new distance indicator for BdHNe. These results, as well as the emitter size and Lorentz factor, appear to be inconsistent with the traditional afterglow model based on synchrotron emission from an ultra-relativistic ($\Gamma \sim 10^2$ – 10^3) collimated jet outflow. We argue, instead, for the possible role of r-process, originating in the binary system, to power the mildly relativistic X-ray source.

34. R. Ruffini, L. Izzo, M. Muccino, G.B. Pisani, J.A. Rueda, Y. Wang, C. Barbarino, C.L. Bianco, M. Enderli, M. Kovacevic; “Induced gravitational collapse at extreme cosmological distances: the case of GRB 090423”; *Astronomy & Astrophysics*, 569, A39 (2014).

Context: The induced gravitational collapse (IGC) scenario has been introduced in order to explain the most energetic gamma ray bursts (GRBs), $E_{iso} = 10^{52} - 10^{54}$ erg, associated with type Ib/c supernovae (SNe). It has led to the concept of binary-driven hypernovae (BdHNe) originating in a tight binary system composed by a FeCO core on the verge of a SN explosion and a companion neutron star (NS). Their evolution is characterized by a rapid sequence of events: 1) The SN explodes, giving birth to a new NS (ν NS). The accretion of SN ejecta onto the companion NS increases its mass up to the critical value; 2) The consequent gravitational collapse is triggered, leading to the formation of a black hole (BH) with GRB emission; 3) A novel feature responsible for the emission in the GeV, X-ray, and optical energy range occurs and is characterized by specific power-law behavior in their luminosity evolution and total spectrum; 4) The optical observations of the SN then occurs.

Aims: We investigate whether GRB 090423, one of the farthest observed GRB at $z = 8.2$, is a member of the BdHN family.

Methods: We compare and contrast the spectra, the luminosity evolution, and the detectability in the observations by *Swift* of GRB 090423 with the corresponding ones of the best known BdHN case, GRB 090618.

Results: Identification of constant slope power-law behavior in the late X-ray emission of GRB 090423 and its overlapping with the corresponding one in GRB 090618, measured in a common rest frame, represents the main result of this article. This result represents a very significant step on the way to using the scaling law properties, proven in Episode 3 of this BdHN family, as a cosmological standard candle.

Conclusions: Having identified GRB 090423 as a member of the BdHN family, we can conclude that SN events, leading to NS formation, can already occur already at $z = 8.2$, namely at 650 Myr after the Big Bang. It is then possible that these BdHNe originate stem from 40-60 M_{\odot} binaries. They are probing the Population II stars after the completion and possible disappearance of Population III stars.

35. M. Muccino, C.L. Bianco, L. Izzo, Y. Wang, M. Enderli, M. Kovacevic, G.B. Pisani, A.V. Penacchioni, R. Ruffini; “The Genuine Short GRB 090227B and the Disguised by Excess GRB 090510”; *Gravitation and*

Cosmology, 20, 197 (2014).

GRB 090227B and GRB 090510, traditionally classified as short gamma-ray Bursts (GRBs), indeed originate from different systems. For GRB 090227B we inferred a total energy of the e^+e^- plasma $E_{e^+e^-}^{tot} = (2.83 \pm 0.15) \times 10^{53}$ erg, a baryon load of $B = (4.1 \pm 0.05) \times 10^{-5}$, and a CircumBurst Medium (CBM) average density $\langle n_{CBM} \rangle = (1.90 \pm 0.20) \times 10^{-5} \text{ cm}^{-3}$. From these results we have assumed the progenitor of this burst to be a symmetric neutron stars (NSs) merger with masses $m = 1.34M_{\odot}$, radii $R = 12.24$ km. GRB 090510, instead, has $E_{e^+e^-}^{tot} = (1.10 \pm 0.06) \times 10^{53}$ erg, $B = (1.45 \pm 0.28) \times 10^{-3}$, implying a Lorentz factor at transparency of $\Gamma = (6.7 \pm 1.7) \times 10^2$, which are characteristic of the long GRB class, and a very high CBM density, $\langle n_{CBM} \rangle = (1.85 \pm 0.14) \times 10^3 \text{ cm}^{-3}$. The joint effect of the high values of Γ and of $\langle n_{CBM} \rangle$ compresses in time and “inflates” in intensity in an extended afterglow, making appear GRB 090510 as a short burst, which we here define as “disguised short GRB by excess” occurring an overdense region with 10^3 cm^{-3} .

36. M. Muccino, C.L. Bianco, L. Izzo, Y. Wang, M. Enderli, G.B. Pisani, A.V. Penacchioni, R. Ruffini; “Two short bursts originating from different astrophysical systems: The genuine short GRB 090227B and the disguised short GRB 090510 by excess”; *Journal of the Korean Physical Society*, 65, 865 (2014).

GRB 090227B and GRB 090510 are two gamma-ray bursts (GRBs) traditionally classified as short bursts. The major outcome of our analysis is that they indeed originate from different systems. In the case of GRB 090227B, from the inferred values of the total energy of the e^+e^- plasma, $E_{e^+e^-}^{tot} = (2.83 \pm 0.15) \times 10^{53}$ erg, the engulfed baryonic mass M_B , expressed as $B = M_B c^2 / E_{e^+e^-}^{tot} = (4.1 \pm 0.05) \times 10^{-5}$, and the circumburst medium (CBM) average density, $\langle n_{CBM} \rangle = (1.90 \pm 0.20) \times 10^{-5} \text{ cm}^{-3}$, we have assumed the progenitor of this burst to be a symmetric neutron star (NS) merger with masses $m = 1.34M_{\odot}$, radii $R = 12.24$ km, and crustal thicknesses of ~ 0.47 km. In the case of GRB 090510, we have derived the total plasma energy, $E_{e^+e^-}^{tot} = (1.10 \pm 0.06) \times 10^{53}$ erg, the Baryon load, $B = (1.45 \pm 0.28) \times 10^{-3}$, and the Lorentz factor at transparency, $\Gamma = (6.7 \pm 1.7) \times 10^2$, which are characteristic of the long GRB class, as well as a very high CBM density, $\langle n_{CBM} \rangle = (1.85 \pm 0.14) \times 10^3 \text{ cm}^{-3}$. The joint effect of the high values of Γ and $\langle n_{CBM} \rangle$ compresses in time and “inflates” in intensity the extended afterglow, making GRB 090510 appear to be a short burst, which we here define as a “disguised short GRB by excess”, occurring

in an overdense region with 10^3 cm^{-3} .

37. R. Ruffini, Y. Wang, M. Kovacevic, C.L. Bianco, M. Enderli, M. Muccino, A.V. Penacchioni, G.B. Pisani, J. Rueda; “GRB 130427A and SN 2013cq: A Multi-wavelength Analysis of An Induced Gravitational Collapse Event”; *The Astrophysical Journal*, 798, 10 (2015).

We have performed our data analysis of the observations by *Swift*, *NuStar* and *Fermi* satellites in order to probe the induced gravitational collapse (IGC) paradigm for GRBs associated with supernovae (SNe), in the “terra incognita” of GRB 130427A. We compare and contrast our data analysis with those in the literature. We have verified that the GRB 130427A conforms to the IGC paradigm by examining the power law behavior of the luminosity in the early 10^4 s of the XRT observations. This has led to the identification of the four different episodes of the “binary driven hypernovae” (BdHNe) and to the prediction, on May 2, 2013, of the occurrence of SN 2013cq, duly observed in the optical band on May 13, 2013. The exceptional quality of the data has allowed the identification of novel features in *Episode 3* including: a) the confirmation and the extension of the existence of the recently discovered “nested structure” in the late X-ray luminosity in GRB 130427A, as well as the identification of a spiky structure at 10^2 s in the cosmological rest-frame of the source; b) a power law emission of the GeV luminosity light curve and its onset at the end of *Episode 2*; c) different Lorentz Γ factors for the emitting regions of the X-ray and GeV emissions in this *Episode 3*. These results make it possible to test the details of the physical and astrophysical regimes at work in the BdHNe: 1) a newly born neutron star and the supernova ejecta, originating in *Episode 1, 2*) a newly formed black hole originating in *Episode 2*, and 3) the possible interaction among these components, observable in the standard features of *Episode 3*.

38. M. Muccino, R. Ruffini, C.L. Bianco, M. Enderli, M. Kovacevic, L. Izzo, A.V. Penacchioni, G.B. Pisani, J.A. Rueda, Y. Wang; “On binary driven hypernovae and their nested late X-ray emission”; *Astronomy Reports*, 59, 581 (2015).

The induced gravitational collapse (IGC) paradigm addresses energetic (10^{52} – 10^{54} erg), long gamma-ray bursts (GRBs) associated to supernovae (SNe) and proposes as their progenitors tight binary systems composed of an evolved FeCO core and a companion neutron star (NS). Their emission is characterized by four specific episodes: *Episode 1*, corresponding to the on-set of the FeCO

SN explosion and the accretion of the ejecta onto the companion NS; Episode 2, related the collapse of the companion NS to a black hole (BH) and to the emission of a long GRB; Episode 3, observed in X-rays and characterized by a steep decay, a plateau phase and a late power-law decay; Episode 4, corresponding to the optical SN emission due to the ^{56}Ni decay. We focus on Episode 3 and we show that, from the thermal component observed during the steep decay of the prototype GRB 090618, the emission region has a typical dimension of $\sim 10^{13}$ cm, which is inconsistent with the typical size of the emitting region of GRBs, e.g., $\sim 10^{16}$ cm. We propose, therefore, that the X-ray afterglow emission originates from a spherically symmetric SN ejecta expanding at $\Gamma \sim 2$ or, possibly, from the accretion onto the newly formed black hole, and we name these systems “binary driven hypernovae” (BdHNe). This interpretation is alternative to the traditional afterglow model based on the GRB synchrotron emission from a collimated jet outflow, expanding at ultra-relativistic Lorentz factor of $\Gamma \sim 10^2 - 10^3$ and originating from the collapse of a single object. We show then that the rest-frame energy band 0.3–10 keV X-ray luminosities of three selected BdHNe, GRB 060729, GRB 061121, and GRB 130427A, evidence a precisely constrained “nested” structure and satisfy precise scaling laws between the average prompt luminosity, $\langle L_{iso} \rangle$, and the luminosity at the end of the plateau, L_a , as functions of the time at the end of the plateau. All these features extend the applicability of the “cosmic candle” nature of Episode 3. The relevance of r-process in fulfilling the demanding scaling laws and the nested structure are indicated.

39. R. Ruffini, J.A. Rueda, C. Barbarino, C. L. Bianco, H. Dereli, M. Enderli, L. Izzo, M. Muccino, A.V. Penacchioni, G.B. Pisani, Y. Wang; “Induced Gravitational Collapse in the BATSE era: the case of GRB 970828”; *Astronomy Reports*, 59, 626 (2015).

Following the recently established “Binary-driven HyperNova” (BdHN) paradigm, we here interpret GRB 970828 in terms of the four episodes typical of such a model. The “Episode 1”, up to 40 s after the trigger time t_0 , with a time varying thermal emission and a total energy of $E_{iso,1st} = 2.60 \times 10^{53}$ erg, is interpreted as due to the onset of an hyper-critical accretion process onto a companion neutron star, triggered by the companion star, an FeCO core approaching a SN explosion. The “Episode 2”, observed up t_0+90 s, is interpreted as a canonical gamma ray burst, with an energy of $E_{tot}^{e^+e^-} = 1.60 \times 10^{53}$ erg, a baryon load of $B = 7 \times 10^{-3}$ and a bulk Lorentz factor at transparency of $\Gamma = 142.5$. From this Episode 2, we infer that the GRB exploded in an environment with a large av-

erage particle density $\langle n \rangle \approx 10^3$ particles/cm³ and dense clouds characterized by typical dimensions of $(4 \div 8) \times 10^{14}$ cm and $\delta n/n \sim 10$. The “Episode 3” is identified from t_0+90 s all the way up to 10^{5-6} s: despite the paucity of the early X-ray data, typical in the BATSE, pre-Swift era, we find extremely significant data points in the late X-ray afterglow emission of GRB 970828, which corresponds to the ones observed in all BdHNe sources. The “Episode 4”, related to the Supernova emission, does not appear to be observable in this source, due to the presence of darkening from the large density of the GRB environment, also inferred from the analysis of the Episode 2.

40. Y. Wang, R. Ruffini, M. Kovacevic, C.L. Bianco, M. Enderli, M. Muccino, A.V. Penacchioni, G.B. Pisani, J.A. Rueda; “Predicting supernova associated to gamma-ray burst 130427a”; *Astronomy Reports*, 59, 667 (2015).

Binary systems constituted by a neutron star and a massive star are not rare in the universe. The Induced Gravitational Gamma-ray Burst (IGC) paradigm interprets Gamma-ray bursts as the outcome of a neutron star that collapses into a black hole due to the accretion of the ejecta coming from its companion massive star that underwent a supernova event. GRB 130427A is one of the most luminous GRBs ever observed, of which isotropic energy exceeds 10^{54} erg. And it is within one of the few GRBs obtained optical, X-ray and GeV spectra simultaneously for hundreds of seconds, which provides an unique opportunity so far to understand the multi-wavelength observation within the IGC paradigm, our data analysis found low Lorentz factor blackbody emission in the Episode 3 and its X-ray light curve overlaps typical IGC Golden Sample, which comply to the IGC mechanisms. We consider these findings as clues of GRB 130427A belonging to the IGC GRBs. We predicted on GCN the emergence of a supernova on May 2, 2013, which was later successfully detected on May 13, 2013.

41. R. Ruffini, M. Muccino, M. Kovacevic, F.G. Oliveira, J.A. Rueda, C.L. Bianco, M. Enderli, A.V. Penacchioni, G.B. Pisani, Y. Wang, E. Zaninoni; “GRB 140619B: a short GRB from a binary neutron star merger leading to black hole formation”; *The Astrophysical Journal*, 808, 190 (2015).

We show the existence of two families of short GRBs, both originating from the merger of binary neutron stars (NSs): family-1 with $E_{iso} < 10^{52}$ erg, leading to a massive NS as the merged core, and family-2 with $E_{iso} > 10^{52}$ erg, leading to a black hole (BH). Following the identification of the prototype

GRB 090227B, we present the details of a new example of family-2 short burst: GRB 140619B. From the spectral analysis of the early ~ 0.2 s, we infer an observed temperature $kT = (324 \pm 33)$ keV of the e^+e^- -plasma at transparency (P-GRB), a theoretically derived redshift $z = 2.67 \pm 0.37$, a total burst energy $E_{e^+e^-}^{tot} = (6.03 \pm 0.79) \times 10^{52}$ erg, a rest-frame peak energy $E_{p,i} = 4.7$ MeV, and a baryon load $B = (5.52 \pm 0.73) \times 10^{-5}$. We also estimate the corresponding emission of gravitational waves. Two additional examples of family-2 short bursts are identified: GRB 081024B and GRB 090510, remarkable for its well determined cosmological distance. We show that marked differences exist in the nature of the afterglows of these two families of short bursts: family-2 bursts, leading to BH formation, consistently exhibit high energy emission following the P-GRB emission; family-1 bursts, leading to the formation of a massive NS, should never exhibit high energy emission. We also show that both the families fulfill an $E_{p,i}-E_{iso}$ relation with slope $\gamma = 0.59 \pm 0.07$ and a normalization constant incompatible with the one for long GRBs. The observed rate of such family-2 events is $\rho_0 = (2.1_{-1.4}^{+2.8}) \times 10^{-4} \text{Gpc}^{-3} \text{yr}^{-1}$.

42. R. Ruffini, Y. Aimuratov, C.L. Bianco, M. Enderli, M. Kovacevic, R. Moradi, M. Muccino, A.V. Penacchioni, G.B. Pisani, J.A. Rueda, Y. Wang; “Induced gravitational collapse in FeCO Core-Neutron star binaries and Neutron star-Neutron star binary mergers”; *International Journal of Modern Physics A*, 30, 1545023 (2015).

We review the recent progress in understanding the nature of gamma-ray bursts (GRBs). The occurrence of GRB is explained by the Induced Gravitational Collapse (IGC) in FeCO Core-Neutron star binaries and Neutron star-Neutron star binary mergers, both processes occur within binary system progenitors. Making use of this most unexpected new paradigm, with the fundamental implications by the neutron star (NS) critical mass, we find that different initial configurations of binary systems lead to different GRB families with specific new physical predictions confirmed by observations.

5.2 Conference proceedings

1. R. Ruffini, M.G. Bernardini, C.L. Bianco, P. Chardonnet, F. Fraschetti, V. Gurzadyan, L. Vitagliano, S.-S. Xue; “The Blackholic energy: long and short Gamma-Ray Bursts (New perspectives in physics and astrophysics from the theoretical understanding of Gamma-Ray Bursts, II)”;

in Proceedings of the XIth Brazilian School on Cosmology and Gravitation, Mangaratiba, Rio de Janeiro (Brazil), July August 2004, M. Novello, S.E. Perez Bergliaffa, Editors; AIP Conference Proceedings, 782, 42 (2005).

We outline the confluence of three novel theoretical fields in our modeling of Gamma-Ray Bursts (GRBs): 1) the ultrarelativistic regime of a shock front expanding with a Lorentz gamma factor ~ 300 ; 2) the quantum vacuum polarization process leading to an electron-positron plasma originating the shock front; and 3) the general relativistic process of energy extraction from a black hole originating the vacuum polarization process. There are two different classes of GRBs: the long GRBs and the short GRBs. We here address the issue of the long GRBs. The theoretical understanding of the long GRBs has led to the detailed description of their luminosities in fixed energy bands, of their spectral features and made also possible to probe the astrophysical scenario in which they originate. We are specially interested, in this report, to a subclass of long GRBs which appear to be accompanied by a supernova explosion. We are considering two specific examples: GRB980425/SN1998bw and GRB030329/SN2003dh. While these supernovae appear to have a standard energetics of 10^{49} ergs, the GRBs are highly variable and can have energetics $10^4 - 10^5$ times larger than the ones of the supernovae. Moreover, many long GRBs occurs without the presence of a supernova. It is concluded that in no way a GRB can originate from a supernova. The precise theoretical understanding of the GRB luminosity we present evidence, in both these systems, the existence of an independent component in the X-ray emission, usually interpreted in the current literature as part of the GRB afterglow. This component has been observed by Chandra and XMM to have a strong decay on scale of months. We have named here these two sources respectively URCA-1 and URCA-2, in honor of the work that George Gamow and Mario Shoenberg did in 1939 in this town of Urca identifying the basic mechanism, the Urca processes, leading to the process of gravitational collapse and the formation of a neutron star and a supernova. The further hypothesis is considered to relate this X-ray source to a neutron star, newly born in the Supernova. This hypothesis should be submitted to further theoretical and observational investigation. Some theoretical developments to clarify the astrophysical origin of this new scenario are outlined. We turn then to the theoretical developments in the short GRBs: we first report some progress in the understanding the dynamical phase of collapse, the mass-energy formula and the extraction

of blackholic energy which have been motivated by the analysis of the short GRBs. In this context progress has also been accomplished on establishing an absolute lower limit to the irreducible mass of the black hole as well as on some critical considerations about the relations of general relativity and the second law of thermodynamics. We recall how this last issue has been one of the most debated in theoretical physics in the past thirty years due to the work of Bekenstein and Hawking. Following these conceptual progresses we analyze the vacuum polarization process around an overcritical collapsing shell. We evidence the existence of a separatrix and a dyadosphere trapping surface in the dynamics of the electron-positron plasma generated during the process of gravitational collapse. We then analyze, using recent progress in the solution of the Vlasov-Boltzmann-Maxwell system, the oscillation regime in the created electron-positron plasma and their rapid convergence to a thermalized spectrum. We conclude by making precise predictions for the spectra, the energy fluxes and characteristic time-scales of the radiation for short-bursts. If the precise luminosity variation and spectral hardening of the radiation we have predicted will be confirmed by observations of short-bursts, these systems will play a major role as standard candles in cosmology. These considerations will also be relevant for the analysis of the long-bursts when the baryonic matter contribution will be taken into account.

2. R. Ruffini, M.G. Bernardini, C.L. Bianco, P. Chardonnet, F. Fraschetti, V. Gurzadyan, L. Vitagliano, S.-S. Xue; "Black hole physics and astrophysics: The GRB-Supernova connection and URCA-1 URCA-2"; in Proceedings of the Tenth Marcel Grossmann Meeting on General Relativity, Rio de Janeiro, Brazil, July 2003, M. Novello, S.E. Perez-Bergliaffa, Editors; p. 369; World Scientific, (Singapore, 2006).

We outline the confluence of three novel theoretical fields in our modeling of Gamma-Ray Bursts (GRBs): 1) the ultrarelativistic regime of a shock front expanding with a Lorentz gamma factor ~ 300 ; 2) the quantum vacuum polarization process leading to an electron-positron plasma originating the shock front; and 3) the general relativistic process of energy extraction from a black hole originating the vacuum polarization process. There are two different classes of GRBs: the long GRBs and the short GRBs. We here address the issue of the long GRBs. The theoretical understanding of the long GRBs has led to the detailed description of their luminosities in fixed energy bands, of their spectral features and made also possible to probe the astrophysical scenario in which they originate. We are specially interested, in this report, to a

subclass of long GRBs which appear to be accompanied by a supernova explosion. We are considering two specific examples: GRB980425/SN1998bw and GRB030329/SN2003dh. While these supernovae appear to have a standard energetics of 10^{49} ergs, the GRBs are highly variable and can have energetics $10^4 - 10^5$ times larger than the ones of the supernovae. Moreover, many long GRBs occurs without the presence of a supernova. It is concluded that in no way a GRB can originate from a supernova. The precise theoretical understanding of the GRB luminosity we present evidence, in both these systems, the existence of an independent component in the X-ray emission, usually interpreted in the current literature as part of the GRB afterglow. This component has been observed by Chandra and XMM to have a strong decay on scale of months. We have named here these two sources respectively URCA-1 and URCA-2, in honor of the work that George Gamow and Mario Shoenberg did in 1939 in this town of Urca identifying the basic mechanism, the Urca processes, leading to the process of gravitational collapse and the formation of a neutron star and a supernova. The further hypothesis is considered to relate this X-ray source to a neutron star, newly born in the Supernova. This hypothesis should be submitted to further theoretical and observational investigation. Some theoretical developments to clarify the astrophysical origin of this new scenario are outlined.

3. M.G. Bernardini, C.L. Bianco, P. Chardonnet, F. Fraschetti, R. Ruffini, S.-S. Xue; "General features of GRB 030329 in the EMBH model"; in Proceedings of the Tenth Marcel Grossmann Meeting on General Relativity, Rio de Janeiro, Brazil, July 2003, M. Novello, S.E. Perez-Bergliaffa, Editors; p. 2459; World Scientific, (Singapore, 2006).

GRB 030329 is considered within the EMBH model. We determine the three free parameters and deduce its luminosity in given energy bands comparing it with the observations. The observed substructures are compared with the predictions of the model: by applying the result that substructures observed in the extended afterglow peak emission (E-APE) do indeed originate in the collision of the accelerated baryonic matter (ABM) pulse with the inhomogeneities in the interstellar medium around the black-hole, masks of density inhomogeneities are considered in order to reproduce the observed temporal substructures. The induced supernova concept is applied to this system and the general consequences that we are witnessing are the formation of a cosmological thriptych of a black hole originating the GRB 030329, the supernova SN2003dh and a young neutron star. Analogies to the system GRB 980425–

SN1998bw are outlined.

4. R. Ruffini, M.G. Bernardini, C.L. Bianco, P. Chardonnet, A. Corsi, F. Frascchetti, S.-S. Xue; “GRB 970228 and its associated Supernova in the EMBH model”; in Proceedings of the Tenth Marcel Grossmann Meeting on General Relativity, Rio de Janeiro, Brazil, July 2003, M. Novello, S.E. Perez-Bergliaffa, Editors; p. 2465; World Scientific, (Singapore, 2006).

The γ -ray burst of 1997 February 28 is analyzed within the Electromagnetic Black Hole model. We first estimate the value of the total energy deposited in the dyadosphere, E_{dya} , and the amount of baryonic matter left over by the EMBH progenitor star, $B = M_B c^2 / E_{dya}$. We then consider the role of the interstellar medium number density n_{ISM} and of the ratio R between the effective emitting area and the total surface area of the γ -ray burst source, in reproducing the prompt emission and the X-ray afterglow of this burst. Some considerations are also done concerning the possibility of explaining, within the theory, the observed evidence for a supernova in the optical afterglow.

5. F. Frascchetti, M.G. Bernardini, C.L. Bianco, P. Chardonnet, R. Ruffini, S.-S. Xue; “Inferences on the ISM structure around GRB980425 and GRB980425-SN1998bw association in the EMBH Model”; in Proceedings of the Tenth Marcel Grossmann Meeting on General Relativity, Rio de Janeiro, Brazil, July 2003, M. Novello, S.E. Perez-Bergliaffa, Editors; p. 2451; World Scientific, (Singapore, 2006).

We determine the four free parameters within the EMBH model for GRB 980425 and deduce its luminosity in given energy bands, its spectra and its time variability in the prompt radiation. We compute the basic kinematical parameters of GRB 980425. In the extended afterglow peak emission the Lorentz γ factor is lower than the critical value 150 which has been found in Ruffini et al. (2002) to be necessary in order to perform the tomography of the ISM surrounding the GRB as suggested by Dermer & Mitman (1999). The detailed structure of the density inhomogeneities as well as the effects of radial apparent superluminal effects are evaluated within the EMBH model. Under the assumption that the energy distribution of emitted radiation is thermal in the comoving frame, time integrated spectra of EMBH model for prompt emission are computed. The induced supernova concept is applied to this system and general consequences on the astrophysical and cosmological scenario are derived.

6. R. Ruffini, M.G. Bernardini, C.L. Bianco, P. Chardonnet, F. Frascchetti,

R. Guida, S.-S. Xue; "GRB 050315: A step in the proof of the uniqueness of the overall GRB structure"; in "GAMMA-RAY BURSTS IN THE SWIFT ERA: Sixteenth Maryland Astrophysics Conference", Washington, DC, USA, November 29th - December 2nd 2005, Stephen S. Holt, Neil Gehrels, John A. Nousek, Editors; AIP Conference Proceedings, 836, 103 (2006).

Using the Swift data of GRB 050315, we progress in proving the uniqueness of our theoretically predicted Gamma-Ray Burst (GRB) structure as composed by a proper-GRB, emitted at the transparency of an electron-positron plasma with suitable baryon loading, and an afterglow comprising the "prompt radiation" as due to external shocks. Detailed light curves for selected energy bands are theoretically fitted in the entire temporal region of the Swift observations ranging over 10^6 seconds.

7. R. Ruffini, M.G. Bernardini, C.L. Bianco, P. Chardonnet, F. Fraschetti, S.-S. Xue; "Theoretical Interpretation of GRB 031203 and URCA-3"; in "Relativistic Astrophysics and Cosmology - Einsteins Legacy", B. Aschenbach, V. Burwitz, G. Hasinger, B. Leibundgut, Editors; Springer-Verlag (2007).
8. R. Ruffini, M.G. Bernardini, C.L. Bianco, L. Caito, P. Chardonnet, M.G. Dainotti, F. Fraschetti, R. Guida, M. Rotondo, G. Vereshchagin, L. Vitagliano, S.-S. Xue; "The Blackholic energy and the canonical Gamma-Ray Burst"; in Proceedings of the XIIth Brazilian School on Cosmology and Gravitation, Mangaratiba, Rio de Janeiro (Brazil), September 2006, M. Novello, S.E. Perez Bergliaffa, Editors; AIP Conference Proceedings, 910, 55 (2007).

Gamma-Ray Bursts (GRBs) represent very likely "the" most extensive computational, theoretical and observational effort ever carried out successfully in physics and astrophysics. The extensive campaign of observation from space based X-ray and γ -ray observatory, such as the *Vela*, CGRO, BeppoSAX, HETE-II, INTEGRAL, *Swift*, R-XTE, *Chandra*, XMM satellites, have been matched by complementary observations in the radio wavelength (e.g. by the VLA) and in the optical band (e.g. by VLT, Keck, ROSAT). The net result is unprecedented accuracy in the received data allowing the determination of the energetics, the time variability and the spectral properties of these GRB sources. The very fortunate situation occurs that these data can be confronted with a mature theoretical development. Theoretical interpretation of the above data

allows progress in three different frontiers of knowledge: **a)** the ultrarelativistic regimes of a macroscopic source moving at Lorentz gamma factors up to ~ 400 ; **b)** the occurrence of vacuum polarization process verifying some of the yet untested regimes of ultrarelativistic quantum field theories; and **c)** the first evidence for extracting, during the process of gravitational collapse leading to the formation of a black hole, amounts of energies up to 10^{55} ergs of black-holic energy — a new form of energy in physics and astrophysics. We outline how this progress leads to the confirmation of three interpretation paradigms for GRBs proposed in July 2001. Thanks mainly to the observations by *Swift* and the optical observations by VLT, the outcome of this analysis points to the existence of a “canonical” GRB, originating from a variety of different initial astrophysical scenarios. The communality of these GRBs appears to be that they all are emitted in the process of formation of a black hole with a negligible value of its angular momentum. The following sequence of events appears to be canonical: the vacuum polarization process in the dyadosphere with the creation of the optically thick self accelerating electron-positron plasma; the engulfment of baryonic mass during the plasma expansion; adiabatic expansion of the optically thick “fireshell” of electron-positron-baryon plasma up to the transparency; the interaction of the accelerated baryonic matter with the interstellar medium (ISM). This leads to the canonical GRB composed of a proper GRB (P-GRB), emitted at the moment of transparency, followed by an extended afterglow. The sole parameters in this scenario are the total energy of the dyadosphere E_{dya} , the fireshell baryon loading M_B defined by the dimensionless parameter $B \equiv M_B c^2 / E_{dya}$, and the ISM filamentary distribution around the source. In the limit $B \rightarrow 0$ the total energy is radiated in the P-GRB with a vanishing contribution in the afterglow. In this limit, the canonical GRBs explain as well the short GRBs. In these lecture notes we systematically outline the main results of our model comparing and contrasting them with the ones in the current literature. In both cases, we have limited ourselves to review already published results in refereed publications. We emphasize as well the role of GRBs in testing yet unexplored grounds in the foundations of general relativity and relativistic field theories.

9. R. Ruffini, M.G. Bernardini, C.L. Bianco, L. Caito, P. Chardonnet, M.G. Dainotti, F. Fraschetti, R. Guida, G. Vereshchagin, S.-S. Xue; “The role of GRB 031203 in clarifying the astrophysical GRB scenario”; in Proceedings of the 6th Integral Workshop - The Obscured Universe, Moscow, (Russia), July 2006, S. Grebenev, R. Sunyaev, C. Winkler, A. Parmar, L.

Ouwehand, Editors; ESA Special Publication, SP-622, 561 (2007).

The luminosity and the spectral distribution of the afterglow of GRB 031203 have been presented within our theoretical framework, which envisages the GRB structure as composed by a proper-GRB, emitted at the transparency of an electron-positron plasma with suitable baryon loading, and an afterglow comprising the “prompt emission” as due to external shocks. In addition to the GRB emission, there appears to be a prolonged soft X-Ray emission lasting for 10^6 – 10^7 seconds followed by an exponential decay. This additional source has been called by us URCA-3. It is urgent to establish if this component is related to the GRB or to the Supernova (SN). In this second case, there are two possibilities: either the interaction of the SN ejecta with the interstellar medium or, possibly, the cooling of a young neutron star formed in the SN 2003lw process. The analogies and the differences between this triptych GRB 031203 / SN 2003lw / URCA-3 and the corresponding ones GRB 980425 / SN 1998bw / URCA-1 and GRB 030329 / SN 2003dh / URCA-2, as well as GRB 060218 / SN 2006aj are discussed.

10. M.G. Bernardini, C.L. Bianco, L. Caito, M.G. Dainotti, R. Guida, R. Ruffini; “GRB970228 and the class of GRBs with an initial spikelike emission: do they follow the Amati relation?”; in *Relativistic Astrophysics Proceedings of the 4th Italian-Sino Workshop*, Pescara (Italy), July 2007, C.L. Bianco, S.-S. Xue, Editors; AIP Conference Proceedings, 966, 7 (2008).

On the basis of the recent understanding of GRB050315 and GRB060218, we return to GRB970228, the first Gamma-Ray Burst (GRB) with detected afterglow. We proposed it as the prototype for a new class of GRBs with “an occasional softer extended emission lasting tenths of seconds after an initial spikelike emission”. Detailed theoretical computation of the GRB970228 light curves in selected energy bands for the prompt emission are presented and compared with observational *BeppoSAX* data. From our analysis we conclude that GRB970228 and likely the ones of the above mentioned new class of GRBs are “canonical GRBs” have only one peculiarity: they exploded in a galactic environment, possibly the halo, with a very low value of CBM density. Here we investigate how GRB970228 unveils another peculiarity of this class of GRBs: they do not fulfill the “Amati relation”. We provide a theoretical explanation within the fireshell model for the apparent absence of such correlation for the GRBs belonging to this new class.

11. C.L. Bianco, M.G. Bernardini, L. Caito, M.G. Dainotti, R. Guida, R. Ruffini;

“The “Fireshell” Model and the “Canonical” GRB Scenario; in *Relativistic Astrophysics Proceedings of the 4th Italian-Sino Workshop, Pescara (Italy), July 2007*, C.L. Bianco, S.-S. Xue, Editors; AIP Conference Proceedings, 966, 12 (2008).

In the “fireshell” model we define a “canonical GRB” light curve with two sharply different components: the Proper-GRB (P-GRB), emitted when the optically thick fireshell of electron-positron plasma originating the phenomenon reaches transparency, and the afterglow, emitted due to the collision between the remaining optically thin fireshell and the CircumBurst Medium (CBM). We outline our “canonical GRB” scenario, originating from the gravitational collapse to a black hole, with a special emphasis on the discrimination between “genuine” and “fake” short GRBs.

12. L. Caito, M.G. Bernardini, C.L. Bianco, M.G. Dainotti, R. Guida, R. Ruffini; “GRB 060614: A Progress Report”; in *Relativistic Astrophysics Proceedings of the 4th Italian-Sino Workshop, Pescara (Italy), July 2007*, C.L. Bianco, S.-S. Xue, Editors; AIP Conference Proceedings, 966, 16 (2008).

The explosion of GRB 060614, detected by the Swift satellite, produced a deep break in the GRB scenario opening new horizons of investigation, because it can't be traced back to any traditional scheme of classification. In fact, it manifests peculiarities both of long bursts and of short bursts. Above all, it is the first case of long duration near GRB without any bright Ib/c associated Supernova. We will show that, in our canonical GRB scenario, this “anomalous” situation finds a natural interpretation and allows us to discuss a possible variation to the traditional classification scheme, introducing the distinction between “genuine” and “fake” short bursts.

13. M.G. Dainotti, M.G. Bernardini, C.L. Bianco, L. Caito, R. Guida, R. Ruffini; “GRB 060218 and the Binaries as Progenitors of GRB-SN Systems”; in *Relativistic Astrophysics Proceedings of the 4th Italian-Sino Workshop, Pescara (Italy), July 2007*, C.L. Bianco, S.-S. Xue, Editors; AIP Conference Proceedings, 966, 25 (2008).

We study the Gamma-Ray Burst (GRB) 060218: a particularly close source at $z = 0.033$ with an extremely long duration, namely $T_{90} \sim 2000$ s, related to SN 2006aj. This source appears to be a very soft burst, with a peak in the spectrum at 4.9 keV, therefore interpreted as an X-Ray Flash (XRF). It fullfills the Amati relation. I present the fitting procedure, which is time consuming. In order

to show its sensitivity I also present two examples of fits with the same value of B and different value of $E_{e^\pm}^{tot}$. We fit the X- and γ -ray observations by *Swift* of GRB 060218 in the 0.1–150 keV energy band during the entire time of observations from 0 all the way to 10^6 s within a unified theoretical model. The free parameters of our theory are only three, namely the total energy $E_{e^\pm}^{tot}$ of the e^\pm plasma, its baryon loading $B \equiv M_B c^2 / E_{e^\pm}^{tot}$, as well as the CircumBurst Medium (CBM) distribution. We justify the extremely long duration of this GRB by a total energy $E_{e^\pm}^{tot} = 2.32 \times 10^{50}$ erg, a very high value of the baryon loading $B = 1.0 \times 10^{-2}$ and the effective CircumBurst Medium (CBM) density which shows a radial dependence $n_{cbm} \propto r^{-\alpha}$ with $1.0 \leq \alpha \leq 1.7$ and monotonically decreases from 1 to 10^{-6} particles/cm³. We recall that this value of the B parameter is the highest among the sources we have analyzed and it is very close to its absolute upper limit expected. By our fit we show that there is no basic differences between XRFs and more general GRBs. They all originate from the collapse process to a black hole and their difference is due to the variability of the three basic parameters within the range of full applicability of the theory. We also think that the smallest possible black hole, formed by the gravitational collapse of a neutron star in a binary system, is consistent with the especially low energetics of the class of GRBs associated with SNe Ib/c.

14. R. Guida, M.G. Bernardini, C.L. Bianco, L. Caito, M.G. Dainotti, R. Ruffini; “The Amati Relation within the Fireshell Model”; in Relativistic Astrophysics Proceedings of the 4th Italian-Sino Workshop, Pescara (Italy), July 2007, C.L. Bianco, S.-S. Xue, Editors; AIP Conference Proceedings, 966, 46 (2008).

In this work we show the existence of a spectral-energy correlation within our “fireshell” model for GRBs. The free parameters of the model are the total energy $E_{tot}^{e^\pm}$ of the e^\pm plasma and its baryon loading $B \equiv M_B c^2 / E_{tot}^{e^\pm}$, characterizing the source, and the parameters describing the effective CircumBurst medium (CBM) distribution, namely its particle number density ρ and its effective emitting area R . We build a sample of pseudo-GRBs, i.e. a set of theoretically simulated light curves, varying the total energy of the electron-positron plasma $E_{tot}^{e^\pm}$ and keeping the same baryon loading; the parametrization used to describe the distribution of the CircumBurst medium is the same as well for all the pseudo-GRBs. The values of these parameters (B , ρ and R) used in this work are equal to the ones assumed to fit GRB050315, a *Swift* burst representing a good example of what in the literature has been addressed as “canonical light curve”. For each GRB of the sample we calculate the νF_ν spectrum

integrating the theoretically computed light curve over the total time, namely from our T_0 , the end of the Proper-GRB (P-GRB), up to the end of our afterglow phase, when the fireshell Lorentz gamma factor is close to unity; we exclude the P-GRB from this spectral computation because, following our “canonical” GRB scenario, this component of the GRB emission is physically different from the other component, that is our afterglow component, so one should take care in no mixing them. We find that the maximum of this spectrum, that is the observed peak energy $E_{p,tot}$, correlates with the initial electron-positron plasma energy $E_{tot}^{e\pm}$ in a way very similar to the Amati one: $E_{p,tot} \propto (E_{tot}^{e\pm})^{0.5}$.

15. R. Guida, M.G. Bernardini, C.L. Bianco, L. Caito, M.G. Dainotti, R. Ruffini; “Theoretical interpretation of the Amati relation within the fireshell model”; in GAMMA-RAY BURSTS 2007: Proceedings of the Santa Fe Conference, Santa Fe (NM, USA), November 2007, M. Galassi, D. Palmer, E. Fenimore, Editors; AIP Conference Proceedings, 1000, 60 (2008).

We discuss within our theoretical “fireshell” model for Gamma-Ray Bursts (GRBs) the theoretical interpretation of the phenomenological correlation between the isotropic-equivalent radiated energy of the prompt emission E_{iso} and the cosmological rest-frame νF_ν spectrum peak energy E_p observed by Amati and collaborators. Possible reasons for some of the outliers of this relation are given.

16. L. Caito, M.G. Bernardini, C.L. Bianco, M.G. Dainotti, R. Guida, R. Ruffini; “GRB 060614: a Fake Short Gamma-Ray Burst”; in GAMMA-RAY BURSTS 2007: Proceedings of the Santa Fe Conference, Santa Fe (NM, USA), November 2007, M. Galassi, D. Palmer, E. Fenimore, Editors; AIP Conference Proceedings, 1000, 301 (2008).

The explosion of GRB 060614 produced a deep break in the GRB scenario and opened new horizons of investigation because it can’t be traced back to any traditional scheme of classification. In fact, it manifests peculiarities both of long bursts and of short bursts and, above all, it is the first case of long duration near GRB without any bright Ib/c associated Supernova. We will show that, in our canonical GRB scenario, this “anomalous” situation finds a natural interpretation and allows us to discuss a possible variation to the traditional classification scheme, introducing the distinction between “genuine” and “fake” short bursts.

17. C.L. Bianco, M.G. Bernardini, L. Caito, M.G. Dainotti, R. Guida, R. Ruffini;

“Short and canonical GRBs”; in GAMMA-RAY BURSTS 2007: Proceedings of the Santa Fe Conference, Santa Fe (NM, USA), November 2007, M. Galassi, D. Palmer, E. Fenimore, Editors; AIP Conference Proceedings, 1000, 305 (2008).

Within the “fireshell” model for the Gamma-Ray Bursts (GRBs) we define a “canonical GRB” light curve with two sharply different components: the Proper-GRB (P-GRB), emitted when the optically thick fireshell of electron-positron plasma originating the phenomenon reaches transparency, and the afterglow, emitted due to the collision between the remaining optically thin fireshell and the CircumBurst Medium (CBM). We outline our “canonical GRB” scenario, with a special emphasis on the discrimination between “genuine” and “fake” short GRBs.

18. C.L. Bianco, M.G. Bernardini, L. Caito, M.G. Dainotti, R. Guida, R. Ruffini, G. Vereshchagin, S.-S. Xue; “The Equations of motion of the “fireshell””; in OBSERVATIONAL EVIDENCE FOR BLACK HOLES IN THE UNIVERSE: Proceedings of the 2nd Kolkata Conference, Kolkata (India), February 2008, S.K. Chakrabarti, A.S. Majumdar, Editors; AIP Conference Proceedings, 1053, 259 (2008).

The Fireshell originating a Gamma-Ray Burst (GRB) encompasses an optically thick regime followed by an optically thin one. In the first one the fireshell self-accelerates from a Lorentz gamma factor equal to 1 all the way to 200-300. The physics of this system is based on the continuous annihilation of electron-positron pairs in an optically thick e^+e^- plasma with a small baryon loading. In the following regime, the optically thin fireshell, composed by the baryons left over after the transparency point, ballistically expands into the CircumBurst Medium (CBM). The dynamics of the fireshell during both regimes will be analyzed. In particular we will re-examine the validity of the constant-index power-law relation between the fireshell Lorentz gamma factor and its radial coordinate, usually adopted in the current literature on the grounds of an “ultrarelativistic” approximation. Such expressions are found to be mathematically correct but only approximately valid in a very limited range of the physical and astrophysical parameters and in an asymptotic regime which is reached only for a very short time, if any.

19. M.G. Bernardini, C.L. Bianco, L. Caito, M.G. Dainotti, R. Guida, R. Ruffini; “The “Canonical” GRBs within the fireshell model”; in OBSERVATIONAL EVIDENCE FOR BLACK HOLES IN THE UNIVERSE: Proceedings of

the 2nd Kolkata Conference, Kolkata (India), February 2008, S.K. Chakrabarti, A.S. Majumdar, Editors; AIP Conference Proceedings, 1053, 267 (2008).

Within the fireshell model we define a “canonical” GRB light curve with two sharply different components: the Proper-GRB (P-GRB), emitted when the optically thick fireshell of electron-positron plasma originating the phenomenon reaches transparency, and the afterglow, emitted due to the collision between the remaining optically thin fireshell and the CircumBurst Medium (CBM). On the basis of the recent understanding of GRB970228 as the prototype for a new class of GRBs with “an occasional softer extended emission lasting tenths of seconds after an initial spikelike emission” we outline our “canonical” GRB scenario, originating from the gravitational collapse to a black hole, with a special emphasis on the discrimination between short GRBs and the ones appearing as such due to their peculiar astrophysical setting.

20. M.G. Dainotti, M.G. Bernardini, C.L. Bianco, L. Caito, R. Guida, R. Ruffini; “GRB 060218: the density mask and its peculiarity compared to the other sources”; in OBSERVATIONAL EVIDENCE FOR BLACK HOLES IN THE UNIVERSE: Proceedings of the 2nd Kolkata Conference, Kolkata (India), February 2008, S.K. Chakrabarti, A.S. Majumdar, Editors; AIP Conference Proceedings, 1053, 283 (2008).

The Swift satellite has given continuous data in the range 0.3150 keV from 0 s to 106 s for GRB060218 associated with SN2006aj. It has an unusually long duration ($T_{90} \sim 2100$ s). We plan to fit the complete γ - and X-ray light curves of this long duration GRB, including the prompt emission and we give peculiar attention to the afterglow lightcurve in order to better constrain the density mask. We apply our “fireshell” model based on the formation of a black hole, giving the relevant references. The initial total energy of the electron-positron plasma $E_{e^\pm}^{tot} = 2.32 \times 10^{50}$ erg has a particularly low value similarly to the other GRBs associated with SNe. For the first time we observe a baryon loading $B = 10^{-2}$ which coincides with the upper limit for the dynamical stability of the fireshell. The effective CircumBurst Medium (CBM) density shows a radial dependence $n_{cbm} \propto r^{-a}$ with $1.0 \leq a \leq 1.7$ and monotonically decreases from 1 to 10^{-6} particles/cm³. Such a behavior is interpreted as due to a fragmentation in the fireshell. Such a fragmentation is crucial in explaining both the unusually large T_{90} and the consequently inferred abnormal low value of the CBM effective density. We present the comparison between the density mask of this source and the ones of a normal GRB 050315 and a fake short, GRB

970228, making some assumptions on the CBM behaviour in the surrounding of the Black hole.

21. L. Caito, M.G. Bernardini, C.L. Bianco, M.G. Dainotti, R. Guida, R. Ruffini; "GRB 060614 in the canonical fireshell model"; in OBSERVATIONAL EVIDENCE FOR BLACK HOLES IN THE UNIVERSE: Proceedings of the 2nd Kolkata Conference, Kolkata (India), February 2008, S.K. Chakrabarti, A.S. Majumdar, Editors; AIP Conference Proceedings, 1053, 291 (2008).

Gamma-Ray Burst (GRB) 060614 is the first nearby long duration GRB clearly not associated to any bright Ib/c Supernova. The explosion of this burst undermines one of the fundamental assumptions of the standard scenario and opens new horizons and hints of investigation. GRB 060614, hardly classifiable as a short GRB, is not either a "typical" long GRB since it occurs in a low star forming region. Moreover, it presents deep similarities with GRB 970228, which is the prototype of the "fake" short bursts, or better canonical GRBs disguised as short ones. Within the "fireshell" model, we test if this "anomalous" source can be a disguised short GRB.

22. L.J. Rangel Lemos, S. Casanova, R. Ruffini, S.S. Xue; "Fermis approach to the study of pp interactions"; in OBSERVATIONAL EVIDENCE FOR BLACK HOLES IN THE UNIVERSE: Proceedings of the 2nd Kolkata Conference, Kolkata (India), February 2008, S.K. Chakrabarti, A.S. Majumdar, Editors; AIP Conference Proceedings, 1053, 275 (2008).

The physics of hadronic interactions found much difficulties for explain the experimental data. In this work we study the approach of Fermi (1950) about the multiplicity of pions emitted in pp interactions and in follow we compare with the modern approach

23. R. Ruffini, A.G. Aksenov, M.G. Bernardini, C.L. Bianco, L. Caito, M.G. Dainotti, G. De Barros, R. Guida, G.V. Vereshchagin, S.-S. Xue; "The canonical Gamma-Ray Bursts and their 'precursors'"; in 2008 NANJING GAMMA-RAY BURST CONFERENCE, Proceedings of the 2008 Nanjing Gamma-Ray Burst Conference, Nanjing (China), June 2008, Y.-F. Huang, Z.-G. Dai, B. Zhang, Editors; AIP Conference Proceedings, 1065, 219 (2008).

The fireshell model for Gamma-Ray Bursts (GRBs) naturally leads to a canonical GRB composed of a proper-GRB (P-GRB) and an afterglow. P-GRBs, introduced by us in 2001, are sometimes considered "precursors" of the main GRB

event in the current literature. We show in this paper how the fireshell model leads to the understanding of the structure of GRBs, with precise estimates of the time sequence and intensities of the P-GRB and the of the afterglow. It leads as well to a natural classification of the canonical GRBs which overcomes the traditional one in short and long GRBs.

24. M.G. Bernardini, C.L. Bianco, L. Caito, M.G. Dainotti, R. Guida, R. Ruffini; “Preliminary analysis of GRB060607A within the fireshell model”; in 2008 NANJING GAMMA-RAY BURST CONFERENCE; Proceedings of the 2008 Nanjing Gamma-Ray Burst Conference, Nanjing (China), June 2008, Y.-F. Huang, Z.-G. Dai, B. Zhang, Editors; AIP Conference Proceedings, 1065, 227 (2008).

GRB060607A is a very distant ($z = 3.082$) and energetic event ($E_{iso} \sim 10^{53}$ erg). Its main peculiarity is that the peak of the near-infrared afterglow has been observed with the REM robotic telescope, allowing to infer the initial Lorentz gamma factor of the emitting system. We present a preliminary analysis of the spectra and light curves of GRB060607A prompt emission within the fireshell model. We show that the N(E) spectrum of the prompt emission, whose behavior is usually described as “simple power-law”, can also be fitted in a satisfactory way by a convolution of thermal spectra as predicted by the model we applied. The theoretical time-integrated spectrum of the prompt emission as well as the light curves in the BAT and XRT energy band are in good agreement with the observations, enforcing the plausibility of our approach. Furthermore, the initial value of Lorentz gamma factor we predict is compatible with the one deduced from the REM observations.

25. C.L. Bianco, M.G. Bernardini, L. Caito, M.G. Dainotti, R. Guida, R. Ruffini; “The “fireshell” model and the “canonical GRB” scenario”; in 2008 NANJING GAMMA-RAY BURST CONFERENCE; Proceedings of the 2008 Nanjing Gamma-Ray Burst Conference, Nanjing (China), June 2008, Y.-F. Huang, Z.-G. Dai, B. Zhang, Editors; AIP Conference Proceedings, 1065, 223 (2008).

The Swift observation of GRB 060614, as well as the catalog analysis by Norris & Bonnell (2006), opened the door “on a new Gamma-Ray Bursts (GRBs) classification scheme that straddles both long and short bursts” (Gehrels et al. 2006). Within the “fireshell” model for the Gamma-Ray Bursts (GRBs) we define a “canonical GRB” light curve with two sharply different components: the

Proper-GRB (P-GRB), emitted when the optically thick fireshell of electron-positron plasma originating the phenomenon reaches transparency, and the afterglow, emitted due to the collision between the remaining optically thin fireshell and the CircumBurst Medium (CBM). We here outline our “canonical GRB” scenario, which implies three different GRB classes: the “genuine” short GRBs, the “fake” or “disguised” short GRBs and the other (so-called “long”) GRBs. We also outline some implications for the theoretical interpretation of the Amati relation.

26. G. De Barros, M.G. Bernardini, C.L. Bianco, L. Caito, M.G. Dainotti, R. Guida, R. Ruffini; “Is GRB 050509b a genuine short GRB?”; in 2008 NANJING GAMMA-RAY BURST CONFERENCE; Proceedings of the 2008 Nanjing Gamma-Ray Burst Conference, Nanjing (China), June 2008, Y.-F. Huang, Z.-G. Dai, B. Zhang, Editors; AIP Conference Proceedings, 1065, 231 (2008).

Within our “fireshell” model we introduced a “canonical” GRB scenario which differentiates physically the “proper GRB” (P-GRB) emission when photons decouple, and the afterglow emission due to interaction of the accelerated baryons with the CircumBurst Medium (CBM). The ratio between energetics of the two components is ruled by the baryon loading of the fireshell. We here analyse the possibility that GRB050509b is the first case of a “genuine” short GRB the ones with smaller baryon loading. In such a case, the GRB050509b “prompt emission” would be dominated by the “proper GRB” and, moreover, the P-GRB total energy would be greater than the afterglow one. Our fit of the afterglow data and of the P-GRB energetics indicates that this source present the smallest baryon loading we ever encountered so far, being on the order of 10^{-4} .

27. G. De Barros, A.G. Aksenov, C.L. Bianco, R. Ruffini, G.V. Vereshchagin; “Fireshell versus Fireball scenarios”; in 2008 NANJING GAMMA-RAY BURST CONFERENCE; Proceedings of the 2008 Nanjing Gamma-Ray Burst Conference, Nanjing (China), June 2008, Y.-F. Huang, Z.-G. Dai, B. Zhang, Editors; AIP Conference Proceedings, 1065, 234 (2008).

We revisit Cavallo and Rees classification based on the analysis of initial conditions in electron-positron-photon plasma which appears suddenly around compact astrophysical objects and gives origin to GRBs. These initial conditions were recently studied in [1,2] by numerical integration of relativistic

Boltzmann equations with collision integrals, including binary and triple interactions between particles. The main conclusion is that the pair plasma in GRB sources quickly reaches thermal equilibrium well before its expansion starts. In light of this work we comment on each of the four scenarios proposed by Cavallo and Rees and discuss their applicability to describe evolution of GRB sources.

28. M.G. Bernardini, C.L. Bianco, L. Caito, M.G. Dainotti, R. Guida, R. Ruffini; “GRB970228 as a prototype for the class of GRBs with an initial spike-like emission”; in Proceedings of the Eleventh Marcel Grossmann Meeting on General Relativity, Berlin, Germany, July 2006, H. Kleinert, R.T. Jantzen, Editors; World Scientific, (Singapore, 2008).

We interpret GRB970228 prompt emission within our “canonical” GRB scenario, identifying the initial spikelike emission with the Proper-GRB (P-GRB) and the following bumps with the afterglow peak emission. Furthermore, we emphasize the necessity to consider the “canonical” GRB as a whole due to the highly non-linear nature of the model we applied.

29. M.G. Bernardini, C.L. Bianco, L. Caito, M.G. Dainotti, R. Guida, R. Ruffini; “GRB980425 and the puzzling URCA1 emission”; in Proceedings of the Eleventh Marcel Grossmann Meeting on General Relativity, Berlin, Germany, July 2006, H. Kleinert, R.T. Jantzen, Editors; World Scientific, (Singapore, 2008).

We applied our “fireshell” model to GRB980425 observational data, reproducing very satisfactorily its prompt emission. We use the results of our analysis to provide a possible interpretation for the X-ray emission of the source S1. The effect on the GRB analysis of the lack of data in the pre-Swift observations is also outlined.

30. C.L. Bianco, M.G. Bernardini, L. Caito, P. Chardonnet, M.G. Dainotti, F. Fraschetti, R. Guida, R. Ruffini, S.-S. Xue; “Theoretical interpretation of ‘long’ and ‘short’ GRBs”; in Proceedings of the Eleventh Marcel Grossmann Meeting on General Relativity, Berlin, Germany, July 2006, H. Kleinert, R.T. Jantzen, Editors; World Scientific, (Singapore, 2008).

Within the “fireshell” model we define a “canonical GRB” light curve with two sharply different components: the Proper-GRB (P-GRB), emitted when the optically thick fireshell of electron-positron plasma originating the phenomenon reaches transparency, and the afterglow, emitted due to the collision between

the remaining optically thin fireshell and the CircumBurst Medium (CBM). We here present the consequences of such a scenario on the theoretical interpretation of the nature of “long” and “short” GRBs.

31. C.L. Bianco, M.G. Bernardini, P. Chardonnet, F. Fraschetti, R. Ruffini, S.-S. Xue; “Theoretical interpretation of luminosity and spectral properties of GRB 031203”; in Proceedings of the Eleventh Marcel Grossmann Meeting on General Relativity, Berlin, Germany, July 2006, H. Kleinert, R.T. Jantzen, Editors; World Scientific, (Singapore, 2008).

We show how an emission endowed with an instantaneous thermal spectrum in the co-moving frame of the expanding fireshell can reproduce the time-integrated GRB observed non-thermal spectrum. An explicit example in the case of GRB 031203 is presented.

32. C.L. Bianco, R. Ruffini; “The ‘Fireshell’ model in the Swift era”; in Proceedings of the Eleventh Marcel Grossmann Meeting on General Relativity, Berlin, Germany, July 2006, H. Kleinert, R.T. Jantzen, Editors; World Scientific, (Singapore, 2008).

We here re-examine the validity of the constant-index power-law relation between the fireshell Lorentz gamma factor and its radial coordinate, usually adopted in the current Gamma-Ray Burst (GRB) literature on the grounds of an “ultrarelativistic” approximation. Such expressions are found to be mathematically correct but only approximately valid in a very limited range of the physical and astrophysical parameters and in an asymptotic regime which is reached only for a very short time, if any.

33. L. Caito, M.G. Bernardini, C.L. Bianco, M.G. Dainotti, R. Guida, R. Ruffini; “Theoretical interpretation of GRB011121”; in Proceedings of the Eleventh Marcel Grossmann Meeting on General Relativity, Berlin, Germany, July 2006, H. Kleinert, R.T. Jantzen, Editors; World Scientific, (Singapore, 2008).

GRB 011121, detected by the BeppoSAX satellite, is studied as a prototype to understand the presence of flares observed by Swift in the afterglow of many GRB sources. Detailed theoretical analysis of the GRB 011121 light curves in selected energy bands are presented and compared with observational data. An interpretation of the flare of this source is provided by the introduction of the three-dimensional structure of the CircumBurst Medium(CBM).

34. M.G. Dainotti, M.G. Bernardini, C.L. Bianco, L. Caito, R. Guida, R. Ruffini; “On GRB 060218 and the GRBs related to Supernovae Ib/c”; in Proceedings of the Eleventh Marcel Grossmann Meeting on General Relativity, Berlin, Germany, July 2006, H. Kleinert, R.T. Jantzen, Editors; World Scientific, (Singapore, 2008).

We study the Gamma-Ray Burst (GRB) 060218: a particularly close source at $z = 0.033$ with an extremely long duration, namely $T_{90} \sim 2000$ s, related to SN 2006aj. This source appears to be a very soft burst, with a peak in the spectrum at 4.9 keV, therefore interpreted as an X-Ray Flash (XRF) and it obeys to the Amati relation. We fit the X- and γ -ray observations by Swift of GRB 060218 in the 0.1150 keV energy band during the entire time of observations from 0 all the way to 106 s within a unified theoretical model. The details of our theoretical analysis have been recently published in a series of articles. The free parameters of the theory are only three, namely the total energy $E_{e^\pm}^{tot}$ of the e^\pm plasma, its baryon loading $B = M_B c^2 / E_{e^\pm}^{tot}$, as well as the CircumBurst Medium (CBM) distribution. We fit the entire light curve, including the prompt emission as an essential part of the afterglow. We recall that this value of the B parameter is the highest among the sources we have analyzed and it is very close to its absolute upper limit expected. We successfully make definite predictions about the spectral distribution in the early part of the light curve, exactly we derive the instantaneous photon number spectrum $N(E)$ and we show that although the spectrum in the co-moving frame of the expanding pulse is thermal, the shape of the final spectrum in the laboratory frame is clearly non thermal. In fact each single instantaneous spectrum is the result of an integration of thousands of thermal spectra over the corresponding EQuiTemporal Surfaces (EQTS). By our fit we show that there is no basic differences between XRFs and more general GRBs. They all originate from the collapse process to a black hole and their difference is due to the variability of the three basic parameters within the range of full applicability of the theory.

35. R. Guida, M.G. Bernardini, C.L. Bianco, L. Caito, M.G. Dainotti, R. Ruffini; “Theoretical interpretation of GRB060124”; in Proceedings of the Eleventh Marcel Grossmann Meeting on General Relativity, Berlin, Germany, July 2006, H. Kleinert, R.T. Jantzen, Editors; World Scientific, (Singapore, 2008).

We show the preliminary results of the application of our “fireshell” model to GRB060124. This source is very peculiar because it is the first event for which

both the prompt and the afterglow emission were observed simultaneously by the three Swift instruments: BAT (15 - 350 keV), XRT (0,2 - 10 keV) and UVOT (170 - 650 nm), due to the presence of a precursor ~ 570 s before the main burst. We analyze GRB060124 within our "canonical" GRB scenario, identifying the precursor with the P-GRB and the prompt emission with the afterglow peak emission. In this way we reproduce correctly the energetics of both these two components. We reproduce also the observed time delay between the precursor (P-GRB) and the main burst. The effect of such a time delay in our model will be discussed.

36. R. Ruffini, M.G. Bernardini, C.L. Bianco, L. Caito, P. Chardonnet, C. Cherubini, M.G. Dainotti, F. Frascetti, A. Geralico, R. Guida, B. Paticelli, M. Rotondo, J. Rueda Hernandez, G. Vereshchagin, S.-S. Xue; "Gamma-Ray Bursts"; in Proceedings of the Eleventh Marcel Grossmann Meeting on General Relativity, Berlin, Germany, July 2006, H. Kleinert, R.T. Jantzen, Editors; World Scientific, (Singapore, 2008).

We show by example how the uncoding of Gamma-Ray Bursts (GRBs) offers unprecedented possibilities to foster new knowledge in fundamental physics and in astrophysics. After recalling some of the classic work on vacuum polarization in uniform electric fields by Klein, Sauter, Heisenberg, Euler and Schwinger, we summarize some of the efforts to observe these effects in heavy ions and high energy ion collisions. We then turn to the theory of vacuum polarization around a Kerr-Newman black hole, leading to the extraction of the blackholic energy, to the concept of dyadosphere and dyadotorus, and to the creation of an electron-positron-photon plasma. We then present a new theoretical approach encompassing the physics of neutron stars and heavy nuclei. It is shown that configurations of nuclear matter in bulk with global charge neutrality can exist on macroscopic scales and with electric fields close to the critical value near their surfaces. These configurations may represent an initial condition for the process of gravitational collapse, leading to the creation of an electron-positron-photon plasma: the basic self-accelerating system explaining both the energetics and the high energy Lorentz factor observed in GRBs. We then turn to recall the two basic interpretational paradigms of our GRB model: 1) the Relative Space-Time Transformation (RSTT) paradigm and 2) the Interpretation of the Burst Structure (IBS) paradigm. These paradigms lead to a "canonical" GRB light curve formed from two different components: a Proper-GRB (P-GRB) and an extended afterglow comprising a raising part, a peak, and a decaying tail. When the P-GRB is energetically predominant

we have a “genuine” short GRB, while when the afterglow is energetically predominant we have a so-called long GRB or a “fake” short GRB. We compare and contrast the description of the relativistic expansion of the electron-positron plasma within our approach and within the other ones in the current literature. We then turn to the special role of the baryon loading in discriminating between “genuine” short and long or “fake” short GRBs and to the special role of GRB 991216 to illustrate for the first time the “canonical” GRB bolometric light curve. We then propose a spectral analysis of GRBs, and proceed to some applications: GRB 031203, the first spectral analysis, GRB 050315, the first complete light curve fitting, GRB 060218, the first evidence for a critical value of the baryon loading, GRB 970228, the appearance of “fake” short GRBs. We finally turn to the GRB-Supernova Time Sequence (GSTS) paradigm: the concept of induced gravitational collapse. We illustrate this paradigm by the systems GRB 980425 / SN 1998bw, GRB 030329 / SN 2003dh, GRB 031203 / SN 2003lw, GRB 060218 / SN 2006aj, and we present the enigma of the URCA sources. We then present some general conclusions.

37. R. Ruffini, A.G. Aksenov, M.G. Bernardini, C.L. Bianco, L. Caito, M.G. Dainotti, G. De Barros, R. Guida, G. Vereshchagin, S.-S. Xue; “The canonical Gamma-Ray Bursts: long, ‘fake’-‘disguised’ and ‘genuine’ short bursts; in PROBING STELLAR POPULATIONS OUT TO THE DISTANT UNIVERSE: CEFALU 2008, Proceedings of the International Conference; Cefal (Italy), September 2008, G. Giobbi, A. Tornambe, G. Raimondo, M. Limongi, L. A. Antonelli, N. Menci, E. Brocato, Editors; AIP Conference Proceedings, 1111, 325 (2009).

The Gamma-Ray Bursts (GRBs) offer the unprecedented opportunity to observe for the first time the black-holic energy extracted by the vacuum polarization during the process of gravitational collapse to a black hole leading to the formation of an electron-positron plasma. The uniqueness of the Kerr-Newman black hole implies that very different processes originating from the gravitational collapse a) of a single star in a binary system induced by the companion, or b) of two neutron stars, or c) of a neutron star and a white dwarf, do lead to the same structure for the observed GRB. The recent progress of the numerical integration of the relativistic Boltzmann equations with collision integrals including 2-body and 3-body interactions between the particles offer a powerful conceptual tool in order to differentiate the traditional “fireball” picture, an expanding hot cavity considered by Cavallo and Rees, as opposed to the “fireshell” model, composed of an internally cold shell of relativistically

expanding electron-positron-baryon plasma. The analysis of the fireshell naturally leads to a canonical GRB composed of a proper-GRB and an extended afterglow. By recalling the three interpretational paradigms for GRBs we show how the fireshell model leads to an understanding of the GRB structure and to an alternative classification of short and long GRBs.

38. M.G. Bernardini, M.G. Dainotti, C.L. Bianco, L. Caito, R. Guida, R. Ruffini; "Prompt emission and X-ray flares: the case of GRB 060607 A"; in PROBING STELLAR POPULATIONS OUT TO THE DISTANT UNIVERSE: CEFALU 2008, Proceedings of the International Conference; Cefal (Italy), September 2008, G. Giobbi, A. Tornambe, G. Raimondo, M. Limongi, L. A. Antonelli, N. Menci, E. Brocato, Editors; AIP Conference Proceedings, 1111, 383 (2009).

GRB 060607A is a very distant and energetic event. Its main peculiarity is that the peak of the near-infrared (NIR) afterglow has been observed with the REM robotic telescope, allowing to estimate the initial Lorentz gamma factor within the fireball forward shock model. We analyze GRB 060607A within the fireshell model. The initial Lorentz gamma factor of the fireshell can be obtained adopting the exact solutions of its equations of motion, dealing only with the BAT and XRT observations, that are the basic contribution to the afterglow emission, up to a distance from the progenitor $r \sim 10^{18}$ cm. According to the "canonical GRB" scenario we interpret the whole prompt emission as the peak of the afterglow emission, and we show that the observed temporal variability of the prompt emission can be produced by the interaction of the fireshell with overdense CircumBurst Medium (CBM) clumps. This is indeed the case also of the X-ray flares which are present in the early phases of the afterglow light curve.

39. C.L. Bianco, M.G. Bernardini, L. Caito, M.G. Dainotti, R. Guida, R. Ruffini; "The 'fireshell' model and the 'canonical GRB' scenario. Implications for the Amati relation"; in PROBING STELLAR POPULATIONS OUT TO THE DISTANT UNIVERSE: CEFALU 2008, Proceedings of the International Conference; Cefal (Italy), September 2008, G. Giobbi, A. Tornambe, G. Raimondo, M. Limongi, L. A. Antonelli, N. Menci, E. Brocato, Editors; AIP Conference Proceedings, 1111, 587 (2009).

Within the "fireshell" model for GRBs we define a "canonical GRB" light curve with two sharply different components: the Proper-GRB (P-GRB), emitted when the optically thick fireshell reaches transparency, and the extended afterglow,

emitted due to the collision between the remaining optically thin fireshell and the CircumBurst Medium (CBM). We here outline our “canonical GRB” scenario, which implies three different GRB classes: the “genuine” short GRBs, the “fake” or “disguised” short GRBs and the other (so-called “long”) GRBs. We will also outline the corresponding implications for the Amati relation, which are opening its use for cosmology.

40. R. Ruffini, A.G. Aksenov, M.G. Bernardini, C.L. Bianco, L. Caito, P. Chardonnet, M.G. Dainotti, G. De Barros, R. Guida, L. Izzo, B. Patricelli, L.J. Rangel Lemos, M. Rotondo, J.A. Rueda Hernandez, G. Vereshchagin, S.-S. Xue; “The Blackholic energy and the canonical Gamma-Ray Burst IV: the ‘long’, ‘genuine short’ and ‘fake disguised short’ GRBs”; in Proceedings of the XIIIth Brazilian School on Cosmology and Gravitation, Mangaratiba, Rio de Janeiro (Brazil), July-August 2008, M. Novello, S.E. Perez Bergliaffa, Editors; AIP Conference Proceedings, 1132, 199 (2009).

We report some recent developments in the understanding of GRBs based on the theoretical framework of the “fireshell” model, already presented in the last three editions of the “Brazilian School of Cosmology and Gravitation”. After recalling the basic features of the “fireshell model”, we emphasize the following novel results: 1) the interpretation of the X-ray flares in GRB afterglows as due to the interaction of the optically thin fireshell with isolated clouds in the CircumBurst Medium (CBM); 2) an interpretation as “fake - disguised” short GRBs of the GRBs belonging to the class identified by Norris & Bonnell; we present two prototypes, GRB 970228 and GRB 060614; both these cases are consistent with an origin from the final coalescence of a binary system in the halo of their host galaxies with particularly low CBM density $n_{cbm} \sim 10^{-3}$ particles/cm³; 3) the first attempt to study a genuine short GRB with the analysis of GRB 050509B, that reveals indeed still an open question; 4) the interpretation of the GRB-SN association in the case of GRB 060218 via the “induced gravitational collapse” process; 5) a first attempt to understand the nature of the “Amati relation”, a phenomenological correlation between the isotropic-equivalent radiated energy of the prompt emission E_{iso} with the cosmological rest-frame νF_{ν} spectrum peak energy $E_{p,i}$. In addition, recent progress on the thermalization of the electron-positron plasma close to their formation phase, as well as the structure of the electrodynamics of Kerr-Newman Black Holes are presented. An outlook for possible explanation of high-energy phenomena in GRBs to be expected from the AGILE and the Fermi satellites are

discussed. As an example of high energy process, the work by Enrico Fermi dealing with ultrarelativistic collisions is examined. It is clear that all the GRB physics points to the existence of overcritical electro-dynamical fields. In this sense we present some progresses on a unified approach to heavy nuclei and neutron stars cores, which leads to the existence of overcritical fields under the neutron star crust.

41. A.G. Aksenov, M.G. Bernardini, C.L. Bianco, L. Caito, C. Cherubini, G. De Barros, A. Geralico, L. Izzo, F.A. Massucci, B. Patricelli, M. Rotonondo, J.A. Rueda Hernandez, R. Ruffini, G. Vereshchagin, S.-S. Xue; "The fireshell model for Gamma-Ray Bursts"; in *The Shocking Universe, Proceedings of the conference held in Venice (Italy), September 2009*, G. Chincarini, P. D'Avanzo, R. Margutti, R. Salvaterra, Editors; *SIF Conference Proceedings*, 102, 451 (2010).

The fireshell model for GRBs is briefly outlined, and the currently ongoing developments are summarized.

42. M.G. Bernardini, C.L. Bianco, L. Caito, L. Izzo, B. Patricelli, R. Ruffini; "The end of the prompt emission within the fireshell model"; in *The Shocking Universe, Proceedings of the conference held in Venice (Italy), September 2009*, G. Chincarini, P. D'Avanzo, R. Margutti, R. Salvaterra, Editors; *SIF Conference Proceedings*, 102, 489 (2010)

The shallow decay emission, revealed by the Swift satellite in the X-ray afterglow of a good sample of bursts, is a puzzle. Within the fireshell model it has been recently proposed an alternative explanation: if we assume that after the prompt phase the system has a range of Lorentz factors, the plateau phase is simply the product of the injection of slower material into the fireshell. This injection produces a modification both in the dynamics of the fireshell and in the spectrum of the emitted radiation. We postulate that this spread in the fireshell Lorentz factor occurs when the fireshell becomes transparent and do not depend on a prolonged activity of the central engine. The aim of this paper is to characterize dynamically the system in order to understand the nature of that material.

43. L. Izzo, M.G. Bernardini, C.L. Bianco, L. Caito, B. Patricelli, R. Ruffini; "GRB 090423 in the fireshell scenario"; in *The Shocking Universe, Proceedings of the conference held in Venice (Italy), September 2009*, G.

Chincarini, P. D'Avanzo, R. Margutti, R. Salvaterra, Editors; SIF Conference Proceedings, 102, 537 (2010).

44. B. Patricelli, M.G. Bernardini, C.L. Bianco, L. Caito, L. Izzo, R. Ruffini, G. Vereshchagin; "A new spectral energy distribution of photons in the fireshell model of GRBs"; in *The Shocking Universe*, Proceedings of the conference held in Venice (Italy), September 2009, G. Chincarini, P. D'Avanzo, R. Margutti, R. Salvaterra, Editors; SIF Conference Proceedings, 102, 559 (2010).

The fireshell model of Gamma Ray Bursts (GRBs) postulates that the emission process is thermal in the comoving frame of the fireshell, but this is just a first approximation. We investigate a different spectrum of photons in the comoving frame in order to better reproduce the observed spectral properties of GRB prompt emission. We introduce a modified thermal spectrum whose low energy slope depends on an index α , left as a free parameter. We test it by comparing the numerical simulations with observed BAT spectra integrated over different intervals of time. We find that the observational data can be correctly reproduced by assuming $\alpha = -1.8$.

45. C.L. Bianco, M.G. Bernardini, L. Caito, G. De Barros, L. Izzo, B. Patricelli, R. Ruffini; "Disguised Short Bursts and the Amati Relation"; in *Deciphering the ancient universe with Gamma-Ray Bursts*, Proceedings of the conference held in Kyoto (Japan), April 2010, N. Kawai, S. Nagataki, Editors; AIP Conference Proceedings, 1279, 299 (2010).

The class of "Disguised short" GRBs implied by the fireshell scenario is presented, with special emphasis on the implications for the Amati relation.

46. L. Izzo, M.G. Bernardini, C.L. Bianco, L. Caito, B. Patricelli, L.J. Rangel Lemos, R. Ruffini; "On GRB 080916C and GRB 090902B observed by the Fermi satellite"; in *Deciphering the ancient universe with Gamma-Ray Bursts*, Proceedings of the conference held in Kyoto (Japan), April 2010, N. Kawai, S. Nagataki, Editors; AIP Conference Proceedings, 1279, 343 (2010).

We propose a possible explanation, in the context of the Fireshell scenario, for the high-energy emission observed in GRB 080916C and GRB 090902B. The physical process underlying this emission consists mainly in the interaction of the baryon in the Fireshell with some high-density region around the burst

site. Moreover we associate the observed delay of the onset of the high-energy emission as due to the P-GRB emission.

47. B. Patricelli, M.G. Bernardini, C.L. Bianco, L. Caito, G. De Barros, L. Izzo, R. Ruffini; "Black Holes in Gamma Ray Bursts"; in *Deciphering the ancient universe with Gamma-Ray Bursts*, Proceedings of the conference held in Kyoto (Japan), April 2010, N. Kawai, S. Nagataki, Editors; AIP Conference Proceedings, 1279, 406 (2010).

Within the fireshell model, Gamma Ray Bursts (GRBs) originate from an optically thick e^\pm plasma created by vacuum polarization process during the formation of a Black Hole (BH). Here we briefly recall the basic features of this model, then we show how it is possible to interpret GRB observational properties within it. In particular we present, as a specific example, the analysis of GRB 050904 observations of the prompt emission light curve and spectrum in the Swift BAT energy band (15-150 keV).

48. M.G. Bernardini, C.L. Bianco, L. Caito, M.G. Dainotti, R. Guida, R. Ruffini; "The GRB classification within the "fireshell" model: short, long and "fake" short GRBs"; in *Proceedings of the 3rd Stueckelberg Workshop on Relativistic Field Theories*, Pescara, Italy, July 2008, N. Carlevaro, R. Ruffini, G.V. Vereshchagin, Editors; Cambridge Scientific Publishers, (UK, 2011).
49. C.L. Bianco, M.G. Bernardini, L. Caito, M.G. Dainotti, R. Guida, R. Ruffini, G.V. Vereshchagin, S.-S. Xue; "Equations of motion of the "fireshell""; in *Proceedings of the 3rd Stueckelberg Workshop on Relativistic Field Theories*, Pescara, Italy, July 2008, N. Carlevaro, R. Ruffini, G.V. Vereshchagin, Editors; Cambridge Scientific Publishers, (UK, 2011).
50. L. Caito, M.G. Bernardini, C.L. Bianco, M.G. Dainotti, R. Guida, R. Ruffini; "GRB 060614: another example of "fake" short burst from a merging binary system"; in *Proceedings of the 3rd Stueckelberg Workshop on Relativistic Field Theories*, Pescara, Italy, July 2008, N. Carlevaro, R. Ruffini, G.V. Vereshchagin, Editors; Cambridge Scientific Publishers, (UK, 2011).
51. G. De Barros, M.G. Bernardini, C.L. Bianco, L. Caito, R. Guida, R. Ruffini; "Analysis of GRB 050509b"; in *Proceedings of the 3rd Stueckelberg Workshop on Relativistic Field Theories*, Pescara, Italy, July 2008, N. Carle-

- evaro, R. Ruffini, G.V. Vereshchagin, Editors; Cambridge Scientific Publishers, (UK, 2011).
52. R. Ruffini, L. Izzo, A.V. Penacchioni, C.L. Bianco, L. Caito, S.K. Chakrabarti, A. Nandi; "GRB 090618: a possible case of multiple GRB?"; in Proceedings of the 25th Texas Symposium on Relativistic Astrophysics, held in Heidelberg (Germany), December 2010, F.M. Rieger, C. van Eldik, W. Hofmann, Editors; PoS(Texas2010), 101.
53. L.J. Rangel Lemos, C.L. Bianco, H.J. Mosquera Cuesta, J.A. Rueda, R. Ruffini; "Luminosity function of BATSE GRBs dominated by extended afterglow"; in Proceedings of the 25th Texas Symposium on Relativistic Astrophysics, held in Heidelberg (Germany), December 2010, F.M. Rieger, C. van Eldik, W. Hofmann, Editors; PoS(Texas2010), 204.
54. R. Ruffini, A.G. Aksenov, M.G. Bernardini, C.L. Bianco, L. Caito, P. Chardonnet, M.G. Dainotti, G. De Barros, R. Guida, L. Izzo, B. Patricelli, L.J. Rangel Lemos, M. Rotondo, J.A. Rueda Hernandez, G. Vereshchagin, She-Sheng Xue; "Black Holes Energetics and GRBs"; in The Sun, the Stars, the Universe and General Relativity: Proceedings of Sobral 2009; S.E. Perez Bergliaffa, M. Novello, R. Ruffini, Editors; Cambridge Scientific Publishers (UK, 2011).
55. C.L. Bianco, L. Amati, M.G. Bernardini, L. Caito, G. De Barros, L. Izzo, B. Patricelli, R. Ruffini; "The class of 'disguised' short GRBs and its implications for the Amati relation"; in GRBs as probes - from the progenitors environment to the high redshift Universe, Proceedings of the conference held in Como (Italy), May 2011, S. Campana, P. D'Avanzo, A. Melandri, Editors; Mem. S.A.It. Suppl., 21, 139 (2012).
56. A.V. Penacchioni, R. Ruffini, L. Izzo, M. Muccino, C.L. Bianco, L. Caito, B. Patricelli; "Evidences for a double component in the emission of GRB 101023"; in GRBs as probes - from the progenitors environment to the high redshift Universe, Proceedings of the conference held in Como (Italy), May 2011, S. Campana, P. D'Avanzo, A. Melandri, Editors; Mem. S.A.It. Suppl., 21, 230 (2012).
57. M.G. Bernardini, C.L. Bianco, L. Caito, L. Izzo, B. Patricelli, R. Ruffini; "The X-Ray Flares of GRB 060607A within the Fireshell Model"; in Proceedings of the Twelfth Marcel Grossmann Meeting on General Relativ-

- ity, Paris, France, July 2009, T. Damour, R.T. Jantzen, R. Ruffini, Editors; World Scientific, (Singapore, 2012).
58. L. Izzo, M.G. Bernardini, C.L. Bianco, L. Caito, B. Patricelli, R. Ruffini; "GRB 090423 in the Fireshell Scenario: A Canonical GRB at Redshift 8.2"; in Proceedings of the Twelfth Marcel Grossmann Meeting on General Relativity, Paris, France, July 2009, T. Damour, R.T. Jantzen, R. Ruffini, Editors; World Scientific, (Singapore, 2012).
59. B. Patricelli, M.G. Bernardini, C.L. Bianco, L. Caito, L. Izzo, R. Ruffini, G.V. Vereshchagin; "A New Spectral Energy Distribution of Photons in the Fireshell Model of GRBs"; in Proceedings of the Twelfth Marcel Grossmann Meeting on General Relativity, Paris, France, July 2009, T. Damour, R.T. Jantzen, R. Ruffini, Editors; World Scientific, (Singapore, 2012).
60. C.L. Bianco, M.G. Bernardini, L. Caito, G. De Barros, L. Izzo, M. Muccino, B. Patricelli, A.V. Penacchioni, G.B. Pisani, R. Ruffini; "Needs for a new GRB classification following the fireshell model: genuine short, disguised short and long GRBs"; in Proceedings of the Gamma-Ray Bursts 2012 Conference, held in Munich (Germany), May 2012, A. Rau, J. Greiner, Editors; PoS(GRB 2012), 043.
61. A.V. Penacchioni, G.B. Pisani, R. Ruffini, C.L. Bianco, L. Izzo, M. Muccino; "The proto-black hole concept in GRB 101023 and its possible extension to GRB 110709B"; in Proceedings of the Gamma-Ray Bursts 2012 Conference, held in Munich (Germany), May 2012, A. Rau, J. Greiner, Editors; PoS(GRB 2012), 042.
62. B. Patricelli, M.G. Bernardini, C.L. Bianco, L. Caito, L. Izzo, R. Ruffini; "GRB 050904: The study of a high redshift GRB within the Fireshell Model"; in Proceedings of the Twelfth Marcel Grossmann Meeting on General Relativity, Paris, France, July 2009, T. Damour, R.T. Jantzen, R. Ruffini, Editors; World Scientific, (Singapore, 2012).
63. L. Izzo, G.B. Pisani, M. Muccino, J.A. Rueda, Y.Wang, C.L. Bianco, A.V. Penacchioni, R. Ruffini; "A common behavior in the late X-ray afterglow of energetic GRB-SN systems"; EAS Publications Series, Volume 61, 595-597 (2013).

64. R. Ruffini; “Black Holes, Supernovae and Gamma Ray Bursts”; in Proceedings of the Thirteenth Marcel Grossmann Meeting on General Relativity, Stockholm, Sweden, July 2012, R.T. Jantzen, K. Rosquist, R. Ruffini, Editors; World Scientific, (Singapore, 2015).
65. M. Muccino, R. Ruffini, C.L. Bianco, L. Izzo, A.V. Penacchioni, G.B. Pisani; “GRB 090227B: The missing link between the genuine short and long GRBs”; in Proceedings of the Thirteenth Marcel Grossmann Meeting on General Relativity, Stockholm, Sweden, July 2012, R.T. Jantzen, K. Rosquist, R. Ruffini, Editors; World Scientific, (Singapore, 2015).
66. A.V. Penacchioni, R. Ruffini, C.L. Bianco, L. Izzo, M. Muccino, G.B. Pisani, J.A. Rueda; “The family of the Induced Gravitational Collapse scenario: The case of GRB 110709B”; in Proceedings of the Thirteenth Marcel Grossmann Meeting on General Relativity, Stockholm, Sweden, July 2012, R.T. Jantzen, K. Rosquist, R. Ruffini, Editors; World Scientific, (Singapore, 2015).
67. A.V. Penacchioni, R. Ruffini, C.L. Bianco, L. Izzo, M. Muccino, G.B. Pisani; “GRB 111228, analysis within the Induced Gravitational Collapse scenario and association with a supernova”; in Proceedings of the Thirteenth Marcel Grossmann Meeting on General Relativity, Stockholm, Sweden, July 2012, R.T. Jantzen, K. Rosquist, R. Ruffini, Editors; World Scientific, (Singapore, 2015).
68. G.B. Pisani, L. Izzo, R. Ruffini, C.L. Bianco, M. Muccino, A.V. Penacchioni, J.A. Rueda, Y. Wang; “On a novel distance indicator for Gamma-Ray Bursts associated with supernovae”; in Proceedings of the Thirteenth Marcel Grossmann Meeting on General Relativity, Stockholm, Sweden, July 2012, R.T. Jantzen, K. Rosquist, R. Ruffini, Editors; World Scientific, (Singapore, 2015).
69. M. Muccino, R. Ruffini, C.L. Bianco, L. Izzo, A.V. Penacchioni, G.B. Pisani; “GRB 090510, explosion of a GRB in the highest circumburst medium even inferred: a disguised short GRB”; in Proceedings of the Thirteenth Marcel Grossmann Meeting on General Relativity, Stockholm, Sweden, July 2012, R.T. Jantzen, K. Rosquist, R. Ruffini, Editors; World Scientific, (Singapore, 2015).

70. L. Izzo, G.B. Pisani, M. Muccino, R. Ruffini, C.L. Bianco, M. Enderli, Y. Wang; “Hints for a physically based GRB distance indicator”; in Proceedings of the Thirteenth Marcel Grossmann Meeting on General Relativity, Stockholm, Sweden, July 2012, R.T. Jantzen, K. Rosquist, R. Ruffini, Editors; World Scientific, (Singapore, 2015).

GRB 130427A AND SN 2013cq: A MULTI-WAVELENGTH ANALYSIS OF AN INDUCED GRAVITATIONAL COLLAPSE EVENT

R. RUFFINI^{1,2,3,4}, Y. WANG^{1,2}, M. ENDERLI^{1,3}, M. MUCCINO^{1,2}, M. KOVACEVIC^{1,3}, C. L. BIANCO^{1,2},

A. V. PENACCHIONI⁴, G. B. PISANI^{1,3}, AND J. A. RUEDA^{1,2,4}

¹ Dip. di Fisica and ICRA, Sapienza Università di Roma, Piazzale Aldo Moro 5, I-00185 Rome, Italy

² ICRA Net, Piazza della Repubblica 10, I-65122 Pescara, Italy; yu.wang@icranet.org

³ Université de Nice Sophia Antipolis, CEDEX 2, Grand Château Parc Valrose, Nice, France

⁴ ICRA Net-Rio, Centro Brasileiro de Pesquisas Físicas, Rua Dr. Xavier Sigaud 150, Rio de Janeiro, RJ 22290-180, Brazil

Received 2014 March 7; accepted 2014 October 17; published 2014 December 11

ABSTRACT

We performed a data analysis of the observations by the *Swift*, *NuStar*, and *Fermi* satellites in order to probe the induced gravitational collapse (IGC) paradigm for gamma-ray bursts (GRBs) associated with supernovae (SNe) in the terra incognita of GRB 130427A. We compare our data analysis with those in the literature. We have verified that GRB 130427A conforms to the IGC paradigm by examining the power law behavior of the luminosity in the early 10^4 s of the XRT observations. This has led to the identification of the four different episodes of the binary driven hypernovae (BdHNe) and to the prediction, on 2013 May 2, of the occurrence of SN 2013cq, which was also observed in the optical band on 2013 May 13. The exceptional quality of the data has allowed the identification of novel features in *Episode 3* including: (1) the confirmation and the extension of the existence of the recently discovered nested structure in the late X-ray luminosity in GRB 130427A, as well as the identification of a spiky structure at 10^2 s in the cosmological rest-frame of the source; (2) a power law emission of the GeV luminosity light curve and its onset at the end of *Episode 2*; and (3) different Lorentz Γ factors for the emitting regions of the X-ray and GeV emissions in this *Episode 3*. These results make it possible to test the details of the physical and astrophysical regimes at work in the BdHNe: (1) a newly born neutron star and the supernova ejecta, originating in *Episode 1*; (2) a newly formed black hole originating in *Episode 2*; and (3) the possible interaction among these components, observable in the standard features of *Episode 3*.

Key words: black hole physics – gamma-ray burst: general – nuclear reactions, nucleosynthesis, abundances – stars: neutron – supernovae: general

1. INTRODUCTION AND SUMMARY OF PREVIOUS RESULTS

That some long gamma-ray bursts (GRBs) and supernovae (SNe) can occur almost simultaneously has been known since the early observations of GRB 980425/SN 1998bw (Galama et al. 1998; Pian et al. 2000). This association of a GRB and an SN occurs most commonly in a family of less energetic long GRBs with the following characteristics: (1) isotropic energies E_{iso} in the range of 10^{49} – 10^{52} erg (Guetta & Della Valle 2007); (2) a soft spectrum with rest-frame peak energy $E_{p,i} < 100$ keV, although the instruments are sensitive up to GeV; and (3) supernova emissions observable up to a cosmological distance $z < 1$. Hereafter we will refer to this family as *family 1*. This is well recognized in the literature; see, e.g., (Maselli et al. 2014).

An alternative family of highly energetic long GRBs that are associated with SNe and that has a much more complex structure exists. Their characteristics are: (1) E_{iso} is in the range 10^{52} – 10^{54} erg; (2) they present multiple components in their spectra and in their overall luminosity distribution, ranging from X-ray to γ -ray all the way to GeV emission. They have peak energies from 100 keV to some MeV; (3) in view of their large energetics, their observation extends to the entire universe all the way up to $z = 8.2$ (Ruffini et al. 2014b). Hereafter we will refer to this family as *family 2*.

There was some doubt that SNe may be associated with very bright long GRBs. Naive energetic arguments said it was unlikely for an SN to be in a powerful GRB within the single star collapse model (see e.g., Maselli et al. 2014).

For some years the issue of the coincidence of very energetic GRBs with SN has represented an authentic terra incognita. It is critical to clarify whether this association of GRBs and SNe is only accidental or if it is necessary, independent of their energetics. Of the 104 long GRBs with known redshift $z < 1$, 19 GRBs associated with SNe belonging to the *family 2* were observed (Kovacevic et al. 2014) before 2014 June, and GRB 130427A, with isotropic energy $E_{\text{iso}} \simeq 10^{54}$ erg, is the most energetic one so far.

In Ruffini et al. (2001, 2008) we introduced the paradigm of induced gravitational collapse (IGC) to explain the astrophysical reasons for the association of GRBs with supernovae. This paradigm indicates that all long GRBs, by norm, must be associated with SNe. The IGC paradigm differs from the traditional collapsar–fireball paradigm (see, e.g., Piran 2005 and references therein). In the collapsar–fireball model, the GRB process is described by a single episode: (1) it is assumed to originate in a “collapsar” (Woosley 1993), (2) the spectral and luminosity analysis is typically time integrated over the entire T_{90} (see e.g., Tavani 1998), and (3) the description of the afterglow is dominated by a single ultra-relativistic jetted emission (see, e.g., in Rhoads 1999; van Eerten et al. 2010; van Eerten & MacFadyen 2012; Nava et al. 2013). In contrast, the IGC paradigm considers a multi-component system, similar to those described by S -matrix in particle physics, as shown in Figure 1: (1) the in-states are represented by a binary system formed by an FeCO core, which is very close to the onset of an SN event and a tightly bound companion neutron star (NS; Ruffini et al. 2008; Rueda & Ruffini 2012; Izzo et al. 2012). The out-states are the creation of a new NS (ν -NS) and black hole

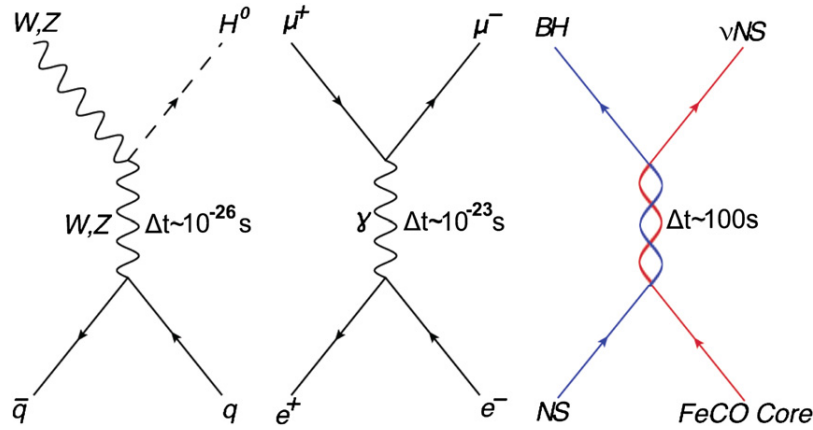


Figure 1. Three different matrices in fundamental physics. The first is the quark matrix leading to a Higgs boson. The middle is the classical electron–positron pair matrix, generating a muon and anti-muon pair. The third matrix is the most recent and it is considered in the present work. Δt is the duration of the intermediate state.

(BH). In the case of particle physics, the S -matrix describes a virtual phenomenon occurring on timescales of 10^{-26} s (Aad et al. 2012, $q\bar{q} \rightarrow WZH^0$) and 10^{-23} s (Bernardini 2004, $e^+e^- \rightarrow \mu^+\mu^-$). In the astrophysical case considered here, the cosmic matrix (C -matrix) describes a real event occurring on timescale ~ 200 s, which is still a very short time when compared to traditional astrophysical timescales. Following the accretion of the SN ejecta onto the companion NS binary, a BH is expected to be created, giving rise to the GRB. (2) Special attention is given to the analysis of the instantaneous spectra in the optical, X-ray, γ -ray, and GeV energy range (as exemplified in this article). (3) Four different episodes are identifiable in the overall emission, each with marked differences in the values of their Lorentz Γ factors (Ruffini et al. 2014c). The possible relevance of a binary system in the explanation of GRBs was already mentioned by Fryer et al. (1999) and Broderick (2005), but the binaries were a trigger to the traditional collapsar model.

The opportunity to probe the IGC paradigm (Izzo et al. 2012) comes from the prototypical source GRB 090618, which is a member of *family 2*. This source has extremely high energetics (i.e., $E_{\text{iso}} = 2.7 \times 10^{53}$ erg), is at a relatively close distance (i.e., $z = 0.54$), and has coverage in all existing γ , X-ray, and optical observatories.

The following results have been obtained (see visualized spacetime diagram in Figure 2):

1. *Episode 1*, which corresponds to the onset of the SN and the accretion process onto the companion NS, was identified in the early 1950 s, with a thermal plus power law component in the spectra (see Izzo et al. 2012, Figure 16), as well as a temporal evolution of the radius of the emitting region expanding from 10^9 cm to 7×10^9 cm (see Izzo et al. 2012, Figure 18). This leads to a precise determination of its overall energetics of 4×10^{52} erg.
2. *Episode 2*, with the GRB emission, follows the onset of gravitational collapse and the BH formation. It was also clearly identified with the following characteristic parameters: an isotropic energy $E_{\text{iso}} = 2.49 \times 10^{53}$, baryon loading $B = 1.98 \times 10^{-3}$, Lorentz factor $\Gamma = 495$ (see Izzo et al. 2012, Figure 4), and peak energy $E_{p,i} = 193$ keV. The average number density of the circumburst medium (CBM) is $\langle n_{\text{CBM}} \rangle = 0.6 \text{ cm}^{-3}$. The characteristic masses of each CBM cloud are of the order $\sim 10^{22} - 10^{24}$ g, at 10^{16} cm in radii (see Izzo et al. 2012, Figure 10).
3. *Episode 3* of GRB 090618, detected by *Swift*-XRT, starts at 150 s after the burst trigger and continues all the way

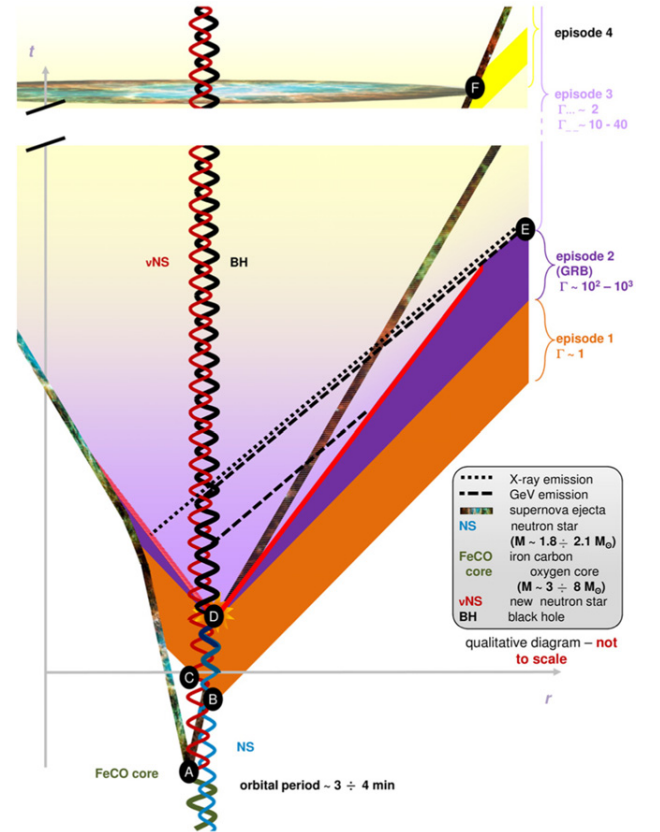


Figure 2. IGC spacetime diagram (not in scale) illustrates four episodes of the IGC paradigm: the nonrelativistic *Episode 1* ($\Gamma \simeq 1$), the relativistic motion of *Episode 2* ($\Gamma \simeq 10^2 \sim 10^3$), the mildly relativistic *Episode 3* ($\Gamma \simeq 2$), and nonrelativistic *Episode 4* ($\Gamma \simeq 1$). There is initially a binary system composed of a massive star (yellow thick line) and a neutron star (blue line). The massive star evolves and explodes as a SN at point A, forming a ν NS (red line). The companion NS accretes the supernova ejecta starting from point B, and collapses into a black hole (black line) at point D; this period from point B to point D is defined as *Episode 1*. Point D is the beginning of *Episode 2*, which is caused by the collision of GRB outflow and interstellar filaments. At point E, *Episode 2* ends and *Episode 3* starts, lasting until the optical signal of the supernova emerges at point F, where *Episode 4* starts. (Credit to M. Enderli for drawing this visualized spacetime diagram.)

up to 10^6 s. It consists of three different parts (Nousek et al. 2006): a first very steep decay; a shallower decay, the plateau; and a final steeper decay with a fixed power law index. It soon became clear that *Episode 3*, which was

previously interpreted in the traditional approach as part of the GRB afterglow (Piran 2005; Rhoads 1999; van Eerten et al. 2010; van Eerten & MacFadyen 2012; Nava et al. 2013), appeared to be the seat of a set of novel independent processes occurring after the end of the GRB emission and preceding the optical observation of the SN, which we indicated as *Episode 4*.

Progress has recently been made in the analysis of *Episode 1*. It is characterized by the explosion of the FeCO core, followed by the hypercritical accretion onto the NS, which leads to the NS reaching critical mass and consequently its induced gravitational collapse to a BH. The hypercritical accretion of the SN ejecta onto the NS has been estimated using the Bondi–Hoyle–Lyttleton formalism to be $10^{-2} M_{\odot} \text{ s}^{-1}$; here M_{\odot} is the solar mass (Bondi & Hoyle 1944; Bondi 1952) (see, e.g., in Rueda & Ruffini 2012). The inflowing material shocks as it piles up onto the NS, producing a compressed layer on top of the NS (see, e.g., Fryer et al. 1996). As this compressed layer becomes sufficiently hot, it triggers the emission of neutrinos that cool the infalling material, allowing it to be accreted into the NS (Zel’dovich et al. 1972; Ruffini & Wilson 1975; Ruffini et al. 1999, 2000; Fryer et al. 1996, 1999). Recently Fryer et al. (2014) presented significant progress in understanding the underlying physical phenomena in the aforementioned hypercritical accretion process of the supernova ejecta into the binary companion neutron star (Ruffini et al. 2008; Rueda & Ruffini 2012). The new treatment, based on the two-dimensional cylindrical geometry smooth particle hydrodynamics code, has numerically simulated the process of hypercritical accretion—the classical Bondi–Hoyle regimes—in the specific case of the IGC paradigm, and led to the first astrophysical application of the neutrino production process considered in Zel’dovich et al. (1972) and in Ruffini & Wilson (1975; see e.g., in R. Ruffini et al., presentation in the Zeldovich-100 meeting)⁵. Indeed the fundamental role of neutrinos’ emission allows the accretion rate process to increase the mass of the binary companion star to its critical value, which leads to the black hole formation giving rise to the GRB in *Episode 2*. These results confirm and quantify the general considerations presented in Rueda & Ruffini (2012).

In *Episode 2* all technical, numerical, and basic physical processes have been tested in the literature, and the fireshell model is now routinely applied to all GRBs (see, e.g., GRB 101023 in Penacchioni et al. 2012 and GRB 110709B in Penacchioni et al. 2013).

The main aim of this paper is dedicated to a deeper understanding of the physical and astrophysical process present in *Episode 3*:

1. to give evidence of the universal properties of *Episode 3* observed in additional sources belonging to *family 2*, as compared to the very high variability of *Episode 1* and *Episode 2* components;
2. to present observations of GRB130427A leading to identification of new physical regimes encountered in *Episode 3* and their interpretation within the IGC paradigm;
3. to give evidence of the predictive power of the observations of *Episode 3* and outline the underlying physical process leading to the characterization of the two aforementioned families of GRBs.

To start we will summarize in the next paragraph some qualifying new features generally observed in *Episode 3* of selected GRBs of *Family 2* and proceed in the following paragraphs to the specific new information acquired about *Episode 3* from GRB 130427A. We will then proceed to the general conclusions.

2. THE QUALIFYING FEATURES OF EPISODE 3

As observations of additional sources fulfilling the IGC paradigm were performed, some precise qualifying features for characterizing *Episode 3* have been found.

1. In some GRBs with known redshift belonging to *family 2* the late X-ray luminosities at times larger than 10^4 s appeared to overlap when duly scaled in the proper rest frame of the GRB source (Penacchioni et al. 2012). This was soon confirmed for a sample of six GRBs (i.e., GRB 060729, GRB 061007, GRB 080319B, GRB090618, GRB 091127, and GRB 111228), which we call the golden sample (*GS*; Pisani et al. 2013); see Figure 3. This unexpected result led to the adoption of the universal luminosity versus time relation in the late X-ray emission of *Episode 3* as a distance indicator. For some GRBs without a known cosmological redshift and exhibiting the general features of the four episodes, we imposed the overlapping of the late power law X-ray emission in *Episode 3* with those of the *GS*, and consequently we inferred the value of the cosmological redshift of the source. This led to inferring the overall energetics of the source and a consistent description of each episode following our theoretical model. This was the case with GRB 101023, which has an inferred redshift $z = 0.9$ and $E_{\text{iso}} = 4.03 \times 10^{53}$ erg (Penacchioni et al. 2012), and GRB 110709B, with inferred redshift $z = 0.75$ and $E_{\text{iso}} = 2.43 \times 10^{52}$ erg (Penacchioni et al. 2013).

The above analysis initially addressed sources with $z < 1$, where the associated SNe are observable. However, there is no reason to doubt that the IGC paradigm also applies to sources for $z > 1$. In this case the SN is not observable with the current optical telescopes, but the existence of all the above episodes, with the exception of *Episode 4* related to the optical observation of the SN, can be verified in principle if they are above the observational threshold, and the members of the *GS* are correspondingly further increased. Indeed, significant results have been reached by observing the fulfillment of the above scaling laws in *Episode 3* of GRB 090423, at $z = 8.2$ (Ruffini et al. 2014b). The occurrence of this overlapping in the late X-ray emission observed by XRT is considered a necessary and sufficient condition to assert that a GRB fulfills the IGC paradigm.

2. The identification of a thermal emission occurring in the initial very steep decay of *Swift*-XRT data of *Episode 3* in GRB 090618 (Ruffini et al. 2014c). We are currently examining other GRBs with this feature, e.g., 060729, 061007, 061121 (Page et al. 2011; Starling et al. 2012; Friis & Watson 2013). From these thermal emissions it is possible to infer the dimensions of the X-ray emitting regions, as well as their Lorentz Γ factors, in this earliest part of *Episode 3* (Ruffini et al. 2014c). A typical mildly relativistic expansion regime with $\Gamma \lesssim 2$ and characteristic radii $R \sim 10^{13}$ cm has been identified (Ruffini et al. 2014c). These observational facts lead to a novel approach to the theoretical understanding of the X-ray emission

⁵ http://www.icranet.org/index.php?option=com_content&task=view&id=747&Itemid=880

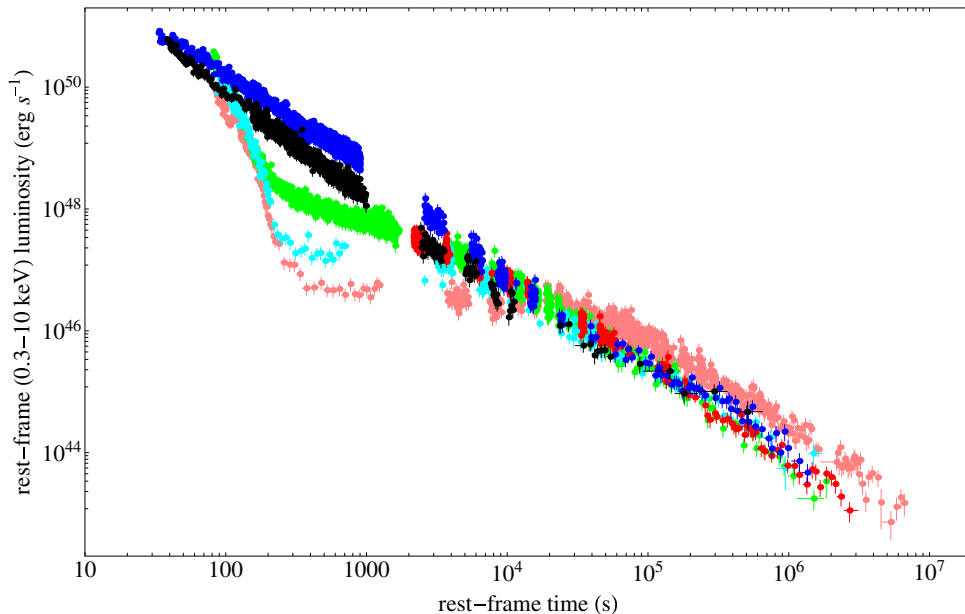


Figure 3. Golden sample scaling law (Pisani et al. 2013). X-ray luminosity light curves of the six GRBs with measured redshift in the 0.310 keV rest-frame energy range: in pink GRB 060729, $z = 0.54$; black GRB 061007, $z = 1.261$; blue GRB 080319B, $z = 0.937$; green GRB 090618, $z = 0.54$; red GRB 091127, $z = 0.49$; and in cyan GRB 111228, $z = 0.713$.

process of *Episode 3*, which is profoundly different from the ultra-relativistic one in the traditional jet afterglow collapsar paradigm model (Piran 2005; Mészáros 2006). We concluded that this emission is not only mildly relativistic, but also linked to a wide-angle emission from the SN ejecta in the absence of any sign of collimation (Ruffini et al. 2014c).

- From the direct comparison of the late X-ray emission of the *GS* sources, we recently identified the appearance of a nested structure, which we illustrate in Figure 4, comparing the corresponding behavior of GRB 130427A with that of *GS* GRB 060729 (Ruffini et al. 2014c). The occurrence of these nested structures shows, among others, that in the case of the most intense sources, the common power law observed for the X-ray luminosities for times larger than 10^4 s does extend to earlier times; see Figure 4. Indeed, for the most intense sources, the common power law behavior is attained at an earlier time and at higher X-ray luminosities than the characteristic timescale indicated in (Pisani et al. 2013); see Figure 3. As we are going to show, in the highly energetic GRB 130427A, this behavior starts at much earlier times around 400 s.

Some of these results were presented by one of the authors in the 2013 Texas Symposium on Relativistic Astrophysics.⁶ There, the sources originating in a tight binary system composed of a FeCO core at the onset of an SN event and a companion NS were named binary driven hypernovae (BdHNe; Ruffini et al. 2014c), in order to distinguish them from the traditional hypernovae (HN).

The occurrence of the three features of *Episode 3* listed previously as obtained by our data analysis are becoming crucial to the theoretical understanding of the GRB–SN phenomenon. They have never been envisaged to exist or predicted in the traditional collapsar–fireball paradigm (Nava et al. 2013; van Eerten & MacFadyen 2012; van Eerten et al. 2010). The IGC

paradigm motivated an attentive data analysis of *Episode 3* and the discovery of its universality has been a by-product.

3. EPISODE 3 IN THE CASE OF GRB 130427A

In what follows we will show how GRB 130427A, which is associated with SN 2013cq and is the most luminous GRB observed in the past 40 yr, offers the longest multi-wavelength observations of *Episode 3* so far. It confirms and extends the above understanding and corresponding scaling laws already observed in X-rays to lower and higher energies. It also allows for the exploration of the occurrence of similar constant power law emission in the high-energy emission (GeV) and in the optical domain. We proceed with our data analysis of the ultra high GeV energy observations (*Fermi*-LAT), those in soft and hard X-rays (*Swift*-XRT and *NuStar*, respectively), as well as of optical observations (*Swift*-UVOT and ground based satellites). Our results are compared to those in the current literature. These observational facts set very specific limits on the Lorentz Γ factor of each component; the corresponding mechanism of emission; and the clear independence of any prolongation of the GRB emission of *Episode 2* to the emission process of *Episode 3*.

The observation of the scaling law in the first 2×10^4 s alone has allowed us to verify the BdHN nature of this source, which necessarily implies the presence of a SN. Consequently, we recall in Section 3.1 that we made the successful prediction of the occurrence of a supernova, which was observed in the optical band, as predicted on 2013 May 2.

In Section 3.2, we summarize our own data reduction of the *Fermi* and *Swift* satellites, and we compare them with those in the current literature.

In Section 3.3, we discuss the finding of a thermal component in the early part of the X-ray emission of *Episode 3*. This is crucial for identifying the existence of the X-ray emission of a regime with low Lorentz factor and small radius, which is typical for supernova ejecta.

⁶ <http://nsm.utdallas.edu/texas2013/proceedings/3/1/Ruffini.pdf>

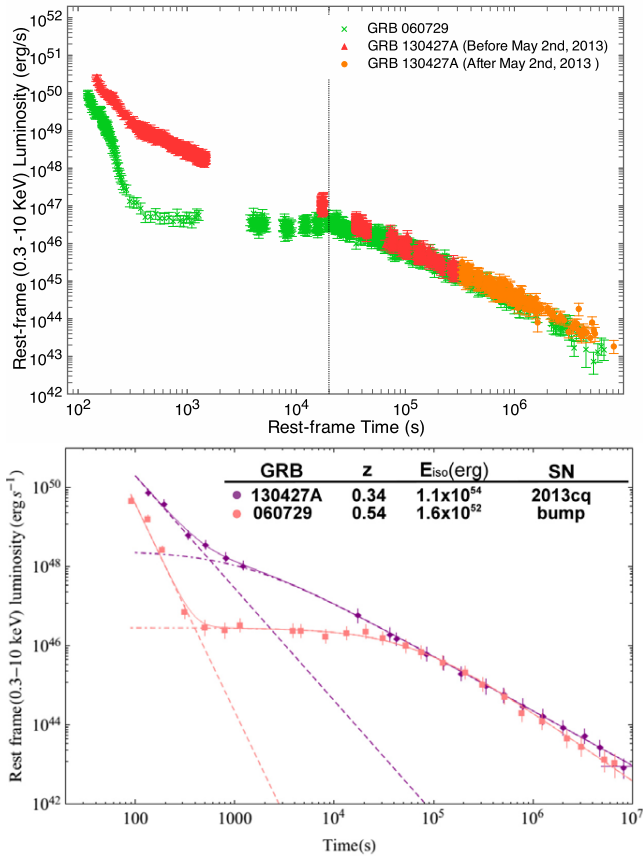


Figure 4. Top: overlapping of GRB 130427A and GRB 060729. The green crosses represent the light curve of GRB 060729. The red triangle and orange dots represent the light curve of GRB 130427A before and after 2013 May 2, respectively. The vertical line marks the time of 2×10^4 s, which is the lower limit for the domain of validity of the Pisani relation prior to GRB 130427A. Bottom: this figure shows that GRB 060729 and GRB 130427A have different magnitudes of the isotropic energy, but exhibit a common scaling law after 2×10^4 s. It also shows that the low isotropic energy GRB 060729 has a longer plateau, while the high isotropic energy GRB 130427A does not display an obvious plateau.

In Section 3.4 we compare the broadband (optical, X-ray, γ -ray, all the way up to GeV) light curves and spectra of *Episode 3*.

In Section 3.5 we point out the crucial difference between the X-, γ -ray, and GeV emission in *Episode-3*.

In Section 3.6 we proceed to a few general considerations on ongoing theoretical activities.

Sections 4 is the summary and conclusions.

3.1. Identification and Prediction

With the appearance of GRB 130427A, we decided to explore the applicability of the IGC paradigm in the terra incognita of GRB energies up to $\sim 10^{54}$ erg. In fact, prior to GRB 130427A, the only known case of an equally energetic source, GRB 080319B, had some evidence of an optical bump (Bloom et al. 2009; Tanvir et al. 2010), but in no way gave detailed information about the SN spectrum or type. We noticed in GRB 130427A the characteristic overlapping of the late X-ray decay in the cosmological rest frame of the source with that of GRB 060729, a member of the golden sample (in red in Figure 4), and from the overlapping we deduced a redshift that was consistent with the observational value $z = 0.34$ (Levan et al. 2013a).

Therefore from the observations of the first 2×10^4 s, GRB 130427A fulfilled the IGC paradigm, and we conclude, solely on this ground, that an SN should be observed under these circumstances. We sent the GCN circular 14526⁷ (Ruffini et al. 2013b) on 2013 May 2 predicting that the optical *R*-band of an SN will reach its peak magnitude in about 10 days in the cosmological rest frame on the basis of the IGC paradigm. Starting from 2013 May 13 the telescopes GTC, Skynet, and HST discovered the signals from the type Ic supernova SN 2013cq (de Ugarte Postigo et al. 2013; Trotter et al. 2013; Levan et al. 2013b, 2014; Xu et al. 2013). We kept updating the X-ray *Swift* data for weeks and confirmed the complete overlapping of the late X-ray luminosities, in the respective cosmological rest frames, of GRB 130427A and GRB 060729 (in orange in Figure 4). From these data it became clear that the power law behavior of the late-time X-ray luminosity with index $\alpha \sim 1.3$ indicated in Pisani et al. (2013)—leading to the new concept of the nesting of the light curves—started in this very energetic source at $\sim 10^2$ s following an initial phase of steeper decay (Ruffini et al. 2014c).

Contrary to the traditional approach that generally considers a GRB to be composed of the prompt emission followed by the afterglow, both of which vary from source to source, the IGC paradigm for *family 2* introduced *Episode 3*, which shows regularities and standard late-time light curves that are largely independent of the GRB energy. It soon became clear that, with *Episode 3*, we were starting to test the details of the physics and astrophysics of as yet unexplored regimes implied by the IGC paradigm: (1) a ν -NS and the SN ejecta, originating in *Episode 1*, (2) a newly formed BH originating in *Episode 2*, and (3) the possible interaction among these components observable in the standard features of *Episode 3*.

The joint observations of the *Swift*, *NuStar*, and *Fermi* satellites have offered the unprecedented possibility of clarifying these new regimes with the addition of crucial observations in the optical, X-ray, and high energy radiation for *Episode 3* of GRB 130427A, leading to equally unexpected results. The remainder of this paper is dedicated to understanding *Episode 3* of this remarkable event.

3.2. Data Analysis of Episode 3 in GRB 130427A

GRB 130427A was first observed by the *Fermi*-GBM at 07:47:06.42 UT on 2013 April 27 (von Kienlin 2013), which we set as the starting time t_0 throughout the entire analysis. After 51.1 s, the Burst Alert Telescope (BAT) on board *Swift* was triggered. The *Swift* Ultra Violet Optical Telescope (UVOT) and the *Swift* X-ray Telescope (XRT) began observing at 181 s and 195 s after the GBM trigger, respectively (Maselli et al. 2013). Because this was an extremely bright burst, successively more telescopes pointed at the source: the Gemini North telescope in Hawaii (Levan et al. 2013a), the Nordic Optical Telescope (NOT) (Xu et al. 2013), and the VLT/X-shooter (Flores et al. 2013), which confirmed the redshift $z = 0.34$.

⁷ GCN 14526: the late X-ray observations of GRB 130427A by *Swift*-XRT clearly show a pattern typical of a family of GRBs associated with supernovae (SNe), following the Induced Gravitational Collapse (IGC) paradigm (Rueda & Ruffini 2012; Pisani et al. 2013). We assume that the luminosity of the possible SN associated with GRB 130427A would be that of 1998bw, as was found in the IGC sample described in Pisani et al. (2013). Assuming the intergalactic absorption in the *I* band (which corresponds to the *R*-band rest frame) and the intrinsic one, with a Milky Way type for the host galaxy, we obtain a magnitude expected for the peak of the SN of $I = 22-23$ occurring 13–15 days after the GRB trigger, namely between the 10th and the 12th of 2013 May. Further optical and radio observations are encouraged.

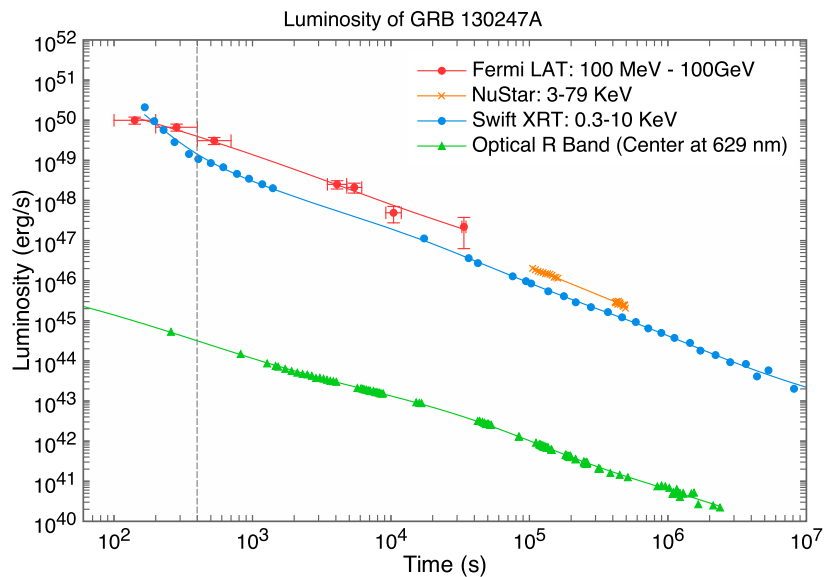


Figure 5. Multi-wavelength light curve of GRB 130427A. The high energy (100 MeV–100 GeV) emission detected by *Fermi*-LAT marked in red, and soft X-ray (0.3–10 keV) data from *Swift*-XRT marked in blue, are deduced from the original data. *NuStar* data (3–79 keV) marked in orange comes from (Kouveliotou et al. 2013). The optical (*R*-band, center at 629 nm) data marked in green comes from ground-based instruments (Perley et al. 2013). The error bars are too small with respect to the data points except for *Fermi*-LAT data. The horizontal error bars of *Fermi*-LAT represent the time bin in which the flux is calculated and vertical bars are statistical 1σ errors on the flux (the systematic error of 10% is ignored). The details in the first tens of seconds are ignored because we are interested in the behavior of the high energy light curve on a longer time scale. The vertical gray dashed line at (~ 400 s) indicates when the constant decaying slope starts. It is clear that all the energy bands have almost the same slope after 400 s in *Episode 3*.

GRB 130427A is one of the few GRBs with an observed adequate fluence in the optical, X-ray, and GeV bands simultaneously for hundreds of seconds. In particular it remained continuously in the LAT field of view until 750 s after the trigger of *Fermi*-GBM (Ackermann et al. 2013), which gives us the best opportunity so far to compare the light curves and spectra in different energy bands, and to verify our IGC paradigm. We did the data reduction of *Fermi* and *Swift* satellites using the following methods.

Fermi. Data were obtained from the Fermi Science Support Center,⁸ and were analyzed using an unbinned likelihood method with Fermi Science Tools v9r27p1.⁹ Event selections *P7SOURCE_V6* and *P7CLEAN_V6* were used, depending on which one gave more stable results. Recommended data cuts were used (e.g., $z_{\max} = 100$ degree). The background is composed of the galactic diffuse emission template and the isotropic emission template, as well as about 60 point sources that are within the 15° radius of the GRB (however, their contribution was found to be negligible). The parameters for the background templates were held fixed during the fit. Luminosity light curve in Figure 5 corresponds to the energy range of 100 MeV to 100 GeV, a circle radius of 15° , with a power law spectra assumption. Because the data points up to the last two give a photon index of $\simeq 2.1$ with small errors, we set the photon index for the last two points to the value 2.1 during the fitting procedure in order to obtain more stable results. The light curve can be obtained with great temporal detail before 750 s. However, because we are interested in the general behavior of *Episode 3*, for simplicity we neglected such a fine temporal structure and rebinned the light curve. Therefore there are only three data points up to 750 s. The spectrum is plotted in Figure 6.

Swift. XRT data were retrieved from UKSSDC¹⁰ and were analyzed by the standard *Swift* analysis software included in the NASA’s Heasoft 6.14 with relevant calibration files.¹¹ In the first 750 s only Windows Timing (WT) data exists and the average count rate exceeds $300 \text{ counts s}^{-1}$; the highest count rate reaches up to $1000 \text{ counts s}^{-1}$, which is far beyond the value of $150 \text{ counts s}^{-1}$ that is suggested for the WT mode as a threshold of considering pile-up effects (Evans et al. 2007). Pile-up effects cause the detector to misrecognize two or more low energy photons as a single high energy photon, which softens the spectrum. We adopted the method proposed by Romano et al. (2006), fitting dozens of spectra from different inner sizes of box annulus selections in order to determine the extent of the distorted region. Taking the time interval 461–750 s as an example, the deviation comes from where the inner size is smaller than six pixels, as shown in Figure 6. Then we applied the standard XRT data analyzing process (Evans et al. 2007, 2009) to obtain the spectrum, as plotted in Figure 6. For the luminosity light curve we split XRT observations in the nominal 0.3–10 keV energy range to several slices with a fixed count number, followed the standard procedure (Evans et al. 2007, 2009), and considered the pile-up correction. The XRT light curves of different bands are shown in Figure 5.

3.3. The X-Ray Qualification of GRB 130427A as a BdHN

Here we first focus on the extended X-ray emission of *Episode 3*, which, as shown, gives the qualifying features for the identification of GRB 130427A as a BdHN. We first identify the power law component of the light curve after the step decay and the end of the plateau. This power law component of GRB 130427A has a power law index $\alpha = -(1.31 \pm 0.01)$ and extends from 400 s to $\sim 10^7$ s without jet breaks. These results are consistent with previous papers (see, e.g., in Perley

⁸ <http://Fermi.gsfc.nasa.gov>

⁹ <http://Fermi.gsfc.nasa.gov/ssc/data/analysis/software/>

¹⁰ <http://www.Swift.ac.uk>

¹¹ <http://heasarc.gsfc.nasa.gov/lheasoft/>

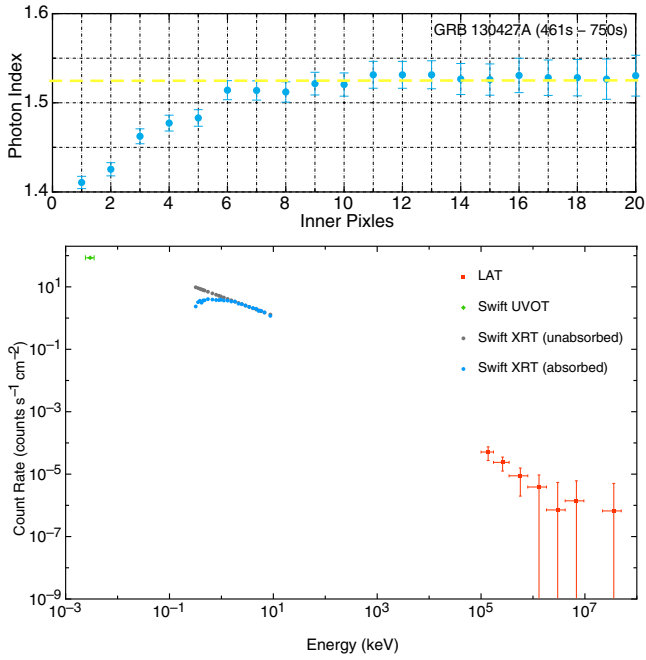


Figure 6. Top: data from the *Swift*-XRT (0.3–10 keV) in the time range of 461–750 s for GRB 130427A. The data shows the photon index for different region selections after considering the pile-up effect. After six inner pixels, the photon index approaches an almost constant value of 1.52. Bottom: spectra of GRB 130427A in the time range of 461–750 s. The green data points are from *Swift*-UVOT (Perley et al. 2013), the blue and gray points come from *Swift*-XRT, and red data correspond to *Fermi*-LAT. The horizontal error bars are energy bins in which the flux is integrated and the vertical ones are 1σ statistical errors on the count rate. The gray data points correspond to unabsorbed *Swift*-XRT data, while the blue ones are obtained with the assumption of absorption.

et al. 2013; Laskar et al. 2013) that find no jet break, but differs from Maselli et al. (2014), who claim a break of the later time light curve.

We turn to an additional crucial point: to confirm that the X-ray emission of *Episode 3* belongs to the SN ejecta and not the GRB. To do this it is crucial, as already done for other sources (Ruffini et al. 2014c), to determine the presence of a thermal component in the early time of *Episode 3* and infer the

temperature and the size of its emitter. By analyzing the XRT data, we find that adding a blackbody component efficiently improves the fit with respect to a single power law from 196 s to 461 s. The corresponding blackbody temperature decreases in that time duration, from 0.5 keV to 0.1 keV, in the observed frame. Figure 7 shows the evolution of the power law plus blackbody spectra in three time intervals. Clearly the flux of the thermal component drops with time, and the temperature corresponding to the peak flux energy decreases. Kouveliotou et al. (2013) found that a single power law is enough to fit the *NuStar* data in the *NuStar* epochs, and the reason could be that the thermal component has faded away or exceeded the observational capacity of the *Swift* satellite in the *NuStar* epochs, which start later than 10^5 s.

By assuming that the blackbody radiation is isotropic in the rest frame, the emitter radius along the line of sight increases from $\sim 0.7 \times 10^{13}$ cm at 196 s to $\sim 2.8 \times 10^{13}$ cm at 461 s in the observed frame. This is orders of magnitude smaller than the emission radius of the GRB, which is larger than 10^{15} cm in the traditional GRB collapsar afterglow model. The size of 10^{13} cm at hundreds of seconds is consistent with the observation of supernova ejecta. After considering the cosmological and the relativistic corrections, $t_a^d \simeq t(1+z)/2\Gamma^2$, where t and t_a^d are the time in the laboratory and observed frame, respectively, and Γ is the Lorentz factor of the emitter, we get an expansion speed of $\sim 0.8c$, corresponding to Lorentz factor $\Gamma = 1.67$. These results contradict the considerations inferred in Maselli et al. (2014) $\Gamma \sim 500$, which invoke a value of the Lorentz factor in the traditional collapsar afterglow model (see, e.g., Mészáros 2006). Again, in the prototypical GRB 090618, the Lorentz factors ($1.5 \leq \Gamma \leq 2.19$) and emission radii ($\sim 10^{13}$ cm) are very similar to those of GRB 130427A presented in Ruffini et al. (2014c). It is interesting that such a thermal component has been also found in the early parts of *Episode 3* of GRB 060729 (adopted in Figure 4) and many other SN associated GRBs (see Ruffini et al. 2014c; Grupe et al. 2007; Starling et al. 2012).

3.4. Discussion of Multi-Wavelength Observations in Episode 3

Now we turn to the most unexpected feature in the analysis of the optical, X-ray, γ -ray, and very high energy emission

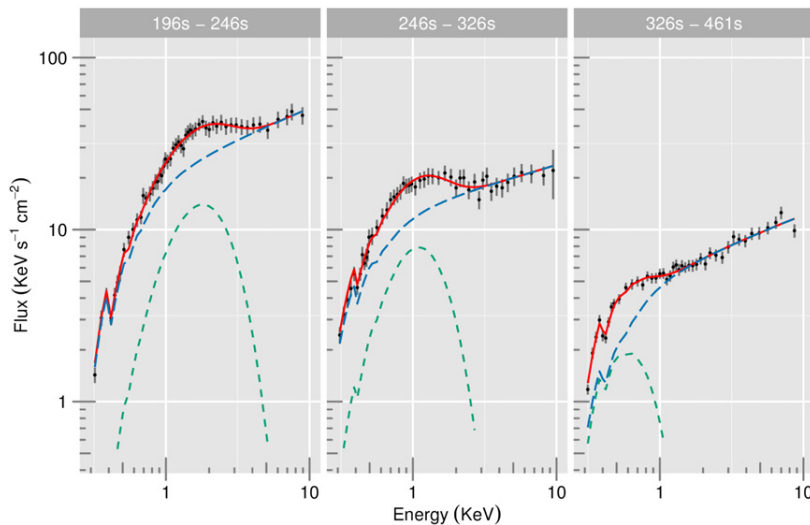


Figure 7. Spectral fitting of three time intervals (196 s–246 s, 246 s–326 s, and 326 s–461 s) in *Episode 3*; the data come from *Swift*-XRT (0.3 KeV–10 KeV, without pile-up area). Black points are the deduced data, the green dashed line presents the thermal component, the blue long-dashed line is the power law component, and the red line shows the combination of these two components. Clearly the flux of thermal component drops and the temperature decreases with time.

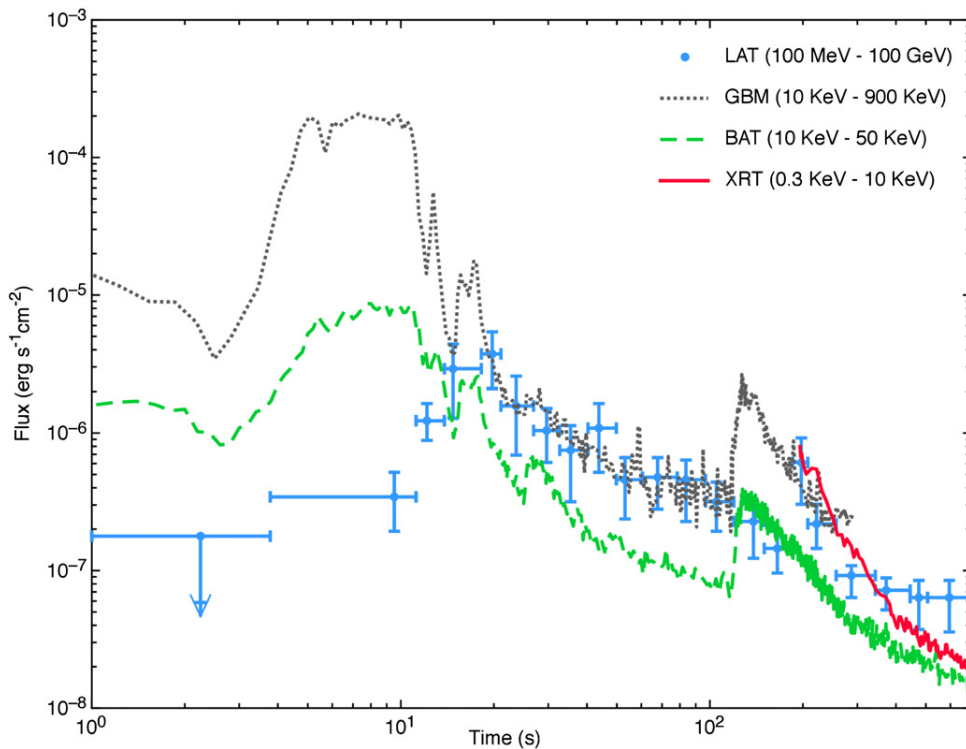


Figure 8. Flux of first 700 s. Blue points are the *Fermi*-LAT high energy emission from 100 MeV until 100 GeV (Ackermann et al. 2013), the gray dotted line represents the *Fermi*-GBM from 10 keV to 900 keV, the green dashed line represents the photons detected by *Swift* BAT from 10 keV to 50 keV, and the red solid line is the soft X-ray *Swift*-XRT detection in the range of 0.3–10 keV. This figure clearly shows that the *Fermi*-LAT emission reaches highest fluence at about 20 s, while the gamma-ray detected by *Fermi*-GBM releases most of the energy within the first 10 s.

in *Episode 3* of GRB 130427A. The optical emission was observed by *Swift*-UVOT and many ground-based telescopes (the *R*-band as an example for the optical observation). The soft X-ray radiation was observed by *Swift*-XRT (0.3–10 keV). Similarly, the hard X-ray radiation was observed by *Swift*-BAT (15–150 keV) and *NuStar* (3–79 keV). The γ -ray radiation was observed by *Fermi*-GBM (8 keV–40 MeV), and the high energy radiation by *Fermi*-LAT (100 MeV–100 GeV). The main result is that strong analogies are found in the late emission at all wavelengths in *Episode 3*. After 400 s these luminosities show a common power law behavior with the same constant index as in the X-ray (and clearly with different normalizations), so by fitting multi-wavelength light curves together we have a power law index $\alpha = -(1.3 \pm 0.1)$.

Turning now to the spectrum, integrated between 461 s and 750 s, the energy range covers 10 orders of magnitude, and the best fit is a broken power law (see Figure 6). In addition to the traditional requirements for the optical supernova emission in *Episode 4*, and the much more energetically demanding requirement for the general multi-wavelength emission of *Episode 3* has to be addressed.

3.5. The Onset of Episode 3

In the previous sections we emphasized the clear evidence of GeV emission and its analogy in the late power law luminosities as functions of the arrival time for the X-ray, optical, and GeV emissions. Equally important in this section is to emphasize some differences between the X-ray, γ -ray, and the high energy GeV emission, especially with respect to the onset of *Episode 3* at the end of prompt emission in *Episode 2* (see Figure 8). We observe:

1. The γ -ray light curves observed by *Fermi*-GBM and hard X-ray observed by *Swift*-BAT have similar shapes. They reach the highest luminosity between 4 s and 10 s during the prompt emission phase of *Episode 2*.
2. The high energy (>100 MeV) GeV emission gradually rises, just after the γ - and X-ray prompt emissions drop down at the end of *Episode 2*: the high energy GeV emission raises to its peak luminosity at about 20 s. The turn on of the GeV emission coincides, therefore, with the onset of our *Episode 3*. These considerations were recently confirmed and extended by the earliest high energy observations in GRB 090510 (Ruffini et al. 2014, in preparation).
3. At about 100 s, the *Swift*-XRT starts to observe the soft X-ray and a sharp spike appears in the hard X-ray and gamma ray bands (see Figure 8). Only at this point does the *Swift*-XRT start to observe soft X-ray. We are currently addressing the occurrence of the spike to the thermal emission observed to follow in the sharp decay of the X-ray luminosity prior to the plateau and the above mentioned common power law decay (Ruffini et al. 2014b).

The detailed analysis of the prolonged emission observed by *Fermi*-LAT in GeV enables us to set specific limits on the Lorentz factor of this high energy emission. We analyzed the GeV emission from ~ 300 s to 2.5×10^4 s, dividing the time interval into seven sub-intervals and in each of them collecting the corresponding maximum photon energy and photon index of the spectral energy distribution, as shown in Ackermann et al. (2013, Figure 2). We focused our attention on the estimate of the Lorentz factor for this high energy component from the usual optical depth formula for pair creation $\tau_{\gamma\gamma}$ (see, e.g., Lithwick & Sari 2001; Gupta & Zhang 2008). We computed, for

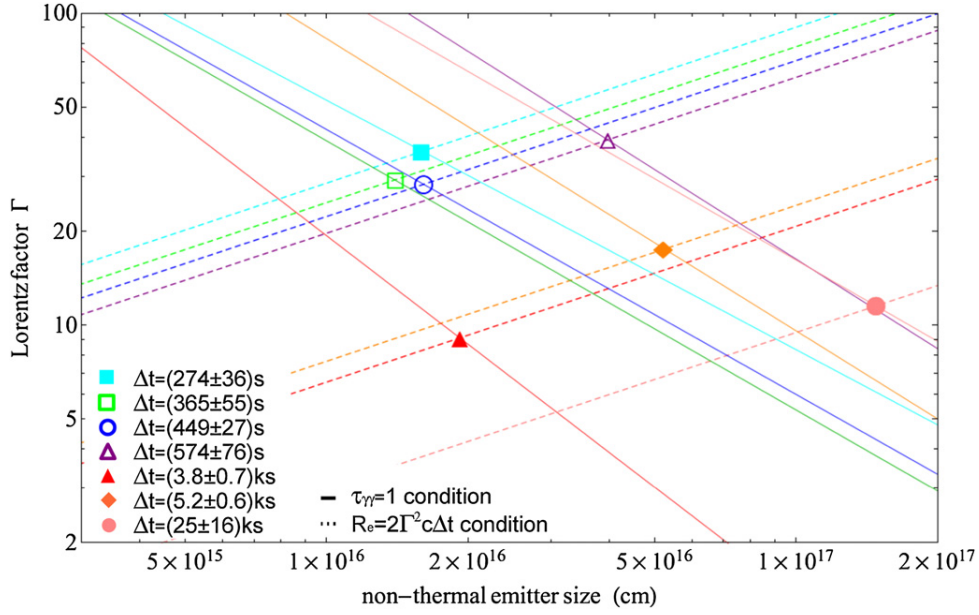


Figure 9. Constraints on the Lorentz factors and the size of the GeV emitting region at the transparency point. Solid curves represent the curves defined by varying the emitting region size from the $\tau_{\gamma\gamma} = 1$ condition; dot-dashed curves represent the radius of the emitter obtained from causality in the ultrarelativistic regime (i.e., $R_{em} = 2\Gamma^2 c\Delta t$). Filled circles correspond to the solutions of both limits. The different colors refer to the time intervals from ~ 273 to 24887 s, in the order cyan, green, blue, purple, red, orange, and pink, respectively.

different values of radii of the emitter, the corresponding Lorentz factors at the transparency condition (i.e., $\tau_{\gamma\gamma} = 1$; see the solid curves in Figure 9). The constraints on the size of the emitting regions come from causality in the ultrarelativistic regime (i.e., $R_{em} = 2\Gamma^2 c\Delta t$), where Δt corresponds to the duration of the time intervals under consideration (see the dot-dashed curves in Figure 9). The values of the Lorentz factor range between ~ 10 and ~ 40 , and correspondingly, the radii of the emitting region at the transparency point are located between $\sim 10^{16}$ cm and $\sim 2 \times 10^{17}$ cm (see the filled circles in Figure 9).

3.6. General Considerations on Recent Theoretical Progress on BdHD

The concurrence of the above well-defined scaling laws and power law of the observed luminosities both in the X-ray and/or in the optical domains in *Episode 3* of GRB 130427A have been considered arguments in favor of looking to the r -process and to heavy nuclei radioactive decay as the energy sources (Ruffini et al. 2014c; see the pioneering work of Li & Paczynski 1998). The extended interaction of the ν -NS and its binary NS companion in the SN ejecta provides an environment for r -processes to create the needed neutron-rich very heavy elements to attribute some of the electromagnetic energy in *Episode 3* to nuclear decay, $\approx 10^{52}$ erg. Alternatively, we are considering emission originating from type-I and type-II Fermi acceleration mechanisms, which are introduced by Fermi precisely to explain the radiation process in the SN remnants (Fermi 1949). In addition these processes can lead to a power law spectrum (Aharonian 2004) that is similar to that presented in this paper and our recent letter (Ruffini et al. 2014c). The GRB emission of *Episode 2* interacting with the SNe ejecta could represent the energy injection long sought by Fermi for the onset of his acceleration mechanism (Fermi 1949).

Both of these processes can operate as energy sources for the mildly relativistic X-ray component and the relativistic GeV emission of *Episode 3*.

We are currently examining additional BdHN sources and giving particular attention to understanding the highest GeV energy emission, which is unexpected in the traditional r -process. The inferred Γ Lorentz factor for the GeV emission points to the possibility of a direct role of the two remaining components in the IGC paradigm: the newly born neutron star (ν NS) and the just born black hole (see Figure 1). There is also the distinct possibility that these two systems have become members of a newly born binary system¹² (Rueda & Ruffini 2012).

4. CONCLUSION

We recall that GRB 130427A is one of the most energetic GRBs ever observed ($E_{iso} \simeq 10^{54}$ erg), with the largest γ -ray fluence and the longest lasting simultaneous optical, X-ray, γ -ray, and GeV observations of the past 40 yr. For this reason we performed our own data analysis of the *Swift* and *Fermi* satellites (see Sections 3) in order to probe the BdHN nature of this source (see Section 3.3) and infer new perspectives for the IGC paradigm and the physical and astrophysical understanding of GRB.

We summarize the main results by showing how the analysis of GRB 130427A should be inserted in a wider context with three different areas: (1) the formulation and the observational consequences of the IGC paradigm; (2) the comprehension induced by the multi-wavelength observations of GRB130427A; and (3) the BDHN versus HN properties. BDHN is relevant in establishing a new alternative distance indicator in astrophysics, which will be summarized in the following.

With reference to the formulation and observational consequences of the IGC paradigm:

1. The IGC paradigm introduces a new experience in astrophysics that has been successfully applied in particle

¹² Presentation of R. Ruffini in Yerevan: <http://www.icranet.org/images/stories/Meetings/meetingArmenia2014/talks/ruffini-1.pdf>

physics: to understand that a system traditionally considered elementary is actually a composed system, and that new components in the system can appear from the influence of collisions or decay. Well-known physical examples are represented by the introduction of the quark (Aad et al. 2012), or the creation of new particles in a decay or collision of elementary particle system: the Fermi theory of beta decay or the mesons production in electron positron collision in storage rings are classical examples. These facts are routinely accepted in particle physics, although Fermi had to explain them at the time (Fermi 1934). In astrophysics this situation is new. To see that a process until recently considered elementary, such as the GRB, does contain four different astrophysical systems, and that the interaction between two of them (i.e., the FeCO core undergoing SN and the companion NS binary) give rise to two different new systems, a ν NS and a BH, and that the entire process occurs in less than 200 s, is a totally new condition. To understand it, a new technical and conceptual approach is needed. The new style of research is more similar to that adopted in particle physics than in classical astronomy; see Figure 1.

2. Possibly the most profound novelty in this approach, for the understanding of GRBs, is the introduction of the four episodes that are summarized in Section 1. The traditional GRB description corresponds to *Episode 2*. *Episode 1* corresponds to the dynamical accretion of the SN ejecta onto the companion NS. We are now considering an enormous rate of accretion of 10^{31} g s^{-1} , which is 10^{15} times larger than that usually considered in the binary X-ray source in systems like Centaurus X-3 or Cygnus X-1 (see e.g., in Giacconi & Ruffini 1975). This process opened a new field of research by presenting the first realization of the hypercritical accretion introduced by Bondi–Hoyle–Littleton, as well as the testing ground of the neutrinos emission pioneered in the Zel’dovich et al. (1972) and Ruffini & Wilson (1975) (see Section 1). The pure analytic simplified solutions in Rueda & Ruffini (2012) are now supported by direct numerical simulation in Fryer et al. (2014, and Figure 1 therein).
3. The main revolution of the IGC paradigm for GRBs comes from the discovery of the universal laws discovered in *Episode 3*, which compare the explosive, irregular phases, varying from source to source in all observed GRBs in *Episode 1* and *Episode 2*. The universality of *Episode 3*, as well as the precise power laws and scaling laws discovered, changes the field of GRB analysis by making it one of time-resolved, high-precision, and reproducible measurements. Additional unexplored physical phenomena occurs in *Episode 3*, adding to the new ultrarelativistic regimes already observed in the *Episode 2* in previous years,¹³ see Figure 3 and Figure 4 as well as Figure 5.

With reference to the comprehension induced by the multi-wavelength observations of GRB130427:

1. Following the work on the *GS* (Pisani et al. 2013) and the more recent work on the nested structures (Ruffini et al. 2014c), we have first verified that the soft X-ray emission of GRB 130427A follows for time $t \simeq 10^4$ s the power law decay described in Pisani et al. (2013). Surprisingly, this most energetic GRB unveils that such power law behavior as already exists at the early time as $t \sim 100$ s (details in

Ruffini et al. 2014c). From the X-ray thermal component observed at the beginning of *Episode 3* following a spiked emission at ~ 100 s, a small Lorentz factor of the emitter is inferred ($\Gamma < 2$). This X-ray emission appears to originate in a mildly relativistic regime with a velocity $v \sim 0.8c$, does not appear to have substantial beaming, and appears to be relatively symmetric with no jet break; see Figure 5 and Ruffini et al. (2014c, Figure 2).

2. We made a multi-wavelength analysis of *Episode 3* where we compared optical data from *Swift*-UVOT and ground-based telescopes, X-ray data from *Swift*-XRT, γ -ray data from *Fermi*-GBM, and very high energy data in the GeV from *Fermi*-LAT. The high energy emission appears to be detectable at the end of the prompt radiation phase in *Episode 2*, when the fluence of the X-ray and γ -ray of the prompt exponentially decreases and becomes transparent for the very high energy photons in the *Fermi*-LAT regime. From the transparency condition of the GeV emission, a Lorentz Gamma factor of 10–40 is deduced. In principle this radiation, although no brake is observed in its power law, could be in principle beamed; see Figure 9.
3. Although the light curves of X-ray and GeV emission appear to be very similar, sharing similar power law decay index, their Lorentz Γ factors appear to be very different, and their physical origins are necessarily different. Within the IGC model, the X-ray and high energy can originate from the interaction of some of the physical components (e.g., neutron star and black hole) that were newly created in the C-matrix: the interaction of the GRBs with the SN ejecta (Ruffini et al. 2014b) may well generate the X-ray emission and the associated thermal component. The high energy should be related to the novel three components (i.e., the BH, the ν NS, and the SN ejecta). From the dynamics it is likely that the ν NS and the BH form a binary system (see e.g., Rueda & Ruffini 2012 and the presentation by one of the authors).¹⁴

With reference to the BDHN versus HN properties:

1. The verification of the BdHN paradigm in GRB 130427A has confirmed that for sources with isotropic energy approximately 10^{54} erg, the common power law behavior is attained at earlier times (i.e., $\sim 10^3$ s) and higher X-ray luminosities than the characteristic timescale indicated in (Pisani et al. 2013) (see Figure 3). From the observation of the constant-index power law behavior in the first 2×10^4 s of the X-ray luminosity light curve, which overlap with the known BdHNe, it is possible to estimate the redshift of the source, the isotropic energy of the GRB, and the fulfillment of the necessary and sufficient condition for predicting the occurrence of the SN after ~ 10 days in the rest frame of the source (see, e.g., GCN 14526). This procedure has been successfully applied to GRB 140512A (R. Ruffini et al., in preparation).
2. The overlap with the *GS* members of the late X-ray emission observed by the *Swift* XRT, referred to as the rest frame of the source, introduces a method to establish an independent distance estimator of the GRBs. Although this method has been amply applied (e.g., GRBs 060729, 061007, 080319, 090618, 091127, 111228A), we also declare that there are some clear outliers to this phenomenon, such as GRB 060614 (Ruffini et al. 2013a), 131202A (Ruffini et al.

¹³ Presentation of R. Ruffini in the 13th Marcel Grossmann Meeting: <http://www.icra.it/mg/mg13>

¹⁴ Presentation of R. Ruffini in Yerevan: <http://www.icranet.org/images/stories/Meetings/meetingArmenia2014/talks/ruffini-1.pdf>

2013c), and 140206A (Ruffini et al. 2014a). These are all cases of great interest and the solution of this contradiction may be of particular astrophysical significance. Particularly interesting is the case of GRB 060614 because the cosmological redshift has not been directly measured and there can be a misidentification of the host galaxy (Cobb et al. 2006).

- As first pointed out in Rueda & Ruffini (2012) and Ruffini et al. (2014c), and further evidenced in Fryer et al. (2014), the crucial factor that may explain the difference between *family 1* and *family 2* GRBs is the initial distance between the FeCO core and its binary NS companion. The accretion from the SN ejecta onto the companion NS, and the consequent emission process decrease, by increasing this distance has consequently hampered the possibility for the binary companion NS to reach its critical mass (see Figures 3 and 4 in Izzo et al. 2012, and the discuss therein). Unlike *family 2*, in *family 1* no BH is formed, no GRB is emitted, and neither *Episode 2* nor *Episode 3* exists—only a softer and less energetic radiation from the accretion onto the neutron star will be observed in these sources. The problem of explaining the coincidence between the GRB and supernova in the case of *family 1* is just a tautology: no GRB in this family exists, only a hypernova (Ruffini et al. 2014c).

This paper addresses recent results on the IGC paradigm applied to long GRBs. The IGC paradigm and the merging of binary neutron stars has also been considered for short GRBs (see e.g., Muccino et al. 2013a, 2013b, 2014; Ruffini et al. 2014c) and is now being further developed.

We acknowledge the use of public data from the *Swift* and *Fermi* data archive. We thank Robert Jantzen for his careful reading and valuable advice. We also thank the editor and the referee for their constant attention and beneficial suggestions, which largely improve this paper. M.E., M.K., and G.B.P. are supported by the Erasmus Mundus Joint Doctorate Program by Grant Numbers 2012-1710, 2013-1471, and 2011-1640, respectively, from the EACEA of the European Commission.

REFERENCES

- Aad, G., Abajyan, T., Abbott, B., et al. 2012, *PhLB*, 716, 1
- Ackermann, M., Ajello, M., Asano, K., et al. 2013, *Sci*, 343, 42
- Aharonian, F. A. 2004, Very High Energy Cosmic Gamma Radiation: A Crucial Window on the Extreme Universe (Singapore: World Scientific Publishing)
- Bernardini, C. 2004, *PhP*, 6, 156
- Bloom, J. S., Perley, D. A., Li, W., et al. 2009, *ApJ*, 691, 723
- Bondi, H. 1952, *MNRAS*, 112, 195
- Bondi, H., & Hoyle, F. 1944, *MNRAS*, 104, 273
- Broderick, A. E. 2005, *MNRAS*, 361, 955
- Cobb, B. E., Bailyn, C. D., van Dokkum, P. G., & Natarajan, P. 2006, *ApJL*, 651, L85
- de Ugarte Postigo, A., Xu, D., Leloudas, G., et al. 2013, GCN Circ., 14646
- Evans, P. A., Beardmore, A. P., Page, K. L., et al. 2007, *A&A*, 469, 379
- Evans, P. A., Beardmore, A. P., Page, K. L., et al. 2009, *MNRAS*, 397, 1177
- Fermi, E. 1934, *Il Nuovo Cimento*, 11, 1
- Fermi, E. 1949, *PhRv*, 75, 1169
- Flores, H., Covino, S., Xu, D., et al. 2013, GCN Circ., 14491
- Friis, M., & Watson, D. 2013, *ApJ*, 771, 15
- Fryer, C. L., Benz, W., & Herant, M. 1996, *ApJ*, 460, 801
- Fryer, C. L., Rueda, J. A., & Ruffini, R. 2014, *ApJ*, 793, L36
- Fryer, C. L., Woosley, S. E., & Hartmann, D. H. 1999, *ApJ*, 526, 152
- Galama, T. J., Vreeswijk, P. M., van Paradijs, J., et al. 1998, *Natur*, 395, 670
- Giacconi, R., & Ruffini, R. 1975, Physics and Astrophysics of Neutron Stars and Black Holes (Amsterdam: North Holland Publishing Co.)
- Grupe, D., Gronwall, C., Wang, X.-Y., et al. 2007, *ApJ*, 662, 443
- Guetta, D., & Della Valle, M. 2007, *ApJL*, 657, L73
- Gupta, N., & Zhang, B. 2008, *MNRAS*, 384, L11
- Izzo, L., Rueda, J. A., & Ruffini, R. 2012, *A&A*, 548, L5
- Kouveliotou, C., Granot, J., Racusin, J. L., et al. 2013, *ApJL*, 779, L1
- Kovacevic, M., Izzo, L., Wang, Y., et al. 2014, *A&A*, 569, A108
- Laskar, T., Berger, E., Zauderer, B. A., et al. 2013, *ApJ*, 776, 119
- Levan, A. J., Cenko, S. B., Perley, D. A., & Tanvir, N. R. 2013a, GCN Circ., 14455
- Levan, A. J., Fruchter, A. S., Graham, J., et al. 2013b, GCN Circ., 1468
- Levan, A. J., Tanvir, N. R., Fruchter, A. S., et al. 2014, *ApJ*, 792, 115
- Li, L.-X., & Paczynski, B. 1998, *ApJL*, 507, L59
- Lithwick, Y., & Sari, R. 2001, *ApJ*, 555, 540
- Maselli, A., Beardmore, A. P., Lien, A. Y., et al. 2013, GCN Circ., 14448
- Maselli, A., Melandri, A., Nava, L., et al. 2014, *Sci*, 343, 48
- Mészáros, P. 2006, *RPPH*, 69, 2259
- Muccino, M., Ruffini, R., Bianco, C. L., Izzo, L., & Penacchioni, A. V. 2013a, *ApJ*, 763, 125
- Muccino, M., Ruffini, R., Bianco, C. L., et al. 2013b, *ApJ*, 772, 62
- Muccino, M., Bianco, C. L., Izzo, L., et al. 2014, *GrCo*, 20, 197
- Nava, L., Sironi, L., Ghisellini, G., Celotti, A., & Ghirlanda, G. 2013, *MNRAS*, 433, 2107
- Nousek, J. A., Kouveliotou, C., Grupe, D., et al. 2006, *ApJ*, 642, 389
- Page, K. L., Starling, R. L. C., Fitzpatrick, G., et al. 2011, *MNRAS*, 416, 2078
- Penacchioni, A. V., Ruffini, R., Bianco, C. L., et al. 2013, *A&A*, 551, A133
- Penacchioni, A. V., Ruffini, R., Izzo, L., et al. 2012, *A&A*, 538, 58
- Perley, D. A., Cenko, S. B., Corsi, A., et al. 2013, *ApJ*, 781, 37
- Pian, E., Amati, L., Antonelli, L. A., et al. 2000, *ApJ*, 536, 778
- Piran, T. 2005, *RMP*, 76, 1143
- Pisani, G. B., Izzo, L., Ruffini, R., et al. 2013, *A&A*, 552, L5
- Rhoads, J. E. 1999, *ApJ*, 525, 737
- Romano, P., Campana, S., Chincarini, G., et al. 2006, *A&A*, 456, 917
- Rueda, J. A., & Ruffini, R. 2012, *ApJL*, 758, L7
- Ruffini, R., Bernardini, M. G., Bianco, C. L., et al. 2008, in 11th Proc. Marcel Grossmann Meeting (Singapore: World Scientific Publishing), 368
- Ruffini, R., Bianco, C. L., Enderli, M., et al. 2013a, GCN Circ., 15560, 1
- Ruffini, R., Bianco, C. L., Enderli, M., et al. 2013b, GCN Circ., 14526
- Ruffini, R., Bianco, C. L., Enderli, M., et al. 2013c, GCN Circ., 15576, 1
- Ruffini, R., Bianco, C. L., Enderli, M., et al. 2014a, GCN Circ., 15794, 1
- Ruffini, R., Bianco, C. L., Frascchetti, F., Xue, S.-S., & Chardonnet, P. 2001, *ApJ*, 555, L117
- Ruffini, R., Izzo, L., Muccino, M., et al. 2014b, *A&A*, 569, A39
- Ruffini, R., Muccino, M., Bianco, C. L., et al. 2014c, *A&A*, 565, L10
- Ruffini, R., Salmonson, J. D., Wilson, J. R., & Xue, S.-S. 1999, *A&A*, 350, 334
- Ruffini, R., Salmonson, J. D., Wilson, J. R., & Xue, S.-S. 2000, *A&A*, 359, 855
- Ruffini, R., & Wilson, J. R. 1975, *PhRvD*, 12, 2959
- Starling, R. L. C., Page, K. L., Pe'er, A., Beardmore, A. P., & Osborne, J. P. 2012, *MNRAS*, 427, 2950
- Tanvir, N. R., Rol, E., Levan, A. J., et al. 2010, *ApJ*, 725, 625
- Tavani, M. 1998, *ApJL*, 497, L21
- Trotter, A., Reichart, D., Haislip, J., et al. 2013, GCN Circ., 1466
- van Eerten, H. J., & MacFadyen, A. I. 2012, *ApJ*, 751, 155
- van Eerten, H. J., Zhang, W., & MacFadyen, A. 2010, *ApJ*, 722, 235
- von Kienlin, A. 2013, GCN Circ., 14473
- Woosley, S. E. 1993, *ApJ*, 405, 273
- Xu, D., de Ugarte Postigo, A., Leloudas, G., et al. 2013, *ApJ*, 776, 98
- Xu, D., de Ugarte Postigo, A., Schulze, S., et al. 2013, GCN Circ., 14478
- Zel'dovich, Y. B., Ivanova, L. N., & Nadezhin, D. K. 1972, *SvA*, 16, 209

On Binary Driven Hypernovae and Their Nested Late X-Ray Emission*

Marco Muccino^{1,2}, Remo Ruffini^{1,2,3,4**}, Carlo Luciano Bianco^{1,2},
Maxime Enderli^{1,3}, Milos Kovacevic^{1,3}, Luca Izzo^{1,2}, Ana Virginia Penacchioni⁴,
Giovanni Battista Pisani^{1,3}, Jorge A. Rueda^{1,2,3,4}, and Yu Wang^{1,2}

¹*Dip. di Fisica and ICRA, Sapienza Università di Roma, Piazzale Aldo Moro 5, I-00185 Rome, Italy*

²*ICRANet, Piazza della Repubblica 10, I-65122 Pescara, Italy*

³*Université de Nice Sophia Antipolis, Nice, CEDEX 2, Grand Château Parc Valrose, France*

⁴*ICRANet-Rio, CBPF, Rua Dr. Xavier Sigaud 150, Rio de Janeiro, RJ, 22290-180 Brazil*

Received January 26, 2015

Abstract—The induced gravitational collapse (IGC) paradigm addresses energetic (10^{52} – 10^{54} erg), long gamma-ray bursts (GRBs) associated to supernovae (SNe) and proposes as their progenitors tight binary systems composed of an evolved FeCO core and a companion neutron star (NS). Their emission is characterized by four specific episodes: Episode 1, corresponding to the on-set of the FeCO SN explosion and the accretion of the ejecta onto the companion NS; Episode 2, related the collapse of the companion NS to a black hole (BH) and to the emission of a long GRB; Episode 3, observed in X-rays and characterized by a steep decay, a plateau phase and a late power-law decay; Episode 4, corresponding to the optical SN emission due to the ^{56}Ni decay. We focus on Episode 3 and we show that, from the thermal component observed during the steep decay of the prototype GRB 090618, the emission region has a typical dimension of $\sim 10^{13}$ cm, which is inconsistent with the typical size of the emitting region of GRBs, e.g., $\sim 10^{16}$ cm. We propose, therefore, that the X-ray afterglow emission originates from a spherically symmetric SN ejecta expanding at $\Gamma \approx 2$ or, possibly, from the accretion onto the newly formed black hole, and we name these systems “binary driven hypernovae” (BdHNe). This interpretation is alternative to the traditional afterglow model based on the GRB synchrotron emission from a collimated jet outflow, expanding at ultra-relativistic Lorentz factor of $\Gamma \sim 10^2$ – 10^3 and originating from the collapse of a single object. We show then that the rest-frame energy band 0.3–10 keV X-ray luminosities of three selected BdHNe, GRB 060729, GRB 061121, and GRB 130427A, evidence a precisely constrained “nested” structure and satisfy precise scaling laws between the average prompt luminosity, $\langle L_{\text{iso}} \rangle$, and the luminosity at the end of the plateau, L_a , as functions of the time at the end of the plateau. All these features extend the applicability of the “cosmic candle” nature of Episode 3. The relevance of r-process in fulfilling the demanding scaling laws and the nested structure are indicated.

DOI: 10.1134/S1063772915070070

1. INTRODUCTION

Gamma-ray bursts (GRBs) are the most powerful explosions in the universe [1], with an isotropic energy release $E_{\text{iso}} = 10^{48}$ – 10^{54} erg. Their classification in short and long GRBs is based on their bi-modal distribution in the observed durations, the so-called T_{90} [2–5], being longer or larger than $T_{90} = 2$ s.

An interesting fact has been the discovery of a temporal coincidence between long GRBs and supernovae (SNe), hypothesized already in 1975 by [6]. In particular, after the first observed connection between GRB 980425 [7] and SN 1998bw [8], the systematic and spectroscopic analysis has evidenced that these associations involve SNe Ib/c SNe [9]. The lack of hydrogen (H) and helium (He) in SN Ib/c spectra, the most likely explanation is that the SN progenitor star is in a binary system with a compact companion, a NS [10–12].

The induced gravitational collapse (IGC) paradigm [13–16] addresses the study of long, energetic (10^{52} – 10^{54} erg) GRBs associated to SNe. It assumes as their progenitor a close binary system composed of an evolved massive star (likely a FeCO

*The text was submitted by the authors in English.

**E-mail: Ruffini@icra.it

Paper was presented at the international conference in honor of Ya.B. Zeldovich 100th Anniversary “Subatomic Particles, Nucleons, Atoms, Universe: Processes and Structure” held in Minsk, Belarus, in March 10–14, 2014. Published by the recommendation of the special Editors: S.Ya. Kilin, R. Ruffini, and G.V. Vereshchagin.

core) in the latest phases of its thermonuclear evolution and a neutron star (NS) companion. We here name these specially energetic systems fulfilling the IGC paradigm “binary driven hypernovae” (BdHNe), to differentiate them from the traditional less energetic hypernovae. From an observational point of view, the complete time sequence of four distinct emission episodes for the BdHNe, observed in GRB 090618 [17], GRB 101023 [18], GRB 110907B [19], and GRB 970828 [20], is well described by the space-time diagram in Fig. 1:

Episode 1 occurs when the FeCO core explodes as SN, originating a new-NS (ν -NS, see A) and triggering an accretion process onto the NS companion (see [15, 16] and B in Fig. 1). In this phase a prolonged interaction between the ν -NS and the NS binary companion occurs (C), leading to a spectrum with an expanding thermal component plus an extra power-law (see Fig. 16 in [17], and Fig. 4 in [20]).

Episode 2 occurs when the companion NS reaches its critical mass and collapses to a black hole (BH), emitting a GRB (D) at Lorentz factors $\Gamma = 10^2 - 10^3$ [for details, see, e.g., 17, 20, 21].

Episode 3, corresponds to the observed X-rays afterglow, which consists of a steep decay, starting at the end point of the prompt emission (see E), and then a plateau phase followed by a late constant power-law decay [see e.g. 17, 18, 20].

Episode 4, not shown in Fig. 1, corresponds to the optical SN emission due to the ^{56}Ni decay [see 22] occurring after $\sim 10 - 15$ days in the cosmological rest-frame. Although the presence of the SN is implicit in all the sources fulfilling the IGC paradigm, it is detectable only for GRBs at $z \leq 1$, in view of the limitations of the current optical telescopes.

In Section 2, we explain the difference in size and the Lorentz factor of the emitting regions of Episodes 1, 2 and 3; for definiteness we use the source with the most complete dataset, GRB 090618. In Section 3, we focus on the luminosity light curve of Episode 3, showing that, for three selected BdHNe (GRBs 060729, 061121 and 130427A) the steep decay, the plateau and the power-law decay of the X-ray luminosities as functions of E_{iso} , and, not only they follow a common power-law behavior with a constant slope in the source rest-frame [23], but they also present a “nested structure.” In Section 4, we examine correlations between the time at the starting point of the constant late power-law decay, t_a^* , the average prompt luminosity, $\langle L_{\text{iso}} \rangle$, and the luminosity at the end of the plateau, L_a , and we draw attention on the possible role of r-process, originating in the binary system of the progenitor, to power the mildly relativistic X-ray source and to explain the above correlations.

2. THE CASE OF GRB 090618

We briefly summarize the differences in the emitting region sizes of Episodes 1, 2, 3 and their corresponding Lorentz factors.

In [17] it was shown that the thermal component of Episode 1 expands from $\sim 10^9$ to $\sim 10^{10}$ cm in a rest-frame timescale of ~ 30 s with an average velocity of $\sim 4 \times 10^8$ cm s $^{-1}$. The total energy of Episode 1 is 4.1×10^{52} erg, well above to the traditional energy expected in the early phases of a SN. This extra energy is here attributed to the accretion of the material of the SN ejecta on the companion NS in the binary system [15, 20].

Episode 2 has been shown to be the ultra-relativistic prompt emission episode (e.g. the actual GRB) originating from the collapse of the NS to a BH. Its isotropic energy is 2.5×10^{53} erg. The characteristic Lorentz factor at the transparency of the Fireshell has been found to be $\Gamma = 490$. The characteristic spatial extension goes all the way up to $\sim 10^{16} - 10^{17}$ cm, reached at the end of Episode 2 (see in particular Fig. 10 in [17]).

The whole Episode 3 has an isotropic energy of $\approx 6 \times 10^{51}$ erg. A striking feature occurs in the early observed 150 s of Episode 3 (see Fig. 2), during its steep decay phase it has been found a thermal component with a decreasing temperature from ~ 0.97 keV to ~ 0.29 keV [24]. The surface radius of the emitter can be inferred from the observed temperature T_o and flux F_{BB} of the thermal component. We have in fact [17]

$$r = \Gamma \frac{d_l}{(1+z)^2} \left(\frac{F_{BB}}{\sigma T_o^4} \right)^{1/2}, \quad (1)$$

where d_l is the luminosity distance in the Λ CDM cosmological model and σ the Stefan–Boltzmann constant. As usually, the Lorentz factor can be written as $\Gamma = 1/\sqrt{1-\beta^2}$, where $\beta = v/c$ is the expansion velocity in units of the speed of light c . In parallel we obtain the relation between the detector arrival time t_a^d , the cosmological rest-frame arrival time t_a^d and the laboratory time t [25]

$$t_a^d \equiv t_a(1+z) = t(1-\beta \cos \theta)(1+z), \quad (2)$$

where θ is the displacement angle of the considered photon emission point from the line of sight. We can then deduce the value of the expansion velocity β , assumed constant, from the ratio between the variation of the emitter radius Δr and the duration of the emission in the laboratory Δt , i.e.,

$$\beta = \frac{\Delta r}{c \Delta t}. \quad (3)$$

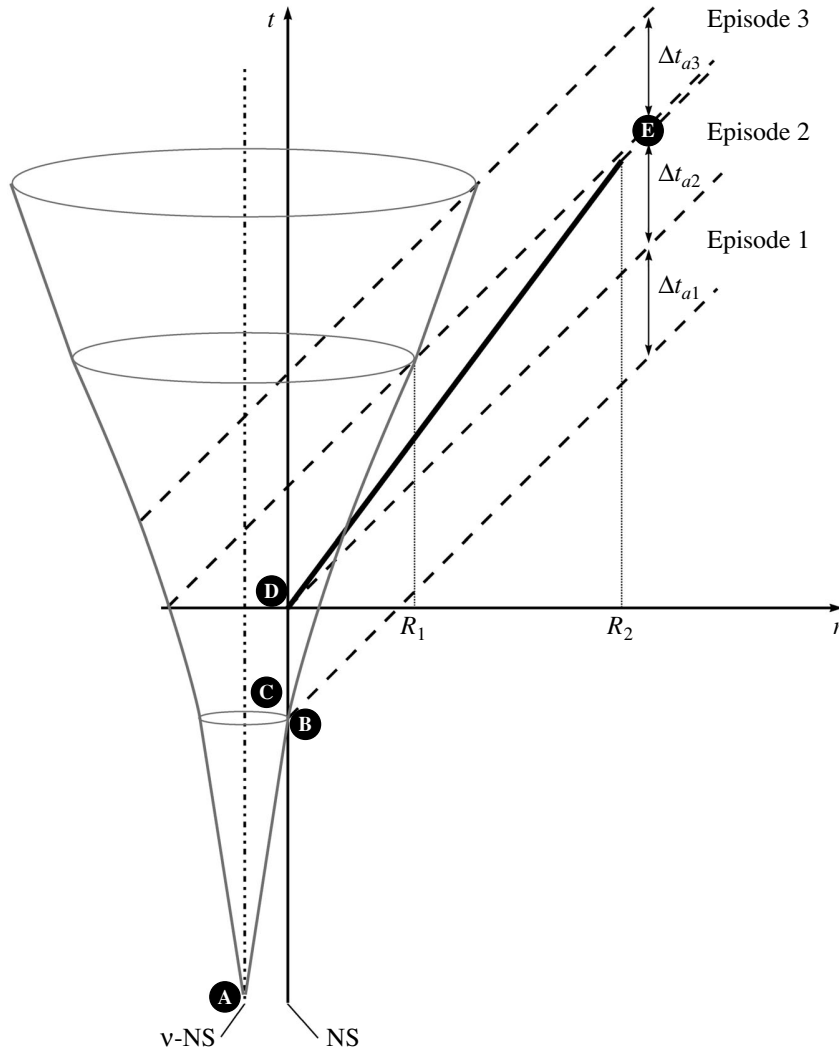


Fig. 1. A schematic diagram emphasizing the relativistic motion of the GRB in Episode 2 at $\Gamma = 490$ (thick line). Compared and contrasted is the interplay with the non-relativistic Episode 1 ($\Gamma = 1$) and Episode 3 ($\Gamma \approx 2$). It is particularly important to realize that the arrival time at the transition between Episode 1 and Episode 2 refers to two different values of the radial coordinate: in Episode 3, R_1 ($\approx 10^{12}$ cm), and Episode 2, R_2 ($\approx 10^{16} - 10^{17}$ cm). This clearly implies that Episode 3 belongs to the SN remnant and not to the GRB. For simplicity we neglect the binary motion as well as some residual BH activity after the completion of the gravitational collapse and/or the activity of the ν -NS and/or the asymmetry in the expanding SN ejecta.

From Eqs. (1)–(3) and using the condition $\beta \leq \cos \theta \leq 1$ [25], we obtain a range of values for the velocity of $0.75 \leq \beta \leq 0.89$, correspondingly, a range of values of the Lorentz factor $1.50 \leq \Gamma \leq 2.19$ and radii of the order of $r \sim 10^{13}$ cm.

As it is clear from Fig. 1, a sharp transition occurs between the end of Episode 2, where the characteristic dimensions reached by the GRB are of the order of $\sim 10^{16} - 10^{17}$ cm, and the emission at the beginning of X-ray luminosity, with an initial size of the order of $\sim 7 \times 10^{12}$ cm. This leads to the conclusion that the X-ray emission originates in the SN ejecta or in

the accretion on the newly born BH and, anyway, not from the GRB.

3. THE BdHNe NESTED EPISODE 3

In [23] it has been shown that the X-ray rest-frame 0.3–10 keV luminosity light curves present a constant decreasing power-law behavior, at times $\geq 10^4$ s, with a typical value of the slope of $-1.7 \leq \alpha_X \leq -1.3$. This feature has been evidenced in a best sample of six BdHNe, namely, 060729, 061007, 080319B, 090618, 091127, and 111228, hereafter *Golden Sample*, see e.g. [23] and Fig. 4, and has been used also to infer the redshifts of GRBs 101023

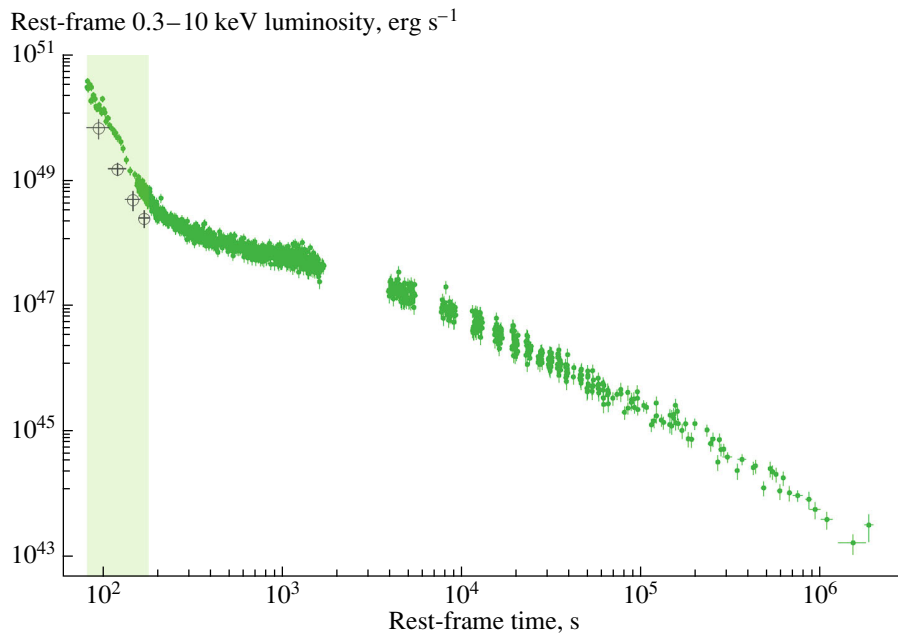


Fig. 2. Rest-frame 0.3–10 keV luminosity light curve of GRB 090618. The shaded region marks the rest-frame time interval in which a thermal component has been found. The black empty circles correspond to the luminosity of this thermal component.

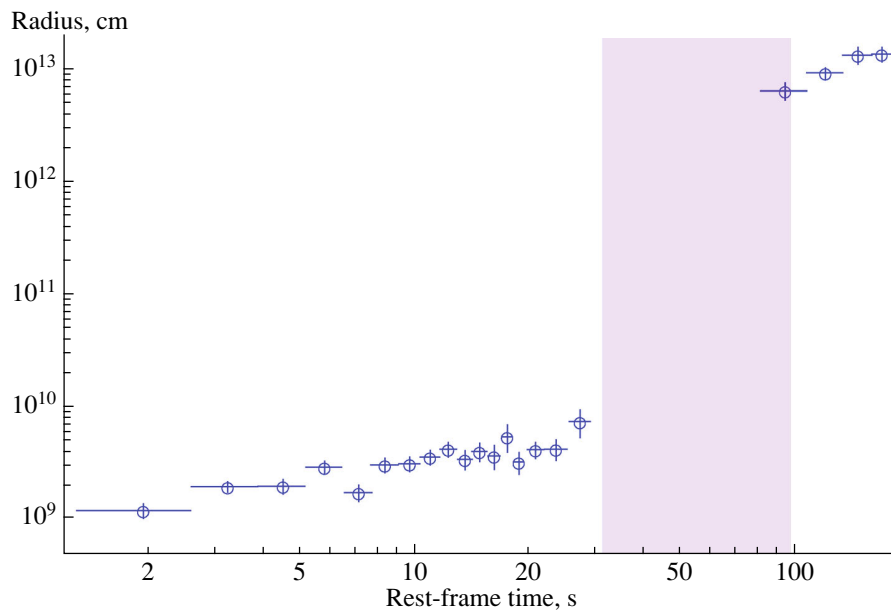


Fig. 3. The radii (open blue circles) of the emitting regions, measured in the cosmological rest-frame. Episode 1 radius ranges from 10^9 cm from 10^{10} cm and expands at $\Gamma \approx 1$. Episode 3 radius, in the early phases of the steep decay, starts from a value of $\approx 7 \times 10^{12}$ cm and expands at $\Gamma \approx 2$. Episode 2 rest-frame duration is indicated by the shaded purple region.

and 110709B [18, 26]. The sufficient selection criteria adopted in [23] to identify the BdHNe were: (a) an isotropic energy of the prompt emission larger than 10^{52} erg, (b) the presence of a precursor (indicated as Episode 1) with a cooling thermal emission in its

spectrum, and (c) a spectroscopical and/or photometric identification of the associated SN (for sources at $z \leq 1$).

The occurrence of GRB 130427A, the most luminous source ever observed in γ -rays with $E_{\text{iso}} \approx 10^{54}$ erg, at $z = 0.34$ [27, 28], led to another important

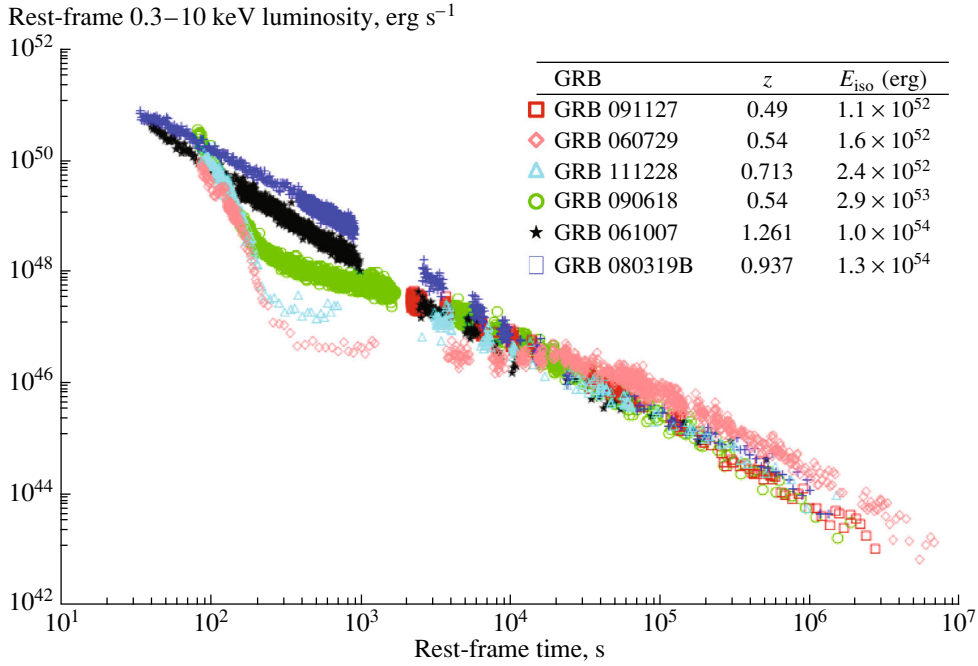


Fig. 4. The X-ray luminosity light curves of the BdHNe members of the Golden Sample (GS): GRB 060729, $z = 0.54$ (pink diamonds); GRB 061007, $z = 1.261$ (black stars); GRB 080319B, $z = 0.937$ (blue crosses); GRB 090618, $z = 0.54$ (green circles); GRB 091127, $z = 0.49$ (red squares); GRB 111228, $z = 0.713$ (cyan triangles).

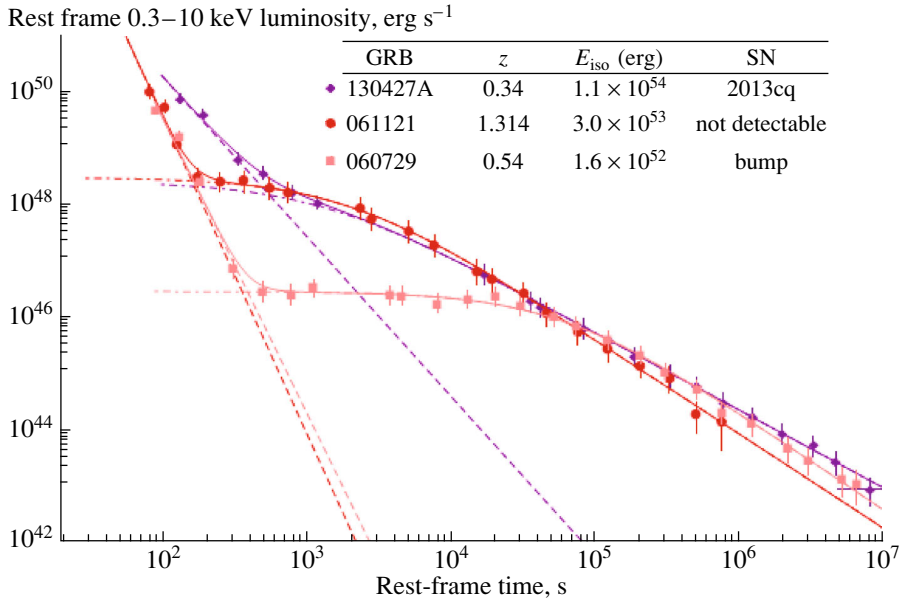


Fig. 5. The rest-frame 0.3–10 keV re-binned luminosity light curves of GRB 130427A (purple diamonds), GRB 061121 (red circles) and GRB 060729 (pink squares). The light curves are fitted by using a power-law for the steep decay phase (dashed lines) and the function in Eq. (4) for the plateau and the late decay phases (dot-dashed curves).

theoretical understanding. Although Episodes 1 and 2 are not clearly separated as in the prototype GRB 090618, the late X-ray luminosity light curve of GRB 130427A evidenced the pattern typical of the BdHNe

and its overlapping with GRB 060729 (see Fig. 5) provided an independent estimate of the redshift of GRB 130427A, in full agreement with the measured value. This allowed also to predict, ~ 10 – 15 days in

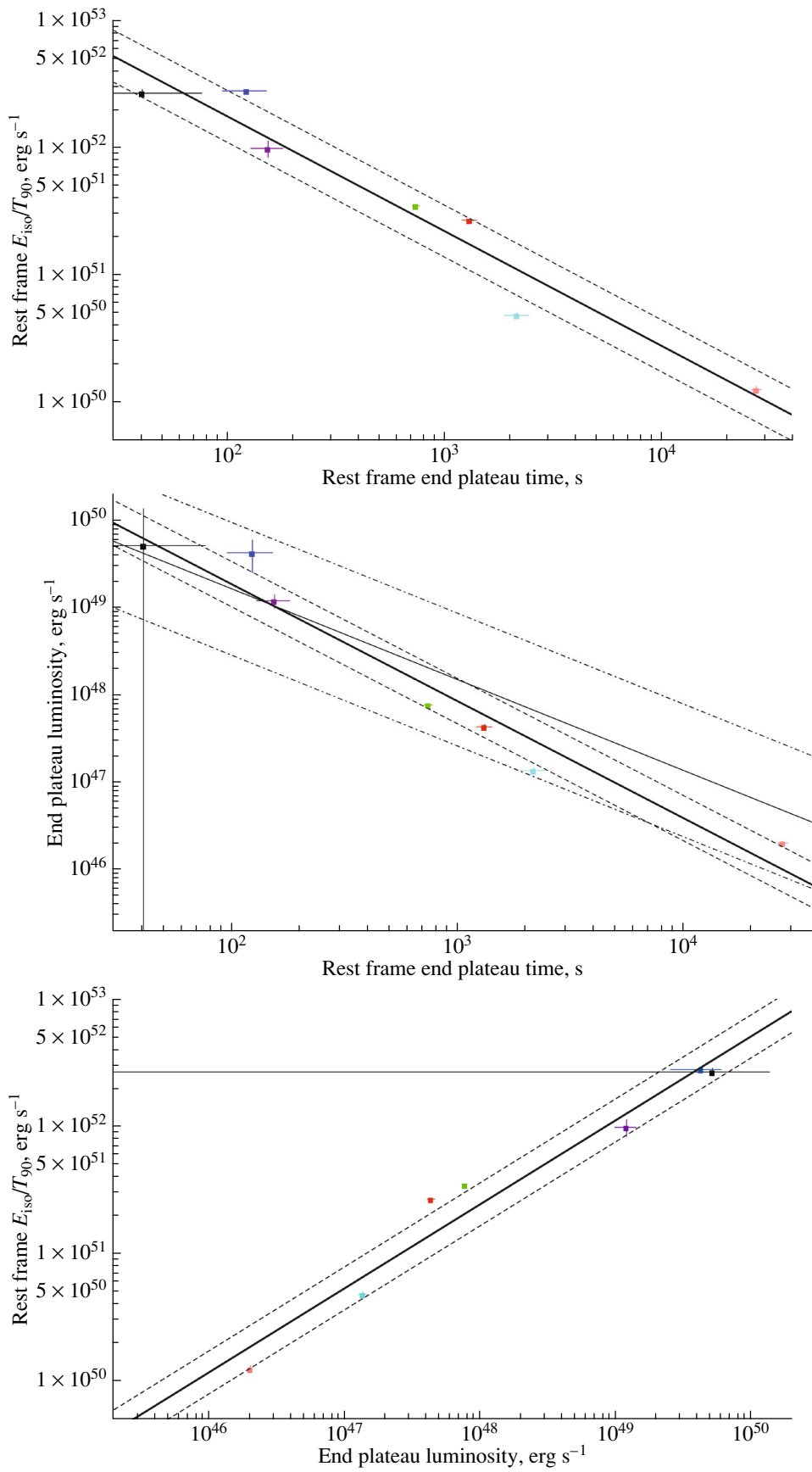


Fig. 6. The $\langle L_{\text{iso}} \rangle - t'_a$ (top panel), the $L_a - t'_a$ (middle panel) and the $\langle L_{\text{iso}} \rangle - L_a$ (bottom panel) correlations (solid gray lines) and the corresponding 1σ confidence levels (dashed gray lines). The source considered in these plots are GRB 060729 (pink), GRB 061007 (black), GRB 080319B (blue), GRB 090618 (green), GRB 091127 (red), GRB 111228A (cyan) and GRB 130427A (purple).

the cosmological rest-frame before its discovery, the occurrence of the associated SN, which has been later confirmed by the observations [29–32]. This led us to the conclusion that only the above conditions a) and c) in [23] are in fact necessary to identify the BdHNe.

GRB 130427A X-ray data have been compared and contrasted also with a third burst, GRB 061121, which shows the general behavior of BdHNe. This burst, at $z = 1.314$ [33], has $E_{\text{iso}} = 3.0 \times 10^{53}$ erg, and its Episode 4 is clearly missing in view of the high cosmological redshift. In Fig. 5, it is shown the comparison between the rebinned rest-frame 0.3–10 keV luminosity light curves of GRBs 130427A (purple diamonds), 060729 (pink squares) and 061121 (red circles). The fitting of their Episode 3 emissions, are modeled by a power-law, which describes the steep decay, and a phenomenological function, which reproduces the plateau and the late decay, both in the rest-frame arrival time t_a

$$L(t_a) = L_p \left(\frac{t_a}{100} \right)^{\alpha_p} + L_X \left(1 + \frac{t_a}{\tau} \right)^{\alpha_X}, \quad (4)$$

where L_p and α_p are the steep decay luminosity (normalized at $t_a = 100$ s) and index, and L_X , α_X and τ are, respectively, the plateau luminosity, the late power-law decay index and the characteristic time-scale of the end of the plateau. From Eq. (4), we have defined the end of the plateau t'_a as the rest-frame time when the luminosity of the plateau is half of the initial one, namely, $t'_a = \tau[(1/2)^{1/\alpha_X} - 1]$, and therefore the corresponding luminosity is $L_a = L_X/2$.

From this fitting procedure, we can conclude that the three considered BdHNe necessary present the following properties:

(a) the selected BdHNe evidence an asymptotic behavior in their X-ray luminosity in the 0.3–10 keV rest frame energy band [23] with a common power-law index $-1.7 \leq \alpha_x \leq -1.3$ for the considered sources;

(b) for the more energetic sources the plateau shrinks and the common power-law decay starts directly from the prompt steep decay with the same slope found at later times;

(c) most remarkably, all the power-law luminosities as functions of the rest-frame time of the BdHNe converge to a common value, independently of their isotropic energy, presenting a “nested” structure, see Fig. 5.

The most important result consists in the fact that in all BdHNe with $z \leq 1$, the common behavior of the power-law decay starts after t'_a , which can occur, for the most energetic sources, much earlier than $t_a \sim 10^4$ s [23].

4. CORRELATIONS FOR THE BDHNE

In order to quantify some additional properties of the plateau phase and of the late power-law decay, in analogy with the procedure by [34–36] we have established correlations from our Eq. (4) for the BdHNe (see Fig. 6): 1) the $\langle L_{\text{iso}} \rangle - t'_a$ (top), 2) the $L_a - t'_a$ by [34] (middle) and 3) the $\langle L_{\text{iso}} \rangle - L_a$ (bottom). In the last correlation, which resembles the one discussed in [35], the averaged luminosity of the prompt is defined as $\langle L_{\text{iso}} \rangle = E_{\text{iso}}/t_{90,a}$, where $t_{90,a}$ is the rest-frame t_{90} duration of the burst. The sources considered in these three correlations correspond to GRB 130427A (purple) and to the BdHNe considered in [23]: GRB 060729 (pink), GRB 061007 (black), GRB 080319B (blue), GRB 090618 (green), GRB 091127 (red) and GRB 111228A (cyan). The parameters of each burst are listed in Table 1. The best fit parameters of the correlations, generally expressed as $\log_{10} Y_i = m_i \log_{10} X_i + q_i$, and their extra scatters σ_i (where $i = 1, \dots, 3$) are summarized in Table 2. As is clear from Table 1, this sample of bursts provides tighter correlations with extra-scatters smaller than the one in [37], $\sigma = 0.76$ for the whole sample of 62 bursts and $\sigma = 0.40$ for the best sub-sample (U0095).

To explain the above nested structure and correlations, we have considered, as a viable energy source, the decay of heavy elements produced in the r-process [38–44]. In the work by [39] it has been shown that the emission from the surface of an optically thick expanding ejecta, in adiabatic regime, provides a flat light curve (see also [45]). This can explain in principle the observed plateau phase of Episode 3, see Fig. 5. After the ejecta becomes transparent, the heating source term due to the nuclear decays of the heavy nuclei, generated via r-process, dominates. The avalanche of decays with different lifetimes provides a total energy release per unit mass per time that follows a power-law distribution, whose decay index has been estimated to be $-1.4 \leq \alpha \leq -1.1$ [46]. These values are strikingly similar to the ones we have found in the late X-ray luminosity.

Table 1. List of the quantities involved in the four correlations in Fig. 6, for each of the considered sources

GRB	E_{iso} (erg)	$\langle L_{\text{iso}} \rangle$ (erg/s)	t'_a (s)	L_a (erg/s)
GRB 060729	$(1.60 \pm 0.07) \times 10^{52}$	$(1.25 \pm 0.08) \times 10^{50}$	$(2.74 \pm 0.14) \times 10^4$	$(2.04 \pm 0.05) \times 10^{46}$
GRB 061007	$(1.05 \pm 0.07) \times 10^{54}$	$(2.67 \pm 0.18) \times 10^{52}$	41 ± 36	$(5.21 \pm \text{unc}) \times 10^{49}$
GRB 080319B	$(1.41 \pm 0.03) \times 10^{54}$	$(2.79 \pm 0.07) \times 10^{52}$	123 ± 28	$(4.3 \pm 1.7) \times 10^{49}$
GRB 090618	$(2.49 \pm 0.02) \times 10^{53}$	$(3.47 \pm 0.03) \times 10^{51}$	741 ± 30	$(7.81 \pm 0.17) \times 10^{47}$
GRB 091127	$(1.62 \pm 0.02) \times 10^{52}$	$(2.68 \pm 0.03) \times 10^{51}$	41 ± 36	$(4.39 \pm 0.26) \times 10^{47}$
GRB 111228A	$(2.41 \pm 0.14) \times 10^{52}$	$(4.79 \pm 0.24) \times 10^{50}$	$(2.17 \pm 0.27) \times 10^3$	$(1.38 \pm 0.10) \times 10^{47}$
GRB 130427A	$(1.05 \pm 0.15) \times 10^{54}$	$(9.8 \pm 1.5) \times 10^{51}$	155 ± 26	$(1.21 \pm 0.21) \times 10^{49}$

5. CONCLUSIONS

Within the IGC scenario, the sub-class of long, extremely energetic (10^{52} – 10^{54} erg) sources is initially driven by a tight binary system, formed by a ν -NS and a companion NS, surrounded by the SN ejecta (see Fig. 1), and are named “BdHNe.” These systems clearly differ from the gravitational collapse of a single massive progenitor star described by the Collapsar model [47–49].

We compared and contrasted the late X-ray luminosities of three BdHNe with different E_{iso} , finding a nested structure. We showed tight correlations between $\langle L_{\text{iso}} \rangle$, L_a and t'_a (see Fig. 6 and Table 2) in agreement with the Dainotti–Willingale ones. The above scaling laws, the nesting, and the initial dimension of $\sim 7 \times 10^{12}$ cm and Lorentz factor of $\Gamma \approx 2$ obtained from the steep decay of the X-ray luminosity of GRB 090618 put stringent limits on alternative theoretical models. They do not appear to be explainable within the traditional fireball jetted model, originating in the synchrotron radiation emitted by a decelerating relativistic shell with $\Gamma \sim 10^2$ and colliding with the circumburst medium at distances $\sim 10^{16}$ cm [see, e.g., 1, 50–52, and reference therein]. We alternatively proposed that the late X-ray luminosity comes from the wide angle emission of the SN ejecta or in the accretion on the newly born BH. Attention is given to the role of the energy release in the SN ejecta from the decay of very heavy nuclei generated by r-process

Table 2. List of the considered correlations and of the corresponding values of m_i , q_i and σ_i

	Correlations	m_i	q_i	σ_i
1	$\langle L_{\text{iso}} \rangle - t'_a$	$-(0.90 \pm 0.09)$	54.0 ± 0.3	0.20 ± 0.05
2	$L_a - t'_a$	$-(1.34 \pm 0.14)$	52.0 ± 0.4	0.26 ± 0.08
3	$\langle L_{\text{iso}} \rangle - L_a$	0.66 ± 0.05	19.7 ± 2.6	0.17 ± 0.05

in binary NSs [39], which may explain the nested structure of the X-ray luminosities, the plateau phase, as well as its energetic and constant index power-law decay (see Fig. 5).

In the case of binary systems with longer periods and/or a lower accretion rate, which do not allow the NS companion to reach its critical mass and to form a BH, Episode 2 is missing. The presence of the companion NS will nevertheless strip the H and He envelopes of the core progenitor star. These sources have low energetic bursts ($E_{\text{iso}} < 10^{52}$ erg), such as GRB 060218 and GRB 980425, and their X-ray luminosity light curves do not overlap with the ones of our more energetic sample of BdHNe. These systems do not conform to the IGC paradigm and are traditional hypernovae.¹

REFERENCES

1. T. Piran, *Rev. Mod. Phys.* **76**, 1143 (2005). <http://link.aps.org/doi/10.1103/RevModPhys.76.1143>
2. R. W. Klebesadel, in *Gamma Ray Bursts*, Ed. by C. Ho, R. I. Epstein, and E. E. Fenimore (Cambridge Univ. Press, 1992), pp. 161–168.
3. J.-P. Dezalay, C. Barat, R. Talon, R. Syunyaev, O. Terekhov, and A. Kuznetsov, in *American Institute of Physics Conference Series*, Vol. 265, Ed. by W. S. Paciesas and G. J. Fishman (American Institute of Physics, Huntsville, Alabama, 1992), pp. 304–309.
4. C. Kouveliotou, C. A. Meegan, G. J. Fishman, N. P. Bhat, M. S. Briggs, T. M. Koshut, W. S. Paciesas, and G. N. Pendleton, *Astrophys. J. Lett.* **413**, L101 (1993).
5. M. Tavani, *Astrophys. J. Lett.* **497**, L21 (1998), [astro-ph/9802192](http://arxiv.org/abs/astro-ph/9802192).
6. G. S. Bisnovatyi-Kogan, V. S. Imshennik, D. K. Nadyozhin, and V. M. Chechetkin, *Astrophys. Space Sci.* **35**, 23 (1975).

¹ <http://nsm.utdallas.edu/texas2013/proceedings/3/1/Ruffini.pdf>

7. E. Pian, L. Amati, L. A. Antonelli, R. C. Butler, E. Costa, G. Cusumano, J. Danziger, M. Feroci, F. Fiore, F. Frontera, et al., *Astrophys. J.* **536**, 778 (2000), astro-ph/9910235.
8. T. J. Galama, P. M. Vreeswijk, J. van Paradijs, C. Kouveliotou, T. Augusteijn, H. Bönhardt, J. P. Brewer, V. Doublier, J.-F. Gonzalez, B. Leibundgut, et al., *Nature (London)* **395**, 670 (1998), astro-ph/9806175.
9. J. Hjorth and J. S. Bloom, in *Gamma-Ray Bursts*, Cambridge Astrophysics Series, Vol. 51, Ed. by C. Kouveliotou, R. A. M. J. Wijers, and S. E. Woosley (Cambridge Univ. Press, 2012), pp. 169–190.
10. K. Nomoto and M. Hashimoto, *Phys. Rep.* **163**, 13 (1988).
11. K. Nomoto, H. Yamaoka, O. R. Pols, E. P. J. van den Heuvel, K. Iwamoto, S. Kumagai, and T. Shigeyama, *Nature (London)* **371**, 227 (1994).
12. K. Iwamoto, K. Nomoto, P. Höflich, H. Yamaoka, S. Kumagai, and T. Shigeyama, *Astrophys. J. Lett.* **437**, L115 (1994).
13. R. Ruffni, M. G. Bernardini, C. L. Bianco, L. Caito, P. Chardonnet, M. G. Dainotti, R. Frascetti, R. Guida, G. Vereshchagin, and S.-S. Xue, in *ESA Special Publication*, Vol. 622 (ESA, 2007), p. 561, 0705.2456.
14. R. Ruffni, M. G. Bernardini, C. L. Bianco, L. Caito, P. Chardonnet, C. Cherubini, M. G. Dainotti, F. Frascetti, A. Geralico, R. Guida, et al., in *Proceedings of the 11th Marcel Grossmann Meeting on Recent Developments in Theoretical and Experimental General Relativity, Gravitation and Relativistic Field Theories*, Ed. by H. Kleinert, R. T. Jantzen, and R. Ruffni (2008), pp. 368–505; arXiv:0804.2837.
15. J. A. Rueda and R. Ruffni, *Astrophys. J. Lett.* **758**, L7 (2012); arXiv:1206.1684.
16. L. Izzo, J. A. Rueda, and R. Ruffni, *Astron. Astrophys.* **548**, L5 (2012); arXiv:1206.2887.
17. L. Izzo, R. Ruffni, A. V. Penacchioni, C. L. Bianco, L. Caito, S. K. Chakrabarti, J. A. Rueda, A. Nandi, and B. Patricelli, *Astron. Astrophys.* **543**, A10 (2012), arXiv:1202.4374.
18. A. V. Penacchioni, R. Ruffni, L. Izzo, M. Muccino, C. L. Bianco, L. Caito, B. Patricelli, and L. Amati, *Astron. Astrophys.* **538**, A58 (2012); arXiv:1112.2970.
19. A. V. Penacchioni, R. Ruffni, C. L. Bianco, L. Izzo, M. Muccino, G. B. Pisani, and J. A. Rueda, *Astron. Astrophys.* **551**, A133 (2013); arXiv:1301.6014.
20. R. Ruffni, J. A. Rueda, C. Barbarino, C. L. Bianco, H. Dereli, M. Enderli, L. Izzo, M. Muccino, A. V. Penacchioni, G. B. Pisani, et al., arXiv: 1311.7432 (2013).
21. R. Ruffni, G. Vereshchagin, and S.-S. Xue, *Phys. Rep.* **487**, 1 (2010); arXiv:0910.0974.
22. D. Arnett, *Space Sci. Rev.* **78**, 559 (1996).
23. G. B. Pisani, L. Izzo, R. Ruffni, C. L. Bianco, M. Muccino, A. V. Penacchioni, J. A. Rueda, and Y. Wang, *Astron. Astrophys.* **552**, L5 (2013); arXiv:1304.1764.
24. K. L. Page, R. L. C. Starling, G. Fitzpatrick, S. B. Pandey, J. P. Osborne, P. Schady, S. McBreen, S. Campana, T. N. Ukwatta, C. Pagani, et al., *Mon. Not. R. Astron. Soc.* **416**, 2078 (2011).
25. C. L. Bianco, R. Ruffni, and S.-S. Xue, *Astron. Astrophys.* **368**, 377 (2001), astro-ph/0102060.
26. A. V. Penacchioni, R. Ruffni, C. L. Bianco, L. Izzo, M. Muccino, G. B. Pisani, and J. A. Rueda, *Astron. Astrophys.* **551**, A133 (2013); arXiv:1301.6014.
27. D. Xu, A. de Ugarte Postigo, S. Schulze, J. Jessen-Hansen, G. Leloudas, T. Kruehler, J. P. U. Fynbo, and P. Jakobsson, *GRB Coordinates Network* **14478**, 1 (2013).
28. H. Flores, S. Covino, D. Xu, T. Kruehler, J. Fynbo, B. Milvang-Jensen, A. de Ugarte Postigo, L. Kaper, and K. Wiersema, *GRB Coordinates Network* **14491**, 1 (2013).
29. A. de Ugarte Postigo, D. Xu, G. Leloudas, T. Kruehler, D. Malesani, J. Gorosabel, C. C. Thone, R. Sanchez-Ramirez, S. Schulze, J. P. U. Fynbo, et al., *GRB Coordinates Network* **14646**, 1 (2013).
30. A. J. Levan, A. S. Fruchter, J. Graham, N. R. Tanvir, J. Hjorth, J. Fynbo, D. Perley, S. B. Cenko, E. Pian, Z. Cano, et al., *GRB Coordinates Network* **14686**, 1 (2013).
31. A. M. Watson, N. Butler, A. Kutyrev, W. H. Lee, M. G. Richer, C. Klein, O. Fox, J. X. Prochaska, J. Bloom, A. Cucchiara, et al., *GRB Coordinates Network* **14666**, 1 (2013).
32. D. Xu, A. de Ugarte Postigo, T. Kruehler, D. Malesani, G. Leloudas, J. P. U. Fynbo, J. Hjorth, S. Schulze, P. Jakobsson, Z. Cano, et al., *GRB Coordinates Network* **14597**, 1 (2013).
33. J. S. Bloom, D. A. Perley, and H. W. Chen, *GRB Coordinates Network* **5826**, 1 (2006).
34. M. G. Dainotti, V. F. Cardone, and S. Capozziello, *Mon. Not. R. Astron. Soc.* **391**, L79 (2008); arXiv:0809.1389.
35. M. G. Dainotti, M. Ostrowski, and R. Willingale, *Mon. Not. R. Astron. Soc.* **418**, 2202 (2011); arXiv:1103.1138.
36. R. Willingale, P. T. O'Brien, J. P. Osborne, O. Godet, K. L. Page, M. R. Goad, D. N. Burrows, B. Zhang, E. Rol, N. Gehrels, et al., *Astrophys. J.* **662**, 1093 (2007); astro-ph/0612031.
37. M. G. Dainotti, V. Fabrizio Cardone, S. Capozziello, M. Ostrowski, and R. Willingale, *Astrophys. J.* **730**, 135 (2011); arXiv:1101.1676.
38. E. M. Burbidge, G. R. Burbidge, W. A. Fowler, and F. Hoyle, *Rev. Mod. Phys.* **29**, 547 (1957).
39. L.-X. Li and B. Paczyński, *Astrophys. J. Lett.* **507**, L59 (1998), astro-ph/9807272.
40. H.-T. Janka, T. Eberl, M. Ruffert, and C. L. Fryer, *Astrophys. J. Lett.* **527**, L39 (1999); astro-ph/9908290.
41. S. Rosswog, R. Speith, and G. A. Wynn, *Mon. Not. R. Astron. Soc.* **351**, 1121 (2004); astro-ph/0403500.
42. R. Oechslin, H.-T. Janka, and A. Marek, *Astron. Astrophys.* **467**, 395 (2007); astro-ph/0611047.
43. S. Goriely, A. Bauswein, and H.-T. Janka, *Astrophys. J. Lett.* **738**, L32 (2011); arXiv:1107.0899.

44. T. Piran, O. Korobkin, and S. Rosswog, arXiv:1401.2166 (2014).
45. W. D. Arnett, *Astrophys. J.* **253**, 785 (1982).
46. B. D. Metzger, G. Martinez-Pinedo, S. Darbha, E. Quataert, A. Arcones, D. Kasen, R. Thomas, P. Nugent, I. V. Panov, and N. T. Zinner, *Mon. Not. R. Astron. Soc.* **406**, 2650 (2010); arXiv:1001.5029.
47. S. E. Woosley, *Astrophys. J.* **405**, 273 (1993).
48. A. I. MacFadyen and S. E. Woosley, *Astrophys. J.* **524**, 262 (1999); astro-ph/9810274.
49. S. E. Woosley and J. S. Bloom, *Ann. Rev. Astron. Astrophys.* **44**, 507 (2006); astro-ph/0609142.
50. R. Sari, T. Piran, and R. Narayan, *Astrophys. J. Lett.* **497**, L17 (1998); astro-ph/9712005.
51. P. Mészáros, *Rep. Prog. Phys.* **69**, 2259 (2006); astro-ph/0605208.
52. N. Gehrels, E. Ramirez-Ruiz, and D. B. Fox, *Ann. Rev. Astron. Astrophys.* **47**, 567 (2009); arXiv:0909.1531.

Induced Gravitational Collapse in the BATSE Era: The Case of GRB 970828*

R. Ruffini^{1,2,3,4**}, L. Izzo^{1,2}, C. L. Bianco^{1,2}, J. A. Rueda^{1,2}, C. Barbarino¹, H. Dereli^{3,5},
M. Enderli^{1,3}, M. Muccino¹, A. V. Penacchioni^{4,6}, G. B. Pisani^{1,3}, and Y. Wang¹

¹*Dip. di Fisica and ICRA, Sapienza Università di Roma, Piazzale Aldo Moro 5, I-00185 Rome, Italy*

²*ICRANet, Piazza della Repubblica 10, I-65122 Pescara, Italy*

³*Universite de Nice Sophia Antipolis, CEDEX 2, Grand Chateau Parc Valrose, Nice, France*

⁴*ICRANet-Rio, CBPF, Rua Dr. Xavier Sigaud 150, Rio de Janeiro, RJ, 22290-18 Brazil*

⁵*Observatoire de la Côte d'Azur, F-06304 Nice, France*

⁶*Instituto Nacional de Pesquisas Espaciais (INPE),
Av. do Astronautas, 1758, Sao Jose dos Campos, SP, Brazil*

Received January 26, 2015

Abstract—Following the recently established “Binary-driven HyperNova” (BdHN) model, we here interpret GRB 970828 in terms of the four episodes typical of such a model. The “Episode 1,” up to 40 s after the trigger time t_0 , with a time varying thermal emission and a total energy of $E_{\text{iso,1st}} = 2.60 \times 10^{53}$ erg, is interpreted as due to the onset of an hyper-critical accretion process onto a companion neutron star, triggered by the companion star, an FeCO core undergoing a SN explosion. The “Episode 2,” observed up $t_0 + 90$ s, is interpreted as a canonical gamma ray burst, with an energy of $E_{\text{tot}}^{e^+e^-} = 1.60 \times 10^{53}$ erg, a baryon load of $B = 7 \times 10^{-3}$ and a bulk Lorentz factor at transparency of $\Gamma = 142.5$. From this Episode 2, we infer that the GRB exploded in an environment with a large average particle density $\langle n \rangle \approx 10^3$ particles/cm³ and dense clouds characterized by typical dimensions of $(4-8) \times 10^{14}$ cm and $\delta n/n \sim 10$. The “Episode 3” is identified from $t_0 + 90$ s all the way up to 10^{5-6} s: despite the paucity of the early X-ray data, typical in the BATSE, pre-Swift era, we find extremely significant data points in the late X-ray afterglow emission of GRB 970828, which corresponds to the ones observed in all BdHNe sources. The “Episode 4,” related to the Supernova emission, does not appear to be observable in this source, due to the presence of darkening from the large density of the GRB environment, also inferred from the analysis of the Episode 2.

DOI: 10.1134/S1063772915070094

1. INTRODUCTION

The Gamma Ray Burst (GRB) 970828 is one of the first GRBs with an observed X-ray and radio afterglow and a determined redshift of $z = 0.9578$ from the identification of its host galaxy [1]. It was detected by the All Sky Monitor (ASM) detector on board the Rossi X-ray Timing Explorer (RXTE) spacecraft [2], and then observed also by the Burst And Transient Source Experiment (BATSE) on board the Compton

Gamma-Ray Observatory [3]. The crucial data on the afterglow of GRB 970828 were collected by the Advanced Satellite for Cosmology and Astrophysics (ASCA) in the 2–10 keV energy range, one day after the RXTE detection [4], and by ROSAT [5] in the (0.1–2.4) keV, one week later. Observations on optical wavelengths failed to detect the optical afterglow [6, 7]. The fluence measured by BATSE implies an isotropic energy for the total emission of $E_{\text{iso}} = 4.2 \times 10^{53}$ erg. This source is still presenting today, after 15 years from its discovery, an extremely rich problematic in the identification of its astrophysical nature.

The recent joint GRB observations made by satellites as Swift [8], Fermi [9], AGILE [10], Konus-WIND [11] in hard X-rays energy range, as well as the follow-up of their afterglow emission in the (0.3–

*The text was submitted by the authors in English.

**E-mail: Ruffini@icra.it

Paper was presented at the international conference in honor of Ya.B. Zeldovich 100th Anniversary “Subatomic Particles, Nucleons, Atoms, Universe: Processes and Structure” held in Minsk, Belarus, in March 10–14, 2014. Published by the recommendation of the special Editors: S.Ya. Kilin, R. Ruffini, and G.V. Vereshchagin.

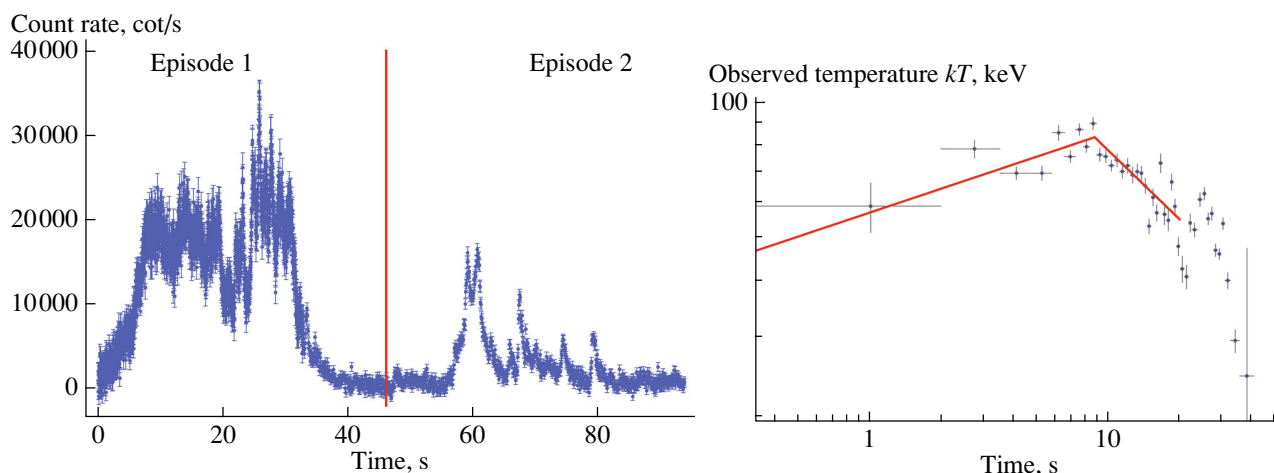


Fig. 1. *Left panel:* BATSE-LAD light curve of GRB 970828 in the 25–1900 keV energy range. *Right panel:* The behavior of the observed temperature in GRB 970828 and the best fit with a broken power-law function of the first 20 s as presented in [22].

10) keV range by the X-Ray Telescope (XRT) [12] on-board Swift, and the corresponding follow-up observations in the optical and radio wavelengths have made possible a new understanding of the entire GRB process. In this paper we start a procedure of revisiting previous GRBs in the BATSE, pre-Swift era, including the new understanding mentioned above. In particular, we apply to GRB 970828 the new Binary-driven HyperNova (BdHN) scenario, in which GRBs associated with Supernovae (SNe) [13, 14], are composed of four different episodes [15–18].

- The “Episode 1” corresponds to the emission from an hyper-critical accretion onto the a neutron star (NS) due to the onset of a Supernova (SN) companion in a close binary system. The hyper-critical accretion induces allows the NS to reach the critical mass [19] finally collapsing to a black hole (BH). In the specific case of GRB 970828, this episode is clearly identified, see Fig. 1. The observed hard X-ray emission is composed of a thermal spectrum plus a power-law component, both evolving in time. The presence of an evolving thermal component allows the determination of the time decay of the blackbody temperature kT (from 80 to 25 keV), in the rest-frame time of 20 s, leading to the estimate of the emitter radius between 5000 and 25 000 km.
- The “Episode 2,” corresponding to the observations of the GRB, is related to the collapse of the NS into a BH. The characteristic parameters of the GRB 970828 are the Lorentz Gamma factor of $\Gamma \approx 150$, the baryon load $B =$

7×10^{-3} and a large circumburst density of the order of 10^3 particles/cm³.

- The “Episode 3,” in soft X-rays, occurs when the prompt emission from the GRB fades away and an additional component, discovered by Swift XRT [20, 21] emerges. It has been shown [18] that this component, in energetic ($E_{\text{iso}} \geq 10^{52}$ erg) BdHNe, when referred to the rest-frame of the source, follows a standard behavior of the light curve evolution. This emission encompasses the SN shock break out and the expanding SN ejecta ($v/c \approx 0.1$). In the case of GRB 970828, the X-ray emission observed by ASCA and ROSAT perfectly overlap with the common trend observed in BdHN systems and exemplified in Fig. 5.
- The “Episode 4” is represented by the observations of the optical emission of the SN, which has been observed in some BdHN sources, with $z \leq 0.9$, [GRB 090618, GRB 060729, GRB 091127, GRB 111228, GRB 080319B, see, e.g., 18]. It is generally hard to detect a SN at $z = 0.9578$ and in the case of GRB 970828 is even more difficult due to the very large presence of circumburst material, which has also hampered the observations of the optical afterglow, making this source a ‘dark’ GRB.

The presence of an evolving thermal component in the first 20 s of the emission of GRB 970828, using BATSE data, has been indicated by [22], where they have considered the emission in the first 20 s of Episode 1. They then have fitted the

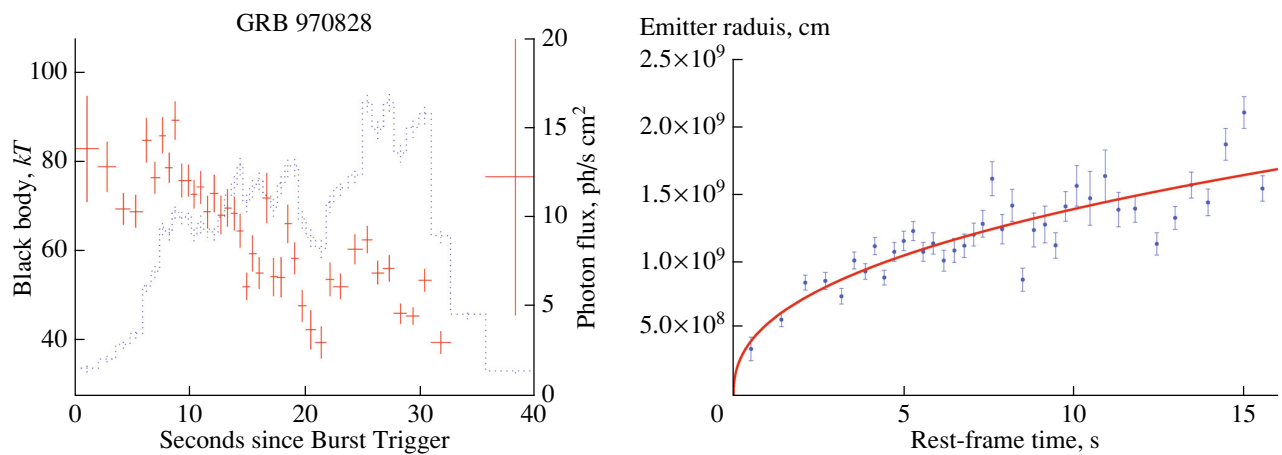


Fig. 2. *Left panel:* The evolution of the temperature kT (red crosses) as obtained from a time-resolved spectral analysis of the first 40 s of emission of GRB 970828. The light curve of the first episode (blue dots) is shown in background. *Right panel:* Evolution of the rest-frame radius of the first episode of GRB 970828. The solid line corresponds to the best fit of this dataset with a power-law function $r \propto t^\delta$, with $\delta = 0.41 \pm 0.04$.

evolution of the temperature kT and the ratio $\mathcal{R} = (Flux_{BB}/\sigma T_{obs}^4)^{1/2}$, where $Flux_{BB}$ is the observed flux of the instantaneous blackbody, σ the Stefan constant, and T_{obs} the observed temperature, whose evolution in time is fitted with a broken power-law function, see Fig. 1. In their theoretical interpretation, this thermal emission was associated to the photospheric GRB emission of a relativistic expanding fireball [23], and they inferred a bulk Lorentz Gamma factor of the expanding plasma, $\Gamma \approx (305 \pm 28)Y_0^{1/4}$, with $Y_0 \geq 1$ the ratio between the entire fireball energy and the energy emitted in γ -rays [23]. Since the fireball photospheric radius is given by $r_{ph} = (\mathcal{R}D\Gamma)/(1.06(1+z)^2)$, with D the luminosity distance of the GRB, they obtain for r_{ph} the value of $2.7 \times 10^{11}Y_0^{1/4}$. In [22], the authors have also attributed the remaining GRB emission to an unspecified engine activity and neglected all data after 20 s. In their own words, “we neglect here late-time episodes of engine activity that occur after ~ 25 and ~ 60 s in this burst.” As we will show in the following of this article, we notice the presence of a thermal component in the first 40 s, and we attribute it to a non-relativistic initial expansion with radius evolving from 2×10^9 to 3×10^{10} cm, see Fig. 2. In addition, we identify the Episode 2 with the GRB emission between $t_0 + 50$ s and $t_0 + 90$ s and the Episode 3 between $10^4 - 10^6$ s.

In Section 2 we give a summary of the observations of GRB 970828 and describe our data analysis. We proceed in Section 3 to the description of Episode 1, with the details of the expanding black

body emitter, the analysis of the non-thermal component and its interpretation in the BdHN paradigm. In Section 4 we describe Episode 2, the authentic GRB emission. It is well explained in the context of the fireshell scenario, see, e.g., [13] for a complete review of the model. In Section 5 we describe Episode 3, pointing out the clear overlapping of the observed late X-ray data within the theoretical expectation of a BdHN member. In Section 6 we discuss about the theoretically expected SN emission, not observed due to the large circumburst medium. Conclusions are given in the last section.

2. DATA ANALYSIS

GRB 970828 was discovered with the All-Sky Monitor (ASM) on board the Rossi X-Ray Timing Explorer (RXTE) on 1997 August 28 [3]. Within 3.6 h the RXTE/PCA scanned the region of the sky around the error box of the ASM burst and detected a weak X-ray source [4, 24]. GRB 970828 was also observed by the Burst and Transient Source Experiment (BATSE) and the GRB experiment on Ulysses [3]. The BATSE-LAD light curve is characterized by two main emission phenomena, see Fig. 1: the first lasts about 40 s and is well described by two main pulses, the second one is more irregular, being composed by several sharp pulses, lasting other 40 s.

The X-ray afterglow was discovered by the ASCA satellite 1.17 days after the GRB trigger [25]. The X-ray afterglow observations continued up to 7–10 days from the burst detection. The optical observations, which started about 4 h after the burst, did not report any possible optical afterglow for GRB 970828 up

Table 1. Spectral analysis (25 keV–1.94 MeV) of the first 40 s of emission in GRB 970828. The following symbols represent: * temperature (keV) of the second black body; † normalization of the power law component in units of $\text{ph cm}^{-2} \text{s}^{-1} \text{keV}^{-1}$

Spectral model	$\alpha (\gamma)$	β	γ_{ext}	E_{peak} (keV)	kT (keV)	χ^2/DOF
Power Law	-1.38 ± 0.01	–	–	–	–	6228.1/115
Cut-off PL	-0.77 ± 0.02	–	–	465.4 ± 10.6	–	203.83/114
Band	-0.60 ± 0.03	-2.15 ± 0.05	–	360.5 ± 12.5	–	106.48/113
Band+PL	-0.41 ± 0.15	-2.41 ± 0.33	-1.47 ± 0.17	335.8 ± 17.6	–	104.12/111
Cutoff + PL	-0.47 ± 0.17	–	-1.28 ± 0.16	338.7 ± 17.9	–	104.28/112
BB + po	–	–	-1.50 ± 0.01	–	63.71 ± 0.92	228.09/113
BB + BB + po	-1.53 ± 0.17	–	$0.010 \pm 0.001^\dagger$	$40.01 \pm 2.05^*$	106.8 ± 6.3	101.78/111

to $R = 23.8$ [7]. However, the observations at radio wavelengths of the burst position, 3.5 h after the initial burst, succeeded in identifying a source at a good significance level of 4.5σ [1] inside the ROSAT error circle ($10''$). The following deep searches for a possible optical counterpart of this radio source led to the identification of an interacting system of faint galaxies, successively recognized as the host galaxy of GRB 970828. The spectroscopic observations of the brightest of this system of galaxies led to the identification of their redshift, being $z = 0.9578$. The lack of an optical transient associated with the afterglow of GRB 970828 can be explained as due to the presence of strong absorption, due to dusty clouds in the burst site environment, whose presence does not affect the X-ray and the radio observations of the GRB afterglow. The absence of an optical afterglow [7], together with the large intrinsic absorption column detected in the ASCA X-ray data [26] and the contemporary detection in radio-wavelengths of the GRB afterglow, imply a very large value for the circum-burst medium (CBM); the variable absorption might be an indication of a strong inhomogeneous CBM distribution.

To analyze in detail this GRB, we have considered the observations of the BATSE-LAD detector, which observed GRB 970828 in the 25–1900 keV energy range, and then we have reduced the data by using the RMFIT software package. For the spectral analysis we have considered the High Energy Resolution Burst (HERB) data, which consist of 128 separate high energy resolution spectra stored during the burst emission. The light curve, shown in Fig. 1, was obtained by using the Medium Energy Resolution (MER) data, which consist of 4.096 16-channel spectra summed from triggered detectors.

3. THE EPISODE 1

3.1. The Onset of the Supernova and the Hyper-Critical Accretion

In analogy to the cases of GRB 090618 [15], we analyze here the first emission episode in GRB 970828 to seek for a thermal signature. We have rebinned the light curve assuming a signal-to-noise ratio for each time bin of 20. This large value of counts per bin allows us to consider a gaussian distribution for the photons in each bin, so in the following we will use a χ^2 statistic.

As often done in GRB analysis, we first perform a time-integrated spectral analysis of the first 40 s of emission, which corresponds to the Episode 1, to identify the best-fit model and the possible presence of thermal features. We make use of different spectral models, see Table 1, to determine the best-fit function. We also check if nested models really improve the best-fit, as in the case of models with an extra power-law component. We find that the best-fit corresponds to a double blackbody model with an extra power-law component. The check between the Band and the double black body plus power law is minimal ($P_{val} = 9\%$) but with this last model we note an improvement of the best fit at high energies.

It has already been emphasized that the integrated spectral analysis often misses the nature of the physical components and also the nature of the underlying physical mechanisms. We perform therefore a time-resolved spectral analysis to determine the existence and the evolution of a thermal component. We find that the double blackbody model observed in the time-integrated spectrum can be explained by the presence of an instantaneous single blackbody with a temperature kT varying in intensity and time, showing a double decay trend. We note that the timing of these trends corresponds to the two main spikes in the observed light curve of this first episode,

see Fig. 2. We have then analyzed this characteristic evolution of the blackbody in both time intervals, corresponding each one to an observed decay trend of the temperature. From the observed flux of the blackbody component $\phi_{BB,obs}$ for each interval, we obtain the evolution of the emitter radius in the rest-frame:

$$r_{em} = \left(\frac{\phi_{BB,obs}}{\sigma T_{obs}^4} \right)^{1/2} \frac{D}{(1+z)^2} \quad (1)$$

whose evolution is shown in Fig. 2. It is very interesting that the radius monotonically increases, without showing an analog double trend which is observed for the temperature, see Fig. 2. The global evolution of the emitter radius is well-described with a power-law function $r = \alpha t^\delta$ and a best fit of the data provides for the $\delta = 0.41 \pm 0.04$ and $\alpha = (5.38 \pm 0.52) \times 10^8$ cm, with an R^2 statistic value of 0.98, see Fig. 2.

It is appropriate to discuss the power law component observed in the time resolved spectra. In BdHNe, the tight geometry of the binary system implies that as the external layers of the SN core starts to expand, an hyper-critical accretion phenomenon is induced onto the NS companion.

3.2. Binary Progenitor and Binary-Driven Hypercritical Accretion

The first estimates of the IGC process [14, 15] were based on a simplified model of the binary parameters and the Bondi–Hoyle–Lyttleton accretion formalism [27–29]. The following discussion is based on the more recent and accurate results presented in [30], in which the collapsing CO cores leading to SN Ic are simulated to calculate realistic profiles for the density and ejection velocity of the SN outer layers. The hydrodynamic evolution of the accreting material falling into the Bondi–Hoyle accretion region is also computed from numerical simulations all the way up to its incorporation onto the NS surface.

The hypercritical accretion onto the NS from the SN ejecta can be estimated from the Bondi–Hoyle–Lyttleton formula

$$\dot{M}_{BHL} = 4\pi r_{BHL}^2 \rho (v^2 + c_s^2)^{1/2}, \quad (2)$$

where ρ is the SN ejecta density, v is the ejecta velocity in the rest-frame of the NS, which includes a component from the ejecta velocity, v_{ej} , and another component from the orbital velocity of the NS, v_{orb} ; c_s is the SN ejecta sound speed, and r_{BHL} is the Bondi radius

$$r_{BHL} = \frac{GM_{NS}}{v^2 + c_s^2}, \quad (3)$$

being G the gravitational constant and M_{NS} is the NS mass. The conditions of the binary system are

such that both the velocity components, v_{orb}, v_{ej} , are typically much larger than the sound speed. The ejecta velocity as a function of time is determined by the explosion energy and the nature of the SN explosion. The orbital velocity depends upon the orbital separation, which in turn depends upon the radius of the CO core and the binary interactions prior to the explosion of the CO core. The effect of the NS magnetic field is negligible in this process [14, 31]: for a neutron star with surface magnetic field $B = 10^{12}$ G, mass $M_{NS} = 1.4 M_\odot$, and radius $r_{NS} = 10^6$ cm, one has that for accretion rates $\dot{M} > 2.6 \times 10^{-8} M_\odot \text{ s}^{-1} = 0.8 M_\odot \text{ yr}^{-1}$, the Alfvén magnetospheric radius satisfies $R_A = [B^2 R^6 / (\dot{M} \sqrt{2GM_{NS}})]^{2/7} < r_{NS}$.

The evolution of the SN ejecta density near the NS companion depends on the SN explosion and the structure of the progenitor just prior to collapse. The compactness of the CO core is such that there is no Roche lobe overflow prior to the SN explosion. The Roche lobe radius can be computed from [32], $R_{L,CO}/a \approx 0.49q^{2/3} / [0.6q^{2/3} + \ln(1 + q^{1/3})]$, where $q = M_{CO}/M_{NS}$. For a CO core progenitor $M_{CO} \approx 5 M_\odot$, $R_{CO} \approx 3 \times 10^9$ cm, no Roche lobe overflow occurs for binary periods $P \geq 2$ min, or binary separations $a \geq 6 \times 10^9$ cm, assuming a NS companion mass $M_{NS} \geq 1.4 M_\odot$.

In order to derive the accretion onto the NS, the explosion has to be modeled. We have recently performed the numerical simulations following two different approaches [30]: the first assuming a homologous outflow with a set explosion energy and a second approach following the collapse, bounce, and explosion of a $20M_\odot$ (zero-age main sequence mass) progenitor. The calculation uses a 1D core-collapse code [33] to follow the collapse and bounce and then injects energy just above the proto-NS to drive different SN explosions mimicking the convective-engine paradigm. With this progenitor and explosion, we produce the density and velocity evolution history at the position of the Bondi–Hoyle surface of the NS companion.

Under the above conditions, we have found from our numerical simulations in [30] that hypercritical accretion rates of up to $10^{-2} M_\odot/\text{s}$ occur in these systems. This infall rate is well above the critical Eddington rate. The Eddington accretion limit, or critical accretion rate makes a series of assumptions: (1) the potential energy gained by the accreting material is released in the form of photons which exert pressure finally reducing the accretion rate, (2) the inflowing material and outflowing radiation is spherically symmetric, (3) the photons are not trapped in the flow and can deposit momentum to the inflowing material, and (4) the opacity is dominated by electron

scattering. However, many of these assumptions break down in the IGC scenario, allowing hypercritical accretion rates.

It can be shown that the photons for the hypercritical accretion rates in the IGC are trapped in the flow. Chevalier [34] derived the trapping radius where photons emitted diffuse outward at a slower velocity than infalling material flows inward:

$$r_{\text{trapping}} = \min[(\dot{M}_{\text{BHL}}\kappa)/(4\pi c), r_{\text{BHL}}] \quad (4)$$

where κ is the opacity (in $\text{cm}^2 \text{g}^{-1}$) and c is the speed of light. If the trapping radius is near or equal to the Bondi radius, the photons are trapped in the flow and the Eddington limit does not apply. We estimate for our CO core a Rosseland mean opacity roughly $5 \times 10^3 \text{ cm}^2 \text{g}^{-1}$, a factor $\sim 10^4$ higher than electron scattering. Combined with our high accretion rates, it is clear that the Eddington limit does not apply in this scenario and hypercritical accretion must occur.

The inflowing material shocks as it piles up onto the NS producing an atmosphere on top of the NS which, by compression, becomes sufficiently hot to emit neutrinos [31, 34–36]. The neutrinos have become then crucial in cooling the infalling material, allowing its incorporation into the NS [31, 37, 38]. We compute the neutrino emission following [31, 38]. We thus take into account e^- and e^+ capture by free protons and neutrons, and pair and plasma $\nu\bar{\nu}$ creation; ν absorption processes include ν_e capture by free neutrons, $\bar{\nu}_e$ by free protons, and $\nu\bar{\nu}$ annihilation. ν scattering includes e^- and e^+ scattering off ν and neutral current opacities by nuclei. The three species ν_e, μ, τ are tracked separately by the transport algorithm.

As material piles up, the accretion shock moves outward. The accretion shock weakens as it moves out and the entropy jump becomes smaller, producing an unstable atmosphere with respect to Rayleigh–Taylor convection. Previous simulations [38, 39] of such instabilities accretion process have shown that they can accelerate above the escape velocity driving outflows from the accreting NS with final velocities approaching the speed of light, causing the ejection of up to 25% of the accreting material. The entropy of the material at the base of our atmosphere, S_{bubble} , is given by [31]:

$$S_{\text{bubble}} = 38.7 \left(\frac{M_{\text{NS}}}{2M_{\odot}} \right)^{7/8} \times \left(\frac{\dot{M}_{\text{BHL}}}{0.1 M_{\odot} \text{s}^{-1}} \right)^{-1/4} \left(\frac{r_{\text{NS}}}{10^6 \text{ cm}} \right)^{-3/8} \quad (5)$$

k_B per nucleon, where r_{NS} is the radius of the NS. The corresponding temperature of the bubble, T_{bubble} ,

is:

$$T_{\text{bubble}} = 195 S_{\text{bubble}}^{-1} \left(\frac{r_{\text{NS}}}{10^6 \text{ cm}} \right)^{-1}. \quad (6)$$

Under the hypercritical accretion of the IGC, the temperature of the bubble when it begins to rise is $T_{\text{bubble}} \sim 5 \text{ MeV}$. If it rises adiabatically, expanding in all dimensions, it drops to 5 keV at a radius of 10^9 cm , far too cool to observe. However, if it is ejected in a jet, as simulated in Fryer [38], it expands laterally but not radially, so we have roughly $\rho \propto r^{-2}$ and $T \propto r^{-2/3}$. In that simplified bubble evolution, the outflow would have a temperature $T_{\text{bubble}} \sim 50 \text{ keV}$ at 10^9 cm and $T_{\text{bubble}} \sim 15 \text{ keV}$ at $6 \times 10^9 \text{ cm}$. This could explain the temperature and size evolution of the blackbody observed in the Episode 1 of BdHNe. For example, the blackbody observed in Episode 1 of GRB 090618 [15] evolves as $T \propto r^{-m}$ with $m = 0.75 \pm 0.09$, in agreement with this simplified theoretical estimate. For the present case of GRB 970828, the fully lateral bubble evolution do not match perfectly, implying that the above simplified picture needs further refinement and/or the presence of other mechanisms. We are currently deepening our analysis of the possible explanation of the thermal emission observed in Episode 1 of BdHNe as based on convective instabilities in the hypercritical accretion process, and the results will be presented elsewhere.

Concerning the power-law component observed in the luminosity of Episode 1 in addition to the blackbody one, we advance the possibility that such a high-energy emission could come from the angular momentum of the binary system as follows.

The angular momentum per unit mass accreting by the NS can be estimated as

$$j_{\text{acc}} \approx \frac{1}{2} \omega_{\text{orb}} r_B^2, \quad (7)$$

where $\omega_{\text{orb}} = v_{\text{orb}}/a$ is the orbital angular velocity, $v_{\text{orb}} = (GM_T/a)^{1/2}$ is the orbital velocity, a the separation distance of the binary components, $M_T = M_{\text{CO}} + M_{\text{NS}}$ is the total mass of the binary. r_B is the Bondi capture radius. From our numerical simulations, we know that when the neutron star reaches the critical mass, the inequality $v_{\text{ej}} \ll v_{\text{orb}}$ is satisfied, so we can approximate Eq. (3) as

$$r_{\text{BHL}} \approx \frac{2GM_{\text{NS}}}{v_{\text{orb}}^2} \rightarrow \frac{2GM_{\text{crit}}}{v_{\text{orb}}^2} = \frac{2GM_{\text{BH}}}{v_{\text{orb}}^2}, \quad (8)$$

where $M_{\text{BH}} = M_{\text{crit}}$, is the mass of the newly-formed black hole, so it equals M_{crit} , the critical mass of the NS.

The black hole can gain angular momentum up to it reaches the maximal value allowed by the Kerr

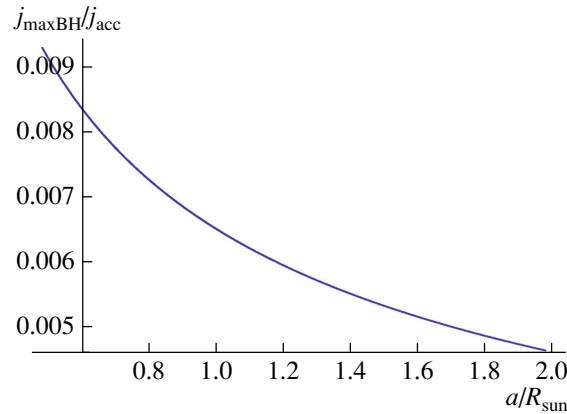


Fig. 3. Maximal black hole to accretion angular momentum ratio, $j_{\text{maxBH}}/j_{\text{acc}}$, as a function of the binary separation in units of solar radius. Here for simplicity we have used $M_{\text{CO}} \approx 6 M_{\odot}$ and $M_{\text{BH}} \approx 3 M_{\odot}$.

solution

$$j_{\text{maxBH}} = \frac{GM_{\text{BH}}}{c}. \quad (9)$$

Therefore we have (see Fig. 3)

$$\begin{aligned} \frac{j_{\text{maxBH}}}{j_{\text{acc}}} &= \frac{1}{2} \frac{M_T}{M_{\text{BH}}} \sqrt{\frac{GM_T}{c^2 a}} \\ &= \frac{1}{2} \left(1 + \frac{M_{\text{CO}}}{M_{\text{BH}}}\right) \sqrt{\frac{G(M_{\text{CO}} + M_{\text{BH}})}{c^2 a}}. \end{aligned} \quad (10)$$

It becomes then clear from the above first simplified estimate that the angular momentum carried out by the accreted material highly exceed the maximal angular momentum that the newly-born black hole can support, and therefore angular momentum dissipation, very likely in form of collimated emission, is likely to occur. We are currently performing numerical simulations of this process in order to assess the validity and accuracy of these first order of magnitude estimates.

3.3. A Possible Explanation for the Non-Thermal Component and the Compactness Problem

It is well known [see 40] that most of GRBs emit a large fraction of observed high-energy photons ($E \gg 1$ MeV) which can interact with low-energy photons to produce electron-positron pairs via $\gamma\gamma \rightarrow e^+e^-$ in a compact region with radius R that, with a naive estimate, can be considered $R < c\delta t \approx 3000$ km. This would imply an optical depth $\tau \gg 1$, but we know that GRB spectra are non-thermal, so we are in presence of a paradox. This issue can be solved assuming a relativistic expansion of the emitting source, with Lorentz factor $\Gamma \gg 1$ [40, 41]. In this case, in fact, we would have $R < 2\gamma^2 c\delta t$ and consequently a decrease of the estimated optical depth [42–44].

The observed high-energy photon spectrum is often modeled by a single power-law $KE^{-\gamma}$, with $E_{\text{min}} < E < E_{\text{max}}$ and power-law index γ . The energy E_{max} is the highest observed photon energy. In the frame of the emitting material, where the photons are assumed to be isotropic, a photon with energy E' can annihilate a second photon with energy E'_{th} , yielding an electron-positron pair. The threshold for this process is described by

$$E'E'_{\text{th}} \geq (m_e c^2)^2, \quad (11)$$

where m_e is the electron mass. If the source is moving toward the observer with a Lorentz factor Γ , then the photons previously analyzed have detected energy of $E = \Gamma E'/(1+z)$ and $E_{\text{th}} \geq \Gamma E'_{\text{th}}/(1+z)$, respectively. Therefore in the observer frame photons with energy E_{max} annihilate only with other photons having energy $E_{\text{max,th}} = [\Gamma m_e c^2/(1+z)]^2 E_{\text{max}}^{-1}$. Although the observed high-energy photon spectrum is a power-law up to 4 MeV in the rest frame of the burst, there is no observational evidence for the presence of a cut-off due to the e^+e^- -pair creation. Therefore we can estimate the minimum Lorentz factor of the non-thermal component allowed by the observations from the maximum energy observed in the first episode $E_{\text{max}} \sim 2$ MeV. From this assumption, it is straightforward to impose that the threshold energy $E_{\text{max,th}}$ for the pair creation process has to be $E_{\text{max,th}} < E_{\text{max}}$, see e.g., case (III) in [45]. It follows then a lower limit on the Lorentz factor from the observed energy E_{max}

$$\Gamma_{\text{min}} \geq \frac{E_{\text{max}}}{m_e c^2} (1+z). \quad (12)$$

We can identify E_{max} with the cut-off energy of the spectrum E_c , but for the moment we treat them as different energies. Following the considerations in [45], we have calculated the averaged number of photons

interacting with E_{\max} from $E_{\max,\text{th}}$ to $E_c \geq E_{\max}$ on the cross-section of the process integrated over all the angles θ

$$\begin{aligned} \langle \sigma N_{\max,\text{th}} \rangle &= 4\pi d_z^2 \Delta t \int_{E_{\max,\text{th}}}^{+\infty} K E^{-\gamma} dE \\ &\times \int_1^{\frac{E_{\max} E}{(m_e c^2)^2}} \frac{3}{16} \sigma_T s ds = \frac{2E_{\max,\text{th}}^{1-\gamma}}{\xi} \end{aligned} \quad (13)$$

and we have correspondingly evaluated the optical depth

$$\tau_{\gamma\gamma} = \frac{\langle \sigma N_{\max,\text{th}} \rangle}{4\pi (\Gamma^2 c \Delta t)^2}, \quad (14)$$

by defining the following quantities

$$\begin{aligned} d_z &= \frac{D}{1+z}, \quad s = \frac{E_{\max} E (1 - \cos \theta)}{2(m_e c^2)^2}, \\ \xi &\equiv \left[\frac{3\pi \sigma_T d_z^2 K \Delta t}{4(\gamma^2 - 1)} \right]^{-1}, \end{aligned}$$

and using the Thomson cross-section σ_T . The condition $\tau_{\gamma\gamma} < 1$ yields to a lower limit on the Lorentz Γ factor. We have applied these considerations to non-thermal spectrum of the first episode of GRB 970828, and considered for Δt in Eq. (14), the whole duration of the first episode in GRB 970828. Therefore, we have calculated an averaged lower limit on the Lorentz factor, i.e., $\Gamma_{\min} = 77$ for the whole first episode. Therefore, a relativistic outflow of the accretion process of the SN onto the companion NS, can explain the origin of the power-law high energy component observed in Episode 1.

4. THE EPISODE 2: THE GRB EMISSION

Turning now to the second emission episode, we have computed the isotropic energies emitted in this episode, by considering a Band model as the best fit for the observed integrated spectra: $E_{\text{iso},2\text{nd}} = 1.6 \times 10^{53}$ erg. In what follows we explain this second emission episode of GRB 970828 as a single canonical GRB emission in the context of the Fireshell scenario.

In this model [46, 47], a GRB originates from an optically thick e^+e^- -plasma created in the process of vacuum polarization, during the process of gravitational collapse leading to a Kerr–Newman black hole [48, 49]. The dynamics of this expanding plasma is described by its total energy $E_{\text{tot}}^{e^+e^-}$, the baryon load $B = M_B c^2 / E_{\text{tot}}^{e^+e^-}$ and the circumburst medium (CBM) distribution around the burst site. The GRB light curve emission is characterized by a first brief

emission, named the proper GRB or P-GRB, originating in the process of the transparency emission of the e^+e^- -plasma, followed by a multi-wavelength emission due to the collisions of the residual accelerated baryons and leptons with the CBM. This latter emission is assumed in a fully radiative regime. Such a condition is introduced for mathematical simplicity and in order to obtain a lower limit on the CBM density. This condition establishes a necessary link between the CBM inhomogeneities and filamentary distribution [50] with the observed structures in the γ and X-ray light curves in the prompt and early afterglow phase. In the spherically symmetric approximation the interaction of the accelerated plasma with the CBM can be described by the matter density distribution n_{CBM} around the burst site and the fireshell surface filling factor $\mathcal{R} = A_{\text{eff}}/A_{\text{vis}}$, which is the ratio between the effective emitting area and the total one [51]. The spectral energy distribution in the comoving frame of the shell is well-described by a “modified” thermal emission model [52], which differs from a classical blackbody model by the presence of a tail in the low-energy range.

In this context, to simulate the second episode of GRB 970828, which is the actual GRB emission, we need to identify the P-GRB signature in the early second episode light curve. From the identification of the P-GRB thermal signature, and the consequent determination of the energy emitted at transparency, we can obtain the value of the baryon load B assuming that the total energy of the e^+e^- -plasma is given by the isotropic energy E_{iso} observed for the second episode of GRB 970828, as it was done for the second episode in GRB 090618, see e.g. [15]. We have then started to seek for a possible thermal signature attributable to the P-GRB emission in the early emission of the second episode. As it is shown in Fig. 4, the early emission of the second episode is characterized by an intense spike, anticipated by a weak emission of 9 s. Our search for the P-GRB emission is concentrated in this time interval, since from the fireshell theory the expected energy of the P-GRB emission, in case of long GRBs for which the baryon load is in between 10^{-3} – 10^{-2} , is of the order of 10^{-2} of the prompt emission. The observed fluence (10–1000 keV) in the P-GRB emission, computed from the fit with the power-law function is $S_{\text{obs}} = (1.54 \pm 0.10) \times 10^{-6}$ erg/cm², which corresponds to an isotropic energy of the P-GRB of $E_{\text{iso,PGRB}} = 1.46 \times 10^{51}$ erg, which is quantitatively in agreement with the energetic of the P-GRB for this GRB (it is $\approx 0.01\%$ the total energy of the second episode, the GRB). However, due to the paucity of photons in this time interval, we are not able to put tight constraints,

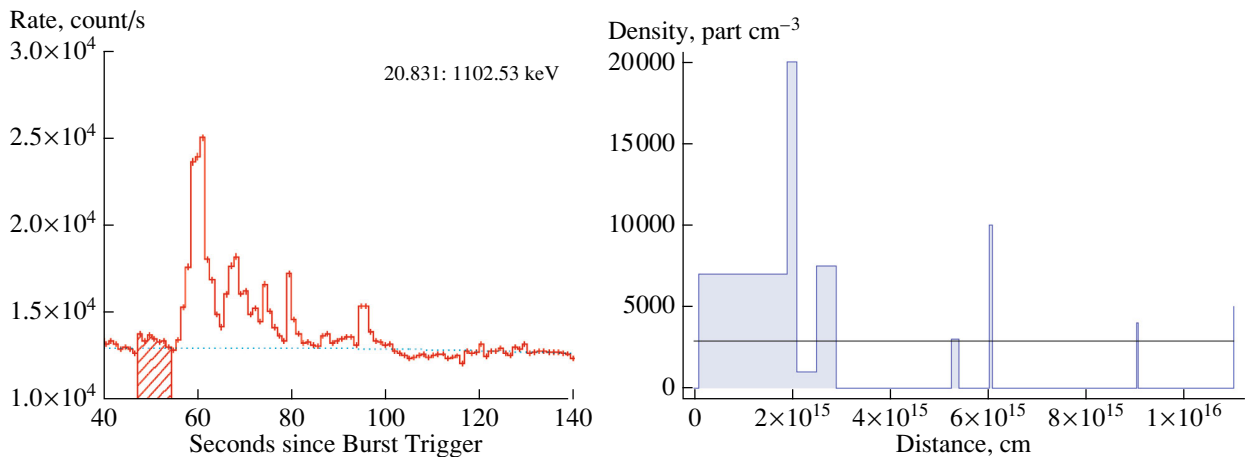


Fig. 4. *Left panel:* Light curve of the second episode in GRB 970828. The dashed region represents the P-GRB emission. *Right panel:* The radial CBM density distribution for GRB 970828. The characteristic masses of each cloud are on the order of $\sim 10^{22}$ g and 10^{15} cm in radii. The black line corresponds to the average value for the particle density.

e.g. about a possible observed temperature of the P-GRB.

With these results, we can estimate the value of the baryon load from the numerical solutions of the fireshell equations of motion. These solutions for four different values of the total e^+e^- -plasma energy are shown in the Fig. 4 of [15]. We find that the baryon load is $B = 7 \times 10^{-3}$, which corresponds to a Lorentz gamma factor at transparency $\Gamma = 142.5$. The GRB emission was simulated with very good approximation by using a density mask characterized by an irregular behavior: all the spikes correspond to spherical clouds with a large particle density $\langle n \rangle \sim 10^3$ part/cm³, and with radius of the order of $(4-8) \times 10^{14}$ cm, see Fig. 4. Considering all the clouds found in our analysis, the average density of the CBM medium is $\langle n \rangle = 3.4 \times 10^3$ particles/cm³. The corresponding masses of the blobs are of the order of 10^{24} g, in agreement with the clumps found in GRB 090618.

5. THE EPISODE 3: THE LATE X-RAY AFTERGLOW

The most remarkable confirmation of the BdHN paradigm applied to GRB 970828, comes from the late X-ray afterglow emission. As shown in [18], from the knowledge of the redshift of the source, we can compute the X-ray luminosity light curve in the common rest frame energy range 0.3–10 keV after $\approx 10^4$ s from the initial GRB emission. However, while in [18] the analysis is based on the available X-ray data (0.3–10 keV) from the Swift-XRT detector, GRB 970828 occurred in the pre-Swift era. Its observational X-ray data are available in the energy range

2–10 keV, since the data were collected by three different satellites: *RXTE*, *ASCA* and *ROSAT*. To further confirm the progenitor mechanism for GRB 970828, we verify the overlapping of the late X-ray data with the ones of the “Golden Sample” (GS) sources presented in [18]. To this aim, we have computed its luminosity light curve L_{rf} in a common rest-frame energy range 0.3–10 keV. Since the observed energy band is different (2–10 keV), the expression for the flux light curve f_{rf} in the 0.3–10 keV rest-frame energy range is not as expressed in Eq. (2) of [18], but it becomes

$$f_{rf} = f_{\text{obs}} \frac{\left(\frac{10}{1+z}\right)^{2-\gamma} - \left(\frac{0.3}{1+z}\right)^{2-\gamma}}{10^{2-\gamma} - 2^{2-\gamma}}, \quad (15)$$

where γ is the photon index of the power-law spectral energy distribution of the X-ray data. All the other data transformations, reported in [18], remain unchanged.

We made use in particular of the *RXTE*-PCA observations and *ASCA* data presented in [26]; the averaged photon indexes are taken from the text, for *RXTE*-PCA ($\gamma \sim 2$), and from Table 1, for the *ASCA* data, of the same paper. The last data-point by *ROSAT* is taken from Fig. 7 in [1], with a corresponding photon index ~ 2 ; the error on the observed flux is the 25% as indicated for the count rate [5]. We show in Fig. 5 the late X-ray (0.3–10 keV) light curve of GRB 970828 and we compare it with some GRBs of the “Golden Sample” presented in [18]: GRB 061007, GRB 080319B, GRB 090618, GRB 091127 and GRB 111228A. The perfect overlap with the late X-ray light curves of BdHN sources confirms the presence of a BdHN mechanism operating also in GRB 970828.

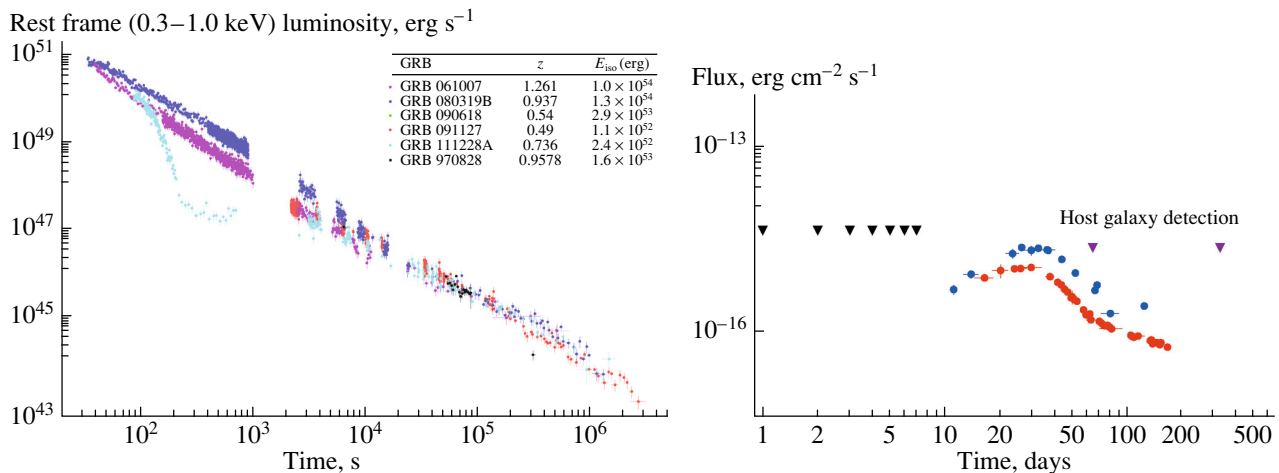


Fig. 5. *Left panel:* The late X-ray (0.3–10 keV) light curves of some GRBs presented in [18] and of GRB 970828 (black open circles). The overlap of the light curve of GRB 970828 with the members of the BdHN class is clearly evident, confirming that an Induced Gravitational Collapse (IGC) mechanism is operating also in GRB 970828. *Right panel:* The light curve of the SN associated with GRB 090618 (green data), the U - (blue line) and R -band (red line) light curve of SN 1998bw transposed at the redshift of GRB 970828, $z = 0.9578$, and not corrected for the intrinsic host-galaxy absorption. The purple and cyan line represents the limit given in the deep images by [1] and [7], respectively.

6. LIMITS ON THE EPISODE 4: SN-RELATED OBSERVATIONS

The analysis of GRB 090618 [15] and GRB 101023 [16] represents an authentic “Rosetta Stone” for the understanding of the GRB-SN phenomenon. The presence of a supernova emission, observed ten days after the burst in the cosmological rest-frame of GRB 090618, was found to have the same luminosity of SN 1998bw [53], the SN related to GRB 980425 and which is the prototype of SNe connected with GRBs [54]. We have transposed the data of the “bump” Rc -band light curve observed in the optical afterglow of GRB 090618, associated to the presence of an underlying supernova [53], to the redshift of GRB 970828. This simple operation concerns only the transformation of the observed flux, under the assumption that the SN has the same intrinsic luminosity. Moreover, we have also transposed the U and R -band light curves of SN 1998bw [55], which is the prototype of a supernova associated to a GRB. From the K -correction transformation formula, the U -band light curve, transposed at $z = 0.9578$, corresponds approximately to the observed R -band light curve, so in principle we should consider the $U = 365$ nm transposed light curve as the actual one observed with the $Rc = 647$ nm optical filter. These transposed light curves are shown in Fig. 5. We conclude that the Supernova emission could have been seen between 20 and 40 days after the GRB trigger, neglecting any possible intrinsic extinction. The optical observations were made up to 7 days from the GRB trigger, reaching a limit of $R \sim 23.8$ [7], and subsequent deeper images after ~ 60 days [1]. So

there are no observations in this time interval. It is appropriate to notice that the R -band extinction value should be large since the observed column density from the X-ray observations of the GRB afterglow is large as well [26]: the computed light curve for the possible SN of GRB 970828 should be lowered by more than 1 magnitude, leading to a SN bump below the $R = 25.2$ limit, see Fig. 5. The presence of very dense clouds of matter near the burst site might have darkened both the supernova emission and the GRB optical afterglow. Indeed we find the presence of clouds in our simulation at the average distances of $\sim 10^{15} - 10^{16}$ cm from the GRB progenitor, with average density of $\langle n \rangle \approx 10^3$ part/cm³ and typical dimensions of $(4-8) \times 10^{14}$ cm, see Fig. 4.

7. CONCLUSIONS

In conclusion, the recent progress in the observations of X and γ -ray emission, with satellites such as Swift, Fermi, AGILE, Suzaku, Coronas-PHOTON, the possibility of observing GRB afterglows with the new generation of optical and radio telescopes, developed since 1997, and the theoretical understanding of the BdHN paradigm, have allowed to revisit the data of GRB 970828 and give a new conceptual understanding of the underlying astrophysical scenario.

We verify in this paper that GRB 970828 is a member of the BdHN family. This new understanding leads to a wealth of information on the different emission episodes which are observed during an IGC process. In Episode 1, we determine the evolution of the thermal component and of the radius of the

Table 2. Spectral analysis (25 keV–1.94 MeV) of the P-GRB emission in the second episode of GRB 970828

Spectral model	γ	β	E_{cutoff} (keV)	kT (keV)	χ^2/DOF
Power-law	-1.18 ± 0.04				91.495/115
Cutoff PL	-1.15 ± 0.08		2251 ± 1800		91.157/114
BB + PL	-1.16 ± 0.06			69.6 ± 40.0	90.228/113
Band	-0.96 ± 0.44	-1.23 ± 0.08	958.8 ± 800.0		90.439/113

blackbody emitter, given by Eq. (1), see Figs. 1, 2. The onset of the SN is here observed for the first time in an unprecedented circumstance: a SN exploding in a close binary system with a companion NS. The energetics are correspondingly much larger than the one to be expected in an isolated SN, and presents an high energy component likely associated to an outflow process in the binary accreting system. In Episode 2, the GRB, we give the details of the CBM structure, see Fig. 4, of the simulation of the light curve and the spectrum of the real GRB emission. We have also shown in Table 2 the final results of the GRB simulation, the total energy of the e^+e^- plasma, the baryon load B , the temperature of the P-GRB kT_{th} and the Lorentz Gamma factor at transparency Γ , as well the average value of the CBM density $\langle n_{\text{CBM}} \rangle$ and the density ratio of the clouds $\delta n/n$. In Episode 3, we have shown that the late afterglow emission observed by ASCA and ROSAT, although limited to few data points, when considered in the cosmological rest-frame of the emitter, presents a successful overlap with the standard luminosity behavior of other members of the BdHN family [18], which is the most striking confirmation that in GRB 970828 an IGC process is working. Finally, from this latter analogy with the late X-ray afterglow decay of the ‘‘Golden Sample’’ [18], and with the optical bump observed in GRB 090618, see Fig. 5, associated to a SN emission [53], we have given reasons why a SN

associated to GRB 970828 was not observable due to the large interstellar local absorption, in agreement with the large column density observed in the ASCA X-ray data [26] and with the large value we have inferred for the CBM density distribution, $\langle n_{\text{CBM}} \rangle \approx 10^3$ particles/cm³.

The possibility to observe the energy distribution from a GRB in a very wide energy range, thanks to the new dedicated space missions, has allowed to definitely confirm the presence of two separate emission episodes in GRBs associated to SNe. Future planned missions, as the proposed Wide Field Monitor detector on board the LOFT mission [56], will allow to observe the thermal decay from these objects down to $kT = 0.5\text{--}1$ keV. It is important to note the possibility that the Large Area Detector, designed for the LOFT mission, will be also able to observe the afterglow emission from times larger than 10^4 s in the rest-frame, allowing to check possible new BdHNE by using the overlapping method described in [18, 57] and consequently estimate the distance, wherever an observed determination of the redshift is missing.

REFERENCES

1. S. G. Djorgovski, D. A. Frail, S. R. Kulkarni, J. S. Bloom, S. C. Odewahn, and A. Diercks, *Astrophys. J.* **562**, 654 (2001); astro-ph/0107539.
2. R. Remillard, A. Wood, D. Smith, and A. Levine, *IAU Circ.* **6726**, 1 (1997).
3. D. Smith, A. Levine, R. Remillard, A. Wood, K. Hurley, C. Kouveliotou, G. Fishman, C. Meegan, V. Connaughton, and J. van Paradijs, *IAU Circ.* **6728**, 1 (1997).
4. A. V. Filippenko, D. Stern, R. R. Treffers, C. Y. Peng, H. E. Bond, M. W. Richmond, T. Murakami, Y. Ueda, M. Ozaki, A. Yoshida, et al., *IAU Circ.* **6729**, 1 (1997).
5. J. Greiner, R. Schwarz, J. Englhauser, P. J. Groot, and T. J. Galama, *IAU Circ.* **6757**, 1 (1997).
6. S. C. Odewahn, S. G. Djorgovski, S. R. Kulkarni, D. A. Frail, T. Herter, F. Fang, X. Xu, O. Pevunova, C. Steidel, K. Adelberger, et al., *IAU Circ.* **6735**, 1 (1997).
7. P. J. Groot, T. J. Galama, J. van Paradijs, C. Kouveliotou, R. A. M. J. Wijers, J. Bloom, N. Tanvir, R. Vanderspek, J. Greiner, A. J. Castro-Tirado, et al., *Astrophys. J. Lett.* **493**, L27 (1998); astro-ph/9711171.

Table 3. Final results of the simulation of GRB 970828 in the fireshell scenario

Parameter	Value
$E_{\text{tot}}^{e^+e^-}$	$(1.60 \pm 0.03) \times 10^{53}$ erg
B	$(7.00 \pm 0.55) \times 10^{-3}$
Γ_0	142.5 ± 57
kT_{th}	(7.4 ± 1.3) keV
$E_{P\text{-GRB,th}}$	$(1.46 \pm 0.43) \times 10^{51}$ erg
$\langle n \rangle$	3.4×10^3 part/cm ³
$\delta n/n$	10 part/cm ³

8. N. Gehrels, G. Chincarini, P. Giommi, K. O. Mason, J. A. Nousek, A. A. Wells, N. E. White, S. D. Barthelmy, D. N. Burrows, L. R. Cominsky, et al., *Astrophys. J.* **611**, 1005 (2004).
9. C. Meegan, G. Lichti, P. N. Bhat, E. Bissaldi, M. S. Briggs, V. Connaughton, R. Diehl, G. Fishman, J. Greiner, A. S. Hoover, et al., *Astrophys. J.* **702**, 791 (2009); arXiv:0908.0450.
10. M. Tavani, G. Barbiellini, A. Argan, F. Boffelli, A. Bulgarelli, P. Caraveo, P. W. Cattaneo, A. W. Chen, V. Cocco, E. Costa, et al., *Astron. Astrophys.* **502**, 995 (2009); arXiv:0807.4254.
11. R. L. Aptekar, D. D. Frederiks, S. V. Golenetskii, V. N. Ilynskii, E. P. Mazets, V. N. Panov, Z. J. Sokolova, M. M. Terekhov, L. O. Sheshin, T. L. Cline, et al., *Space Sci. Rev.* **71**, 265 (1995).
12. D. N. Burrows, J. E. Hill, J. A. Nousek, J. A. Kennea, A. Wells, J. P. Osborne, A. F. Abbey, A. Beardmore, K. Mukerjee, A. D. T. Short, et al., *Space Sci. Rev.* **120**, 165 (2005); arXiv:astro-ph/0508071.
13. R. Ruffini, M. G. Bernardini, C. L. Bianco, L. Caito, P. Chardonnet, M. G. Dainotti, F. Frascchetti, R. Guida, G. Vereshchagin, and S.-S. Xue, in *Proceedings of the 6th Integral Workshop on the Obscured Universe*, Ed. by S. Grebenev, R. Sunyaev, C. Winkler, A. Parmar, and L. Ouweland, vol. SP-622 of *ESA Special Publication* (2007), p. 561; arXiv:0705.2456.
14. J. A. Rueda and R. Ruffini, *Astrophys. J. Lett.* **758**, L7 (2012); arXiv:1206.1684.
15. L. Izzo, R. Ruffini, A. V. Penacchioni, C. L. Bianco, L. Caito, S. K. Chakrabarti, J. A. Rueda, A. Nandi, and B. Patricelli, *Astron. Astrophys.* **543**, A10 (2012); arXiv:1202.4374.
16. A. V. Penacchioni, R. Ruffini, L. Izzo, M. Muccino, C. L. Bianco, L. Caito, B. Patricelli, and L. Amati, *Astron. Astrophys.* **538**, A58 (2012); arXiv:1112.2970.
17. A. V. Penacchioni, R. Ruffini, C. L. Bianco, L. Izzo, M. Muccino, G. B. Pisani, and J. A. Rueda, *Astron. Astrophys.* **551**, A133 (2013); arXiv:1301.6014.
18. G. B. Pisani, L. Izzo, R. Ruffini, C. L. Bianco, M. Muccino, A. V. Penacchioni, J. A. Rueda, and Y. Wang, *Astron. Astrophys.* **552**, L5 (2013); arXiv:1304.1764.
19. R. Belvedere, D. Pugliese, J. A. Rueda, R. Ruffini, and S.-S. Xue, *Nucl. Phys. A* **883**, 1 (2012); arXiv:1202.6500.
20. B. Zhang, Y. Z. Fan, J. Dyks, S. Kobayashi, P. Mészáros, D. N. Burrows, J. A. Nousek, and N. Gehrels, *Astrophys. J.* **642**, 354 (2006); astro-ph/0508321.
21. J. A. Nousek, C. Kouveliotou, D. Grupe, K. L. Page, J. Granot, E. Ramirez-Ruiz, S. K. Patel, D. N. Burrows, V. Mangano, S. Barthelmy, et al., *Astrophys. J.* **642**, 389 (2006); astro-ph/0508332.
22. A. Pe'er, F. Ryde, R. A. M. J. Wijers, P. Mészáros, and M. J. Rees, *Astrophys. J. Lett.* **664**, L1 (2007); astro-ph/0703734.
23. P. Mészáros, *Ann. Rev. Astron. Astrophys.* **40**, 137 (2002); astro-ph/0111170.
24. F. E. Marshall, J. K. Cannizzo, and R. H. D. Corbet, *IAU Circ.* **6727**, 1 (1997).
25. T. Murakami, Y. Ueda, A. Yoshida, N. Kawai, F. E. Marshall, R. H. D. Corbet, and T. Takeshima, *IAU Circ.* **6732**, 1 (1997).
26. A. Yoshida, M. Namiki, D. Yonetoku, T. Murakami, C. Otani, N. Kawai, Y. Ueda, R. Shibata, and S. Uno, *Astrophys. J. Lett.* **557**, L27 (2001); astro-ph/0107331.
27. F. Hoyle and R. A. Lyttleton, *Proc. Cambridge Philos. Soc.* **35**, 405 (1939).
28. H. Bondi and F. Hoyle, *Mon. Not. R. Astron. Soc.* **104**, 273 (1944).
29. H. Bondi, *Mon. Not. R. Astron. Soc.* **112**, 195 (1952).
30. C. L. Fryer, J. A. Rueda, and R. Ruffini, *Astrophys. J. Lett.* **793**, L36 (2014); arXiv:1409.1473.
31. C. L. Fryer, W. Benz, and M. Herant, *Astrophys. J.* **460**, 801 (1996); astro-ph/9509144.
32. P. P. Eggleton, *Astrophys. J.* **268**, 368 (1983).
33. C. Fryer, W. Benz, M. Herant, and S. A. Colgate, *Astrophys. J.* **516**, 892 (1999); astro-ph/9812058.
34. R. A. Chevalier, *Astrophys. J.* **346**, 847 (1989).
35. Y. B. Zeldovich, L. N. Ivanova, and D. K. Nadyozhin, *Sov. Astron.* **16**, 209 (1972).
36. J. C. Houck and R. A. Chevalier, *Astrophys. J.* **376**, 234 (1991).
37. R. Ruffini and J. Wilson, *Phys. Rev. Lett.* **31**, 1362 (1973).
38. C. L. Fryer, *Astrophys. J.* **699**, 409 (2009); arXiv:0711.0551.
39. C. L. Fryer, F. Herwig, A. Hungerford, and F. X. Timmes, *Astrophys. J. Lett.* **646**, L131 (2006); astro-ph/0606450.
40. T. Piran, *Phys. Rep.* **314**, 575 (1999); astro-ph/9810256.
41. M. Ruderman, in *Proceedings of the 7th Texas Symposium on Relativistic Astrophysics*, Ed. by P. G. Bergman, E. J. Fenyves, and L. Motz, *Ann. (N.Y.) Acad. Sci.* **262**, 164 (1975).
42. E. Woods and A. Loeb, *Astrophys. J.* **453**, 583 (1995); astro-ph/9503070.
43. Y. Lithwick and R. Sari, *Astrophys. J.* **555**, 540 (2001); astro-ph/0011508.
44. B. Zhang and A. Pe'er, *Astrophys. J. Lett.* **700**, L65 (2009); 0904.2943.
45. N. Gupta and B. Zhang, *Mon. Not. R. Astron. Soc.* **384**, L11 (2008); arXiv:0708.2763.
46. R. Ruffini, C. L. Bianco, F. Frascchetti, S.-S. Xue, and P. Chardonnet, *Astrophys. J. Lett.* **555**, L107 (2001); astro-ph/0106531.
47. R. Ruffini, C. L. Bianco, F. Frascchetti, S.-S. Xue, and P. Chardonnet, *Astrophys. J. Lett.* **555**, L117 (2001); astro-ph/0106534.
48. D. Christodoulou and R. Ruffini, *Phys. Rev. D* **4**, 3552 (1971).
49. T. Damour and R. Ruffini, *Phys. Rev. Lett.* **35**, 463 (1975).
50. R. Ruffini, C. L. Bianco, S.-S. Xue, P. Chardonnet, F. Frascchetti, and V. Gurzadyan, *Int. J. Mod. Phys. D* **14**, 97 (2005); astro-ph/0411760.

51. R. Ruffini, M. G. Bernardini, C. L. Bianco, P. Chardonnet, F. Fraschetti, V. Gurzadyan, L. Vitagliano, and S.-S. Xue, in *Proceedings of the 11th Brazilian School of Cosmology and Gravitation*, Ed. by M. Novello and S. E. Perez Bergliaffa, AIP Conf. Ser. **782**, 42 (2005); astro-ph/0503476.
52. B. Patricelli, M. G. Bernardini, C. L. Bianco, L. Caito, G. de Barros, L. Izzo, R. Ruffini, and G. V. Vereshchagin, *Astrophys. J.* **756**, 16 (2012); arXiv:1206.5605.
53. Z. Cano, D. Bersier, C. Guidorzi, R. Margutti, K. M. Svensson, S. Kobayashi, A. Melandri, K. Wiersema, A. Pozanenko, A. J. van der Horst, et al., *Mon. Not. R. Astron. Soc.* **413**, 669 (2011); arXiv:1012.1466.
54. M. Della Valle, *Int. J. Mod. Phys. D* **20**, 1745 (2011).
55. T. J. Galama, P. M. Vreeswijk, J. van Paradijs, C. Kouveliotou, T. Augusteijn, H. Bönhardt, J. P. Brewer, V. Doublier, J.-F. Gonzalez, B. Leibundgut, et al., *Nature (London)* **395**, 670 (1998); astro-ph/9806175.
56. M. Feroci, J. W. den Herder, E. Bozzo, D. Barret, S. Brandt, M. Hernanz, M. van der Klis, M. Pohl, A. Santangelo, L. Stella, et al., *SPIE Conf. Ser.* **8443**, 2 (2012); arXiv:1209.1497.
57. L. Izzo, G. B. Pisani, M. Muccino, J. A. Rueda, Y. Wang, C. L. Bianco, A. V. Penacchioni, and R. Ruffini, in *Gamma-ray Bursts: 15 Years of GRB Afterglows*, EAS Publications Series, Vol. 61, Ed. by A. J. Castro-Tirado, J. Gorosabel, and I. H. Park (European Astron. Soc., 2013), p. 595; arXiv:1210.8034.

Predicting Supernova Associated to Gamma-Ray Burst 130427A*

Y. Wang^{1,2}, R. Ruffini^{1,2,3,4**}, M. Kovacevic^{1,2}, C. L. Bianco^{1,2}, M. Enderli^{1,2},
M. Muccino^{1,2}, A. V. Penacchioni⁴, G. B. Pisani^{1,2}, and J. A. Rueda⁴

¹*Dip. di Fisica and ICRA, Sapienza Università di Roma,
Piazzale Aldo Moro 5, I-00185 Rome, Italy*

²*ICRANet, Piazza della Repubblica 10, I-65122 Pescara, Italy*

³*Université de Nice Sophia Antipolis, CEDEX 2, Grand Château Parc Valrose, Nice, France*

⁴*ICRANet-Rio, Centro Brasileiro de Pesquisas Físicas,
Rua Dr. Xavier Sigaud 150, Rio de Janeiro, RJ, 22290-180 Brazil*

Received January 26, 2015

Abstract—Binary systems constituted by a neutron star and a massive star are not rare in the universe. The Induced Gravitational Gamma-ray Burst (IGC) paradigm interprets Gamma-ray bursts as the outcome of a neutron star that collapses into a black hole due to the accretion of the ejecta coming from its companion massive star that underwent a supernova event. GRB 130427A is one of the most luminous GRBs ever observed, of which isotropic energy exceeds 10^{54} erg. And it is within one of the few GRBs obtained optical, X-ray and GeV spectra simultaneously for hundreds of seconds, which provides an unique opportunity so far to understand the multi-wavelength observation within the IGC paradigm, our data analysis found low Lorentz factor blackbody emission in the Episode 3 and its X-ray light curve overlaps typical IGC Golden Sample, which comply to the IGC mechanisms. We consider these findings as clues of GRB 130427A belonging to the IGC GRBs. We predicted on GCN the emergence of a supernova on May 2, 2013, which was later successfully detected on May 13, 2013.

DOI: 10.1134/S1063772915070148

1. INTRODUCTION: IGC PARADIGM

The Induced Gravitational Collapse (IGC) GRB paradigm describes a naturally evolutionary consequence of a binary system composed by a massive star and a neutron star, and includes four episodes corresponding to (1) Neutron star collapses into a black hole due to the accretion of the ejecta coming from its companion massive star that undergoes a supernova [1]. (2) The electron–positron pairs generated from the dyadosphere ballistically expands and engulfs baryonic matter, later collides at ultra-relativistic velocities with the ISM and filaments, which gives origin to the GRB [2]. (3) The starting of final steeper decay of the lightcurve, usually follows a plateau or a power-law with a constant decay index [3]. (4) The emergence of supernova in

optical band, normally nearly 10 days after the GRB trigger in its rest frame.

2. PREDICTION

The IGC paradigm demands special characteristics for the GRBs generated in the aforementioned binary system, such as the thermal radiation from accretion and supernova remnant, the overlapping of late afterglow and so on [4, 5]. In [3] we list some GRBs complying to the IGC paradigm, we call these GRBs the golden sample. After the first days' observation of the GRB 130427A, we found this new GRB exhibited similar features of the golden sample, especially the overlapping of the late decay with the golden sample, shown in Figure 1, which makes us consider this new GRB as a member of the IGC GRBs, immediately we send a letter to GCN on May 2, 2013, predicting that a supernova would appear in about 10 days [6]. Indeed, starting from May 13, 2013, the telescopes GTC, VLT and HST observed the signals of this supernova.

In this presentation, we will mainly discuss some evidences making GRB 130427A belong to the IGC

*The text was submitted by the authors in English.

**E-mail: Ruffini@icra.it

Paper was presented at the international conference in honor of Ya.B. Zeldovich 100th Anniversary “Subatomic Particles, Nucleons, Atoms, Universe: Processes and Structure” held in Minsk, Belarus, in March 10–14, 2014. Published by the recommendation of the special Editors: S.Ya. Kilin, R. Ruffini, and G.V. Vereshchagin.

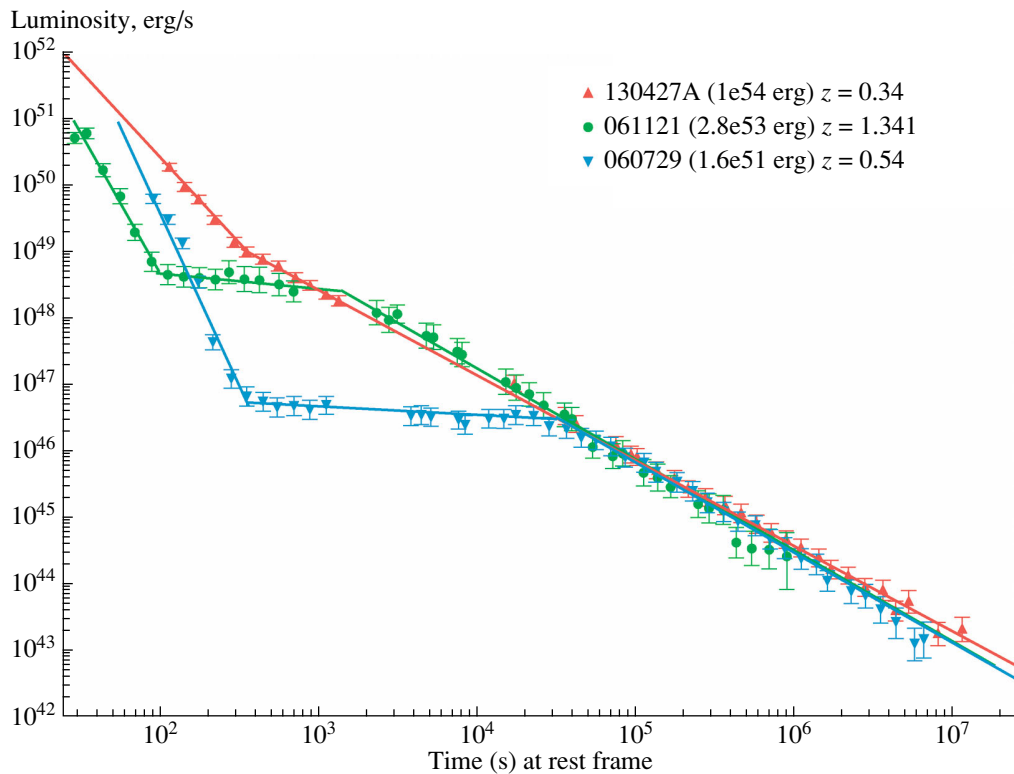


Fig. 1. An example of GRB 130427A overlaps two GBBs with different magnitude of isotropic energy from Golden Sample. GRBs' name, isotropic energy, and redshift are shown on the figure.

GRBs, specially the low Lorentz factor thermal radiator, and the multi-wave length observation in the Episode 3 of the GRB 130427A.

3. OBSERVATION AND DATA ANALYSIS

GRB 130427A was triggered by the *Fermi*-GBM at 07:47:06.42 UT on April 27, 2013 [7]. And the *Swift* Burst Alert Telescope (BAT) was triggered 51.1 s later. The *Swift* X-ray Telescope (XRT) and the *Swift* Ultra Violet Optical Telescope (UVOT) began observing 195 s and 181 s after the GBM trigger respectively [8]. On the ground, the Gemini North telescope at Hawaii [9], the Nordic Optical Telescope (NOT) [10] and the VLT/X-shooter [11] also took part in the observation and detected the redshift $z = 0.34$.

GRB 130427A is one of the few GRBs which has hundreds of seconds simultaneous data in the optical, x-ray and GeV emission [12], especially precious is its GeV emission, due to the long duration, high intensity and containing the highest energy photon (95.3 GeV) ever observed [13].

Following the standard procedure [14–16], we did the data reduction of Fermi and Swift satellite, using an unbinned likelihood method with Fermi Science

Tools v9r27p1 and NASA's Heasoft 6.14 with relevant calibration files. Data were obtained from Fermi Science Support Center,¹ and UKSSDC² light curve and spectrum are shown in Figs. 2 and 4. For the spectrum, we select 196–461 s because Swift XRT started observation at 195 s (Maselli et al. 2013), and the thermal component, which we are especially interested in, gradually fades away after 461 s.

4. THERMAL RADIATION IN EPISODE 3

By analyzing the X-ray data from 195 s to 461 s, we found that adding a blackbody component could efficiently improve the fitting solely by a single power law, the obtained blackbody temperature is in the range of 0.3 keV to 0.5 keV, if the blackbody radiation is isotropic, the radiation radius can be deduced from about 7×10^{12} cm to 2.8×10^{13} cm, with the expansion speed at $0.8c$, c is the speed of light. By analyzing the optical absorption lines of GRB associated supernovae, normally the speed of supernovae at about 10 days after the GRB trigger is around $0.1c$, the classical supernova theory holds the opinion that before the supernova appearing in optical band,

¹ <http://fermi.gsfc.nasa.gov>

² <http://www.swift.ac.uk>

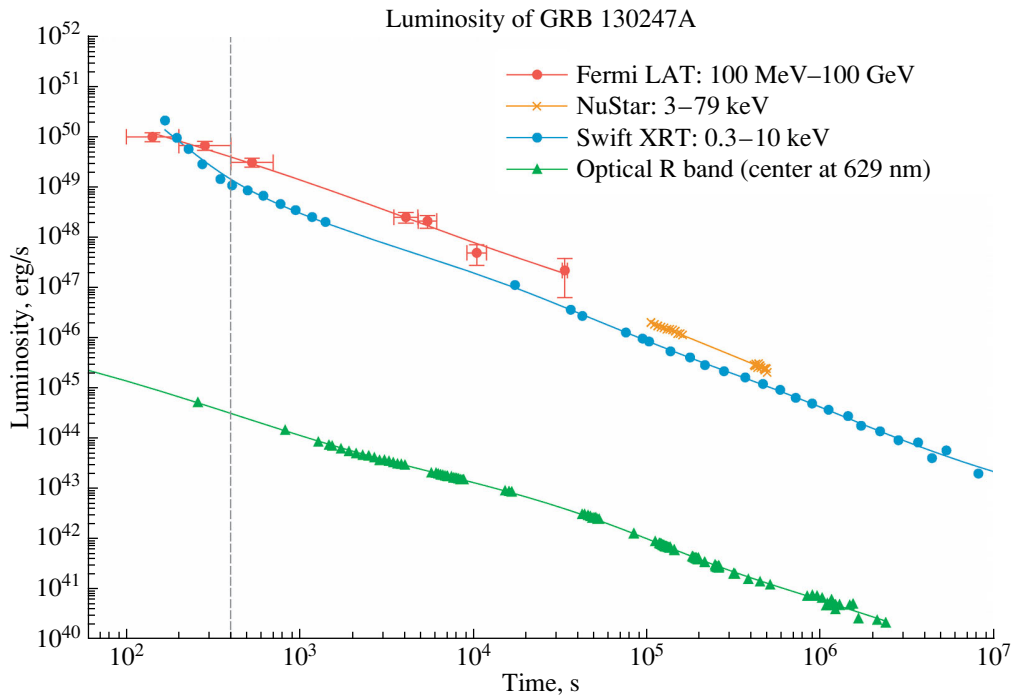


Fig. 2. The Multi-wavelength lightcurve of GRB 130247A. The GeV emission from Fermi LAT (red) and soft X-ray from Swift XRT (blue) are deduced from the original data. NuStar [17] provides higher energy X-ray than Swift XRT. The optical R band data comes from ground based telescopes [18]. The vertical dash line splits Episode 2 and Episode 3.

it undergoes a period of deceleration, from which we legitimately infer that the blackbody with the speed of $0.8c$ in the GRB 130427A probably is the supernova ejecta that IGC paradigm searches. For the GRB 130427A, or the broader IGC GRBs, the discovery of the supernova ejecta obviously is a key clue for predicting the emergence of supernova in the optical band.

5. MULTI-WAVELENGTH ANALYSIS

In the IGC paradigm, we separate Episode 2 and Episode 3 by the ending time of the prompt emission. Figure 3 demonstrates the light curve of the first 2 episodes, and Fig. 2 shows the light curve of Episode 3. The very high energy (100 MeV–100 GeV) emission is quite dim in the first 10 s when gamma and X-ray dominate the emission, then the very high energy emission raises up coincidentally with the gamma and hard X-ray prompt emissions dropping down. There is no soft X-ray observation during the first prompt emission, *Swift*-XRT starts to observe soft X-ray from 195 s, and the soft X-ray fluence is higher than the γ -ray observed by *Fermi*-GBM. Soft X-ray may have a flare between 100 s and 200 s, if it shares similar evolution as hard X-ray observed by *Swift*-BAT. In Fig. 2, clearly, the light curves of multi-wavelength from optical, X-ray to GeV follow power law decay,

and share similar decaying slope after the bending point around 400 s. We are currently attempting to link the mechanism of the possible soft X-ray flare to the thermal emission inside it, a direct and reasonable explanation is the existence of an extra process.

In the Episode 3, light curves have similar slope, but the spectra which extends 10 magnitudes of orders, from optical to GeV emission, can not be fitted by a single power law very well, instead the broken power-law gives a better fitting, the X-ray part has a photon index 1.6 ± 0.2 , and the GeV part has a softer photon index 1.9 ± 0.1 , shown in Fig. 4. As far as we know, this is the only relatively explicit multi-wavelength spectrum including GeV emission lasts for hundreds of seconds.

The IGC paradigm considers GeV emission originated from the interaction of neutron star and black hole, and the gamma-ray is described by fireshell model [2], the intensive X-ray and gamma-ray photos block the GeV photons at the beginning of the GRB, which could explain the behavior of GeV emission in Fig. 2. Also in the IGC paradigm, the collision between GRB outflow and supernova remnant is inevitable, which always happens around 100 s [19], and consequently emits thermal photons at the radius about 10^{12} cm, this collision may explain the flare and the associated thermal component.

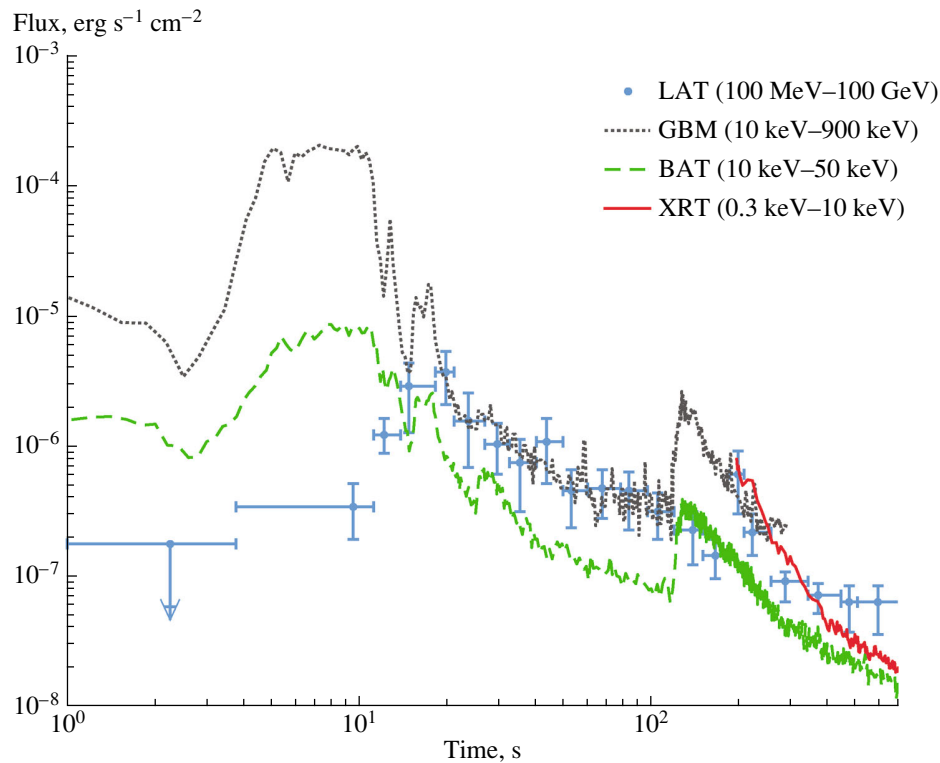


Fig. 3. Flux of first 700 s. Blue points are the *Fermi*-LAT high energy emission from 100 MeV till 100 GeV, grey dotted line represents the *Fermi*-GBM, from 10 keV to 900 keV, green dashed line represents the photons detected by *Swift* BAT from 10 keV to 50 keV, and red solid line is the soft X-ray *Swift*-XRT detection, in the range of 0.3 keV to 10 keV. From this figure, clearly the *Fermi*-LAT emission reaches highest fluence at about 20 s while the gamma-ray detected by *Fermi*-GBM releases most of the energy within the first 10 s.

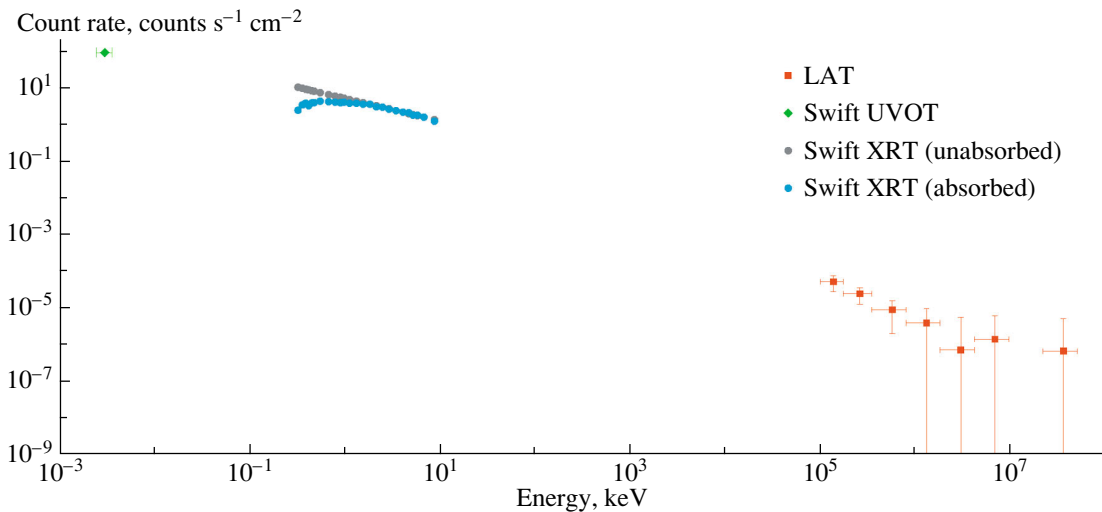


Fig. 4. Spectrum of GRB 130427A between 195 s and 461 s: Swift UVOT (green), Swift XRT (blue), and Fermi LAT (red).

6. CONCLUSION

In conclusion, first of all, the Pisani relation of the power-law overlapping [3], which is independent of energy and observed in all the golden sample,

this energetic GRB 130427A unveils such typical power-law behavior already exists at the early time as $t \sim 100$ s. Secondly, the thermal emission coming from the GRB outflow and SN remnant collision in

the early seconds of Episode 3 confirms the supernova event. Finally the multi-wavelength behavior occurs in optical, X-ray and GeV emissions conform to the IGC paradigm.

REFERENCES

1. J. A. Rueda and R. Ruffini, *Astrophys. J. Lett.* **758**, L7 (2012).
2. R. Ruffini, G. Vereshchagin, and S.-S. Xue, *Phys. Rep.* **487**, 1 (2010).
3. G. B. Pisani, L. Izzo, R. Ruffini, C. L. Bianco, M. Muccino, A. V. Penacchioni, J. A. Rueda, and Y. Wang, *Astron. Astrophys.* **552**, L5 (2013).
4. L. Izzo, J. A. Rueda, and R. Ruffini, *Astron. Astrophys.* **548**, L5 (2012).
5. A. V. Penacchioni, R. Ruffini, L. Izzo, M. Muccino, C. L. Bianco, L. Caito, B. Patricelli, and L. Amati, *Astron. Astrophys.* **538**, 58 (2012).
6. R. Ruffini, C. L. Bianco, M. Enderli, M. Muccino, A. V. Penacchioni, G. B. Pisani, J. A. Rueda, N. Sahakyan, Y. Wang, and L. Izzo, *GCN Circ.* **14526** (2013).
7. A. von Kienlin, *GCN Circ.* **14473** (2013).
8. A. Maselli, A. P. Beardmore, A. Y. Lien, V. Mangano, C. J. Mountford, K. L. Page, D. M. Palmer, and M. H. Siegel, *GCN Circ.* **14448** (2013).
9. A. J. Levan, S. B. Cenko, D. A. Perley, and N. R. Tanvir, *GCN Circ.* **14455** (2013).
10. D. Xu, A. de Ugarte Postigo, S. Schulze, J. Jessen-Hansen, G. Leloudas, T. Kruehler, J. P. U. Fynbo, and P. Jakobsson, *GCN Circ.* **14478** (2013).
11. H. Flores, S. Covino, D. Xu, T. Kruehler, J. Fynbo, B. Milvang-Jensen, A. de Ugarte Postigo, L. Kaper, and K. Wiersema, *GCN Circ.* **14491** (2013).
12. M. Ackermann, M. Ajello, K. Asano, W. B. Atwood, M. Axelsson, L. Baldini, J. Ballet, G. Barbiellini, M. G. Baring, D. Bastieri, et al., *Science* **343**, 42 (2013).
13. Y.-Z. Fan, P. H. T. Tam, F.-W. Zhang, Y.-F. Liang, H.-N. He, B. Zhou, R.-Z. Yang, Z.-P. Jin, and D.-M. Wei, *Astrophys. J.* **776**, 95 (2013).
14. P. Romano, S. Campana, G. Chincarini, J. Cummings, G. Cusumano, S. T. Holland, V. Mangano, T. Mineo, K. L. Page, V. Pal'shin, et al., *Astron. Astrophys.* **456**, 917 (2006).
15. P. A. Evans, A. P. Beardmore, K. L. Page, L. G. Tyler, J. P. Osborne, M. R. Goad, P. T. O'Brien, L. Vetere, J. Racusin, D. Morris, et al., *Astron. Astrophys.* **469**, 379 (2007).
16. P. A. Evans, A. P. Beardmore, K. L. Page, J. P. Osborne, P. T. O'Brien, R. Willingale, R. L. C. Starling, D. N. Burrows, O. Godet, L. Vetere, et al., *Mon. Not. R. Astron. Soc.* **397**, 1177 (2009).
17. C. Kouveliotou, J. Granot, J. L. Racusin, E. Bellm, G. Vianello, S. Oates, C. L. Fryer, S. E. Boggs, F. E. Christensen, W. W. Craig, et al., *Astrophys. J.* **779**, L1 (2013).
18. D. A. Perley, S. B. Cenko, A. Corsi, N. R. Tanvir, A. J. Levan, D. A. Kann, E. Sonbas, K. Wiersema, W. Zheng, X. H. Zhao, et al., *Astrophys. J.* **781**, 37 (2013).
19. R. Ruffini, G. V. Vereshchagin, and Y. Wang (2014, in preparation).

GRB 140619B: A SHORT GRB FROM A BINARY NEUTRON STAR MERGER LEADING TO BLACK HOLE FORMATION

R. RUFFINI^{1,2,3,4}, M. MUCCINO^{1,2}, M. KOVACEVIC^{1,3}, F. G. OLIVEIRA^{1,3}, J. A. RUEDA^{1,2,4}, C. L. BIANCO^{1,2},

M. ENDERLI^{1,3}, A. V. PENACCHIONI^{4,5}, G. B. PISANI^{1,2}, Y. WANG^{1,2}, AND E. ZANINONI⁴

¹Dip. di Fisica and ICRA, Sapienza Università di Roma, Piazzale Aldo Moro 5, I-00185 Rome, Italy; ruffini@icra.it

²ICRANet, Piazza della Repubblica 10, I-65122 Pescara, Italy

³Université de Nice Sophia Antipolis, CEDEX 2, Grand Château Parc Valrose, Nice, France

⁴ICRANet-Rio, Centro Brasileiro de Pesquisas Físicas, Rua Dr. Xavier Sigaud 150, Rio de Janeiro, RJ, 22290-180, Brazil

⁵Instituto Nacional de Pesquisas Espaciais, Av. dos Astronautas, 1758, São José dos Campos, SP, 12227-010, Brazil

Received 2014 November 30; accepted 2015 June 15; published 2015 August 4

ABSTRACT

We show the existence of two families of short gamma-ray bursts (GRBs), both originating from the merger of binary neutron stars (NSs): family-1 with $E_{\text{iso}} < 10^{52}$ erg, leading to a massive NS as the merged core, and family-2 with $E_{\text{iso}} > 10^{52}$ erg, leading to a black hole (BH). Following the identification of the prototype GRB 090227B, we present the details of a new example of family-2 short burst: GRB 140619B. From the spectral analysis of the early ~ 0.2 s, we infer an observed temperature $kT = (324 \pm 33)$ keV of the e^+e^- -plasma at transparency (P-GRB), a theoretically derived redshift $z = 2.67 \pm 0.37$, a total burst energy $E_{e^+e^-}^{\text{tot}} = (6.03 \pm 0.79) \times 10^{52}$ erg, a rest-frame peak energy $E_{p,i} = 4.7$ MeV, and a baryon load $B = (5.52 \pm 0.73) \times 10^{-5}$. We also estimate the corresponding emission of gravitational waves. Two additional examples of family-2 short bursts are identified: GRB 081024B and GRB 090510, remarkable for its well determined cosmological distance. We show that marked differences exist in the nature of the afterglows of these two families of short bursts: family-2 bursts, leading to BH formation, consistently exhibit high energy emission following the proper-GRB emission; family-1 bursts, leading to the formation of a massive NS, should never exhibit high energy emission. We also show that both the families fulfill an $E_{p,i}-E_{\text{iso}}$ relation with slope $\gamma = 0.59 \pm 0.07$ and a normalization constant incompatible with the one for long GRBs. The observed rate of such family-2 events is $\rho_0 = (2.1_{-1.4}^{+2.8}) \times 10^{-4}$ Gpc⁻³ yr⁻¹.

Key words: gamma-ray burst: general

1. INTRODUCTION

The phenomenological classification of gamma-ray bursts (GRBs) based on their prompt emission observed T_{90} durations defines “long” and “short” bursts which are, respectively, longer or shorter than $T_{90} = 2$ s (Dezalay et al. 1992; Klebesadel 1992, pp. 161–168; Kouveliotou et al. 1993; Tavani 1998). Short GRBs have been often indicated as originating from binary neutron star (NS) mergers (see, e.g., Goodman 1986; Paczynski 1986; Eichler et al. 1989; Narayan et al. 1991; Meszaros & Rees 1997; Rosswog et al. 2003; Lee et al. 2004; Berger 2014).

An ample literature exists of short GRBs with a measured redshift, isotropic burst energy $E_{\text{iso}} < 10^{52}$ erg and rest-frame spectral peak energy $E_{p,i} < 2$ MeV (see, e.g., Berger 2014 and references therein). Thanks to extensive data provided by the *Swift*-XRT instrument (Burrows et al. 2005), it is possible to observe the long lasting X-ray afterglow of these short bursts to identify their host galaxies and to compute their cosmological redshifts. They have been observed in both early- and late-type galaxies with older stellar population ages (see, e.g., Berger 2014 for details), and at systematically larger radial offsets from their host galaxies than long GRBs (Sahu et al. 1997; van Paradijs et al. 1997; Bloom et al. 2006; Troja et al. 2008; Fong et al. 2010; Berger 2011; Kopač et al. 2012). None of these afterglows appears to have the specific power law signature in the X-ray luminosity when computed in the source rest-frame, as found in some long GRBs (see, e.g., Ruffini et al. 2014).

In the meantime, considerable progress has been obtained in the theoretical understanding of the equilibrium configuration of NSs, in their mass–radius relation (see Figure 2 in Section 2), and especially in the theoretical determination of the value of the NS critical mass for gravitational collapse $M_{\text{crit}}^{\text{NS}}$ (Rotondo et al. 2011; Rueda et al. 2011; Belvedere et al. 2012). This has led to a theoretical value $M_{\text{crit}}^{\text{NS}} = 2.67 M_{\odot}$ (Belvedere et al. 2012). Particularly relevant to this determination has been the conceptual change of paradigm of imposing global charge neutrality (Belvedere et al. 2012) instead of the traditional local charge neutrality (LCN) still applied in the current literature (see, e.g., Haensel et al. 2007 and references therein).

Similarly, noteworthy progress has been achieved in the determination of the masses of galactic binary pulsars. Of the greatest relevance has been the direct observation of NS masses larger than $2 M_{\odot}$ (see Antoniadis et al. 2013 and Section 2). In the majority of the observed cases of binary NSs the sum of the NS masses, $M_1 + M_2$, is indeed smaller than $M_{\text{crit}}^{\text{NS}}$ and, given the above determination of the NS critical mass, their coalescence will never lead to a black hole (BH) formation (see Figure 3 in Section 2). This of course offers a clear challenge to the traditional assumption that all short GRBs originate from BH formation (see, e.g., Berger 2014 and references therein).

Motivated by the above considerations, we propose in this article the existence of two families of short GRBs, both originating from NS mergers: the difference between these two families depends on whether the total mass of the merged core

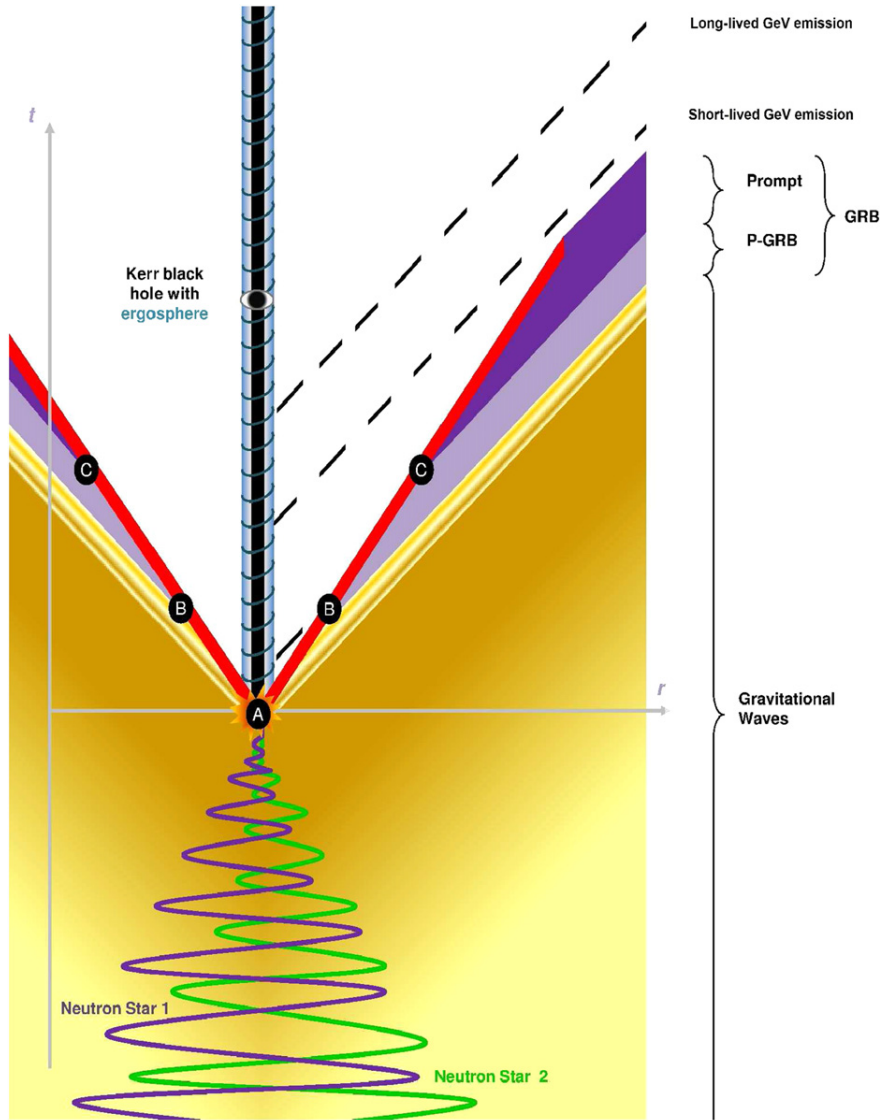


Figure 1. Space–time diagram of family-2 short GRBs. The orbital separation between the two NSs decreases due to the emission of GWs, until the merging occurs and a family-2 short GRB is emitted. Following the fireshell model (see Section 3): (A) vacuum polarization occurs while the event horizon is formed and a fireshell of e^+e^- plasma self-accelerates radially outwards; (B) the fireshell, after engulfing the baryons, keeps self-accelerating and reaches the transparency when the P-GRB is emitted; (C) the accelerated baryons interact with the local CBM giving rise to the prompt emission. The remnant of the merger is a Kerr BH. The accretion of a small (large) amount of orbiting matter onto the BH can lead to the short lived but very energetic 0.1–100 GeV emission observed in GRB 081024B, GRB 090510, and GRB 140619B. The absence of such an emission in GRB 090227B is due to the absence of observations of *Fermi*-LAT.

is smaller or larger than $M_{\text{crit}}^{\text{NS}}$. We assume that family-1 coincides with the above mentioned less energetic short GRBs with $E_{\text{iso}} < 10^{52}$ erg and the coalescence of the merging NSs leads to a massive NS as the merged core. We assume that family-2 short bursts with $E_{\text{iso}} > 10^{52}$ erg originate from a merger process leading to a BH as the merged core. The presence of the BH allows us to address the GRB nature within the fireshell model (Ruffini et al. 2001a, 2001b, 2001c) leading to specific signatures in the luminosity, spectra and time variability observed in two very different components: the proper-GRB (P-GRB) and the prompt emission (see Section 3). The prototype is GRB 090227B, which we already analyzed within the fireshell model in Muccino et al. (2013). We also assume that the BH gives rise to the short-lived ($\lesssim 10^2$ s in the observer frame) and very energetic GeV emission which has been found to be present in all these family-2 short GRBs,

when *Fermi*-LAT data are available. This article is mainly dedicated to giving the theoretical predictions and the observational diagnostics to support the above picture.

In Section 4 we recall the results obtained in the case of the prototype of family-2 short GRBs: GRB 090227B (Muccino et al. 2013). The analysis of its P-GRB emission led to a particularly low value of the baryon load, $B \sim 10^{-5}$, as well as to the prediction of the distance corresponding to a redshift $z = 1.61$, and consequently to $E_{e^+e^-}^{\text{tot}} = 2.83 \times 10^{53}$ erg. From the analysis of the spectrum and the light curve of the prompt emission we inferred an average circumburst medium (CBM) density $\langle n_{\text{CBM}} \rangle \sim 10^{-5} \text{ cm}^{-3}$ typical of galactic halos of GRB host galaxies.

In Section 5 we summarize the observations of a second example of such family-2 short bursts, GRB 140619B, and our data analysis from 8 keV up to 100 GeV. We also point out the

lack of any observed X-ray afterglow following the prompt emission (Maselli & D’Avanzo 2014).

In Section 6 we address GRB 140619B within the fireshell model and compare and contrast the results with those of the prototype, GRB 090227B (Muccino et al. 2013). In Section 6.1, from the fireshell equations of motion, we theoretically estimate and predict the value of the redshift of the source, $z = 2.67 \pm 0.37$. Consequently, we derive the burst energy $E_{\text{iso}} > 10^{52}$ erg and the value of the baryon load $B \sim 10^{-5}$. In Section 6.2 we infer an average density of the CBM $\langle n_{\text{CBM}} \rangle \sim 10^{-5} \text{ cm}^{-3}$ from fitting the prompt emission light curve and spectra. This parameter is typical of the galactic halo environment and further confirms a NS–NS merger as the progenitor for GRB 140619B (see Section 6.3 and Figure 1).

In Section 7 we discuss the possibility for Advanced LIGO to detect the emission of gravitational waves (GWs) from such a binary NS progenitor. From the dynamics of the above system, the total energy emitted in GW radiation corresponds to $E_{\text{GW}}^T = 7.42 \times 10^{52}$ erg, computed during the entire inspiral phase all the way up to the merger. This gives a signal below the sensitivity of the Advanced LIGO interferometer.

In Section 8 we focus on the short-lived ($\Delta t \approx 4$ s) but significant 0.1–100 GeV emission (see Figure 1). We first address the issue of whether this is a peculiarity of GRB 140619B, or whether the GeV emission can be considered to be a common feature of all these family-2 short GRBs. We first return to GRB 090227B to see how to explain the absence of observations of the GeV emission from this source, and we find a simple reason: GRB 090227B was outside the nominal LAT field of view (FOV, see Ackermann et al. 2013, and Section 4). We then turn our attention to another source, GRB 090510, which presents many of the common features of the family-2 short GRBs. Especially noteworthy is the presence of a high energy GeV emission lasting $\sim 10^2$ s, much longer than the one of GRB 140619B. The presence of an X-ray afterglow in GRB 090510 is fortunate and particularly important, though lacking a scaling law behavior (Ruffini et al. 2014), since it has allowed the optical identification of the source and the determination of its distance and its cosmological redshift $z = 0.903$. The corresponding isotropic energy and intrinsic peak spectral energy are, respectively, $E_{\text{iso}} > 10^{52}$ erg and $E_{p,i} = (7.89 \pm 0.76)$ MeV, typical again of family-2 short bursts. We then compare and contrast this high energy emission and their corresponding X-ray emissions in the family-2 short GRB 140619B and GRB 090510 with the afterglow of the family-1 short GRBs (see Figure 13 and Berger 2014).

In Section 9 we give an estimate for the rate of the family-2 short GRBs.

In Section 10 we discuss the existence of the new $E_{p,i}-E_{\text{iso}}$ relation for all short GRBs introduced by Zhang et al. (2012) and Calderone et al. (2015), with a power-law similar to the one of the Amati relation (Amati et al. 2008) for long GRBs, but with a different amplitude. Finally we draw our conclusions.

2. MOTIVATION FROM GALACTIC BINARY NS AND NS THEORY

Recent theoretical progress has been achieved in the understanding of the NS equation of state and equilibrium configuration and of the value of its critical mass $M_{\text{crit}}^{\text{NS}}$. In Rotondo et al. (2011) it has been shown to be impossible to

impose the LCN condition on a self-gravitating system of degenerate neutrons, protons, and electrons in β -equilibrium within the framework of relativistic quantum statistics and the Einstein–Maxwell equations. The equations of equilibrium of NSs, taking into account strong, weak, electromagnetic, and gravitational interactions in general relativity and the equilibrium conditions based on the Einstein–Maxwell–Thomas–Fermi equations along with the constancy of the general relativistic Fermi energies of particles, the “Klein potentials,” throughout the configuration have been presented in Rueda et al. (2011) and Belvedere et al. (2012), where a theoretical estimate of $M_{\text{crit}}^{\text{NS}} \approx 2.67 M_{\odot}$ has been obtained. The implementations of the above results by considering the equilibrium configurations of slowly rotating NSs by using the Hartle formalism has been presented in Belvedere et al. (2014a). Then in Rueda et al. (2014) a detailed study was made of the transition layer between the core and crust of NSs at the nuclear saturation density, and its surface tension and Coulomb energy have been calculated. A comprehensive summary of these results for both static and uniformly rotating NSs is discussed in Belvedere et al. (2014b). The absolute upper limit on the angular momentum of a rotating NS fulfilling the above microscopical conditions has been obtained in Cipolletta et al. (2015).

A vast number of tests have been performed in fitting the data of pulsars (Deneva et al. 2012; Lattimer 2012; Antoniadis et al. 2013; Kramer 2014). In particular, the high value of the recently measured mass of PSR J0348+0432, $M = (2.01 \pm 0.04) M_{\odot}$ (Antoniadis et al. 2013), favors stiff nuclear equations of state, like the one adopted in Belvedere et al. (2012) based on relativistic nuclear mean field theory à la Boguta & Bodmer (1977), which leads to the above theoretical estimate of $M_{\text{crit}}^{\text{NS}}$ (see also Figure 2). This value is supported by the above observational constraints, and in any case, is well below the absolute upper limit of $3.2 M_{\odot}$ for a non-rotating NS (Rhoades & Ruffini 1974).

If we turn to the binary NSs within our Galaxy (see Figure 3) we notice that only in a subset of them is the total mass of the components larger than $M_{\text{crit}}^{\text{NS}}$ and can lead to a BH in their merging process.⁶

Given this general understanding, we have identified the characteristic properties of family-2 short bursts, whose prototype was identified in GRB 090227B (Muccino et al. 2013). Equally important has been the identification of the observed characteristic features of family-1 short GRBs which will be discussed in the following sections.

⁶ During the refereeing process, an approach by Fryer et al. (2015) based on a combination of binary NS merger nuclear physics models and population synthesis appeared. They infer that for a maximum nonrotating NS mass of $M_{\text{crit}}^{\text{NS}}$ above 2.3–2.4 M_{\odot} , less than 4% of the NS mergers produces short GRBs by gravitational collapse to a BH. Here we go one step further by indicating the theoretical predictions characterizing short GRBs originating from the massive NS formation (family-1) and the ones originating from BH formation (family-2). We indicate: (a) the specific spectral features, (b) the presence of the GeV emission originating from the BH, and (c) the fulfillment of the $E_{p,i}-E_{\text{iso}}$ relation (see Zhang et al. 2012; Calderone et al. 2015, and Section 10). The paper by Fryer et al. (2015) was followed by Lawrence et al. (2015) where the authors examine the value of $M_{\text{crit}}^{\text{NS}}$ for a family of equations of state and concluded that a reasonable fraction of double NS mergers may produce neither short GRBs nor BHs. Here we again go one step further by indicating that in the case of a merged core with a mass smaller than $M_{\text{crit}}^{\text{NS}}$ leading to a massive NS, a less energetic short GRB with a softer emission tail indeed occurs (family-1 short bursts). We show also that these short GRBs fulfill the above $E_{p,i}-E_{\text{iso}}$ relation (see Section 10).

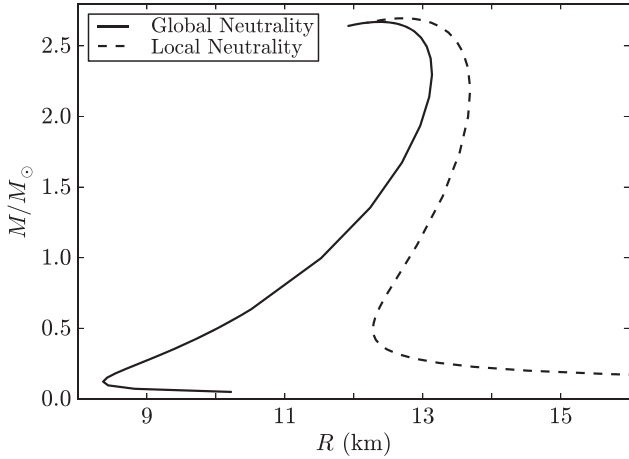


Figure 2. Mass–radius relation obtained with the local and the new global neutrality equilibrium configurations, by applying the NL3 nuclear model. Figure reproduced from Belvedere et al. (2012).

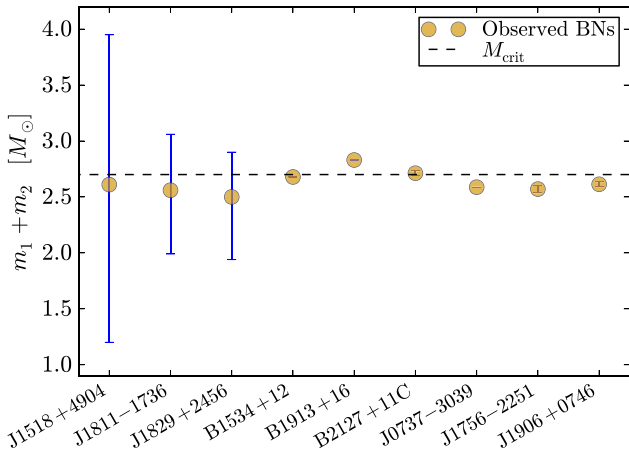


Figure 3. Plot of the binary NSs with known total masses ($M_1 + M_2$, in solar masses) and the corresponding uncertainties. The horizontal dashed line marks the critical NS mass of $2.67 M_\odot$ (Belvedere et al. 2012). Systems beyond this value lead to BH formation. Masses taken from Zhang et al. (2011) and Antoniadis (2014).

The crucial role of $M_{\text{crit}}^{\text{NS}}$ has been also shown in the corresponding analysis of long GRBs in distinguishing between the two different families (Ruffini et al. 2015) in the induced gravitational collapse paradigm (Izzo et al. 2012a; Rueda & Ruffini 2012; Fryer et al. 2014).

3. THE FIRESHELL MODEL

It is well known that the majority of the astrophysical community working on GRBs envisages the spectral and temporal analysis of both short and long GRBs considering their whole emission as a single event (see, e.g., Ackermann et al. 2013). This picture follows the conceptual framework of the “fireball model” (see, e.g., Sari et al. 1998; Piran 2005; Meszaros 2006, and reference therein).

The “fireshell model” (Ruffini et al. 2001a, 2001b, 2001c) has instead addressed a specific time-resolved spectral analysis leading to distinct signatures and to the identification of different astrophysical regimes within the same GRB (see, e.g., Izzo et al. 2010; Izzo et al. 2012b; Muccino et al. 2013; Ruffini et al. 2013 and references therein). This has led to introduction

of the concept of binary mergers of NS–NS and of FeCO–NS together with a set of new paradigms in order to describe the complexity of GRB phenomena within a “Cosmic-Matrix” approach (Ruffini 2015a).

In the fireshell model (Ruffini et al. 2001a, 2001b, 2001c) GRBs originate from an optically thick e^+e^- plasma (Damour & Ruffini 1975; Ruffini & Xue 2008; Ruffini et al. 2010) during the gravitational collapse to a BH. Such an e^+e^- plasma is confined to an expanding shell and reaches thermal equilibrium almost instantaneously (Aksenov et al. 2007). The annihilation of these pairs occurs gradually, while the expanding shell, called the *fireshell*, self-accelerates up to ultra relativistic velocities (Ruffini et al. 1999) and engulfs the baryonic matter (of mass M_B) left over in the process of collapse. The baryon load thermalizes with the pairs due to the large optical depth (Ruffini et al. 2000).

Assuming spherical symmetry of the system, the dynamics in the optically thick phase is fully described by only two free initial parameters: the total energy of the plasma $E_{e^+e^-}^{\text{tot}}$ and the baryon load B (Ruffini et al. 2000). Only solutions with $B \leq 10^{-2}$ are characterized by regular relativistic expansion; for $B \geq 10^{-2}$ turbulence and instabilities occur (Ruffini et al. 2000). The fireshell continues to self-accelerate until it reaches the transparency condition and a first flash of thermal radiation, the P-GRB, is emitted (Ruffini et al. 2001b). The radius r_{tr} at which the transparency occurs, the theoretical temperature (blueshifted toward the observer kT_{blue}), the Lorentz factor Γ_{tr} , as well as the amount of the energy emitted in the P-GRB are functions of $E_{e^+e^-}^{\text{tot}}$ and B (see, e.g., Ruffini et al. 2001b; Ruffini et al. 2009, and Figure 4).

After transparency, the residual expanding plasma of leptons and baryons collides with the CBM giving rise to multi-wavelength emission: the prompt emission. Assuming the fully radiative condition, the structures observed in the prompt emission of a GRB are described by two quantities associated with the environment: the CBM density profile n_{CBM} , which determines the temporal behavior of the light curve, and the fireshell surface filling factor $\mathcal{R} = A_{\text{eff}}/A_{\text{vis}}$, in which A_{eff} is the effective emitting area of the fireshell, and A_{vis} is its total visible area (Ruffini et al. 2002, 2005). This second parameter takes into account the inhomogeneities in the CBM and its filamentary structure (Ruffini et al. 2004).

The emission process of the collision between the baryons and the CBM is described in the comoving frame of the shell as a modified blackbody (BB) spectrum. This spectrum is obtained by the introduction of an additional phenomenological parameter α which characterizes the departure of the slope of the low energy part of the comoving spectrum from the purely thermal one (see Patricelli et al. 2012, for details). The nonthermal spectral shape of the observed GRB is then produced by the convolution of a very large number of modified thermal spectra with different temperatures and different Lorentz and Doppler factors. This convolution is performed over the surfaces of constant arrival time for photons at the detector (EquiTemporal Surfaces, EQTS, Bianco & Ruffini 2005a, 2005b), encompassing the total observation time. The observed hard-to-soft spectral variation comes out naturally from the decrease with time of the comoving temperature and of the bulk Lorentz Γ factor. This effect is amplified by the curvature effect due to the EQTS which produces the observed time lag in the majority of the GRBs.

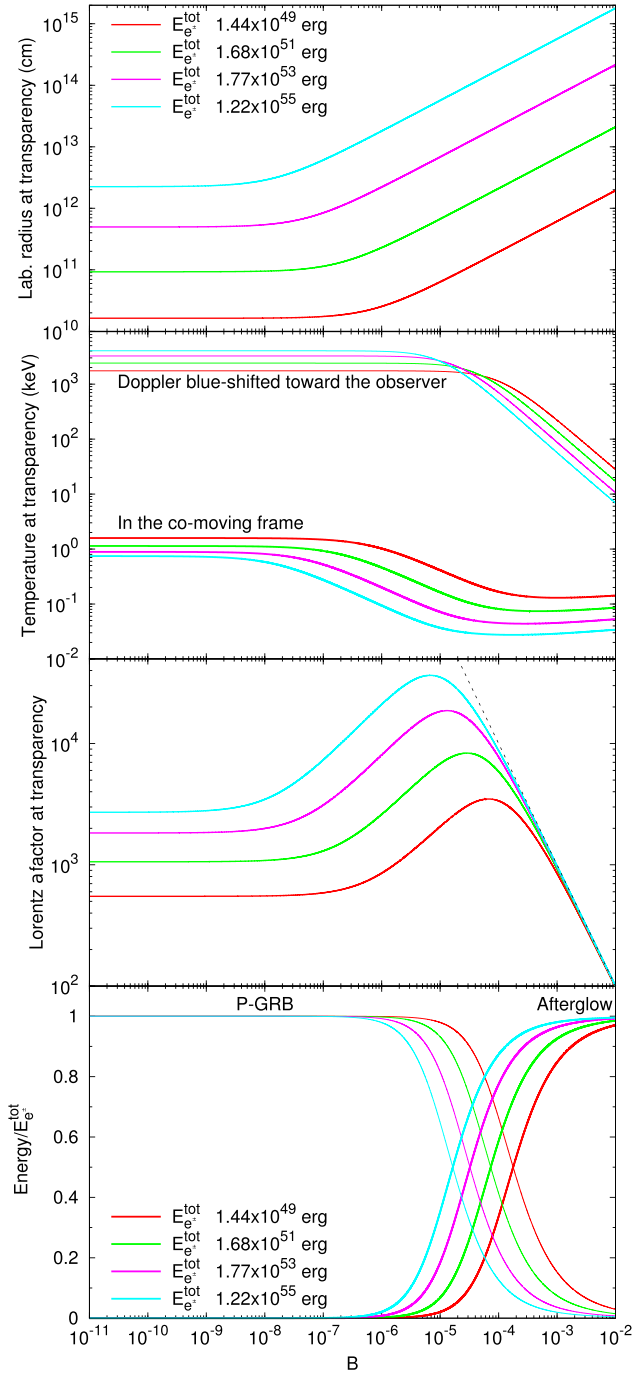


Figure 4. Main quantities of the fireshell model at transparency for selected values of $E_{e^+e^-}^{\text{tot}}$: the radius in the laboratory frame, the temperatures of the plasma in the co-moving frame and blueshifted toward the observer, the Lorentz Γ factor, and the fraction of energy radiated in the P-GRB and in the prompt emission as functions of B .

The canonical GRB light curve within the fireshell model is then characterized by a first (mainly thermal) emission due to the transparency of the e^+e^- -photon-baryon plasma, the P-GRB. A multi-wavelength emission, the prompt emission, follows due to the collisions between the accelerated baryons and the CBM.

The fireshell model has originally described the process of vacuum polarization due to the overcritical electromagnetic

field occurring at the moment of BH formation (Damour & Ruffini 1975). The formalism has been developed by considering a large number of relativistic quantum effects in the electrodynamics proposed for the NS crust (Belvedere et al. 2012, 2014a; Rueda et al. 2014), as well as on quantum-electrodynamics processes ongoing in the gravitational collapse (Han et al. 2012; Ruffini & Xue 2013). This has led to the results summarized in Figure 4.

The first description of the e^+e^- plasma within the fireshell model was performed under the simplified assumption of spherical symmetry (the dyadosphere; see, e.g., Preparata et al. 1998). The corresponding structure in the axially symmetric Kerr-Newman geometry has been considered (the dyadotorus; see, e.g., Cherubini et al. 2009; Ruffini 2009) and could possibly be tested.

The general formalism of the fireshell model can also be applied to any optically thick e^+e^- plasma in the presence of a baryon load, like the one created during the merging of binary NSs from $\nu\bar{\nu} \rightarrow e^+e^-$ (see, e.g., Salmonson & Wilson 2002 and references therein).

The P-GRB addresses the fully relativistic fundamental physics aspects of the model, in particular the acceleration process of the e^+e^- -baryon plasma, the collapsing NS quantum-electrodynamics, and the BH physics. The prompt emission addresses the conceptually simpler problem of the interaction of the accelerated baryons with the CBM, which does not allow nor require, by its own nature, a detailed description.

4. SUMMARY OF THE RESULTS FOR GRB 090227B: THE PROTOTYPE OF THE FAMILY-2 SHORT GRBS

GRB 090227B is a bright short burst with an overall emission lasting ~ 0.9 s and total fluence of 3.79×10^{-5} erg cm^{-2} in the energy range 8 keV–40 MeV. This burst was significantly detected only in the LAT Low Energy (LLE) data since it was outside the nominal LAT FOV (Ackermann et al. 2013). However, only one transient-class event with energy above 100 MeV has been associated with the GRB (Ackermann et al. 2013).

The time-resolved spectral analysis on the time scale as short as 16 ms, made possible by the *Fermi*-GBM (Meegan et al. 2009), has allowed the identification of the P-GRB in the early 96 ms of emission. The corresponding thermal component has a temperature $kT = (517 \pm 28)$ keV (see the upper plots of Figure 9 in Muccino et al. 2013). The subsequent emission, fit by a Band function (see lower plots of Figure 9 in Muccino et al. 2013), has been identified with the prompt emission.

Due to the absence of an optical identification, a direct measurement of the cosmological redshift was not possible. From the temperature and flux of the P-GRB thermal component it was possible to derive (see Figure 4) a theoretical cosmological redshift $z = 1.61 \pm 0.14$, as well as the baryon load $B = (4.13 \pm 0.05) \times 10^{-5}$, the total plasma energy $E_{e^+e^-}^{\text{tot}} = (2.83 \pm 0.15) \times 10^{53}$ erg, and the extremely high Lorentz Γ factor at transparency $\Gamma_{\text{tr}} = (1.44 \pm 0.01) \times 10^4$ (see Section 4.1 in Muccino et al. 2013). Consequently, an average CBM number density $\langle n_{\text{CBM}} \rangle = (1.90 \pm 0.20) \times 10^{-5}$ cm^{-3} has been determined which is typical of galactic halos where NS-NS mergers migrate, owing to natal kicks imparted to the binaries at birth (see, e.g., Narayan et al. 1992; Bloom et al. 1999; Fryer et al. 1999; Belczynski et al. 2006; Berger 2014).

In Muccino et al. (2013) it was concluded that the progenitor of GRB 090227B is a binary NS. For simplicity and as a lower limit, the masses of the two NS have been assumed to be the same, e.g., $M_1 = M_2 = 1.34 M_\odot$, so that the total merged core mass is $>M_{\text{crit}}^{\text{NS}}$ and therefore a BH is formed. This conclusion was drawn in view of the large total energy, $E_{e^+e^-}^{\text{tot}} = 2.83 \times 10^{53}$ erg. Correspondingly, the energy emitted via GWs, $\sim 9.7 \times 10^{52}$ erg, has been estimated in Oliveira et al. (2014).

5. OBSERVATIONS AND DATA ANALYSIS OF GRB 140619B

At 11:24:40.52 UT on 2014 June 19, the *Fermi*-GBM detector (Connaughton et al. 2014) triggered and located the short and hard burst GRB 140619B (trigger 424869883/140619475). The on-ground calculated location, using the GBM trigger data, was R.A.(J2000) = $08^{\text{h}}54^{\text{m}}$ and decl. (J2000) = $-3^\circ42'$, with an uncertainty of 5° (statistical only). The location of this burst was 32° from the LAT boresight at the time of the trigger, and the data from the *Fermi*-LAT showed a significant increase in the event rate (Kocevski et al. 2014). The burst was also detected by *Suzaku*-WAM (Iwakiri et al. 2014), showing a single pulse with a duration of ~ 0.7 s (50 keV–5 MeV). The analysis from 48.7 to 71.6 ks after the GBM trigger by the *Swift*-XRT instrument in the FOV of the *Fermi*-GBM and LAT, was completely in Photon Counting mode (Maselli & D’Avanzo 2014). No bright X-ray afterglow was detected within the LAT error circle. This set an upper limit on the energy flux in the observed 0.3–10 keV energy band of $\approx 9.24 \times 10^{-14}$ erg/(cm² s), assuming a photon index $\gamma = 2.2$. Therefore, no optical follow-up was possible and thus the redshift of the source is unknown.

We have analyzed the *Fermi*-GBM and LAT data in the energy range 8 keV–40 MeV and 20 MeV–100 GeV, respectively. We have downloaded the GBM TTE (Time-Tagged Events) files,⁷ suitable for short or highly structured events, and analyzed them by using the RMFIT package.⁸ The LLE data⁹, between 20–100 MeV, and the high energy data¹⁰, between 100 MeV–100 GeV, were analyzed by using the Fermi-science tools.¹¹ In Figure 5 we have reproduced the 64 ms binned GBM light curves corresponding to detectors NaI-n6 (8–260 keV, top panel) and BGO-b1 (260 keV–20 MeV, second panel), the 64 ms binned LLE light curve (20–100 MeV, third panel) and the 192 ms binned high-energy channel light curve (0.1–100 GeV, bottom panel). All the light curves are background subtracted. The NaI-n6 light curve shows a very weak signal, almost at the background level, while the BGO-b1 signal is represented by a short hard pulse, possibly composed by two sub-structures, with a total duration of $T_{90} \approx 0.7$ s. The vertical dashed line in Figure 5 represents the on-set of both LAT light curves, i.e., ~ 0.2 s after the GBM trigger. In principle, this allows us to determine the time interval within which the P-GRB emission takes place.

We have subsequently performed the time-integrated and time-resolved spectral analyses focused on the GBM data in the energy range 8 keV–40 MeV.

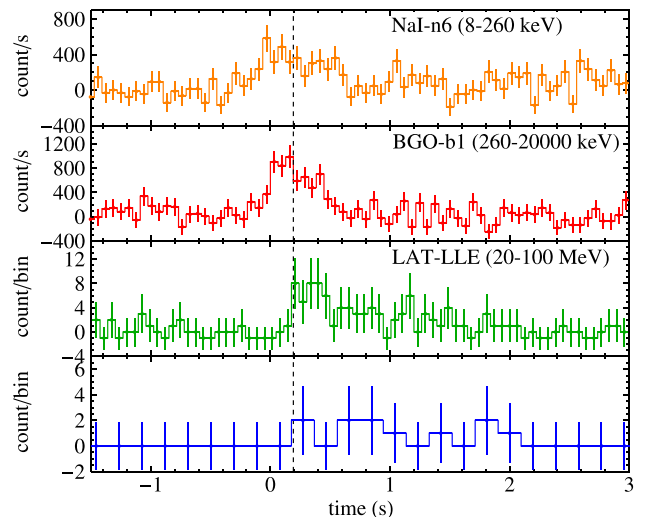


Figure 5. Background subtracted light curves of GRB 140619B from various detectors in various energy bands. From the top to the bottom panel: the 64 ms binned light curves from the NaI-n6 (8–260 keV, top panel) and BGO-b1 (260 keV–20 MeV, second panel) detectors, the 64 ms binned LLE light curve (20–100 MeV, third panel), and the 192 ms binned high-energy channel light curve (100 MeV–100 GeV, bottom panel).

5.1. Time-integrated Spectral Analysis

We have performed a time-integrated spectral analysis in the time interval from $T_0 - 0.064$ s to $T_0 + 0.640$ s, which corresponds to the T_{90} duration of the burst. We have indicated the trigger time by T_0 and have considered the following spectral models: Comptonization (Compt) and a Band function (Band et al. 1993). The corresponding plots are shown in Figure 6 and the results of the fits are listed in Table 1. From a statistical point of view, the Compt model provides the best fit to the data. In fact the Band function, which has an additional parameter with respect to the Compt model, improves the fit by only $\Delta\text{C-STAT} = 2.53$, where $\Delta\text{C-STAT}$ is the difference between the two C-STAT values of the Compt and Band models. If we consider $\Delta\text{C-STAT}$ as a χ^2 variable for the change in the number of the model parameters Δn (in this case $\Delta n = 1$), and assuming that the Compt model is nested within the Band model,¹² we conclude that the Band model improves the fit only at the 89% significance level, and anyway less than 2σ . Therefore it is not enough to reject the Compt model. The most interesting feature of the Compt model consists of its low-energy index, which is consistent with $\alpha \sim 0$. We proceed now to a time-resolved analysis to investigate the possibility that in the early phases of the prompt emission the spectrum is consistent with a BB spectrum, i.e., $\alpha \approx 1$, which corresponds to the signature of P-GRB emission.

5.2. Time-resolved Spectral Analysis

We performed the time-resolved spectral analysis by selecting time intervals with fluences larger than $\approx 10^{-6}$ erg cm⁻² in order to collect enough photons. Consequently, we have selected two time intervals that correspond to the main spike and the less intense structure (see the BGO-b1 light curve in Figure 6). The first time interval, from T_0 to

¹² The Compt model can be considered a particular case of the Band model with $\beta \rightarrow -\infty$.

⁷ <ftp://legacy.gsfc.nasa.gov/fermi/data/gbm/bursts>

⁸ http://Fermi.gsfc.nasa.gov/ssc/data/analysis/rmfit/vc_rmfit_tutorial.pdf

⁹ http://fermi.gsfc.nasa.gov/ssc/observations/types/grbs/lat_grbs/

¹⁰ <http://fermi.gsfc.nasa.gov/cgi-bin/ssc/LAT/LATDataQuery.cgi>

¹¹ <http://fermi.gsfc.nasa.gov/ssc/data/analysis/documentation/Cicerone/>

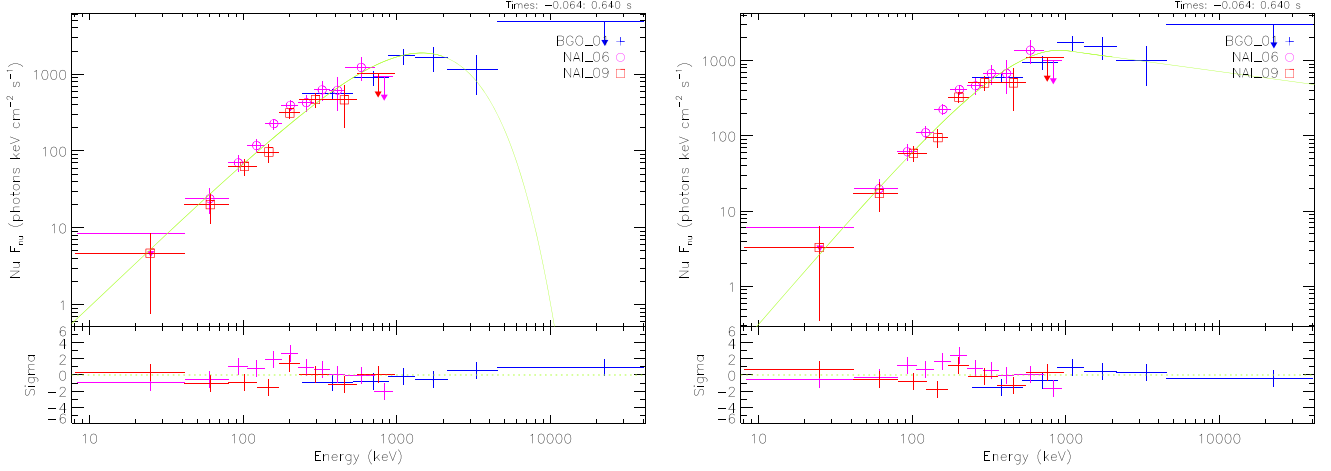


Figure 6. Combined NaI-n6, n9+BGO-b1 νF_ν spectra of GRB 140619B in the T_{90} time interval. The fit using the Compt spectral model is shown on the left, while the Band model fit is on the right.

Table 1
Summary of the Time-integrated (T_{90}) and Time-resolved (ΔT_1 and ΔT_2) Spectral Analyses

ΔT	Model	K (ph keV $^{-1}$ cm $^{-2}$ s $^{-1}$)	kT (keV)	E_p (keV)	α	β	F_{tot} (erg cm $^{-2}$ s $^{-1}$)	C-STAT/DOF
T_{90}	Compt	$(7.7 \pm 1.1) \times 10^{-3}$...	1456 ± 216	-0.09 ± 0.18	...	$(5.75 \pm 0.75) \times 10^{-6}$	365.09/346
	Band	$(7.8 \pm 1.3) \times 10^{-3}$...	908 ± 199	-0.38 ± 0.37	-2.28 ± 0.31	$(7.4 \pm 1.8) \times 10^{-6}$	362.56/345
ΔT_1	Compt	$(6.3 \pm 2.0) \times 10^{-3}$...	1601 ± 287	0.26 ± 0.32	...	$(9.4 \pm 1.6) \times 10^{-6}$	318.92/346
	BB	$(7.5 \pm 2.2) \times 10^{-8}$	324 ± 33	$(8.5 \pm 1.2) \times 10^{-6}$	323.86/347
ΔT_2	Compt	$(7.2 \pm 1.4) \times 10^{-3}$...	1283 ± 297	-0.11 ± 0.26	...	$(4.38 \pm 0.89) \times 10^{-6}$	391.65/346
	BB	$(3.8 \pm 1.1) \times 10^{-7}$	156 ± 15	$(2.33 \pm 0.28) \times 10^{-6}$	392.23/347

Note. In each column are listed, respectively, the time interval ΔT , the adopted spectral model, the normalization constant K of the fitting function, the BB temperature kT , the peak energy E_p , the low-energy α and high-energy β photon indexes, the total energy flux F_{tot} in the range 8 keV–40 MeV, and the value of the C-STAT over the number of degrees of freedom (dof).

$T_0 + 0.192$ s, is hereafter referred to as ΔT_1 , while the subsequent emission, from $T_0 + 0.192$ s to $T_0 + 0.640$ s, is designated by ΔT_2 .

In the ΔT_1 time interval, to identify the P-GRB, we have performed a spectral analysis by considering the BB and Compt spectral models. The spectra and the corresponding fits are shown in Figure 7 and the best fit parameters are listed in Table 1. As reported in Table 1, the Compt and the BB models are both viable. However, the value of the low-energy index of the Compt model in the ΔT_1 time interval, $\alpha = 0.26 \pm 0.32$, is consistent within three σ with $\alpha = 1$, which is the low energy index of a BB. We conclude that the BB model is an acceptable fit to the data and the best “physical model” of the ΔT_1 time interval and therefore identify it with the P-GRB emission. The corresponding observed temperature is $kT = (324 \pm 33)$ keV (see Table 1).

We then performed a spectral analysis on the time interval ΔT_2 to identify the prompt emission. We have again considered the Compt and BB spectral models (see Figure 8 and Table 1). By looking at Figure 8, it is immediately clear that the BB model does not adequately fit the data at energies larger than 1 MeV. Therefore the Compt model is favored. Its low-energy index, $\alpha = -0.11 \pm 0.26$, indicates that the spectral energy distribution in the ΔT_2 time interval is broader than that of the BB model. The Compt model is consistent with the spectral model adopted in the fireshell model and described in Patricelli et al. (2012) for the prompt emission.

In the next section we interpret the above data within the fireshell theoretical framework.

6. APPLICATION OF THE FIRESHLL MODEL TO GRB 140619B

After the P-GRB and the prompt emission identification, we have followed the same analysis described in Muccino et al. (2013) to determine the cosmological redshift, the baryon load and all the other physical quantities characterizing the plasma at the transparency point (see Figure 4). It is appropriate to underline that a remarkable difference between the long and the short GRBs is considered: the P-GRB emission in long GRBs represents on average the 1%–5% of the overall emission (see, e.g., the cases of GRB 970828, Ruffini et al. 2013, and GRB 090618, Izzo et al. 2012b), while in the cases of the short GRBs 090227B and 140619B (see Section 6.1), the P-GRB emissions represent $\sim 40\%$ of the overall observed fluence.

6.1. Redshift Estimate in Fireshell Model

From the observed P-GRB and total fluences, respectively, $S_{\text{BB}} = F_{\text{tot}}(\Delta T_1)\Delta T_1$ and $S_{\text{tot}} = F_{\text{tot}}(T_{90})T_{90}$ (see values in Table 1), we have estimated the ratio

$$\frac{E_{\text{P-GRB}}}{E_{e^-e^+}^{\text{tot}}} \approx \frac{4\pi d_l^2 S_{\text{BB}}/(1+z)}{4\pi d_l^2 S_{\text{tot}}/(1+z)} = \frac{S_{\text{BB}}}{S_{\text{tot}}} = (40.4 \pm 7.8)\%, \quad (1)$$

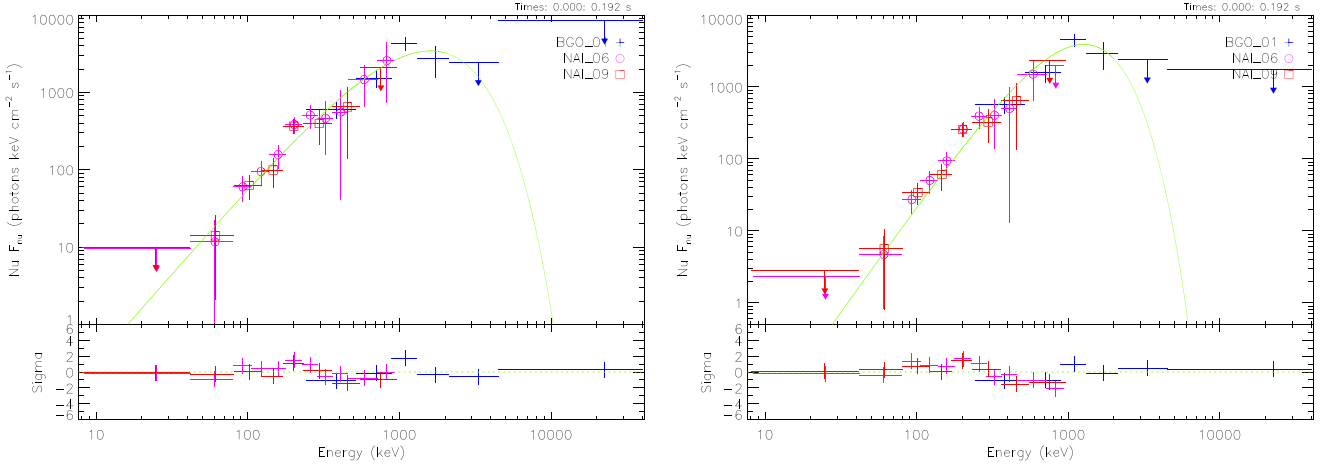


Figure 7. Same considerations as in Figure 6, in the ΔT_1 time interval, comparing Compt (left panel) and BB (right panel) models.

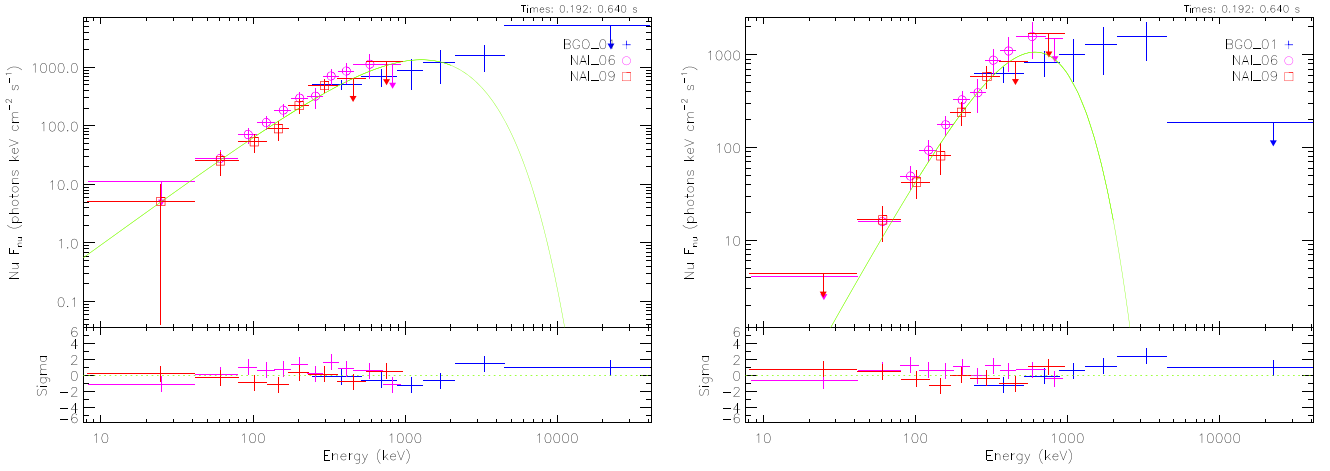


Figure 8. Same considerations as in Figure 6, in the ΔT_2 time interval, comparing Compt (left panel) and BB (right panel) models.

where the theoretically computed energy of the P-GRB, E_{P-GRB} , has been constrained by the observed thermal emission, E_{BB} , and we have imposed $E_{e^+e^-}^{\text{tot}} \equiv E_{\text{iso}}$. In Equation (1) the luminosity distance d_l and the redshift z of the source do not enter into the final computation.

From the last diagram in Figure 4, it is clear that for the value in Equation (1), we have different possible parameters ($E_{e^+e^-}^{\text{tot}}$, B) and for each of them we can determine the corresponding kT_{blue} (see the top diagram in Figure 4). Finally, from the ratio between kT_{blue} and the observed P-GRB temperature kT , we can estimate the redshift, i.e., $kT_{\text{blue}}/kT = (1+z)$. To obtain the correct value of z and then the right parameters $[E_{e^+e^-}^{\text{tot}}(z), B(z)]$, we have made use of the isotropic energy formula

$$E_{\text{iso}} = 4\pi d_l^2 \frac{S_{\text{tot}}}{(1+z)} \frac{\int_{1/(1+z)}^{10000/(1+z)} E N(E) dE}{\int_8^{40000} E N(E) dE}, \quad (2)$$

in which $N(E)$ is the photon spectrum of the burst and the integrals are due to the K -correction on S_{tot} (Schaefer 2007). From the initial constraint $E_{\text{iso}} \equiv E_{e^+e^-}^{\text{tot}}$, we have found $z = 2.67 \pm 0.37$, which leads to $B = (5.52 \pm 0.73) \times 10^{-5}$

and $E_{e^+e^-}^{\text{tot}} = (6.03 \pm 0.79) \times 10^{52}$ erg. All the quantities so determined are summarized in Table 2. The analogy with the prototypical source GRB 090227B, for which we have $E_{P-GRB} = (40.67 \pm 0.12)\% E_{e^+e^-}^{\text{tot}}$ and $B = (4.13 \pm 0.05) \times 10^{-5}$, is very striking (Muccino et al. 2013).

We now proceed with the analysis of the subsequent emission to derive the properties of the surrounding CBM.

6.2. Analysis of the Prompt Emission

Having determined the initial conditions for the fireshell, i.e., $E_{e^+e^-}^{\text{tot}} = 6.03 \times 10^{52}$ erg and $B = 5.52 \times 10^{-5}$, the dynamics of the system is uniquely established. In particular, we obtain the Lorentz factor at transparency, $\Gamma_{\text{tr}} = 1.08 \times 10^4$, and we can simulate the light curve and the spectrum of the prompt emission. To reproduce the pulses observed especially in the BGO-b1 light curve (see Figure 5) we have derived the radial distributions of the CBM number density and of the filling factor \mathcal{R} around the burst site (see Table 3 and Figure 9). The errors in the CBM number density and in \mathcal{R} are defined as the maximum possible variation of the parameters to guarantee agreement between the simulated light curve and the observed data. The final simulation of the BGO-b1 light curve (260 keV–40 MeV) is shown in Figure 10.

Table 2

The Results of the Simulation of GRB 090227B in the Fireshell Model

Fireshell Parameter	Value
$E_{e^+e^-}^{\text{tot}}$ (erg)	$(6.03 \pm 0.79) \times 10^{52}$
B	$(5.52 \pm 0.73) \times 10^{-5}$
Γ_{tr}	$(1.08 \pm 0.08) \times 10^4$
r_{tr} (cm)	$(9.36 \pm 0.42) \times 10^{12}$
kT_{blue} (keV)	$(1.08 \pm 0.08) \times 10^3$
z	2.67 ± 0.37
$\langle n_{\text{CBM}} \rangle$ (cm^{-3})	$(4.7 \pm 1.2) \times 10^{-5}$

Interestingly, the average CBM number density in GRB 140619B, $\langle n_{\text{CBM}} \rangle = (4.7 \pm 1.2) \times 10^{-5} \text{ cm}^{-3}$ (see Table 3), is very similar to that of the prototype GRB 090227B, $\langle n_{\text{CBM}} \rangle = (1.90 \pm 0.20) \times 10^{-5} \text{ cm}^{-3}$. In both the cases the CBM densities are typical of the galactic halo environment.

We turn now to the spectrum of the prompt emission using the spectral model described in Patricelli et al. (2012) with a phenomenological parameter $\alpha = -1.11$. From fitting the light curve in the energy range 260 keV–40 MeV, we have extended the simulation of the corresponding spectrum down to 8 keV to check overall agreement with the observed data. The final result is plotted in Figure 11, where the rebinned NaI-n6 and n9 and BGO-b1 data in the ΔT_2 time interval show their agreement with the simulation; the lower panel in Figure 11 shows the residuals of the data around the fireshell simulated spectrum.

The fireshell approach is different from the fireball one, where the sharp luminosity variations observed in the prompt emission are attributed to the prolonged and variable activity of the “inner engine” (see, e.g., Rees & Meszaros 1994; Ramirez-Ruiz & Fenimore 2000; Piran 2004).

In the fireshell model, the observed time variability of the prompt emission is produced by the interaction of the accelerated baryons of the fireshell with the CBM “clumps” (see, e.g., Ruffini et al. 2002, 2006; Patricelli et al. 2012). The issue of the time variability in GRB light curves has been long debated. Zhang et al. (2006) and Nakar & Granot (2007) indicated difficulties in producing short time variability from CBM inhomogeneities. The opposite point of view has been expressed by Dermer & Mitman (1999) and Dermer (2006, 2008). In the fireshell model it has been shown that, from the correct computation of the equations of motion of the shell, of the EQTS, and of the Lorentz factor (Bianco & Ruffini 2005a, 2005b, and Section 3), the short time scale variability of GRB light curves occurs in regimes with the larger values of the Lorentz factor, when the total visible area of the emission region is very small and “dispersion” in arrival time of the luminosity peaks is negligible. Therefore the short time scale variability indeed can be produced by the CBM inhomogeneities (see Section 3 in Patricelli et al. 2012). This has been verified in the present case of GRB 140619B, where the values of the Lorentz factor Γ and the total transversal size of the fireshell visible area d_v at the initial radius of the CBM cloud are explicitly indicated in Table 3. These values of d_v are smaller than the thickness of the inhomogeneities ($\Delta r \approx 10^{16}$ – 10^{17} cm) and fully justify the adopted spherical symmetry approximation (Ruffini et al. 2002, 2006; Patricelli et al. 2012). Consequently, a finer description of each substructure in the spikes observed in the light curve is not necessary and does not

change the substantial agreement of the model with the observational data, which is provided by the average densities and the filling factors in Table 3.

6.3. The Progenitor System

In analogy with the case of GRB 090227B (see, e.g., Muccino et al. 2013; Oliveira et al. 2014), we conclude that the progenitor of GRB 140619B is a NS–NS merger. As a lower limit, we have considered the simplest case by assuming two NSs with the same mass M_{NS} such that the total mass would be larger than the NS critical mass $M_{\text{crit}}^{\text{NS}}$, e.g., $2M_{\text{NS}} \gtrsim M_{\text{crit}}^{\text{NS}}$. This condition is clearly necessary for the formation of a BH and the consequent application of the fireshell model. It is also appropriate here to recall that only a subset of binary NSs mergers can fulfill this stringent requirement (see Figure 3). This will strongly affect the estimate of the rate of these family-2 short GRBs, when compared with the usual expected binary NS rate (see Section 9 and Conclusions).

Referring to the work of Belvedere et al. (2012) on nonrotating NSs in the global charge neutrality treatment with all the fundamental interactions taken into account properly, we have considered two NSs with mass $M_{\text{NS}} = 1.34 M_{\odot} = 0.5M_{\text{crit}}^{\text{NS}}$ and corresponding radius $R = 12.24$ km. As a working hypothesis we assume that in the NS merger the crustal material from both NSs contributes to the GRB baryon load, while the NS cores collapse to a BH. For each NS the crustal mass from the NL3 nuclear model is $M_c = 3.63 \times 10^{-5} M_{\odot}$, so the total NS merger crustal mass is $M_{2c} = 2M_c = 7.26 \times 10^{-5} M_{\odot}$. On the other hand, the baryonic mass engulfed by the e^+e^- plasma before transparency is $M_B = E_{e^+e^-}^{\text{tot}} B/c^2 = (1.86 \pm 0.35) \times 10^{-6} M_{\odot}$, so we can conclude that only a small fraction of the crustal mass contributes to the baryon load, namely $M_B = (2.56 \pm 0.48)\% M_{2c}$. This value is consistent with the global charge neutrality condition adopted in Belvedere et al. (2012). The usually adopted LCN condition leads instead to a crustal mass $M_c^{\text{LCN}} \sim 0.2 M_{\odot}$ (see, e.g., Belvedere et al. 2012; Oliveira et al. 2014), which would be inconsistent with the small value of the baryon load inferred above.

7. ON THE GWS EMISSION AND THE DETECTABILITY OR ABSENCE THEREOF

Following the previous work on GRB 090227B (Oliveira et al. 2014), we now estimate the emission of GWs of the binary NS progenitor of the short GRB 140619B using the effective-one-body (EOB) formalism (Buonanno & Damour 1999, 2000; Damour et al. 2000; Damour 2001; Damour & Nagar 2010) and assess the detectability of the emission by the Advanced LIGO interferometer.¹³ The EOB formalism maps the conservative dynamics of a binary system of nonspinning objects onto the geodesic dynamics of a single body of reduced mass $\mu = M_1 M_2 / M$, with total binary mass $M = M_1 + M_2$. The effective metric is a modified Schwarzschild metric with a rescaled radial coordinate, $r = c^2 r_{12} / (GM)$, where r_{12} is the distance between the two stars. The binary binding energy as a function of the orbital frequency Ω is given by $E_b(\Omega) = Mc^2 [\sqrt{1 + 2\nu(\hat{H}_{\text{eff}} - 1)} - 1]$, where the effective Hamiltonian $\hat{H}_{\text{eff}}^2 = A(u) + p_{\phi}^2 B(u)$ depends on the radial

¹³ <http://www.advancedligo.mit.edu>

Table 3
The Density and Filling Factor Masks of GRB 140619B

Cloud	Distance (cm)	$n_{\text{CBM}} \text{ (cm}^{-3}\text{)}$	\mathcal{R}	Γ	$d_v \text{ (cm)}$
1th	1.50×10^{15}	$(1.2 \pm 0.2) \times 10^{-5}$	$(2.8 \pm 0.3) \times 10^{-11}$	1.08×10^4	2.76×10^{11}
2nd	1.20×10^{17}	$(9.2 \pm 1.1) \times 10^{-6}$...	2.07×10^3	1.16×10^{14}
3rd	1.70×10^{17}	$(2.5 \pm 0.5) \times 10^{-4}$	$(3.5 \pm 0.6) \times 10^{-10}$	1.84×10^3	1.85×10^{14}

Note. In each column are listed, respectively, the CBM cloud, the corresponding initial radius away from the BH, the number density, the filling factor, the Lorentz factor, and the total transversal size of the fireshell visible area.

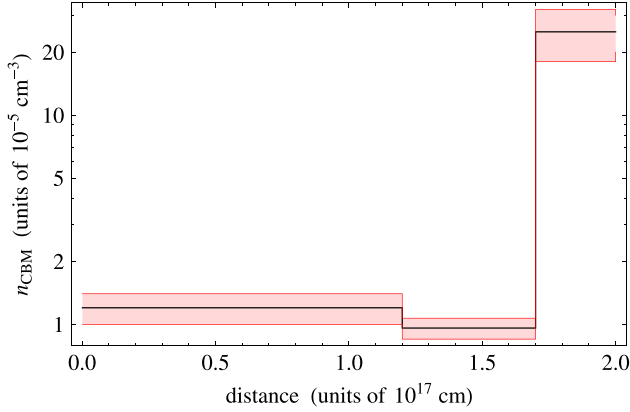


Figure 9. Radial CBM number density distribution of GRB 140619B (black line) and its range of validity (red shaded region).

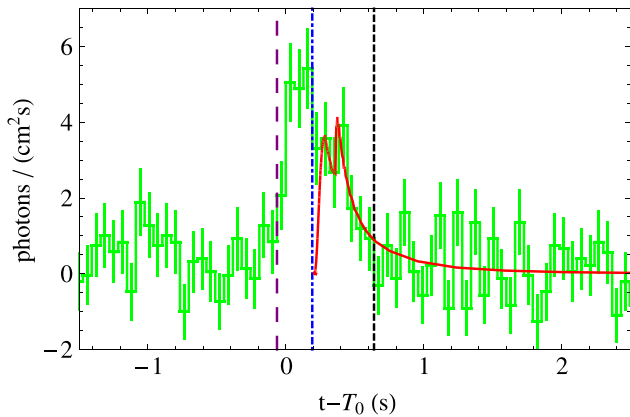


Figure 10. BGO-b1 (260 keV–40 MeV) simulated light curve of the prompt emission of GRB 140619B (solid red line). Each spike corresponds to the CBM number density profile described in Table 2 and Figure 9. The blue dotted-dashed vertical line marks the end of the P-GRB emission. The purple long-dashed and the black dashed vertical lines indicate, respectively, the starting and the ending times of the T_{90} time interval. Clearly visible outside of this time interval is the background noise level. The continuation of the simulation after T_{90} is due to the residual large angle emission of the EQTS (Bianco & Ruffini 2005a, 2005b) due to the density profile indicated in Table 3.

potential $A(u)$ of the variable $u = 1/r$ and $B(u) = u^2 A(u)$, while the angular momentum for the circular orbit is given by $p_\phi^2 = -A'(u)/[u^2 A(u)]'$, where a prime stands for the derivative with respect to u (see, e.g., Bini & Damour 2013 for further details). In order to obtain the derivative of the effective Hamiltonian \dot{H}_{eff} as a function of Ω , we must use the chain rule together with the relation $\Omega = \Omega(u)$ following from the angular

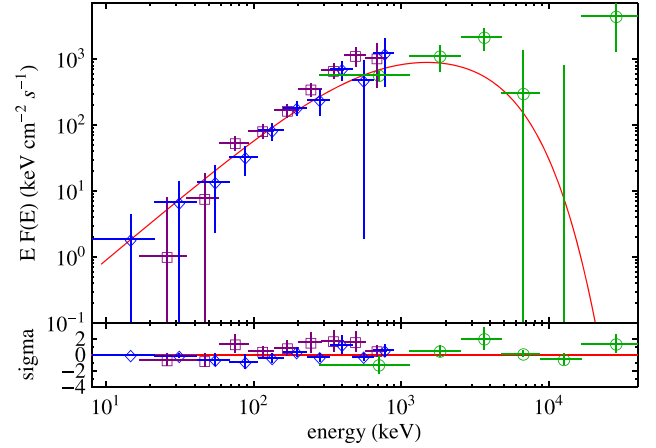


Figure 11. Top panel: comparison between the 8–900 keV data from the NaI-n6 (purple squares) and n9 (blue diamonds) detectors, and the 260 keV–40 MeV data from the BGO-b1 detector (green circles), and the simulation within the fireshell model (solid red curve) in the time interval ΔT_2 . Bottom panel: the residuals of the above mentioned data with the simulation.

Hamilton equation of motion in the circular case $GM\Omega(u) = (1/u)\partial H/\partial p_\phi = MA(u)p_\phi(u)u^2/(H\dot{H}_{\text{eff}})$, where G is the gravitational constant. Finally we obtain the rate of orbital energy loss through emission of GWs from the related derivative $dE_b/d\Omega$.

Using the well known matched filtering technique, we compute the signal-to-noise ratio (S/N) from the Fourier transform of the signal $h(t) = h_+ F_+ + h_\times F_\times$, where $h_{+, \times}$ are functions that depend on the direction and polarization of the source and $F_{+, \times}$ depend on the direction of the detector. By making an rms average over all possible source directions and wave polarizations, i.e., $\langle F_+^2 \rangle = \langle F_\times^2 \rangle = 1/5$, we obtain (see Flanagan & Hughes 1998 for details)

$$\langle (S/N)^2 \rangle = \int_{f_{\min}}^{f_{\max}} df_d \frac{h_c^2(f_d)}{5f_d^2 S_h^2(f_d)}, \quad (3)$$

where $S_h(f)$ is the strain noise spectral density (in units $1/\sqrt{\text{Hz}}$) of the interferometer. We have also introduced the characteristic GW amplitude, h_c , defined using the Fourier transform of the GW form $h(t)$, $h_c(f) = f|\tilde{h}(f)|$, and it is given by

$$h_c^2(f) = \frac{2(1+z)^2}{\pi^2 d_L^2} \frac{dE_b}{df} [(1+z)f_d], \quad (4)$$

with z the cosmological redshift, $f_d = f/(1+z)$ the GW frequency at the detector, $f = \Omega/\pi$ the frequency in the source frame, f_{\min} the minimal bandwidth frequency of the detector, and $f_{\max} = f_c/(1+z)$ the maximal bandwidth frequency,

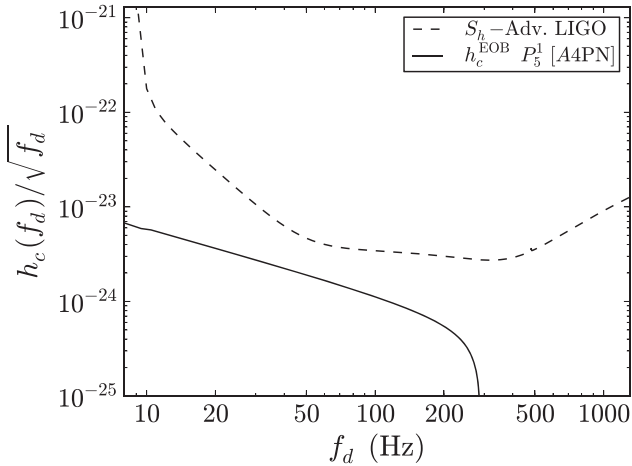


Figure 12. Sensitivity curve of Advanced LIGO $S_h(f)$ (dashed black curve) and the characteristic gravitational amplitude $h_c(f_d)/\sqrt{f_d}$ (solid black curve) of the binary NS progenitor of GRB 140619B, as a function of the frequency at the detector f_d . The EOB radial potential $A(u)$ was calculated using values for the coefficients in the 4th order post-Newtonian (PN) approximation and P_5^1 is the Padé approximant of order (1, 5).

where $f_c = \Omega_c/\pi$ is the binary contact frequency and d_L is the luminosity distance. In Figure 12 we show the strain-noise sensitivity of Advanced LIGO, $S_h(f)$, and the characteristic gravitational amplitude per square root frequency, $h_c(f_d)/\sqrt{f_d}$, both plotted as functions of the frequency at the detector f_d .

Following the above procedure we obtained for the short GRB 140619B a very low value $\langle S/N \rangle \approx 0.21$ compared to the value $S/N = 8$ needed for an optimal positive detection. The low value of the S/N is clearly due to the large cosmological distance to the source, $d \approx 21$ Gpc. Although the rms-averaged S/N we have computed might improve by a factor $\approx 5/2$ for an optimally located and polarized source (e.g. $\langle F_+^2 \rangle = 1$ and $\langle F_\times^2 \rangle = 0$) with an optimal face-on orbit ($\cos i = 1$), in the case of GRB 140619B it would increase only to a maximal value $S/N(\text{opt}) \approx 0.5$. From the dynamics of the system, we also find that this binary emits a total energy of $E_{\text{GW}}^T = 7.42 \times 10^{52}$ erg in gravitational radiation during the entire inspiral phase all the way up to the merger.

8. CONSIDERATIONS ON THE GEV EMISSION OF GRB 140619B

In addition to the analogies with GRB 090227B, GRB 140619B presents a novelty of special interest: a short-lived emission (~ 4 s) observed at energies $\gtrsim 0.1$ GeV. The light curve of this emission shows a rising part which peaks at ~ 2 s, followed by a decaying tail emission lasting another ~ 2 s in the observer frame (see Figure 13(b)). Since GRB 140619B was in the LAT FoV during the entire observational period, the absence of emission after ~ 4 s has been attributed to a cut-off intrinsic to the source. We divided the overall emission into four time intervals (see Figure 13(b)), each of them lasting 1 s. The corresponding spectra are best fit by power-law models. The total isotropic energy of the 0.1–100 GeV emission is $E_{\text{LAT}} = (2.34 \pm 0.91) \times 10^{52}$ erg.

In complete analogy with the GeV emission emitted in the binary-driven hypernovae (BdHNe), we attribute this high energy radiation to the newly formed BH. This identification is clearer here in view of the absence of a supernova (SN) and the

related constant power-law emission in X-rays, when measured in the cosmological rest-frame of the BdHN (Ruffini et al. 2014, 2015; Ruffini 2015b).

The presence of this GeV emission is not a peculiarity of GRB 140619B, but is a common feature of all these family-2 short GRBs. In line with this, the apparent absence of the GeV emission in GRB 090227B has already been discussed in Section 5: it can be explained simply by the fact that this source was outside the nominal LAT FoV. The significant detection in the LLE channel and the presence of only one transient-class event with energy above 100 MeV associated with the GRB (Ackermann et al. 2013) confirms that in optimal conditions the GeV emission from GRB 090227B should have been detected.

Now consider GRB 090510, which has the characteristics of the family-2 short GRBs ($E_{\text{iso}} > 10^{52}$ erg and $E_{p,i} > 2$ MeV), including the presence of a high energy GeV emission lasting $\sim 10^2$ s. This high energy emission continues up to the signal goes below the LAT threshold (Ackermann et al. 2013). The new feature of GRB 090510, among the family-2 short GRBs, is a well determined cosmological redshift inferred from the optical observations. The corresponding distance indeed coincides with the one theoretically predicted in the fireshell binary merger model (M. Muccino et al. 2015, in preparation).

In Figure 13(a) we compare and contrast the afterglows of the traditional low energetic short GRBs (see Berger 2014, for a review) with those of the family-2 short GRB 140619B (see Figure 13(b)) and GRB 090510 (see Figure 13(c)). In Figure 1 we show the evolution of the NS–NS merger generating a family-2 short GRB. In this system the conservation laws for total energy and the total angular momentum have to be satisfied during and following the binary NS merger (J. A. Rueda et al. 2015, in preparation). One of the most important issues is the determination of the dimensionless angular momentum $cJ/(GM^2)$ of the newly born BH (where J and M are, respectively, the BH spin angular momentum and mass). These considerations have been applied to GRB 090510 (M. Muccino et al. 2015, in preparation).

Before closing, we call attention to GRB 081024B, which we are currently addressing within the fireshell model (Y. Aimuratov et al. 2015, in preparation), and which shows all the typical features of the family-2 short GRBs, including a distinctive GeV emission. In conclusion, we can safely assert that all family-2 short GRBs, when the observational requirements are fulfilled, present a short-lived but very intense GeV emission, which in our interpretation originates from the newly formed BH.

In Table 4 we listed the redshift, $E_{p,i}$, E_{iso} , and the GeV isotropic emission energy E_{LAT} in the rest-frame energy band 0.1–100 GeV of the three family-2 short GRBs discussed here. In computing E_{iso} we have inserted the energy computed in the rest-frame energy band 1–10000 keV.

9. THE RATE OF FAMILY-2 SHORT GRBS

With the identification of three family-2 short GRBs, namely GRB 090227B and GRB 140619B, with theoretically inferred redshifts, and GRB 090510 with a measured redshift, all of them detected by the *Fermi* satellite, we are now in a position to give an estimate of the expected rate ρ_0 of such events. Following Soderberg et al. (2006) and Guetta & Della Valle (2007), for these sources we have computed the 1 s peak photon flux f_p in the energy band 1–1000 keV, which is 16.98

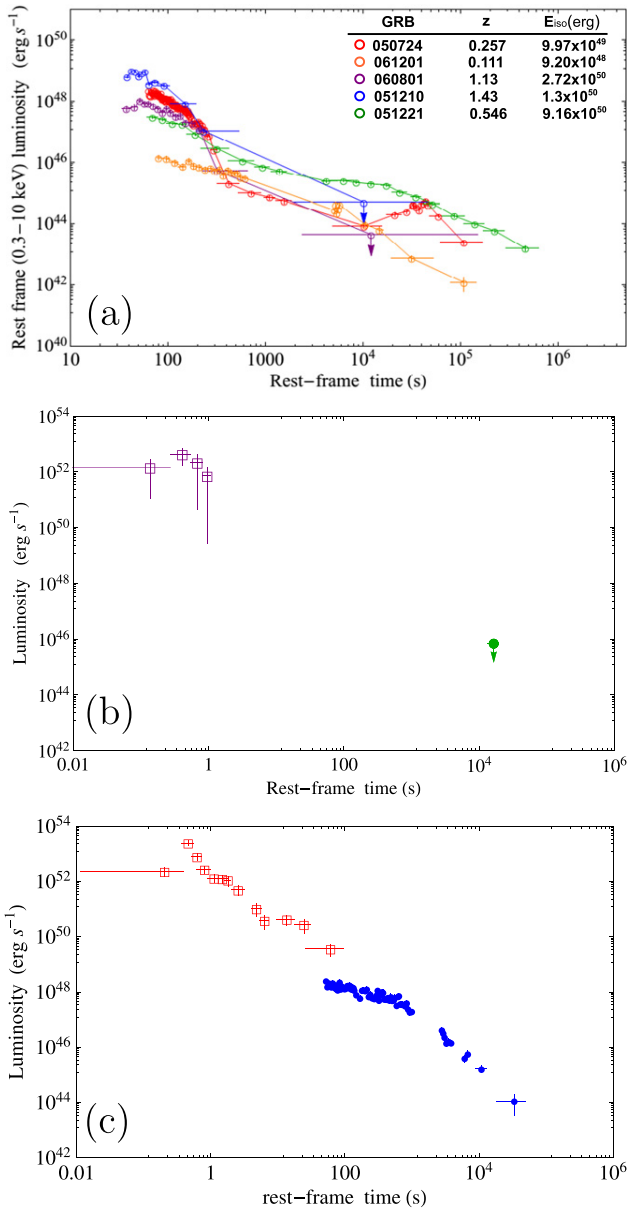


Figure 13. Top panel (a): the rebinned rest-frame 0.3–10 keV X-ray luminosities of weak short GRBs leading to massive NSs; the corresponding bursts, redshifts and energies are indicated in the legend. In their afterglows there is no regular power-law behavior at late times and no nesting (Ruffini et al. 2014). Middle panel (b): the short lived rest-frame 0.1–100 GeV isotropic luminosity light curve (purple squares) and the rest-frame 0.3–10 keV upper limit, as set from the analysis of GRB 140619B outlined in Section 3 (green circle). Bottom panel (c): the long lived rest-frame 0.1–100 GeV (red squares) and the rest-frame 0.3–10 keV (blue circles) isotropic luminosity light curves of GRB 090510.

photons $\text{cm}^{-2} \text{s}^{-1}$ for GRB 090227B, 9.10 photons $\text{cm}^{-2} \text{s}^{-1}$ for GRB 090510, and 4.97 photons $\text{cm}^{-2} \text{s}^{-1}$ for GRB 140619B. From the spectral parameters for each source, we have computed f_p for various redshifts until it coincided with the corresponding threshold peak flux f_T which is the limiting peak photon flux allowing burst detection (see the analysis in Band 2003 for details). In this way we have evaluated for each source the maximum redshift z_{max} at which the burst would have been detected and, then, the corresponding maximum comoving volume V_{max} . For GRB 140619B we

Table 4

The Redshift, the Rest-frame Peak Spectral Energy, the Isotropic Energy E_{iso} in the Rest-frame Energy Band 1–10000 keV, and the GeV Isotropic Emission energy E_{LAT} in the Rest-frame Energy Band 0.1–100 GeV of the Four family-2 Short GRBs Discussed Here

GRB	z	$E_{p,i}$ (MeV)	E_{iso} (10^{52} erg)	E_{LAT} (10^{52} erg)
081024B	>3.0	>8.2	>2.4	>2.7
090227B	1.61 ± 0.14	5.89 ± 0.30	28.3 ± 1.5	...
090510	0.903 ± 0.003	7.89 ± 0.76	3.95 ± 0.21	5.78 ± 0.60
140619B	2.67 ± 0.37	5.34 ± 0.79	6.03 ± 0.79	2.34 ± 0.91

Note. The values indicated for GRB 081024B will be Discussed in Y. Aimuraton et al. (2015, in preparation).

obtain $f_p \equiv f_T = 1.03$ photons $\text{cm}^{-2} \text{s}^{-1}$ at maximum redshift $z_{140619B}^{\text{max}} = 5.49$; for GRB 090227B, which is the brightest one, we find $f_p \equiv f_T = 1.68$ photons $\text{cm}^{-2} \text{s}^{-1}$ at a maximum redshift $z_{090227B}^{\text{max}} = 5.78$; finally, for GRB 090510, we get $f_p \equiv f_T = 1.96$ photons $\text{cm}^{-2} \text{s}^{-1}$ at a maximum redshift $z_{090510}^{\text{max}} = 2.25$. Correspondingly we have computed V_{max} .

The empirical rate can be evaluated as

$$\rho_0 = \left(\frac{\Omega_F}{4\pi} \right)^{-1} \frac{N}{V_{\text{max}} T_F}, \quad (5)$$

where $N = 3$ is the number of identified energetic NS–NS short bursts, $\Omega_F \approx 9.6$ sr is the average Fermi solid angle, and $T = 6$ years is the Fermi observational period. We infer a local rate of $\rho_0 = (2.6_{-1.9}^{+4.1}) \times 10^{-4} \text{ Gpc}^{-3} \text{ yr}^{-1}$, where the attached errors are determined from the 95% confidence level of the Poisson statistic (Gehrels 1986). At $z \geq 0.9$, the above inferred rate provides an expected number of events $N_{>} = 4_{-3}^{+6}$, which is consistent with the above three observed events during the Fermi observational period. Also at $z \leq 0.9$ our estimate $N_{<} = 0.2_{-0.14}^{+0.31}$ is consistent with the absence of any family-2 short GRB detection.

With the inclusion of GRB 081024B, with a theoretically estimated redshift $z > 3$ (more details will appear in Y. Aimuraton et al. 2015, in preparation), the above rate remains stable with smaller error bars, i.e., $\rho_0 = (2.1_{-1.4}^{+2.8}) \times 10^{-4} \text{ Gpc}^{-3} \text{ yr}^{-1}$. This inferred rate is different from that of the long GRBs, recently estimated to be $\rho_{\text{L-GRB}} = 1.3_{-0.6}^{+0.7} \text{ Gpc}^{-3} \text{ yr}^{-1}$ (Wanderman & Piran 2010), and also from the estimates of the family-1 short GRBs given in the literature (without a beaming correction $\rho_{\text{short}} = 1\text{--}10 \text{ Gpc}^{-3} \text{ yr}^{-1}$; see e.g., Berger 2014 and Clark et al. 2014).

Such a low rate can be explained based upon the existing data of binary NSs within our Galaxy (see Section 2). From Figure 3 we notice that only a subset of them has the sum of the masses of the components larger than the critical NS mass and can collapse to a BH in their merger process. Only this subset can lead to a family-2 short GRB.

10. THE FAMILY-2 SHORT GRBS AND THE $E_{p,i}$ – E_{ISO} RELATION FOR SHORT GRBS

Now we discuss some general considerations for the new $E_{p,i}$ – E_{iso} relation for short GRBs (Zhang et al. 2012; Calderone et al. 2015), with a power law similar to the one of the Amati

relation for long GRBs (Amati et al. 2008), but different amplitude. This yet unexplained difference discourages the use of the Amati relation as an astronomical tool. All four family-2 short GRBs satisfy this new $E_{p,i}-E_{\text{iso}}$ relation (see the quantities listed in Table 4). We call attention to the need to investigate the physical reasons for the validity of this universal $E_{p,i}-E_{\text{iso}}$ relation, which appears to be satisfied by family-1 short bursts, where the binary NS merger does not lead to BH formation, and also the family-2 short bursts, where BHs are formed and reveal their presence by giving rise to the short-lived but significant GeV emission.

11. CONCLUSIONS

In this article we have predicted the occurrence of two different kinds of short GRBs originating from binary NS mergers, based on

- (a) the analysis of GRB 090227B, the prototype of short bursts originating from a binary NS leading to BH formation (Muccino et al. 2013),
- (b) the recent progress in the determination of the mass–radius relation of NSs and the determination of their critical mass $M_{\text{crit}}^{\text{NS}} \approx 2.67 M_{\odot}$ (Rotondo et al. 2011; Rueda et al. 2011, 2014; Belvedere et al. 2012, 2014a, 2014b), and
- (c) the recently measured mass of PSR J0348+0432, $M = (2.01 \pm 0.04) M_{\odot}$ (Antoniadis et al. 2013), establishing an absolute lower limit on $M_{\text{crit}}^{\text{NS}}$, and the remarkable information gained from radio observations of binary NS systems in our own Galaxy (Zhang et al. 2011; Antoniadis 2014).

The first kind of short GRBs, which we call family-1, are the most common ones with $E_{\text{iso}} < 10^{52}$ erg and rest-frame spectral peak energy $E_{p,i} < 2$ MeV, originating from binary NS mergers with merged core mass smaller than $M_{\text{crit}}^{\text{NS}}$ and leading, therefore, to a massive NS, possibly with a companion. We identify these family-1 short bursts with the ones extensively quoted in literature (see, e.g., Berger 2014 for a review).

The second kind of short GRBs, which we call family-2, are those with $E_{\text{iso}} > 10^{52}$ erg and harder spectra with $E_{p,i} > 2$ MeV, originating from binary NS mergers with merged core mass larger than $M_{\text{crit}}^{\text{NS}}$. These family-2 short bursts satisfy the necessary condition to form a BH, following the example of the prototype GRB 090227B (Muccino et al. 2013).

The application of the fireshell model (Ruffini et al. 2001a, 2001b, 2001c) to the family-2 short GRB 140619B analyzed here has allowed the determination of the physical parameters of this source: the identification of the P-GRB emission in the early ~ 0.2 s of its light curve, the theoretical cosmological redshift of $z = 2.67 \pm 0.37$ and consequently the total burst energy $E_{e^+e^-}^{\text{tot}} = (6.03 \pm 0.79) \times 10^{52}$ erg, the baryon load $B = (5.52 \pm 0.73) \times 10^{-5}$, and a Lorentz Γ factor at transparency $\Gamma_{\text{tr}} = (1.08 \pm 0.08) \times 10^4$. The analysis of the prompt emission has also led to the determination of the CBM density, $\langle n_{\text{CBM}} \rangle = (4.7 \pm 1.2) \times 10^{-5} \text{ cm}^{-3}$, typical of the galactic halo environment, where NS–NS binaries migrate to, due to natal kicks imparted to them at birth (see, e.g., Narayan et al. 1992; Bloom et al. 1999; Fryer et al. 1999; Belczynski et al. 2006; Berger 2014), clearly supporting the binary NS merger hypothesis of this source. Unexpectedly, we have found the existence of a short-lived and

very intense GeV emission, just after the P-GRB occurrence and during and after the prompt emission phase, which has led us to conclude that this high energy emission originates from the newly formed BH.

While this article was being refereed, we have discovered three additional examples of these family-2 short bursts: GRB 081024B, GRB 090510, and GRB 090227B. These have given evidence that all these family-2 short bursts indeed show the existence of high energy emission, with the sole exception of GRB 090227B, which at the time of the observation was outside the nominal LAT FOV.

In summary we formulate some norms and theoretical predictions.

- (1) All family-1 short GRBs have an extended X-ray afterglow (see, e.g., Figure 13(a) and Berger 2014). When computed in the rest-frame 0.3–10 keV energy band they do not show any specific power-law behavior (Pisani et al. 2013) or the “nesting” properties (Ruffini et al. 2014) which have been discovered in some long GRBs. We predict that family-1 short GRBs, originating from a binary merger to a massive NS, should never exhibit high energy emission. The upper limit of 10^{52} erg can be simply understood in terms of a merger leading to a massive NS.
- (2) All family-2 short GRBs have been observed not to have prominent X-ray or optical afterglows. They all have short-lived but very energetic GeV emissions (see, e.g., Figures 13(b) and (c)), when LAT data are available. The upper limit of 10^{54} erg can be also simply understood in terms of a merger leading to BH formation.
- (3) The high energy emission episode in family-2 short GRBs always occurs at the end of the P-GRB emission, during and after the prompt emission phase. This fact uniquely links the high energy emission to the occurrence of the newly born BH. The prompt emission phase studied within the fireshell model has also allowed the determination of a large number of essential astrophysical parameters, both of the source (e.g., $E_{e^+e^-}^{\text{tot}}$ and B) and of the CBM (e.g., α , n_{CBM} , and \mathcal{R}).

It is interesting that the very simplified conditions encountered in the short GRBs in the absence of a SN event, which characterize the long GRBs (Ruffini et al. 2015), have allowed definite progress in understanding some fundamental GRB properties, e.g., the correlation of high energy emission to the BH formation. They can be adapted to the case of long GRBs. The points summarized above go a long way toward reaching a better understanding of family-1 and family-2 long GRBs (Ruffini et al. 2015), as well as of the BdHNe (Ruffini et al. 2014). We are confident that GRB 140619B is one of the best examples of short GRBs obtained with the current space technology. We sincerely hope that the results of our research will lead to new missions with greater collecting area and time resolution in X- and gamma-rays.

We thank the referee for requesting additional observational support for our theoretical fireshell binary merger model. This has motivated us to improve the connection of our theoretical work with the observations, resulting in this new version of the manuscript. We are especially grateful to S. Campana and C. L. Fryer for useful suggestions in improving some conceptual and observational arguments, and to L. Izzo for the detailed analysis of the high energy emission. M.E., M.K. and F.G.O.

are supported by the Erasmus Mundus Joint Doctorate Program by grant Nos. 2012-1710, 2013-1471, and 2012-1710, respectively, from the EACEA of the European Commission. A.V.P. and E.Z. acknowledge the support by the International Cooperation Program CAPES-ICRANet financed by CAPES-Brazilian Federal Agency for Support and Evaluation of Graduate Education within the Ministry of Education of Brazil. This work made use of data supplied by the UK *Swift* Science Data Centre at the University of Leicester.

REFERENCES

- Ackermann, M., Ajello, M., Asano, K., et al. 2013, *ApJS*, **209**, 11
- Aksenov, A. G., Ruffini, R., & Vereshchagin, G. V. 2007, *PhRvL*, **99**, 125003
- Amati, L., Guidorzi, C., Frontera, F., et al. 2008, *MNRAS*, **391**, 577
- Antoniadis, J. 2015, in *Gravitational Wave Astrophysics*, ed. C. F. Sopuerta (Cham, Switzerland: Springer International Publishing), 1
- Antoniadis, J., Freire, P. C. C., Wex, N., et al. 2013, *Sci*, **340**, 448
- Band, D., Matteson, J., Ford, L., et al. 1993, *ApJ*, **413**, 281
- Band, D. L. 2003, *ApJ*, **588**, 945
- Belczynski, K., Perna, R., Bulik, T., et al. 2006, *ApJ*, **648**, 1110
- Belvedere, R., Boshkayev, K., Rueda, J. A., & Ruffini, R. 2014a, *NuPhA*, **921**, 33
- Belvedere, R., Pugliese, D., Rueda, J. A., Ruffini, R., & Xue, S.-S. 2012, *NuPhA*, **883**, 1
- Belvedere, R., Rueda, J. A., & Ruffini, R. 2014b, *JKPS*, **65**, 897
- Berger, E. 2011, *NewAR*, **55**, 1
- Berger, E. 2014, *ARA&A*, **52**, 43
- Bianco, C. L., & Ruffini, R. 2005a, *ApJL*, **633**, L13
- Bianco, C. L., & Ruffini, R. 2005b, *ApJL*, **620**, L23
- Bini, D., & Damour, T. 2013, *PhRvD*, **87**, 121501
- Bloom, J. S., Prochaska, J. X., Pooley, D., et al. 2006, *ApJ*, **638**, 354
- Bloom, J. S., Sigurdsson, S., & Pols, O. R. 1999, *MNRAS*, **305**, 763
- Boguta, J., & Bodmer, A. R. 1977, *NuPhA*, **292**, 413
- Buonanno, A., & Damour, T. 1999, *PhRvD*, **59**, 084006
- Buonanno, A., & Damour, T. 2000, *PhRvD*, **62**, 064015
- Burrows, D., Hill, J., Nousek, J., et al. 2005, *SSRv*, **120**, 165
- Calderone, G., Ghirlanda, G., Ghisellini, G., et al. 2015, *MNRAS*, **448**, 403
- Cherubini, C., Geralico, A., J. A. Rueda, H., & Ruffini, R. 2009, *PhRvD*, **79**, 124002
- Cipolletta, F., Cherubini, C., Filippi, S., Rueda, J. A., & Ruffini, R. 2015, *PhRvD*, submitted (arXiv:1506.05926)
- Clark, J., Evans, H., Fairhurst, S., et al. 2014, arXiv:1409.8149
- Connaughton, V., Zhang, B.-B., Fitzpatrick, G., & Roberts, O. 2014, *GCN*, 16419, 1
- Damour, T. 2001, *PhRvD*, **64**, 124013
- Damour, T., Jaranowski, P., & Schäfer, G. 2000, *PhRvD*, **62**, 084011
- Damour, T., & Nagar, A. 2010, *PhRvD*, **81**, 084016
- Damour, T., & Ruffini, R. 1975, *PhRvL*, **35**, 463
- Deneva, J. S., Freire, P. C. C., Cordes, J. M., et al. 2012, *ApJ*, **757**, 89
- Dermer, C. D. 2006, *NCimB*, **121**, 1331
- Dermer, C. D. 2008, *ApJ*, **684**, 430
- Dermer, C. D., & Mitman, K. E. 1999, *ApJL*, **513**, L5
- Dezalay, J.-P., Barat, C., Talon, R., et al. 1992, AIP Conf. Ser. 265, ed. W. S. Paciesas & G. J. Fishman (Melville, NY: AIP), 304
- Eichler, D., Livio, M., Piran, T., & Schramm, D. N. 1989, *Natur*, **340**, 126
- Flanagan, É. É., & Hughes, S. A. 1998, *PhRvD*, **57**, 4535
- Fong, W., Berger, E., & Fox, D. B. 2010, *ApJ*, **708**, 9
- Fryer, C. L., Belczynski, K., Ramirez-Ruiz, E., et al. 2015, *ApJ*, submitted (arXiv:1504.07605)
- Fryer, C. L., Rueda, J. A., & Ruffini, R. 2014, *ApJL*, **793**, L36
- Fryer, C. L., Woosley, S. E., & Hartmann, D. H. 1999, *ApJ*, **526**, 152
- Gehrels, N. 1986, *ApJ*, **303**, 336
- Goodman, J. 1986, *ApJL*, **308**, L47
- Guetta, D., & Della Valle, M. 2007, *ApJL*, **657**, L73
- Haensel, P., Potekhin, A. Y., & Yakovlev, D. G. (ed.) 2007, *Astrophysics and Space Science Library 326, Neutron Stars 1: Equation of State and Structure* (New York: Springer)
- Han, W.-B., Ruffini, R., & Xue, S.-S. 2012, *PhRvD*, **86**, 084004
- Iwakiri, W., Tashiro, M., Terada, Y., et al. 2014, *GCN*, 16457, 1
- Izzo, L., Bernardini, M. G., Bianco, C. L., et al. 2010, *JKPS*, **57-3**, 551
- Izzo, L., Rueda, J. A., & Ruffini, R. 2012a, *A&A*, **548**, L5
- Izzo, L., Ruffini, R., Penacchioni, A. V., et al. 2012b, *A&A*, **543**, A10
- Klebesadel, R. W. 1992, in *Gamma-Ray Bursts—Observations, Analyses and Theories*, ed. C. Ho, R. I. Epstein, & E. E. Fenimore (Cambridge: Cambridge Univ. Press)
- Kocevski, D., Longo, F., Vianello, G., et al. 2014, *GCN*, 16421, 1
- Kopač, D., D'Avanzo, P., Melandri, A., et al. 2012, *MNRAS*, **424**, 2392
- Kouveliotou, C., Meegan, C. A., Fishman, G. J., et al. 1993, *ApJL*, **413**, L101
- Kramer, M. 2014, *IJMPD*, **23**, 30004
- Lattimer, J. M. 2012, *ARNPS*, **62**, 485
- Lawrence, S., Tervala, J. G., Bedaque, P. F., & Miller, M. C. 2015, *ApJ*, in press (arXiv:1505.00231)
- Lee, W. H., Ramirez-Ruiz, E., & Page, D. 2004, *ApJL*, **608**, L5
- Maselli, A., & D'Avanzo, P. 2014, *GCN*, 16424, 1
- Meegan, C., Lichti, G., Bhat, P. N., et al. 2009, *ApJ*, **702**, 791
- Meszáros, P. 2006, *RPPH*, **69**, 2259
- Meszáros, P., & Rees, M. J. 1997, *ApJL*, **482**, L29
- Muccino, M., Ruffini, R., Bianco, C. L., Izzo, L., & Penacchioni, A. V. 2013, *ApJ*, **763**, 125
- Nakar, E., & Granot, J. 2007, *MNRAS*, **380**, 1744
- Narayan, R., Paczynski, B., & Piran, T. 1992, *ApJL*, **395**, L83
- Narayan, R., Piran, T., & Shemi, A. 1991, *ApJL*, **379**, L17
- Oliveira, F. G., Rueda, J. A., & Ruffini, R. 2014, *ApJ*, **787**, 150
- Paczynski, B. 1986, *ApJL*, **308**, L43
- Patricelli, B., Bernardini, M. G., Bianco, C. L., et al. 2012, *ApJ*, **756**, 16
- Piran, T. 2004, *RvMP*, **76**, 1143
- Piran, T. 2005, *RvMP*, **76**, 1143
- Pisani, G. B., Izzo, L., Ruffini, R., et al. 2013, *A&A*, **552**, L5
- Preparata, G., Ruffini, R., & Xue, S. 1998, *A&A*, **338**, L87
- Ramirez-Ruiz, E., & Fenimore, E. E. 2000, *ApJ*, **539**, 712
- Rees, M. J., & Meszáros, P. 1994, *ApJL*, **430**, L93
- Rhoades, C. E., & Ruffini, R. 1974, *PhRvL*, **32**, 324
- Rosswog, S., Ramirez-Ruiz, E., & Davies, M. B. 2003, *MNRAS*, **345**, 1077
- Rotondo, M., Rueda, J. A., Ruffini, R., & Xue, S.-S. 2011, *PhLB*, **701**, 667
- Rueda, J. A., & Ruffini, R. 2012, *ApJL*, **758**, L7
- Rueda, J. A., Ruffini, R., Wu, Y.-B., & Xue, S.-S. 2014, *PhRvC*, **89**, 035804
- Rueda, J. A., Ruffini, R., & Xue, S.-S. 2011, *NuPhA*, **872**, 286
- Ruffini, R. 2009, in *The Kerr Spacetime*, ed. D. L. Wiltshire, M. Visser, & S. Scott (Cambridge: Cambridge Univ. Press)
- Ruffini, R. 2015a, ARep, in press
- Ruffini, R. 2015b, Proc. of the 2nd Cesar Lattes Meeting, ed. U. Barres de Almeida et al., in press
- Ruffini, R., Aksenov, A. G., Bernardini, M. G., et al. 2009, AIP Conf. Ser. 1132, ed. M. Novello & S. Perez (Melville, NY: AIP), 199
- Ruffini, R., Bernardini, M. G., Bianco, C. L., et al. 2005, AIP Conf. Ser. 782, Xlth Brazilian School of Cosmology and Gravitation, ed. M. Novello & S. E. Perez Bergliaffa (Melville, NY: AIP), 42
- Ruffini, R., Bernardini, M. G., Bianco, C. L., et al. 2006, AIP Conf. Ser. 836, Gamma-Ray Bursts in the Swift Era, ed. S. S. Holt, N. Gehrels & J. A. Nousek (Melville, NY: AIP), 103
- Ruffini, R., Bianco, C. L., Chardonnet, P., Frascchetti, F., & Xue, S. 2002, *ApJL*, **581**, L19
- Ruffini, R., Bianco, C. L., Frascchetti, F., Xue, S.-S., & Chardonnet, P. 2001a, *ApJL*, **555**, L117
- Ruffini, R., Bianco, C. L., Frascchetti, F., Xue, S.-S., & Chardonnet, P. 2001b, *ApJL*, **555**, L113
- Ruffini, R., Bianco, C. L., Frascchetti, F., Xue, S.-S., & Chardonnet, P. 2001c, *ApJL*, **555**, L107
- Ruffini, R., Bianco, C. L., Xue, S.-S., et al. 2004, *IJMPD*, **13**, 843
- Ruffini, R., Izzo, L., Muccino, M., et al. 2013, ARep, submitted (arXiv:1311.7432)
- Ruffini, R., Muccino, M., Bianco, C. L., et al. 2014, *A&A*, **565**, L10
- Ruffini, R., Salmonson, J. D., Wilson, J. R., & Xue, S. 2000, *A&A*, **359**, 855
- Ruffini, R., Salmonson, J. D., Wilson, J. R., & Xue, S.-S. 1999, *A&A*, **350**, 334
- Ruffini, R., Vereshchagin, G., & Xue, S.-S. 2010, *PhR*, **487**, 1
- Ruffini, R., Wang, Y., Enderli, M., et al. 2015, *ApJ*, **798**, 10
- Ruffini, R., & Xue, S.-S. 2008, AIP Conf. Ser. 1059, ed. D.-S. Lee & W. Lee (Melville, NY: AIP), 72
- Ruffini, R., & Xue, S.-S. 2013, *PhLA*, **377**, 2450
- Sahu, K. C., Livio, M., Petro, L., et al. 1997, *Natur*, **387**, 476
- Salmonson, J. D., & Wilson, J. R. 2002, *ApJ*, **578**, 310
- Sari, R., Piran, T., & Narayan, R. 1998, *ApJL*, **497**, L17
- Schaefer, B. E. 2007, *ApJ*, **660**, 16
- Soderberg, A. M., Kulkarni, S. R., Nakar, E., et al. 2006, *Natur*, **442**, 1014
- Tavani, M. 1998, *ApJL*, **497**, L21
- Troja, E., King, A. R., O'Brien, P. T., Lyons, N., & Cusumano, G. 2008, *MNRAS*, **385**, L10
- van Paradijs, J., Groot, P. J., Galama, T., et al. 1997, *Natur*, **386**, 686
- Wanderman, D., & Piran, T. 2010, *MNRAS*, **406**, 1944
- Zhang, B., Fan, Y. Z., Dyks, J., et al. 2006, *ApJ*, **642**, 354
- Zhang, C. M., Wang, J., Zhao, Y. H., et al. 2011, *A&A*, **527**, A83
- Zhang, F.-W., Shao, L., Yan, J.-Z., & Wei, D.-M. 2012, *ApJ*, **750**, 88

Induced gravitational collapse in FeCO Core–Neutron star binaries and Neutron star–Neutron star binary mergers

R. Ruffini,^{1,2,3,4,5,*} Y. Aimuratov,^{1,5} C. L. Bianco,^{1,2} M. Enderli,^{1,5}
M. Kovacevic,^{1,5} R. Moradi,^{1,5} M. Muccino,¹ A. V. Penacchioni,^{3,4}
G. B. Pisani,¹ J. A. Rueda^{1,2} and Y. Wang^{1,2,†}

¹*Dip. di Fisica, Sapienza University of Rome and ICRA,
Piazzale Aldo Moro 5, I-00185, Rome, Italy*

²*ICRANet, Piazzale della Repubblica 10, I-65122 Pescara, Italy*

³*ICRANet, Centro Brasileiro de Pesquisas Fisicas,
rua Dr. Xavier Sigaud 150, 22290-180, Rio de Janeiro, Brazil*

⁴*ICRANet, Av dos Astronautas 1758 Jd. Granja BR S José dos Campos,
SP 12227-010, Brazil*

⁵*Université de Nice Sophie Antipolis, Nice,
CEDEX 2 Grand Château Parc Valrose, France*

**ruffini@icra.it*

†*yu.wang@icranet.org*

Published 19 October 2015

We review the recent progress in understanding the nature of gamma-ray bursts (GRBs). The occurrence of GRB is explained by the Induced Gravitational Collapse (IGC) in FeCO Core–Neutron star binaries and Neutron star–Neutron star binary mergers, both processes occur within binary system progenitors. Making use of this most unexpected new paradigm, with the fundamental implications by the neutron star (NS) critical mass, we find that different initial configurations of binary systems lead to different GRB families with specific new physical predictions confirmed by observations.

Keywords: Black hole; supernova; gamma ray burst.

1. Introduction

Supernovae (SNe) have been known and studied for a long time, from 1054 A.D. to the classic work of Baade and Zwicky in 1934,^{1–3} to the discovery of pulsar in 1967,⁴ leading the identification of the first NS in the Crab nebula originated from the SN phenomenon. It has become clear that a NS has harbored for thousands of years inside that SN remnant, and the main energetics of the SN is from the loss of NS rotational energy.

Observations of GRBs date from the detection by the Vela satellites in the early 1970s, see e.g. in Ref. 5. Just after the announcement of GRBs, out of first principle, we indicated in Ref. 6 that GRBs could originate in the process of gravitational

collapse, leading to the birth of a black hole (BH), and we theoretically predicted consequently have energetics of the order of $10^{54} (M_{BH}/M_{\odot})$ erg, namely equivalent to the release of $\sim M_{\odot}c^2$ in few tens of seconds, here M_{BH} is the mass of BH and M_{\odot} is the solar mass.

It has only been after the observations by the Beppo-Sax satellite and the optical identification of GRBs that their enormous energetics, 10^3 – 10^4 times larger than those of SNe, have been confirmed and they coincide the theoretical prediction made on the ground of the BH mass-energy formula.⁶

From these premises, it was introduced the basic paradigm, see e.g. in Ref. 7 and the references there in, that the SN originated from the formation of a NS, and a GRB originated from the formation of a BH. These two astrophysical systems conceptually have consequently been assumed to be member of two conceptually distinct families.

This situation has become even more intricate and interesting after the unexpected observation of a temporal coincidence between the emission of a GRB and a SN, see e.g. GRB 980425⁸ and SN 1998bw.⁹ The explanation of this coincidence has gradually led from GRBs and SNe been traditionally considered as a single star event to a much more rich and complex comic many-body interaction and therefore to the introduction of a cosmic matrix: C-matrix. This totally unprecedented situation has led to the opening of a new understanding of a vast number of unknown domains of physics and astrophysics.

1.1. *Crab nebula — Supernova as prove of the existence of neutron star*

Of all the objects in the sky, none has been richer than the Crab nebula in results for physics, astronomy and astrophysics. Although a result of the 1054 A.D. SN observed by Chinese, Japanese and Korean astronomers, the nebula itself was not identified till 1731, and not associated with that SN until the last century, but it has been of interest to astronomers, and later astrophysicists and theoretical physicists ever since, even very recently, see e.g. the discovery by Agile of the giant flare discovered in September 2010.¹⁰ It was only in 1968 that a rotational pulsar was discovered at its center following the predicted existence of rapidly rotating NSs by John Wheeler. This is a absolutely first for the field for astronomy and astrophysics: in that decade hundreds of neutron stars observed as pulsars.

Independently from these successes, there still remains to explain an outstanding physical process needed to model this object: the expulsion of the shell of the SN remnant during the process of gravitational collapse to a NS. We are currently gaining some understanding of the physical processes governing NSs, motivated by the research on GRBs and BH formation which is being fully exploited to this end at the present time. The understanding of BH formation and consequently of the emission of GRBs is likely to lead, in this Faustian effort to learn the laws of nature, to the understanding of the process of NS formation and the expulsion of the remnant in the SN explosion.

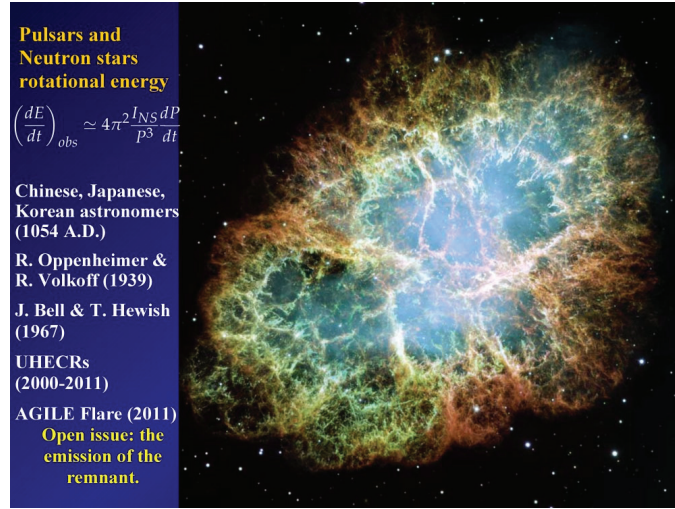


Fig. 1. Hubble Space Telescope photograph (2005) of the Crab Nebula.

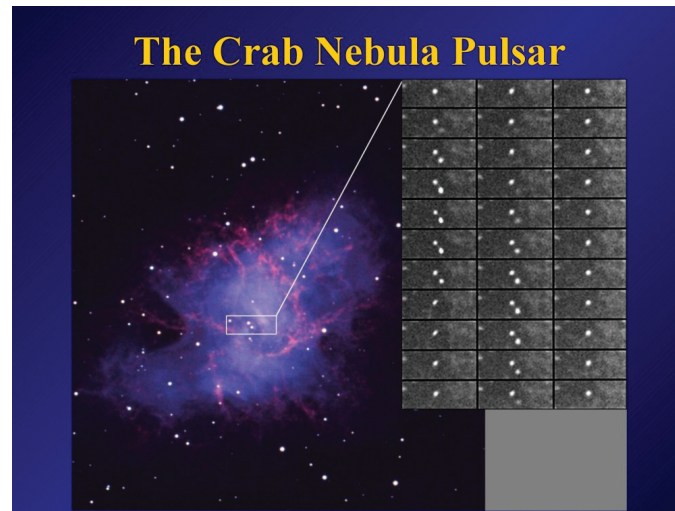


Fig. 2. The sequence of black and white images on the right is separated by one millisecond intervals, from which it is clear that the left star is a pulsar with a period of $P = 33$ milliseconds. This period changes with a rate dP/dt of 12.5 microseconds per year. The fact that the loss of rotational energy of a NS star with moment of inertia I is given by $dE/dt \propto -I(1/P^3)dP/dt$ explains precisely the energetics of the pulsar and proves at once the existence of NSs.¹¹

That NSs exist in nature has been proven by the direct observation of pulsars. The year 1967 marked the discovery of the first pulsar, observed at radio wavelengths in November 28, 1967 by Jocelyn Bell Burnell and Antony Hewish.⁴ Just a few months later, the pulsar NP0532 was found in the Crab Nebula (see Fig. 1) and observed first at radio wavelengths and soon after at optical wavelengths (see Fig. 2).

The discovery of NSs led our small group working around John Wheeler in Princeton (see Fig. 3), to go one step further and to direct our main attention to the study of a even more extreme phenomenon: the continuous gravitational collapse of a core with mass later than the critical NS mass introduced by Oppenheimer

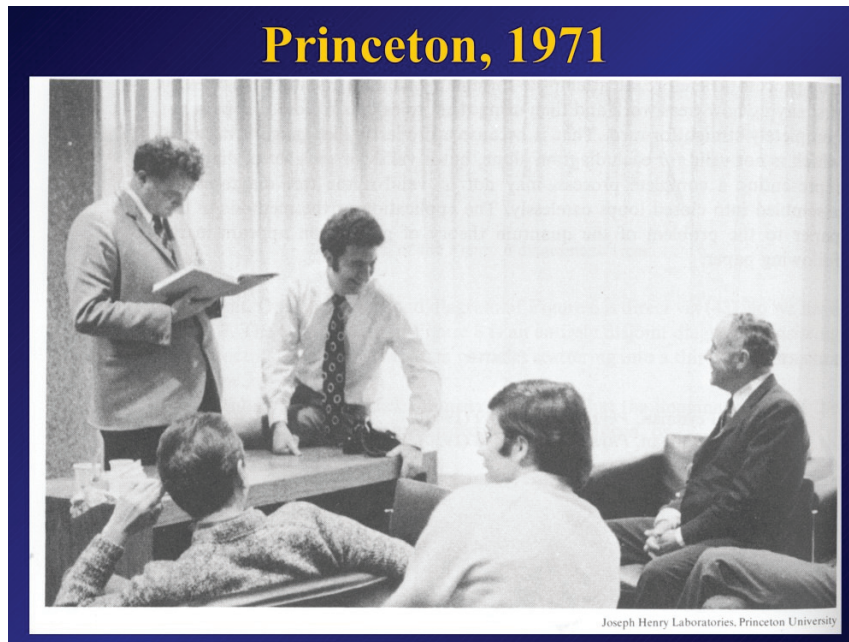


Fig. 3. Standing to the left T. Regge, sitting on the desk R. Ruffini and sitting on the chair J. A. Wheeler.

and his students. This soon led to the celebrated articles “Introducing the Black Hole” by J. A. Wheeler and R. Ruffini.¹² The work in Princeton addressed the topic of BHs, gravitational waves (GWs) and cosmology. A summary of that work can be found in Ref. 13, where a vast number of topics considered for the first time of relativistic astrophysics was reconsidered, including the cross-sections of GW detectors, the possible sources of GWs and especially, an entirely new family of phenomena occurring around BHs.

1.2. *The BH mass-energy formula*

A most important result in understanding the physics and astrophysics of BHs has been the formulation of the BH mass-energy formula. From this formula, indeed, it became clear that up to 50% of the mass-energy of a BH could be extracted by using reversible transformations.¹⁴ It then followed that during the formation of a BH, some of the most energetic processes in the universe could exist, releasing an energy of the order of $\sim 10^{54}$ erg for a few solar masses BH.

1.3. *VELA satellites and GRBs*

In Ref. 15 I described how the observations of the Vela satellites were fundamental in discovering GRBs, see Fig. 4. Initially it was difficult to model GRBs to understand their nature since their distance from the earth was unknown, and their energetics is consequently undefined. Thousands of models were presented, see e.g. in Ref. 16, attempting to explain their nature which was a profound mystery. Just a few months after the public announcement of their discovery,⁵ T. Damour, a collaborator at

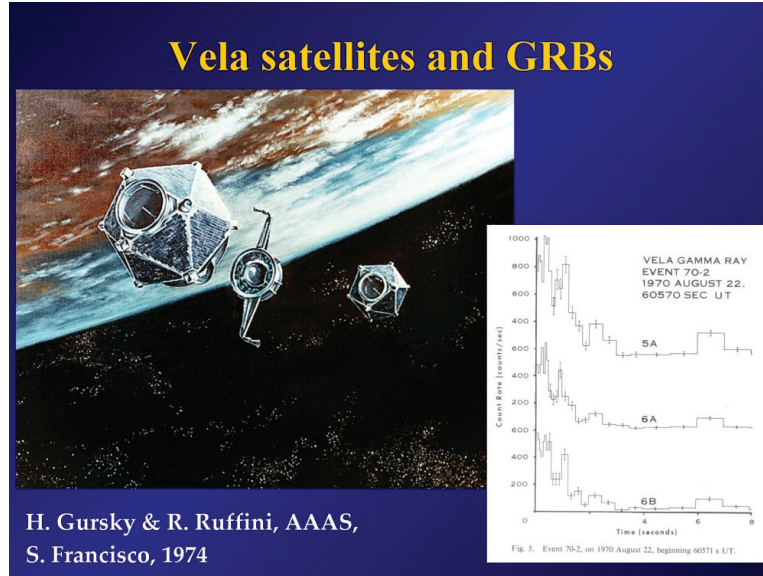


Fig. 4. The Vela satellites, see e.g. the I. Strong’s chapter in Ref. 5.

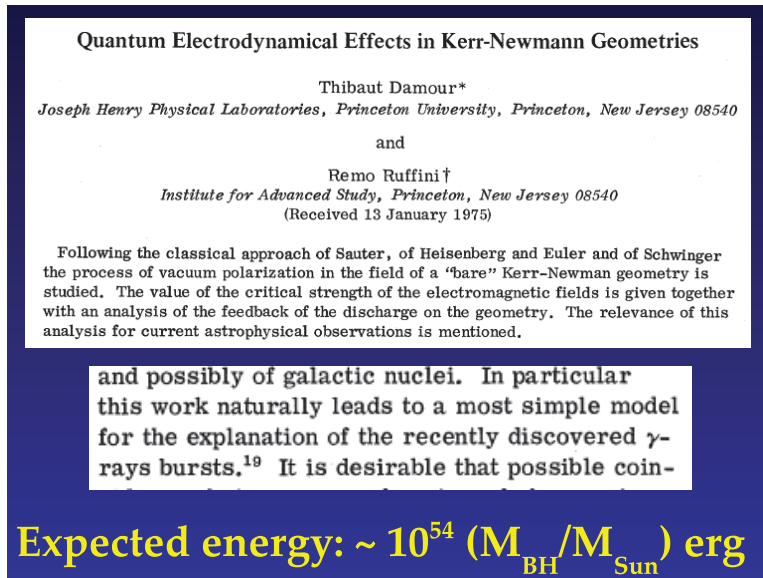


Fig. 5. The classic paper Ref. 6 by Damour and Ruffini on the extractable energy of a Kerr–Newman BH through vacuum polarization.

Princeton, and I formulated a theoretical model based on the extractable energy of a Kerr–Newmann BH through a vacuum polarization process as the origin of GRBs, see Fig. 5. In our paper,⁶ we pointed out that vacuum polarization occurring in the field of electromagnetic in Kerr–Newman BHs could release a vast e^+e^- plasma which self-accelerates and gives origin to the GRB phenomenon. Energetics for GRBs all the way up to $\sim 10^{55}$ ergs where theoretically predicted for a $10M_{\odot}$ BH. The dynamics of this e^-e^+ plasma was first studied by J. R. Wilson and myself with the collaboration of S.-S. Xue and J. D. Salmonson.^{17,18}

2. Classification of Short and Long GRBs

The launching of the Compton satellite with the BATSE detectors on-board led to important discoveries: the homogeneous distribution of GRBs in the universe and the classification of short-duration GRB with $T_{90} < 2$ second and long-duration GRB with $T_{90} > 2$ second, T_{90} means the duration containing 90% of total energy in the observer's frame.

The crucial contribution to understand the nature of GRBs came from the Beppo-Sax satellite which led to a more precise definition of their positions in the sky obtained using a wide field X-ray camera and a narrow field instrumentation. This enabled the optical identification of GRBs and the determination of their cosmological redshift, and consequently of their energetics, which turned out to be up to $\sim 10^{55}$ erg, precisely the value predicted by Damour and Ruffini in Ref. 6. Since that time no fewer than ten different X- and γ -ray observatory missions and numerous observations at optical and radio wavelengths on the ground have allowed us to reach unprecedented amount of high quality observational data and consequently a deeper understanding of the nature of GRBs.

The observational classification based on T_{90} reflects the GRB's central engine. In the single core collapse model, the progenitor of long GRB is a massive star which collapses to a black hole. The short GRB is due to the merger of two compact objects (NS–NS or NS–black hole). In the IGC model of long GRBs, the progenitor is a very special binary system. We will also show that both long and short GRBs have two distinct binary progenitors, see Sec. 3.

Many previous articles, e.g. Refs. 19–21, simply plot the histograms of T_{90} using the observed T_{90} . Two Gaussian distributions depicting short and long GRBs are obtained. We here plot our T_{90} histogram, shown in Fig. 6, with three improvements: (1) If one wants to compare the physics of GRBs, observer's frame cannot tell the

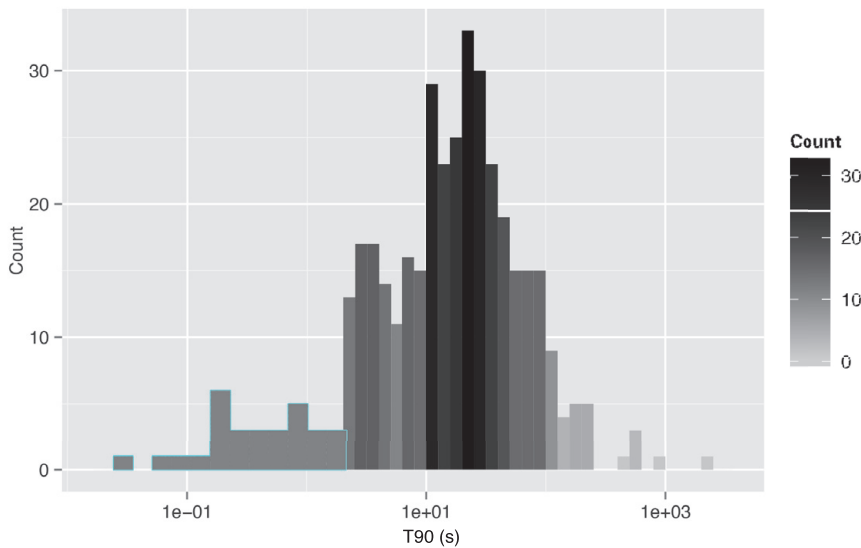


Fig. 6. T_{90} of GRBs with known redshift, blue frame contains short bursts with $T_{90} < 2$.

real T_{90} duration since GRBs are cosmological events with different redshift, we only consider those GRBs with known redshift and we transfer them to their rest frame. Duration decreases in GRB’s rest frame, consequently more GRBs with $T_{90} < 2s$; (2) satellites are limited when GRB’s flux is not adequate, it brings the effect that for some distant GRBs, T_{90} only contains the brightest part of the prompt emission, long GRBs are mis-classified as short ones, for example, GRB 090423, one of the farthest observed GRB at $z = 8.2$, has been discussed in detail in Ref. 22; (3) currently none of the satellite has a full energy coverage, each one observes a different energy band, as a result, the T_{90} from these satellites are different, we normalize T_{90} to the energy band of *Swift*-BAT, from 15 keV to ~ 150 keV.

3. Induced Gravitational Collapse Model

In Refs. 23 and 24, we have introduced the IGC paradigm in order to explain the astrophysical reasons for the conceptually unexpected association of GRBs with SNe. This IGC paradigm indicates that all long GRBs, by norm, have to be associated with a SN occurring in a binary system with a NS. The IGC paradigm differs from the traditional single star core collapsar model. In the collapsar-fireball model the GRB process is described by a single episode^{25–27} and references therein: (1) it is assumed to originate in a “collapsar”;²⁸ (2) the description of the late X-ray emission is dominated by a single ultra-relativistic jetted emission,^{29–33} shown in Fig. 7. There is a very fundamental different between the particle S-Matrix and cosmic C-Matrix, the in-state and the out-state in S-Matrix is reversible, oppositely the C-Matrix is not reversible. This is conceptually profound in the nature of general relativity which is not invariant for time reversal.

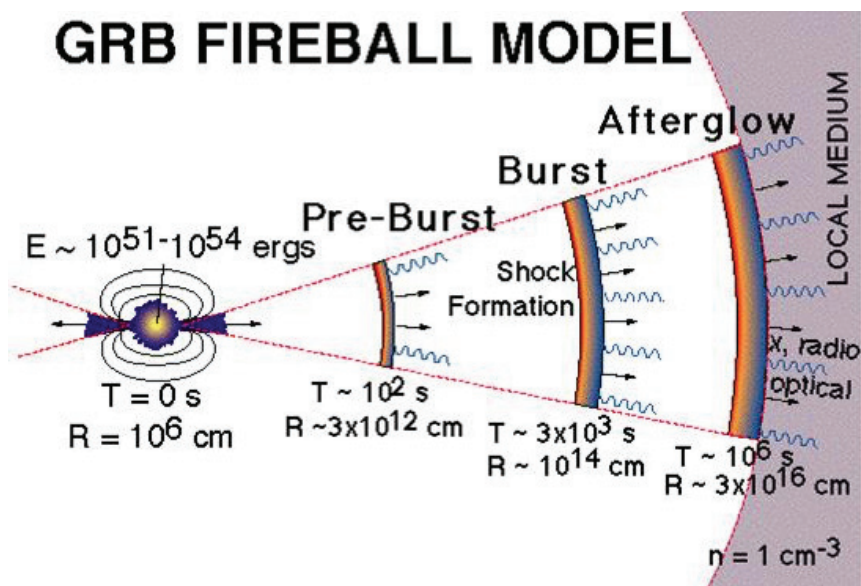


Fig. 7. Demonstration of fireball model, the central engine, the burst, the afterglow and the ISM (Figure is from Swift UK website).

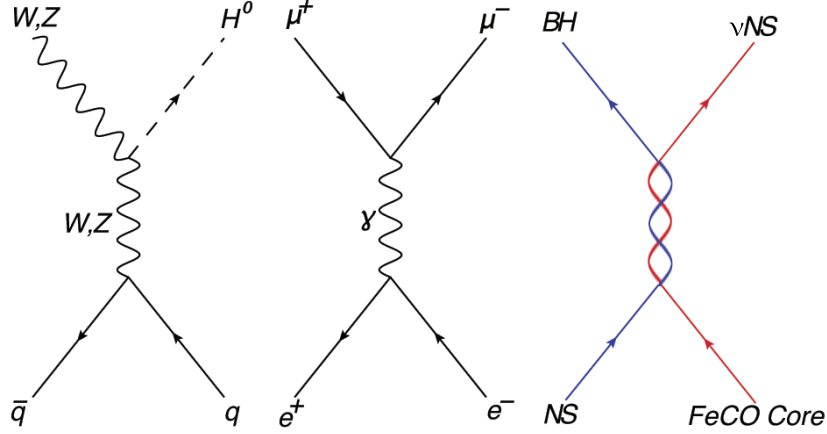


Fig. 8. Three different matrixes in the fundamental physics, first one is the quark matrix leading to Higgs boson. In the middle is the classical electron-positron pair matrix, generating muon and anti-muon pair. And the third matrix is the most recent one, which is considered in the present work, see e.g. in Ref. 7.

In contrast, the IGC paradigm considers a multi-component system, similar to the ones described by S -matrix in particle physics. For example, Fig. 8, the cosmic matrix of long GRBs: (1) the “in-states” are represented by a binary system formed by a FeCO core, very close to the onset of a SN event, and a tightly bound companion NS.^{24,34,35} The “out-states” are the creation of a new NS (ν -NS) and a black hole (BH). In the case of particle physics the S -matrix describes virtual phenomena occurring on time scales of 10^{-26} s for $q\bar{q} \rightarrow WZH^0$ ³⁶ and 10^{-23} s for $e^+e^- \rightarrow \mu^+\mu^-$.³⁷ In the astrophysical case, the cosmic matrix (C -matrix) describes real event occurring on timescale ~ 200 s, still a very short time when compared to traditional astrophysical time scales. Following the accretion of the SN ejecta onto the companion NS, a BH is created when the critical mass of a NS is reached, giving origin to the GRB; (2) special attention is given to the analysis of the instantaneous spectra in optical, X-ray, γ -ray and GeV energy range (as exemplified in this article); (3) four different episodes are identifiable in the overall emission, each with marked differences in the values of their Lorentz Γ factors.³⁸ Actually the possible relevance of a binary system in the explanation of GRBs was already mentioned in a pioneering work of Refs. 39 and 40, but the binaries in their case are triggers to the traditional collapsar model.

3.1. Families and episodes of GRBs

We here divide both long and short GRBs into two families respectively, namely family-1 and family-2, by a simple but fundamental threshold $E_{\text{iso}} \sim 10^{52}$ erg. This value corresponds to the minimal release of binding energy during the process that a NS, in a binary system as the initial state of IGC scenario, accretes enough matter to reach its critical mass and collapses to a black hole. This crucial result was obtained during many discussions I had with J. A. Rueda and Y. Wang in the preparation of the paper Ref. 41, such a distinction was first proposed for the long GRBs.

3.1.1. *Families of long GRBs*

Continued observations of massive stars have demonstrated that most, if not all, massive stars are in binary systems.^{42–44} A large fraction (50–75%) of these systems are in tight binaries that interact during the evolution (e.g. mass transfer, common envelope phase). The high binary fraction has led to a growing consensus that most type Ib/Ic SN progenitors are produced in interacting binary systems.^{45–49} Since the type of SNe associated to long-duration GRBs are of type Ic,⁵⁰ it is not surprising that binaries, often involving interactions of a massive star with a compact companion, have been invoked to produce GRB-SNe to remove the hydrogen envelope, spin up the star, or both.^{39,48,51–54} For the long GRBs, the IGC model requires a tight binary (produced in a common envelope phase) between a massive CO star (a star that has lost its hydrogen envelope and helium shell) and a NS companion.³⁴ Due to different configurations of binary system, especially the separation between two stars, two families of long GRBs are produced depending on whether or not a black hole formed.

The IGC paradigm is composed of four episodes, we delineate the family-2 long GRBs ($E_{\text{iso}} > 10^{52}$ erg, $T_{90} > 2$ s) which includes the most complete process, see Fig. 9.

Episode 1 originates in a unstable FeCO core leading to a SN event and the accretion onto the companion NS via the Bondi–Hoyle hypercritical accretion process.^{55,56} At the end of this episode, as the NS reaches its critical mass, it collapses to a BH.³⁴ It has become evident that the energetics of episode 1 is markedly different from the one of an isolated FeCO core that undergoes a SN and it is very sensitive to its binary nature and to the distance a between the SN and the NS: the tighter the binary system, the more energetic is episode 1. In GRB 130427A, a good prototype of such an extremely energetic emission occurs. The discovery of episode 1 offers the possibility of probing some of the pioneering works on “hypercritical accretion” by Refs. 57–59 which can in principle be tested with the possible observation of associated neutrino emission process.

In episode 2, along the direction of observer, a cavity is formed due to the accretion. In the vicinity of a black hole, the quantum electro-dynamical process occurring in the formation of the black hole leads to e^+e^- plasma which expands to ultra-relativistic velocity, a part of the plasma passes the cavity and interacts with the circumburst medium giving rise to a part of the prompt emission (see Refs. 61, 62 and references therein). The continuous accretion from SN ejecta on the newly formed black hole also contributes to the prompt emission. The physical picture in this episode is fundamentally important, it connects episode 1 and affects episodes 3, we propose an educative mimic as a simplification, the Chinese fortune cookie, shown in Fig. 11, which I developed with Y. Wang and our group in many conceptual discussions. The SN locates at the center, the cookie itself represents the SN ejecta, and the companion NS, which later becomes a black hole, locates inside the cavity that is carved by the effect of accretion onto the NS.

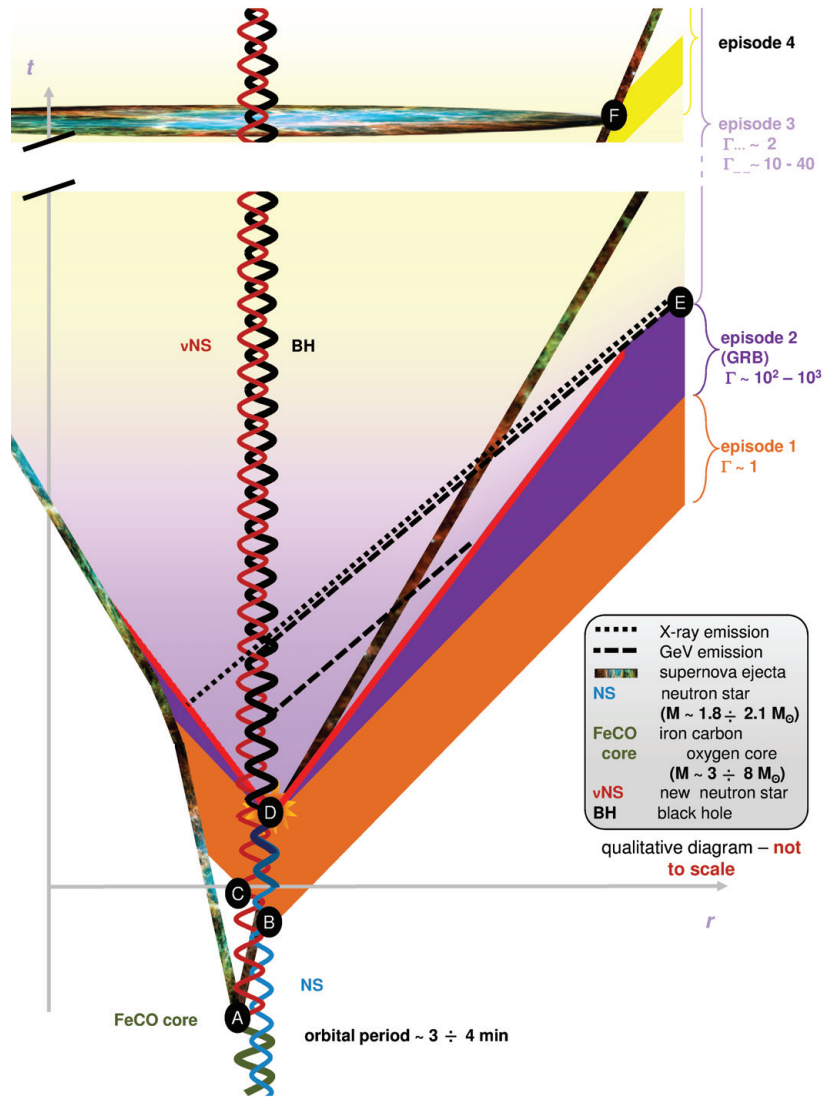


Fig. 9. The initial configuration is composed of an evolved, likely FeCO stellar core and a companion NS. (a) The core undergoes a SN and creates a new NS and its remnant; (b) beginning of the accretion of SN ejecta onto the companion NS, emitting episode 1; (c) the new NS interacts with mission from the episode 1; (d) accretion of the SN ejecta on the companion NS induces he black hole formation and the emission of e^+e^- plasma fireshell; (e) transition point between episode 2 and episode 3 which originates from the collision between the GRB ingoing to the SN remnant and collides with the ejecta originating binary driven hypernova (BdHN); (f) the SN optical signal peaks after tens of days.

Episode 3 is in our view mainly related to the SN ejecta. At this moment, we assume a novel idea which is quite different from the traditional approach, relating the so-called afterglow to the GRB phenomena, it is my opinion that the afterglow which clearly follows the prompt emission of the GRB is actually originating not in the GRB but is related to the SN ejecta. The SNe indeed are heated and accelerated as the collision of a portion of the e^+e^- plasma does not escape form the cavity indicated in Fig. 11. This concept can be visualized in the qualitative picture shown in Fig. 9, we compare and contrast that two cases of the long and short GRBs, only

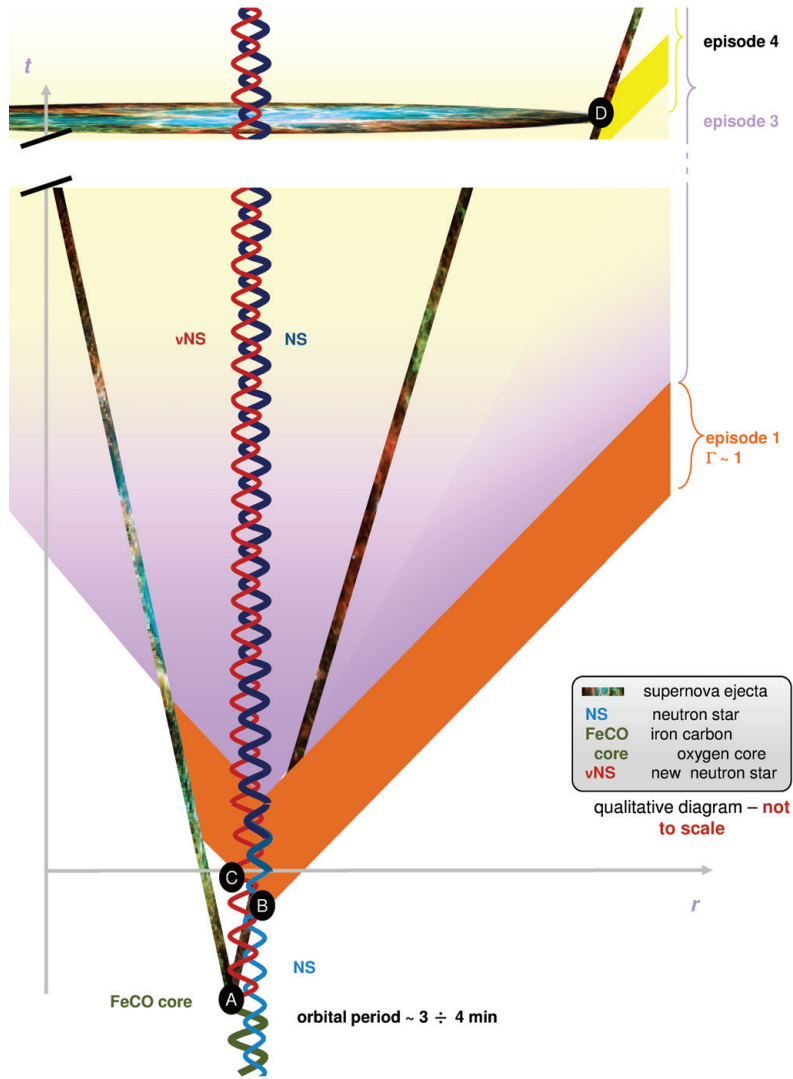


Fig. 10. The initial configuration is composed of an evolved, likely FeCO stellar core and a companion NS. (a) The core undergoes a SN and creates a new NS and its remnant; (b) beginning of the accretion of SN ejecta onto the companion NS, emitting episode 1; (c) the new NS interacts with mission from the episode 1, but the companion NS does not accrete enough matter to induce a black hole formation, no episode 2; (d) the SN optical signal peaks after tens of days.

in the long GBBs, episode 3 starts with a steeper decay of the X-ray light curve, in the 0.3–10 keV energy range, is followed by a plateau and then by a power-law decay with a almost constant index $-1.3 \lesssim \alpha \lesssim -1.7$. The overlapping of this late power-law decay which is measured in the rest-frame of the source, originally observed at times larger than 2×10^4 s,⁶³ has been considered the qualifying test for assuring the GRB to follow the IGC paradigm: a necessary and sufficient condition for the appearance of a SN at a later time, after 10 days in cosmological rest frame. The overlapping has also been used to probe the cosmological redshift of GRBs⁶⁴ and has led to consider the episode 3 as a “cosmic distance indicator”.⁶³ It is by now clear that the energy of the episode 3 is a standard feature, which is largely independent from the energy of the GRB.⁶³

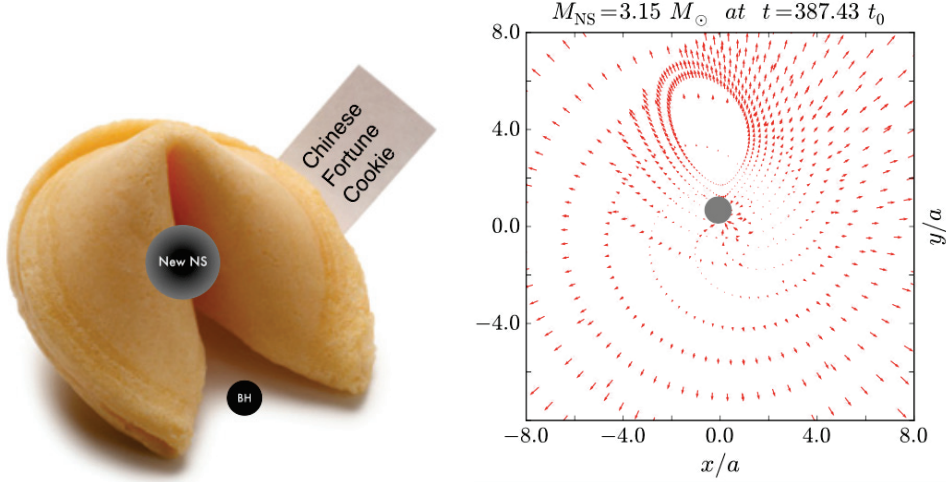


Fig. 11. Left: The shape of IGC episode 2 is similar to the Chinese fortune cookie. Right: Two dimensional simulation of the SN ejecta velocity field at $387.43 t_0$, $t_0 = 3.82$ s, a is the initial separation of two stars, the NS has been accreted to 3.15 solar masses.⁶⁰

Episode 4 is related to the optical appearance of the SN. This observational fact may very well be the consequence of a standard mass of the initial FeCO core.

Family 1 long GRB with $E_{\text{iso}} < 10^{52}$ erg, see Fig. 10, initially has a similar picture as the family-2 long GRB, a massive FeCO core collapse to a SN and the companion star accretes its ejecta, the difference is the binary components are too separated that the companion NS cannot accrete enough mass to form a black hole. As the result, there is no episode 2, because the formation of e^+e^- plasma relies on the BH, which absents in this family. Its episode 3 is simply an outcome of a hyper-nova, different from family-2 which goes through the heating and acceleration process, consequently, the nested and overlapped features do not appear in this family, and its luminosity of late X-ray emission is generally lower than Family-2 long GRB. In episode 4, a type Ib/c SN appears in the optical band in 10 – 20 days after the trigger of GRB, the same as Family-2. Most of energy of family-1 GRB is in X-ray, we call family-1 long GRB as X-ray flash (XRF).

3.1.2. Families of short GRBs

Progress has been obtained in the theoretical understanding of the equilibrium configuration of NSs, in their mass–radius relation, and especially in the theoretical determination of the value of the NS critical mass for gravitational collapse $M_{\text{crit}}^{\text{NS}}$.^{65,66} This has led to a theoretical value $M_{\text{crit}}^{\text{NS}} = 2.67M_{\odot}$, for instance for the NL3 equation of state.⁶⁷ Particularly relevant to this determination has been the conceptual change of paradigm of imposing global charge neutrality⁶⁷ instead of the traditional local charge neutrality still applied in the current literature, see, e.g. Ref. 68 and references therein. Similarly, noteworthy progress has been achieved in the determination of the masses of Galactic binary pulsars. Of the greatest relevance has been the direct observation of NS masses larger than $2M_{\odot}$,⁶⁹ pointing to

a very stiff nuclear equation of state hence to a large value of the NS critical mass, as pointed out above. In the majority of the observed cases of Galactic binary NSs, the sum of the NS masses, $M_1 + M_2$, is indeed smaller than $M_{\text{crit}}^{\text{NS}}$ and, given the above determination of the NS critical mass, their coalescence will never lead to a BH formation. This of course offers a clear challenge to the traditional assumption that all short GRBs originate from BH formation, see e.g., Refs. 70, 71 and references therein.

Two families of short GRBs, both originating from NS mergers exist, and the difference between these two families depends on whether the total mass of the merged core is smaller or larger than $M_{\text{crit}}^{\text{NS}}$. This point has been clarified in many discussions with M. Muccino and J. A. Rueda and published in Ref. 71. The first family corresponding to the above mentioned less energetic short GRBs with $E_{\text{iso}} < 10^{52}$ erg, in which coalescence of the merging NSs leads to a massive NS as the merged core. In view of their relatively low value energetics, and the attributes of their hard X-ray spectra in the gamma-rays, we indicate them as short gamma flashes (S-GRFs). Paradoxically all the short bursts published in Ref. 70 belong to this class, and S-GRFs do not originate from the a process of the BH formation. The second family of short bursts with $E_{\text{iso}} > 10^{52}$ erg originate instead from a merger process leading to a BH as the merged core, in view of the hardness of the spectra and the high energetics of this class of short bursts, these sources deserve the name of short GRBs (S-GRBs). It is appropriate to remind that both long GRBs and short GRBs with $E_{\text{iso}} > 10^{52}$ lead to a BH formation, and both of them appear to have prominent GeV emission.

4. The IGC Paradigm for Long GRBs and Five Physical and Astrophysical Processes

The IGC paradigm integrates many physical and astrophysical processes:

- (1) The hypercritical accretion in episode 1.
- (2) The GRB emission in episode 2 composed by the P-GRB and the prompt emission, and possibly additional phase of hypercritical accretion.
- (3) The overlapping and nesting of the late X-ray emission in episode 3. item The GeV emission.
- (4) The SN observations.

4.1. *The Hypercritical accretion in episode 1*

In episode 1 of IGC paradigm, the SN explosion and the GRB occur following a precise time sequence as depicted in Fig. 9: explosion of the CO core → hypercritical accretion onto the NS → the critical mass is reached → gravitational collapse to a BH is induced → emission of the GRB. In episode 2, a part of the ejecta can continue the accretion onto the black hole producing significant emission in the most energetic GRBs. The theoretical framework and the first estimates of the hypercritical accretion onto the NS as a function of the nature of the binary parameters were

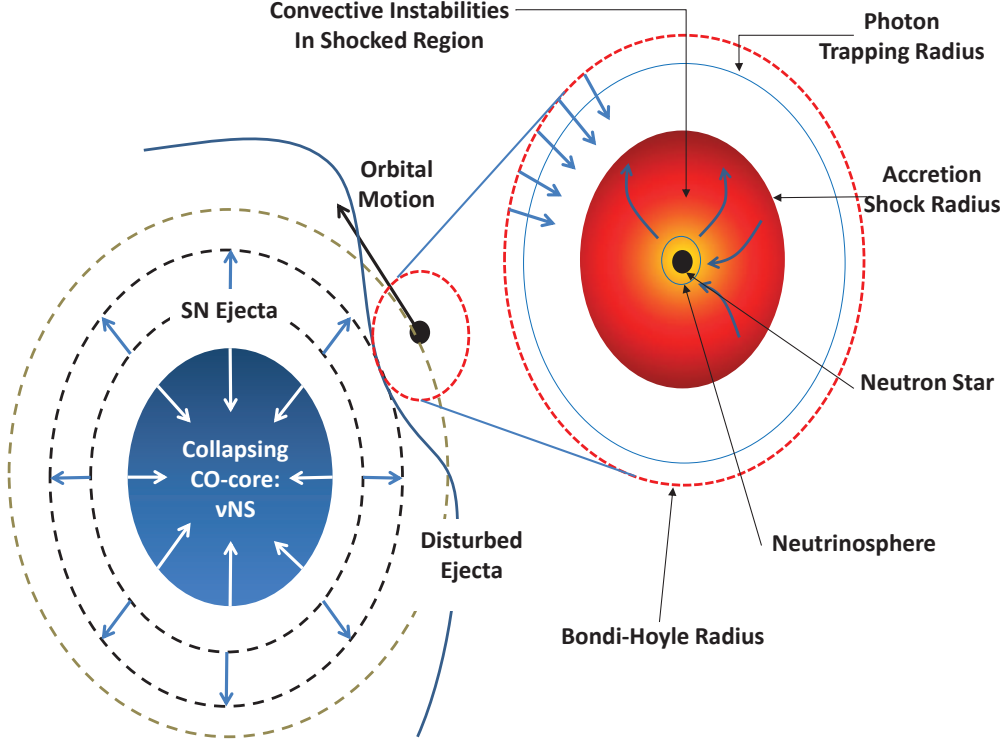


Fig. 12. Induced gravitational collapse scenario.

first presented in Ref. 34, see Fig. 12. The first more realistic numerical simulations of the IGC is performed by using more detailed SN explosions coupled to hypercritical accretion models from previous simulations of SN fallback in Refs. 59, 72, 73, and more recently Ref. 60 present the first estimates of the angular momentum transported by the SN ejecta, and perform numerical simulations of the angular momentum transfer to the NS during the hyper-accretion process in full general relativity.

For a wide variety of X-ray binaries, see e.g. in Ref. 74, the Eddington limit places a very fundamental role. In the present case of hypercritical accretion from the SN ejecta onto the companion NS within the IGC scenario, the Eddington limit plays no role since the photons are trapped in the flow. The trapping radius of photons emitted diffuse outward at a slower velocity than infalling material flows inward:⁷⁵

$$r_{\text{trapping}} = \min[(\dot{M}_{\text{BHL}}\kappa)/(4\pi c), r_{\text{BHL}}], \quad (1)$$

where κ is the opacity (in $\text{cm}^2 \text{g}^{-1}$) and c is the speed of light. If the trapping radius is larger or equal to the Bondi–Hoyle radius, the photons are trapped in the flow and the Eddington limit does not apply. The inflowing material shocks as it piles up onto the NS, producing an atmosphere on top of the NS, for details, see Refs. 57, 59, 75, 76. As the atmosphere compresses, it becomes sufficiently hot to emit neutrinos which cool the infalling material, allowing it to be incorporated into the NS. For details of the simulation of this process, we refer the reader to Refs. 59, 73, 77.

As material piles onto the NS and the atmosphere radius, the accretion shock moves outward. The accretion shock weakens as it moves out and the entropy jump (derived from the shock jump conditions) becomes smaller. This creates an atmosphere that is unstable to Rayleigh–Taylor convection. Simulations of these accretion atmospheres show that these instabilities can accelerate above the escape velocity driving outflows from the accreting NS with final velocities approaching the speed of light, ejecting up to 25% of the accreting material.^{73,78}

For the typical hypercritical accretion conditions of the ICG, the temperature of the bubble when it begins to rise is $T_{\text{bubble}} \sim 5$ MeV. If it rises adiabatically, expanding in all dimensions, its temperature drops to 5 keV at a radius of 10^9 cm, far too cool to observe. However, if it is ejected in a preferred direction due to the presence of angular momentum, as simulated by Ref. 73, it may expand in the lateral direction but not in the radial direction, so $\rho \propto r^2$ and $T \propto r^{-2/3}$. In this scenario, the bubble outflow would have $T_{\text{bubble}} \sim 50$ keV at 10^9 cm and $T_{\text{bubble}} \sim 15$ keV at 6×10^9 cm. This could explain the temperature and size evolution of the blackbody emitter observed in the episode 1 of several GRBs, see, e.g., in Refs. 63, 64, 79–81. We are currently deepening our analysis of the possible explanation of the thermal emission observed in episode 1 as due to the convective instabilities in the accretion process.

GRB 090618, as a typical example, its episode 1 lasts from 0 to 50 s and the episode 2 is from 50 s to 151 s after the trigger time, shown in Fig. 14. The blackbody emission observed in episode 1 of GRB 090618⁷⁹ evolves as $T \propto r^{-m}$ with $m = 0.75 \pm 0.09$, whose lower value is in striking agreement with the above simplified theoretical estimate.⁷⁹ The spectrum of episode 1 is shown in Fig. 13.

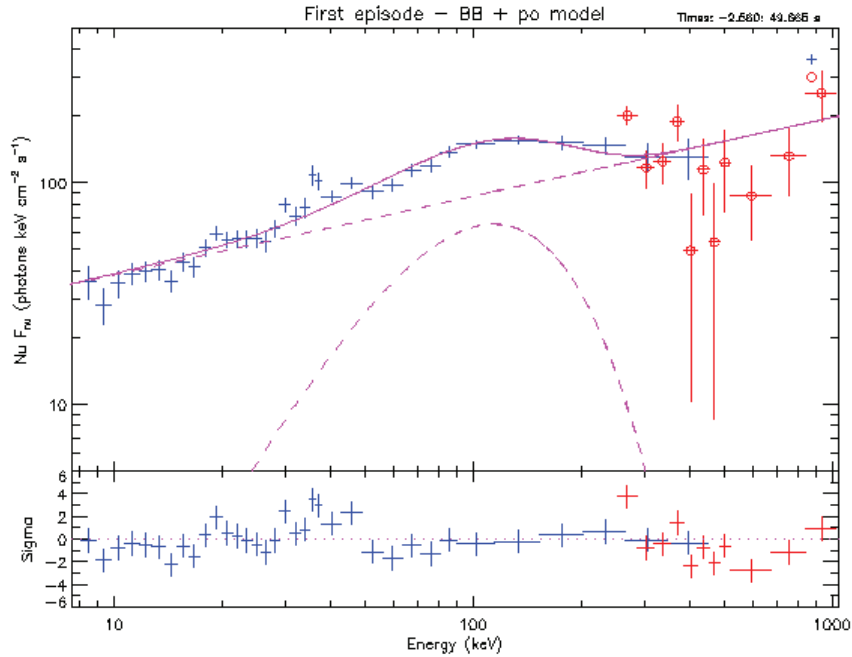


Fig. 13. Time-integrated spectra for the first episode (from 0 to 50 s) of GRB 090618 fitted blackbody + power-law (right) models with temperature $T = 32.07 \pm 1.85$ keV.

4.2. *The GRB emission in episode 2: P-GRB and the prompt emission*

According to the uniqueness theorem for stationary, the process of gravitational collapse of a core whose mass is larger than the NS critical mass will generally lead to a black hole. The creation of critical electric fields and consequent process of pair creation by vacuum polarization are expected to occur in the late phases of gravitational collapse when the gravitational energy of the collapsing core is transformed into an electromagnetic energy and eventually in e^+e^- pairs. Episode 2 starts from such an optically thick e^+e^- plasma in thermal equilibrium, with a total energy of $E_{\text{tot}}^{e^\pm}$. We call the evolution of this plasma shell as the fireshell model.

This plasma is initially confined between the radius r_h of a BH and the dyadosphere radius

$$r_{ds} = r_h \left[2\alpha \frac{E_{\text{tot}}^{e^+e^-}}{m_e c^2} \left(\frac{\hbar/m_e c}{r_h} \right)^3 \right]^{1/4}, \quad (2)$$

where α is the usual fine structure constant, \hbar the Planck constant, c the speed of light, and m_e the mass of the electron. The lower limit of $E_{\text{tot}}^{e^\pm}$ is assumed to coincide with the observed isotropic energy E_{iso} emitted in X-rays and gamma rays alone in the GRB.

The rate equation for the e^+e^- pair plasma and its dynamics have been described in Ref. 18. This plasma engulfs the baryonic material left over from the process of gravitational collapse having a mass M_B , still maintaining thermal equilibrium between electrons, positrons, and baryons. The baryon load is measured by the dimensionless parameter $B = M_B c^2 / E_{\text{tot}}^{e^+e^-}$. Reference 77 showed that no relativistic expansion of the plasma exists for $B > 10^{-2}$. The fireshell is still optically thick and self-accelerates to ultra-relativistic velocities.⁸² Then the fireshell becomes transparent and the P-GRB is emitted.⁸³ The final Lorentz gamma factor at transparency can vary over a wide range between 10^2 and 10^4 as a function of $E_{\text{tot}}^{e^+e^-}$ and B . For its final determination it is necessary to explicitly integrate the rate equation for the e^+e^- annihilation process and evaluate, for a given BH mass and a given e^+e^- plasma radius, at what point the transparency condition is reached.¹⁸ After transparency, along the direction pointing to the observer, the remaining accelerated baryonic matter still expands ballistically and starts to slow down from collisions with the CBM and filaments, producing a big amount of gamma-ray and X-ray photons in the GRB prompt emission.

We adopted a pragmatic approach in our fireshell model by making full use of the knowledge of the equations of motion, of the EQTS formulations,⁸⁴ and of the correct relativistic transformations between the comoving frame of the fireshell and the observer frame. Figure 14 shows an example of our simulation, the light curve of GRB 090618 in episode 2 starting from about 50 s.

As discussed in Subsec. 3.1.1 and shown in Fig. 11, that e^+e^- dyadosphere can only be generated when the accretion reaches a critical mass, which means such

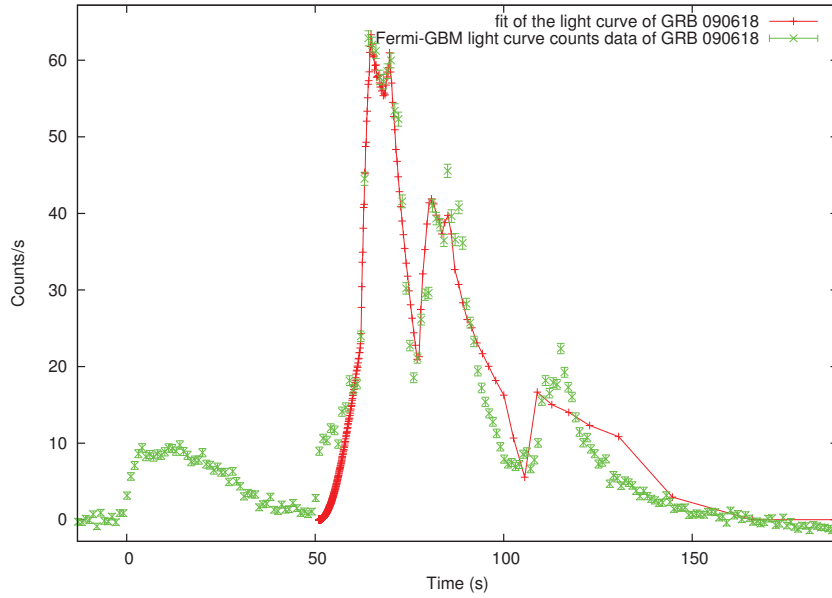


Fig. 14. Simulated light curve of the episode 2 of GRB 090618, from 58 s to 150 s, in the energy band 8–440 keV.

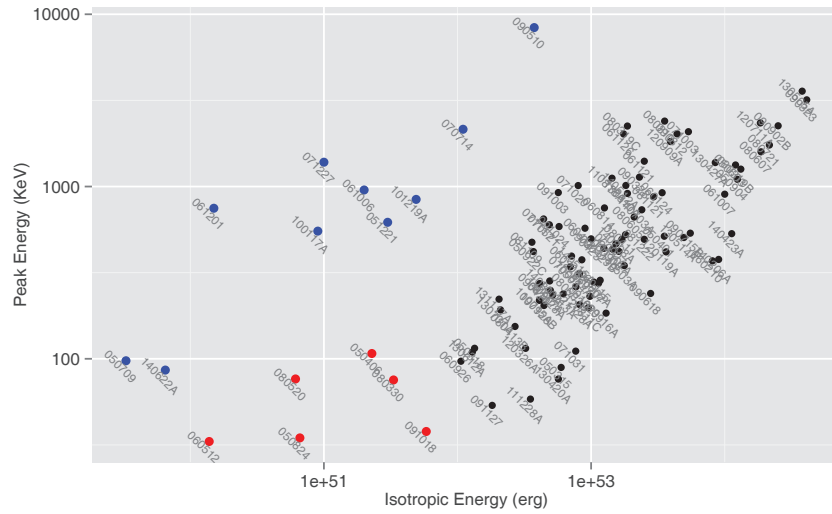


Fig. 15. The relation of isotropic energy and peak energy. Blue points are short GRBs, red and black points are long GRBs.

fireshell of plasma appears just in family-2 GRBs. As a result, the prompt emission of family-2 GRBs is a combination of outcome from the fireshell and the accretion onto black hole, while for the family-1 GRBs, solely accretion provides the energy. From the theory and simulation of hypercritical accretion, we already know that accretion generates X-ray photons with tens of keV, that photon's energy could peak at hundreds of keV, even some MeV since the accretion onto the newly formed BH, not just a NS. More over, the presence of angular momentum jets high Lorentz factor material, which generates high energy spectrum. In the observational aspect, shown in Fig. 15, confirms our simulations.

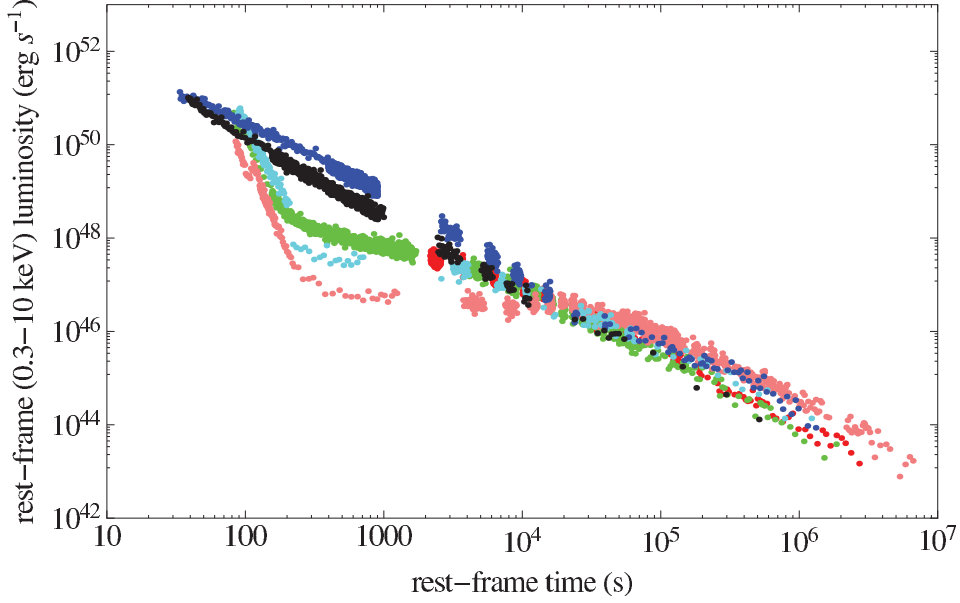


Fig. 16. (Color online) The X-ray luminosity light curves of the BdHNe members of the Golden Sample: GRB 060729, $z = 0.54$ (pink diamonds); GRB 061007, $z = 1.261$ (black stars); GRB 080319B, $z = 0.937$ (blue crosses); GRB 090618, $z = 0.54$ (green circles); GRB 091127, $z = 0.49$ (red squares); GRB 111228, $z = 0.713$ (cyan triangles).⁶³

4.3. The overlapping and nested of the late x-ray emission in episode 3

The photons in episode 3 have two origins, one is the heated SN ejecta, which contributes photons in the X-ray and lower energy, and the second is GeV photons originated from the interaction of black hole with newly born NS from the SN and the SN ejecta.⁷² This section we mainly focus on the X-ray emission from the SN ejecta.

It has been shown that the X-ray rest-frame 0.3–10 keV luminosity light curves present a constant decreasing power-law behavior, at times $\gtrsim 10^4$ s, with a typical value of the slope of $-1.7 \lesssim \alpha_X \lesssim -1.3$. This feature has been evidenced in a best sample of six GRBs, namely GRB 060729, 061007, 080319B, 090618, 091127, and 111228, hereafter *Golden Sample*, see e.g. in Ref. 63 and Fig. 16, and has been used also to infer the redshifts of GRBs 101023 and 110709B.^{80,85}

In Fig. 17, we compare the rebinned rest-frame 0.3–10 keV luminosity light curves of GRBs 130427A (purple), 060729 (pink) and 061121 (red). Their episode 3 emissions, are modeled by using the following phenomenological function of the rest-frame arrival time t_a ,

$$L(t_a) = L_p \left(\frac{t_a}{100} \right)^{\alpha_p} + L_X \left(1 + \frac{t_a}{\tau} \right)^{\alpha_X}, \quad (3)$$

where L_p and α_p are the steep decay luminosity (at $t_a = 100$ s) and index, and L_X , α_X and τ , respectively, are the plateau luminosity, the late power-law decay index and the characteristic time-scale of the end of the plateau.

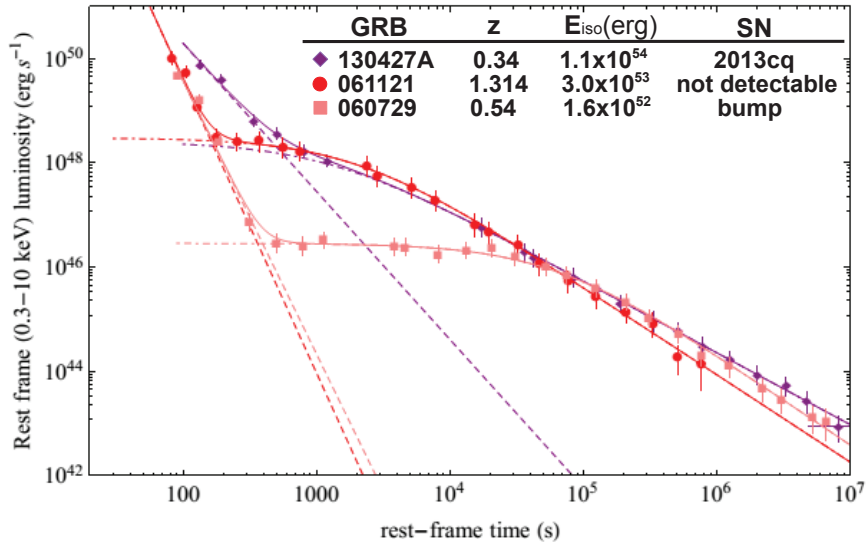


Fig. 17. (Color online) The rest-frame 0.3–10 keV re-binned luminosity light curves of GRB 130427A (purple diamonds), GRB 061121 (red circles) and GRB 060729 (pink squares). The light curves are fitted by using a power-law for the steep decay phase (dashed lines) and the function in Eq. (3) for the plateau and the late decay phases (dot-dashed curves).³⁸

From this fitting procedure, we conclude that the IGC GRBs exemplified in Fig. 17 share the following properties:

- the power-law decay, for the more energetic sources, starts directly from the steep decay, well before the $t_a \approx 2 \times 10^4$ s as indicated in Ref. 63. Consequently the plateau shrinks for increasing E_{iso} (see Fig. 17);
- the luminosities in the power-law decay are uniquely functions of the cosmological rest-frame arrival time t_a , independently on the E_{iso} of each source (see Fig. 17);
- most remarkably, the overlapping of the X-ray light curves reveals a “nested” structure of episodes 3.

In GRB 130427A, the precise power-law decay of episode 3 in the X-rays is also observed in other wavelengths. In Fig. 18 are compared the data by the Fermi-LAT (100 MeV–100 GeV, red), the Swift-XRT (0.3–10 keV, blue), the NuStar⁸⁶ (3–79 keV, orange) and the Swift-UVOT⁸⁷ (optical R-band, green). Details are given in Ref. 41.

4.4. The GeV emission

It has always been a challenging topic of explaining GeV photons since the launch of Fermi satellite and the observation by Fermi-LAT. In the traditional collapse-fireball model, GeV photons originate from the same plasma outflow as lower energy ones, though the radiation mechanism participated varies. In the IGC paradigm, as we described, photons from optical to gamma-ray have many different origins in each on of the four episodes. The GeV photons instead have a different origin

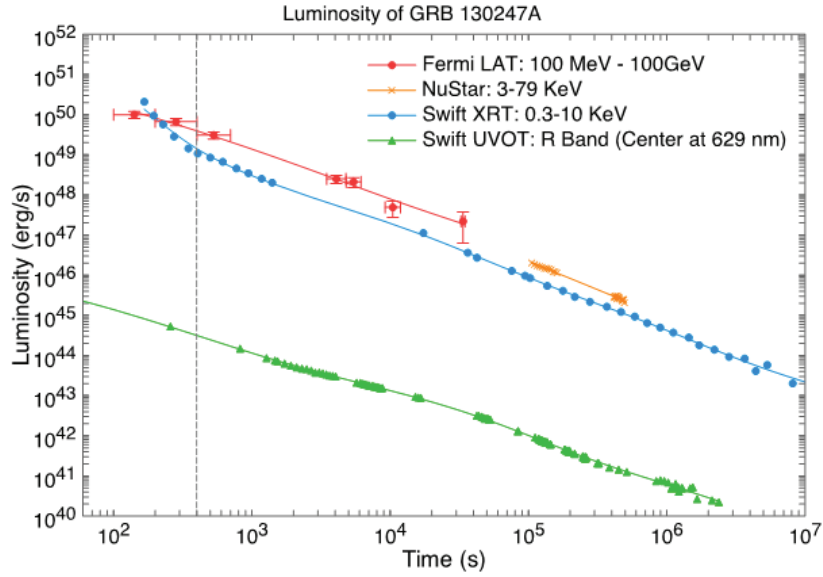


Fig. 18. (Color online) Multi-wavelength light curve of GRB 130427A from the data by the Fermi-LAT (100 MeV–100 GeV, red circles with errors), the Swift-XRT (0.3–10 keV, blue circles), the NuStar⁸⁶ (3–79 keV, orange crosses) and the R-band optical from Swift-UVOT⁸⁷ (green triangles).⁴¹

from all the others: they originate from the interaction of newly born black hole with the NS from the SN and the SN ejecta. The most significant factor for the identification of being originating from the black hole is the observation that the high GeV emission occurs after the emission of the P-GRB, which coincides with the moment of the formation of the blackhole.^{60,72} In this sense, GeV photons only exist in family-2 GRBs which possess a black hole, see Fig. 19 for family-2 long GRBs.

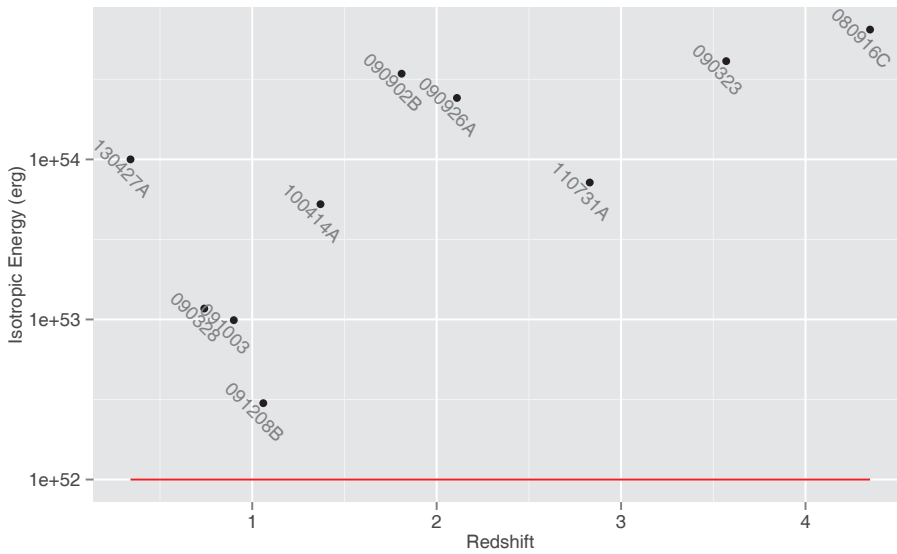


Fig. 19. GRBs with observed > 1 GeV photons, the horizontal redline indicates isotropic energy equals to 10^{52} erg, GRBs above this line are belong to family-2.

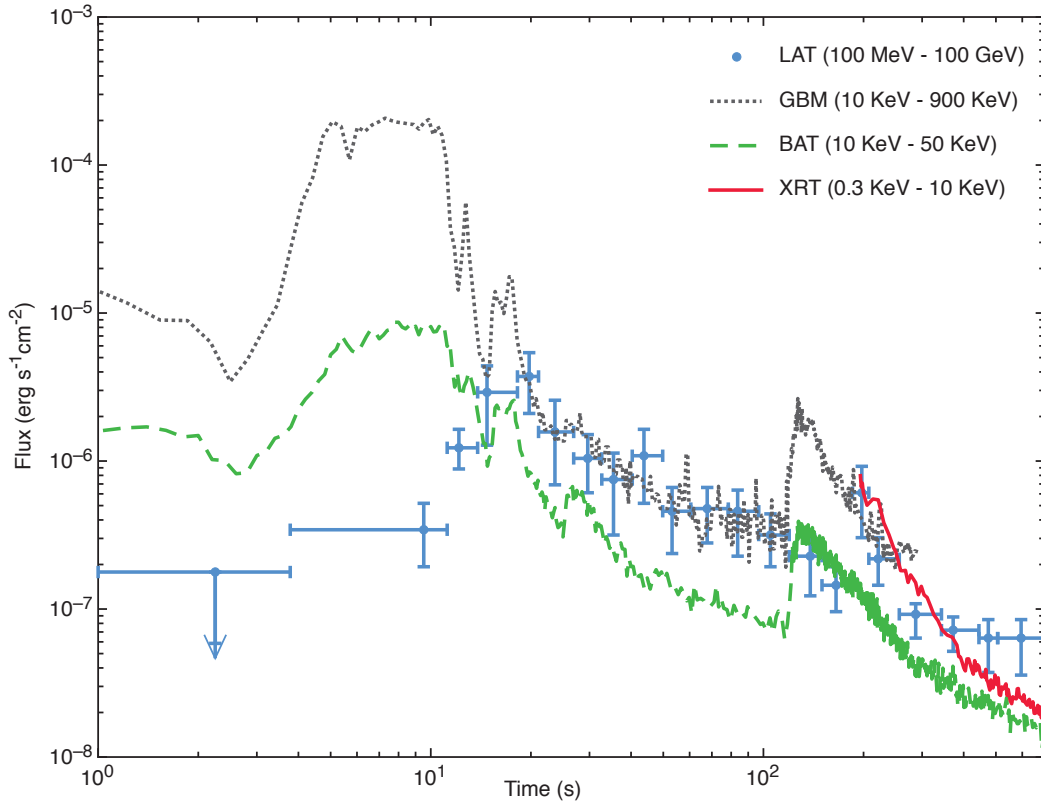


Fig. 20. Flux of first 700 s. Blue points are the *Fermi*-LAT high energy emission from 100 MeV till 100 GeV,⁸⁸ grey dotted line represents the *Fermi*-GBM, from 10 keV to 900 keV, green dashed line represents the photons detected by *Swift* BAT from 10 keV to 50 keV, and red solid line is the soft X-ray *Swift*-XRT detection, in the range of 0.3 KeV to 10 KeV. From this figure, clearly the *Fermi*-LAT emission reaches highest fluence at about 20 s while the gamma-ray detected by *Fermi*-GBM releases most of the energy within the first 10 s.⁴¹

GRB 130427A is one of the few GRBs with an observed adequate fluence in the optical, X-ray and GeV bands simultaneously for hundreds of seconds. In particular it remained continuously in the LAT field of view until 750 s after the trigger of *Fermi*-GBM,⁸⁸ which gives us the best opportunity so far to investigate different energy bands together, especially for the GeV photons. The first 700 s light curve is shown in Fig. 20, obviously, The GeV emission is quite dim in the first 10 s when gamma- and X-ray dominate the emission, then the GeV emission raises up coincidentally with the gamma and hard X-ray prompt emissions dropping down, the reason is at the beginning the intensive X-ray and gamma-ray photos block the GeV photons which are produced in the center. Such phenomena are common in many GRBs, shown in Fig. 21.

4.5. *Supernova appearance*

In the IGC, the occurrence of all the long GRBs require the explosion of SN. Normally the confirmation of SN is by detecting its optical emission from the nuclear decay of the ejecta at about 10 to 20 days after the GRB trigger. There are many

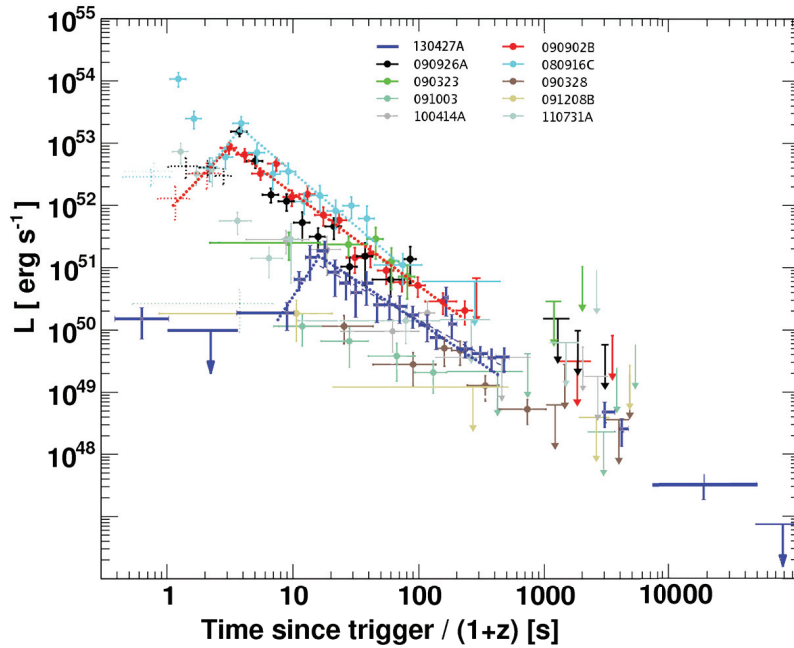


Fig. 21. Light curves of Fermi-LAT emission (100 MeV to 100 GeV), figure is from the first Fermi-LAT gamma-Ray burst catalog,⁸⁹ complemented.

reasons obstruct the optical detection, for instance, Poor localizations of bursts, contamination from host galaxy, and most important that GRB is a cosmological event with high redshift, but due to metal absorption, photons below ~ 400 nm are especially difficult to be detected, essentially no optical flux from GRB-SNe at $z > 1.2$.⁵⁴ Table 1 from Ref. 90 contains all the 35 confirmed GRB-SN connections updated to the 31 May 2014. Clearly, their isotropic energy vary many magnitudes from 10^{48} erg till 10^{54} erg, containing both family-1 and family-2 GRBs.

We had a successful prediction of SN appearance for GRB 130427A/SN2013cq. From the observations of the episode 3, GRB 130427A has been confirmed to fulfill the IGC paradigm, and we conclude, solely on this ground, that a SN should necessarily be observed under these circumstances. We sent the GCN circular 14526^{a91} on May 2, 2013 predicting that the optical R-band of a SN will reach its peak magnitude in about 10 days in the cosmological rest-frame on the basis of the IGC paradigm, and we encouraged the further observation. Indeed, starting from May 13, 2013, the telescopes GTC, Skynet and HST discovered the signals from the type Ic SN SN 2013cq.^{92–96}

^aGCN 14526: The late X-ray observations of GRB 130427A by *Swift*-XRT clearly evidence a pattern typical of a family of GRBs associated to SN following the IGC paradigm.^{34,63} We assume that the luminosity of the possible SN associated to GRB 130427A would be the one of 1998bw, as found in the IGC sample described in Ref. 63. Assuming the intergalactic absorption in the I-band (which corresponds to the R-band rest-frame) and the intrinsic one, assuming a Milky Way type for the host galaxy, we obtain a magnitude expected for the peak of the SN of $I = 22-23$ occurring 13–15 days after the GRB trigger, namely between the 10th and the 12th of May 2013. Further optical and radio observations are encouraged.

Table 1. The sample of the 35 confirmed GRB-SN connections updated to the 31 May 2014, from Ref. 90.

GRB	E_{iso} (erg)	Discovered by	z	SN identification	SN name
970228	1.86×10^{52}	BATSE/SAX	0.695	bump	
980326	5.60×10^{51}	BATSE/SAX	1(?)	bump	
980425	6.38×10^{47}	BATSE	0.0085	spec.	SN1998bw
990712	7.80×10^{51}	SAX	0.434	bump	
991208	2.59×10^{53}	SAX	0.706	bump	
000911	7.80×10^{53}	Konus-WIND	1.058	bump	
010921	1.10×10^{52}	HETE	0.45	bump	
011121	9.90×10^{52}	Ulysses	0.36	bump	SN 2001ke
020305	$0.7\text{-}4.6 \times 10^{51}$	Ulysses	0.2-0.5	bump	
020405	1.28×10^{53}	Ulysses	0.695	bump	
020410	2.20×10^{52}	Konus-WIND	~ 0.5	bump	
021211	1.30×10^{52}	HETE	1.006	spec.	SN 2002lt
030329	1.70×10^{52}	Konus-WIND	0.168	spec.	SN 2003dh
030723	1.60×10^{53}	HETE	< 1	bump	
031203	9.99×10^{49}	INTEGRAL	0.105	spec.	SN 2003lw
040924	1.10×10^{52}	HETE	0.86	bump	
041006	3.50×10^{52}	HETE	0.716	bump	
050525A	3.39×10^{52}	Konus-WIND	0.606	spec.	SN 2005nc
060218	1.66×10^{49}	Swift	0.033	spec.	SN 2006aj
060729	1.60×10^{52}	Swift	0.54	bump	
070419	7.90×10^{51}	Swift	0.97	bump	
080319B	1.30×10^{54}	Swift	0.937	bump	
081007	2.50×10^{51}	Swift	0.5295	bump	SN2008hw
090618	2.90×10^{53}	Fermi-GBM	0.54	bump	
091127	1.60×10^{52}	Fermi-GBM	0.49	bump	SN 2009nz
100316D	9.81×10^{48}	Swift	0.059	spec.	SN 2010bh
101219B	4.39×10^{51}	Fermi-GBM	0.55	spec.	SN 2010ma
111228A	7.52×10^{52}	Fermi-GBM	0.714	bump	
120422A	1.28×10^{51}	Swift	0.283	spec.	SN 2012bz
120714B	4.51×10^{51}	Swift	0.3984	spec.	SN 2012eb
120729A	2.30×10^{52}	Swift	0.80	bump	
130215A	3.10×10^{52}	Fermi-GBM	0.597	spec.	SN 2013ez
130427A	9.57×10^{53}	Fermi-GBM	0.3399	spec.	SN 2013cq
130702A	7.80×10^{50}	Fermi-GBM	0.145	spec.	SN 2013dx
130831A	4.56×10^{51}	Konus-WIND	0.4791	spec.	SN 2013fu

5. Conclusions

The nature of GRBs is presenting itself as one of the richest diagnostics ever encountered within physics and astrophysics. It is clear that phenomena never before explored in this domain can now be submitted to theoretical and observational scrutiny. In analogy with the S-matrix of particle physics, for long GRBs a cosmic matrix (C-matrix), in which the in-states are a NS and an evolved core undergoing

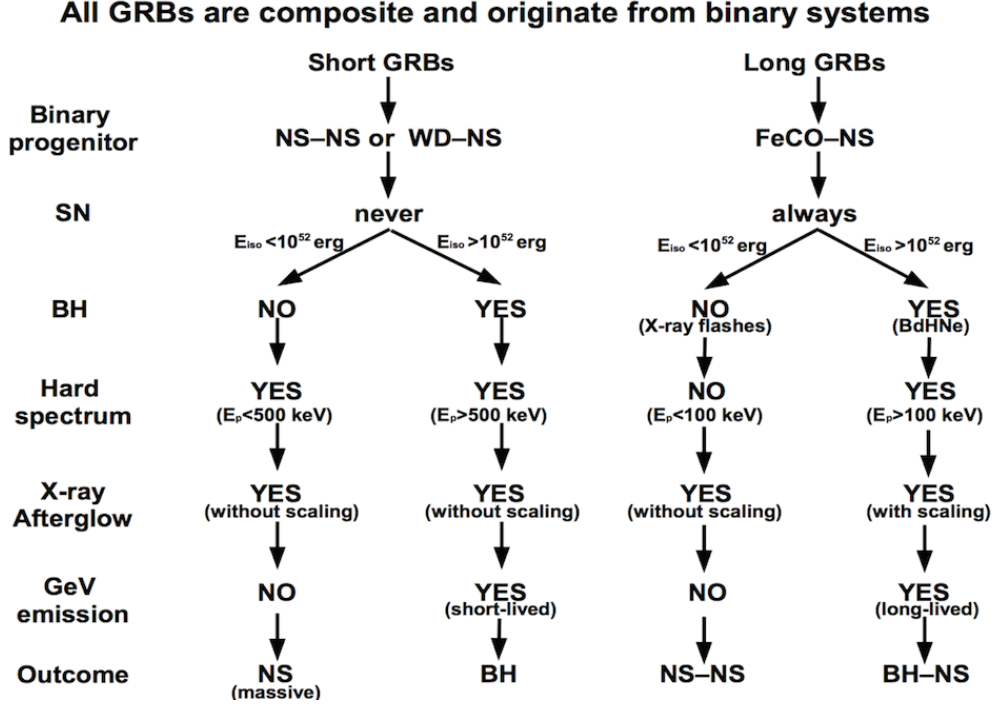


Fig. 22. All GRBs are composited and originated from binary systems, they follow four different routes of evolution. For long GRBs, the in-states are a NS and an evolved core undergoing a SN explosion in a binary system, and the out-states are a BH and a newly-born NS.⁴¹ For short GRBs, the in-states are two compact stars in a binary system, and the out-states is a BH or a NS.³⁸

a SN explosion in a binary system, and the out-states are a BH and a newly-born NS. For short GRBs, the in-states are two compact stars in a binary system, and the out-states is a BH or a NS. Fig. 22 shows that all GRBs are composited and originated from binary systems, they follow four different routes of evolution. In the induced gravitational collapse we have introduced, GRBs are classified to two families depending on the formation of black hole. We discussed several physical processes and phenomena in these families, namely the hypercritical accretion which initials the occurrence of GRB, the formation of e^-e^+ plasma as the causation of non-thermal emission in the prompt phase and the heating of SN ejecta, this heated and accelerated SN ejecta afterwards lead to the observation of spikes in the X-ray emission, as well as the overlapped and nested structures of late X-ray emissions. We also discussed GeV photons have a unique origination of the interaction between the black hole and newly born NS. And in the last section we show the connection of GRB and SN, and our successful prediction of SN 2013cq associated to GRB 130427A.

The cosmic matrix is at the basis of this new physics and relativistic astrophysics. Until now we have emphasized the action around the black hole, or the absence of it. Much work is still ahead in covering all possible interactions between the massive neutron star, the newly born neutron star, the supernova ejecta, and the newly born black hole.

Acknowledgments

I am very thankful to the president of the Chinese Academy of Sciences, Prof. Chunli Bai, to have promoted the 4th Galileo-Xu Guangqi meeting held in China, with the participation of so many young and distinguished scientists. Thanks to the presence of Prof. Frank C.N. Yang and his noble words expressed remembering Fermi will be a standing memory for all the participants to the 14th Marcel Grossmann meeting. My gratitude to Prof. Ronggen Cai, Prof. Yueliang Wu, and Prof. Yaping Zhang, for their work of preparing this splendid meeting and its publication. To many Chinese participants I confirm my usual happiness for their thought-provoking questions and discussion.

References

1. W. Baade and F. Zwicky, *Proc. Natl. Acad. Sci.* **20**, 254 (1934), doi:10.1073/pnas.20.5.254.
2. W. Baade and F. Zwicky, *Proc. Natl. Acad. Sci.* **20**, 259 (1934), doi:10.1073/pnas.20.5.259.
3. W. Baade and F. Zwicky, *Phys. Rev.* **46**, 76 (1934), doi:10.1103/PhysRev.46.76.2.
4. A. Hewish, S. J. Bell, J. D. H. Pilkington, P. F. Scott and R. A. Collins, *Nature* **217**, 709 (1968), doi:10.1038/217709a0.
5. H. Gursky and R. Ruffini (eds.), Neutron stars, black holes and binary X-ray sources, in *Proceedings of the Annual Meeting*, San Francisco, Calif., February 28, 1974, Astrophysics and Space Science Library, Vol. 48 (1975).
6. T. Damour and R. Ruffini, *Phys. Rev. Lett.* **35**, 463 (1975), doi:10.1103/PhysRevLett.35.463.
7. R. Ruffini, *Int. J. Mod. Phys. D* **20**, 1797 (2011), arXiv:1107.0862 [astro-ph.HE], doi:10.1142/S0218271811019876.
8. E. Pian *et al.*, *Astrophys. J.* **536**, 778 (2000), astro-ph/9910235, doi:10.1086/308978.
9. T. J. Galama *et al.*, *Nature* **395**, 670 (1998), astro-ph/9806175, doi:10.1038/27150.
10. M. Tavani *et al.*, *Science* **331**, 736 (2011), arXiv:1101.2311 [astro-ph.HE], doi:10.1126/science.1200083.
11. A. Finzi and R. A. Wolf, *Astrophys. J.* **153**, 865 (1968), doi:10.1086/149711.
12. R. Ruffini and J. A. Wheeler, *Phys. Today* **24**, 30 (1971), doi:10.1063/1.3022513.
13. M. Rees, R. Ruffini and J. A. Wheeler, Black holes, gravitational waves and cosmology: An introduction to current research (1974).
14. D. Christodoulou and R. Ruffini, *Phys. Rev. D* **4**, 3552 (1971), doi:10.1103/PhysRevD.4.3552.
15. D. L. Wiltshire, M. Visser and S. Scott (eds.), The ergosphere and dyadosphere of black holes, in *The Kerr Spacetime* (2009).
16. W. Janke, W. A. Pelster, H. J. Schmidt and M. Bachmann (eds.), Analogies, new paradigms and observational data as growing factors of relativistic astrophysics (2011).
17. R. Ruffini, J. D. Salmonson, J. R. Wilson and S.-S. Xue, *Astron. Astrophys.* **350**, 334 (1999), arXiv:astro-ph/9907030.
18. R. Ruffini, J. D. Salmonson, J. R. Wilson and S.-S. Xue, *Astron. Astrophys.* **359**, 855 (2000), arXiv:astro-ph/0004257.
19. J. P. Norris, T. L. Cline, U. D. Desai and B. J. Teegarden, Frequency of fast, narrow gamma-ray bursts and burst classification, in *American Institute of Physics Conference Series*, Vol. 115, ed. S. E. Woosley (AIP, 1984), pp. 367–372.

20. J.-P. Dezalay, C. Barat, R. Talon, R. Syunyaev, O. Terekhov and A. Kuznetsov, Short cosmic events — A subset of classical GRBs?, in *American Institute of Physics Conference Series*, Vol. 265, eds. W. S. Paciesas and G. J. Fishman (AIP, 1992), pp. 304–309.
21. C. Kouveliotou et al., *Astrophys. J. Lett.* **413**, L101 (1993), doi:10.1086/186969.
22. R. Ruffini et al., *Astron. Astrophys.* **569**, A39 (2014), arXiv:1404.1840 [astro-ph.HE], doi:10.1051/0004-6361/201423457.
23. R. Ruffini, C. L. Bianco, F. Frascchetti, S.-S. Xue and P. Chardonnet, *Astrophys. J. Lett.* **555**, L117 (2001), arXiv:astro-ph/0106534, doi:10.1086/323177.
24. R. Ruffini, On gamma-ray bursts, in *The Eleventh Marcel Grossmann Meeting on Recent Developments in Theoretical and Experimental General Relativity, Gravitation and Relativistic Field Theories*, eds. H. Kleinert, R. T. Jantzen and R. Ruffini (2008), pp. 368–505, arXiv:0804.2837.
25. P. Mészáros, *Rep. Prog. Phys.* **69**, 2259 (2006), arXiv:astro-ph/0605208, doi:10.1088/0034-4885/69/8/R01.
26. T. Piran, *Rev. Mod. Phys.* **76**, 1143 (2005), doi:10.1103/RevModPhys.76.1143.
27. P. Kumar and B. Zhang, *Phys. Rep.* **561**, 1 (2015), arXiv:1410.0679 [astro-ph.HE], doi:10.1016/j.physrep.2014.09.008.
28. S. E. Woosley, *Astrophys. J.* **405**, 273 (1993), doi:10.1086/172359.
29. J. E. Rhoads, *Astrophys. J.* **525**, 737 (1999), arXiv:astro-ph/9903399, doi:10.1086/307907.
30. Y. Z. Fan, D. M. Wei and C. F. Wang, *Astron. Astrophys.* **424**, 477 (2004), arXiv:astro-ph/0405392, doi:10.1051/0004-6361:20041115.
31. B. Zhang et al., *Astrophys. J.* **642**, 354 (2006), arXiv:astro-ph/0508321, doi:10.1086/500723.
32. H. van Eerten, W. Zhang and A. MacFadyen, *Astrophys. J.* **722**, 235 (2010), arXiv:1006.5125 [astro-ph.HE], doi:10.1088/0004-637X/722/1/235.
33. L. Nava, L. Sironi, G. Ghisellini, A. Celotti and G. Ghirlanda, *Mon. Not. R. Astron. Soc.* **433**, 2107 (2013), arXiv:1211.2806 [astro-ph.HE], doi:10.1093/Monthly Notices of the Royal Astronomical Society/stt872.
34. J. A. Rueda and R. Ruffini, *The Astrophys. J. Lett.* **758**, L7 (2012), arXiv:1206.1684 [astro-ph.HE], doi:10.1088/2041-8205/758/1/L7.
35. L. Izzo, J. A. Rueda and R. Ruffini, *Astron. Astrophys.* **548**, L5 (2012), arXiv:1206.2887 [astro-ph.HE], doi:10.1051/0004-6361/201219813.
36. G. Aad et al., *Phys. Lett. B* **716**, 1 (2012), arXiv:1207.7214 [hep-ex], doi:10.1016/j.physletb.2012.08.020.
37. C. Bernardini, *Phys. Perspec.* **6**, 156 (2004), doi:10.1007/s00016-003-0202-y.
38. R. Ruffini et al., *Astron. Astrophys.* **565**, L10 (2014), arXiv:1404.3946 [astro-ph.HE], doi:10.1051/0004-6361/201423812.
39. C. L. Fryer, S. E. Woosley and D. H. Hartmann, *Astrophys. J.* **526**, 152 (1999), arXiv:astro-ph/9904122, doi:10.1086/307992.
40. A. E. Broderick, *Mon. Not. R. Astron. Soc.* **361**, 955 (2005), arXiv:astro-ph/0411778, doi:10.1111/j.1365-2966.2005.09220.x.
41. R. Ruffini et al., *Astrophys. J.* **798**, 10 (2015), arXiv:1405.5723 [astro-ph.HE], doi:10.1088/0004-637X/798/1/10.
42. N. Smith, J. A. Morse, N. R. Collins and T. R. Gull, *Astrophys. J. Lett.* **610**, L105 (2004), arXiv:astro-ph/0406408, doi:10.1086/423341.
43. H. A. Kobulnicky and C. L. Fryer, *Astrophys. J.* **670**, 747 (2007), doi:10.1086/522073.

44. H. Sana *et al.*, *Science* **337**, 444 (2012), arXiv:1207.6397 [astro-ph.SR], doi:10.1126/science.1223344.
45. K. Nomoto and M. Hashimoto, *Phys. Rep.* **163**, 13 (1988), doi:10.1016/0370-1573(88)90032-4.
46. P. Podsiadlowski, P. C. Joss and J. J. L. Hsu, *Astrophys. J.* **391**, 246 (1992), doi:10.1086/171341.
47. E. De Donder and D. Vanbeveren, *Astron. Astrophys.* **333**, 557 (1998).
48. C. L. Fryer *et al.*, *Publ. Astron. Soc. Pac.* **119**, 1211 (2007), arXiv:astro-ph/0702338, doi:10.1086/523768.
49. S.-C. Yoon, S. E. Woosley and N. Langer, *Astrophys. J.* **725**, 940 (2010), arXiv:1004.0843 [astro-ph.SR], doi:10.1088/0004-637X/725/1/940.
50. M. Della Valle, *Int. J. Mod. Phys. D* **20**, 1745 (2011), doi:10.1142/S0218271811019827.
51. C. L. Fryer and S. E. Woosley, *Astrophys. J. Lett.* **502**, L9 (1998), arXiv:astro-ph/9804167, doi:10.1086/311493.
52. C. L. Fryer and A. Heger, *Astrophys. J.* **623**, 302 (2005), arXiv:astro-ph/0412024, doi:10.1086/428379.
53. E. P. J. van den Heuvel and S.-C. Yoon, *Astrophys. Space Sci.* **311**, 177 (2007), arXiv:0704.0659, doi:10.1007/s10509-007-9583-8.
54. S. E. Woosley and J. S. Bloom, *Annu. Rev. Astron. Astrophys.* **44**, 507 (2006), arXiv:astro-ph/0609142, doi:10.1146/annurev.astro.43.072103.150558.
55. H. Bondi and F. Hoyle, *Mon. Not. R. Astron. Soc.* **104**, 273 (1944).
56. H. Bondi, *Mon. Not. R. Astron. Soc.* **112**, 195 (1952).
57. Y. B. Zel’dovich, L. N. Ivanova and D. K. Nadezhin, *Sov. Astron.* **16**, 209 (1972).
58. G. S. Bisnovaty-Kogan and S. A. Lamzin, *Sov. Astron.* **28**, 187 (1984).
59. C. L. Fryer, W. Benz and M. Herant, *Astrophys. J.* **460**, 801 (1996), arXiv:astro-ph/9509144, doi:10.1086/177011.
60. L. Becerra, F. Cipolletta, C. L. Fryer, J. A. Rueda and R. Ruffini, arXiv:1505.07580 [astro-ph.HE].
61. R. Ruffini *et al.*, The blackholic energy and the canonical gamma-ray burst IV: The “long,” “genuine short” and “fake-disguised short” GRBs, in *American Institute of Physics Conference Series*, Vol. 1132, eds. M. Novello and S. Perez (AIP, 2009), pp. 199–266, arXiv:0907.5517 [astro-ph.HE].
62. R. Ruffini, G. Vereshchagin and S.-S. Xue, *Phys. Rep.* **487**, 1 (2010), arXiv:0910.0974 [astro-ph.HE], doi:10.1016/j.physrep.2009.10.004.
63. G. B. Pisani *et al.*, *Astron. Astrophys.* **552**, L5 (2013), arXiv:1304.1764 [astro-ph.HE], doi:10.1051/0004-6361/201220829.
64. A. V. Penacchioni *et al.*, *Astron. Astrophys.* **538**, A58 (2012), arXiv:1112.2970 [astro-ph.HE], doi:10.1051/0004-6361/201118403.
65. M. Rotondo, J. A. Rueda, R. Ruffini and S.-S. Xue, *Phys. Lett. B* **701**, 667 (2011), arXiv:1106.4911 [gr-qc], doi:10.1016/j.physletb.2011.06.041.
66. J. A. Rueda, R. Ruffini and S.-S. Xue, *Nucl. Phys. A* **872**, 286 (2011), arXiv:1104.4062 [gr-qc], doi:10.1016/j.nuclphysa.2011.09.005.
67. R. Belvedere, D. Pugliese, J. A. Rueda, R. Ruffini and S.-S. Xue, *Nucl. Phys. A* **883**, 1 (2012), arXiv:1202.6500 [astro-ph.SR], doi:10.1016/j.nuclphysa.2012.02.018.
68. P. Haensel, A. Y. Potekhin and D. G. Yakovlev (eds.), *Neutron Stars 1: Equation of State and Structure*, Astrophysics and Space Science Library, Vol. 326 (2007).
69. J. Antoniadis *et al.*, *Science* **340**, 448 (2013), arXiv:1304.6875 [astro-ph.HE], doi:10.1126/science.1233232.

70. E. Berger, *Annu. Rev. Astron. Astrophys.* **52**, 43 (2014), arXiv:1311.2603 [astro-ph.HE], doi:10.1146/annurev-astro-081913-035926.
71. R. Ruffini et al., *Astrophys. J.* **808**, 190 (2015), arXiv:1412.1018 [astro-ph.HE], doi:10.1088/0004-637X/808/2/190.
72. C. L. Fryer, J. A. Rueda and R. Ruffini, *Astrophys. J. Lett.* **793**, L36 (2014), arXiv:1409.1473 [astro-ph.HE], doi:10.1088/2041-8205/793/2/L36.
73. C. L. Fryer, *Astrophys. J.* **699**, 409 (2009), arXiv:0711.0551, doi:10.1088/0004-637X/699/1/409.
74. R. Giacconi and R. Ruffini (eds.), *Physics and astrophysics of neutron stars and black holes* (1978).
75. R. A. Chevalier, *Astrophys. J.* **346**, 847 (1989), doi:10.1086/168066.
76. J. C. Houck and R. A. Chevalier, *Astrophys. J.* **376**, 234 (1991), doi:10.1086/170272.
77. R. Ruffini and J. Wilson, *Phys. Rev. Lett.* **31**, 1362 (1973), doi:10.1103/PhysRevLett.31.1362.
78. C. L. Fryer, F. Herwig, A. Hungerford and F. X. Timmes, *Astrophys. J. Lett.* **646**, L131 (2006), arXiv:astro-ph/0606450, doi:10.1086/507071.
79. L. Izzo et al., *Astron. Astrophys.* **543**, A10 (2012), arXiv:1202.4374 [astro-ph.HE], doi:10.1051/0004-6361/201117436.
80. A. V. Penacchioni et al., *Astron. Astrophys.* **551**, A133 (2013), arXiv:1301.6014 [astro-ph.HE], doi:10.1051/0004-6361/201220679.
81. R. Ruffini et al., *Astron. Rep.* **59**, 626 (2015), doi:10.1134/S1063772915070094.
82. R. Ruffini, *Astron. Astrophys. Suppl. Ser.* **138**, 513 (1999), arXiv:astro-ph/9905072, doi:10.1051/aas:1999331.
83. R. Ruffini, C. L. Bianco, F. Frascetti, S.-S. Xue and P. Chardonnet, *Astrophys. J. Lett.* **555**, L113 (2001), arXiv:astro-ph/0106532, doi:10.1086/323176.
84. C. L. Bianco and R. Ruffini, *Astrophys. J. Lett.* **620**, L23 (2005), arXiv:astro-ph/0501390, doi:10.1086/428500.
85. A. V. Penacchioni et al., *Int. J. Mod. Phys. Conf. Ser.* **23**, 254 (2013), doi:10.1142/S2010194513011409.
86. C. Kouveliotou et al., *Astrophys. J. Lett.* **779**, L1 (2013), arXiv:1311.5245 [astro-ph.HE], doi:10.1088/2041-8205/779/1/L1.
87. D. A. Perley et al., *Astrophys. J.* **781**, 37 (2014), arXiv:1307.4401 [astro-ph.HE], doi:10.1088/0004-637X/781/1/37.
88. M. Ackermann et al., *Science* **343**, 42 (2014), doi:10.1126/science.1242353.
89. M. Ackermann et al., *Astrophys. J.* **209**, 11 (2013), arXiv:1303.2908 [astro-ph.HE], doi:10.1088/0067-0049/209/1/11.
90. M. Kovacevic et al., *Astron. Astrophys.* **569**, A108 (2014), arXiv:1408.6227 [astro-ph.HE], doi:10.1051/0004-6361/201424700.
91. R. Ruffini et al., *GRB Coordinates Network* **14526**, 1 (2013).
92. A. de Ugarte Postigo et al., *GRB Coordinates Network* **14646**, 1 (2013).
93. A. Trotter et al., *GRB Coordinates Network* **1466** (2013).
94. A. J. Levan et al., *GRB Coordinates Network* **14686**, 1 (2013).
95. A. J. Levan et al., *Astrophys. J.* **792**, 115 (2014), arXiv:1307.5338 [astro-ph.HE], doi:10.1088/0004-637X/792/2/115.
96. D. Xu et al., *Astrophys. J.* **776**, 98 (2013), arXiv:1305.6832 [astro-ph.HE], doi:10.1088/0004-637X/776/2/98.